Technicc

1. Report No.	2. Government Accession No.	3. Recipient's Catalog No.
FHWA/TX-93+1210-5F		

4. Title and Subtitle	5. Report Date
DESIGN GUIDELINES FOR TRANSFER, DEVELOPMENT AND DEBONDING OF LARGE DIAMETER SEVEN WIRE STRANDS IN PRETENSIONED CONCRETE GIRDERS	January 1993
	6. Performing Organization Code

7. Author(s)	8. Performing Organization Report No.
Bruce W. Russell and Ned H. Burns	Research Report 1210-5F

9. Performing Organization Name and Address	10. Work Unit No. (TRAIS)
Center for Transportation Research The University of Texas at Austin 3208 Red River, Suite 200 Austin, Texas 78705-2650	11. Contract or Grant No. Research Study 3-5-89/2-1210
	13. Type of Report and Period Covered Final
12. Sponsoring Agency Name and Address Texas Department of Transportation Transportation Planning Division, Research Section P. O. Box 5051 Austin, Texas 78763-5051	14. Sponsoring Agency Code

15. Supplementary Notes

Study conducted in cooperation with the U.S. Department of Transportation, Federal Highway Administration. Research Study Title: "Influence of Debonding Strands on Behavior of Composite Prestressed Concrete Bridge Girders"

16. Abstract

Recently, a new and larger seven-wire strand was offered by industry for use in pretensioned concrete. The new strand size, 0.6 inches in diameter, has 40 percent greater area and 40 percent greater capacity than the current industry standard, 0.5-inch-diameter strand. Larger strand sizes can lead to improved efficiency of pretensioned structures; however, larger strands require greater bond forces to anchor the strands.

In October of 1988, the FHWA issued a moratorium suspending the use of 0.6-inch strand in pretensioned applications. Recent studies had indicated that current design provisions were inadequate. Additional restrictions were placed on smaller sizes of strands. The limitaations were adopted on an interim basis until additional research could substantiate or restructure current industry standards. One objective of this investigation is to determine the transfer and development length of 0.5-inch- and 0.6-inch-diameter prestressing strands.

The debonding, or blanketing, of strands is an alternative to draping strands in order to control the maximum concrete stresses. Debonding strands can simplify girder construction; draping strand is more difficult and more dangerous. Likewise, debonded strands enjoy economical advantages compared to draped strands. The second objective of this research is to develop design guidelines for the use of debonded strands in pretensioned concrete beams.

A testing program was conducted that included measurement of transfer lengths, measurement of development lengths, and testing the behavior and performance of beams made with debonded strands. A simple analytical model was developed to predict the behavior of pretensioned bond. Bond failure is predicted based on the distress caused by cracks when they propagate through the anchorage zone of prestressing strands. Tests showed that the model accurately predicts strand anchorage, or, conversely, bond failure.

Based on the experimental data, it was determined that bond failure would be prevented if no cracking occurred in the anchorage zone of a pretensioned strand. Design recommendations are made for transfer length, development length, and the use of debonded strands.

17. Key Words	18. Distribution Statement
debonding, strands, 0.5-inch-diameter strand, pretensioned concrete, bond failure, development length, transfer length, anchorage zone, cracks, draped strands, beams, compression stresses	No restrictions. This document is available to the public through the National Technical Information Service, Springfield, Virginia 22161.

19. Security Classif. (of this report)	20. Security Classif. (of this page)	21. No. of Pages	22. Price
Unclassified	Unclassified	300	

DESIGN GUIDELINES FOR TRANSFER, DEVELOPMENT AND DEBONDING OF LARGE DIAMETER SEVEN WIRE STRANDS IN PRETENSIONED CONCRETE GIRDERS

by

Bruce W. Russell and Ned H. Burns

Research Report 1210-5F

"Influence of Debonding Strands on Behavior of Composite Prestressed Concrete Bridge Girders"
Research Project 3-5-89/2-1210

conducted for the

Texas Department of Transportation

in cooperation with the

U.S. Department of Transportation
Federal Highway Administration

by the

CENTER FOR TRANSPORTATION RESEARCH
Bureau of Engineering Research
THE UNIVERSITY OF TEXAS AT AUSTIN

January 1993

NOT INTENDED FOR CONSTRUCTION,
BIDDING OR PERMIT PURPOSES

N.H. Burns, P.E. (Texas No. 20801)
Research Supervisor

The contents of this report reflect the views of the authors, who are responsible for the facts and accuracy of the data presented herein. The contents do not necessarily reflect the official views or policies of the Federal Highway Administration or the Texas Department of Transportation. This report does not constitute a standard, specification, or regulation.

There was no invention or discovery conceived or first actually reduced to practice in the course of or under this contract, including any art, method, process, machine, manufacture, design or composition of matter, or any new and useful improvement thereof, or any variety of plant which is or may be patentable under the patent laws of the United States of America or any foreign country.

PREFACE

This is the fifth and final report from an extensive experimental testing program concerning the bond of pretensioned strands. This final report discusses transfer length, development length and flexural bond behavior from a comprehensive point of view.

In the first report, results from the transfer length tests were discussed. The second report discussed the effects of transverse post-tensioning on flexural bond. The third report examines the development length that should be required for pretensioned strands and the fourth report examines design provisions for the use of debonded strands. This report provides the comprehensive analysis of all the data from the entire project and general design recommendations are given.

The research was conducted as part of Research Program 3-5-89-1210, entitled "*Influence of Debonding of Strands on Behavior of Composite Prestressed Bridge Girders*." This project was modified in March 1989 to include transfer length and development length testing for 0.6-inch strands. The work performed under that first modification is reported primarily in the first three reports. A second modification was adopted for the fiscal year 91-92 to perform repeated load tests on full-sized composite girders. These tests are reported in Chapter 7.

The research was conducted at the Phil M. Ferguson Structural Engineering Laboratory (FSEL) as a part of the overall research program for the Center for Transportation Research of The University of Texas at Austin. The work was sponsored jointly by the Texas Department of Transportation (TxDOT) and the Federal Highway Administration (FHWA). Liaison is maintained with TxDOT through the Technical Coordinator, Mr. David P. Hohmann and with FHWA through Ms. Susan N. Lane, Structural Research Engineer.

The program was directed by Dr. Ned H. Burns, the Associate Dean of Engineering for Academic Affairs and Zarrow Centennial Professor of Engineering at The University of Texas at Austin. Dr. Michael E. Kreger, Associate Professor of Civil Engineering has assisted the project by reviewing the efforts. Graduate Research Assistants who have made significant contributions to this research are Mr. Asit Baxi, Mr. Leslie ZumBrunnen, Mr. Riyad Aboutaha, Mr. Bruce Lutz, Mr. Ozgur Egilmez, Mr. Ozgur Unay, Mr. Raheel Malik and Dr. Bruce W. Russell. Appreciation is also extended to Mr. Andy Linseisen, Mr. George Mayfield, and Mr. "Rusty" Barnhill.

SUMMARY

Recently, a new and larger seven-wire strand was offered by industry for use in pretensioned concrete. The new strand size, 0.6 inches in diameter, has 40% greater area and has 40% greater capacity than the current industry standard, 0.5 inch strand. Larger strand sizes can lead to improved efficiency of pretensioned structures; however, larger strands require greater bond forces to restrain the strands.

In October of 1988, the Federal Highway Administration (FHWA) issued a moratorium suspending the use of 0.6-inch diameter strand in pretensioned applications and the required development lengths for smaller strand sizes were increased. Recent research had indicated that current design provisions were inadequate.[39] The limitations were adopted on an interim basis until additional research could substantiate or restructure current industry standards. One objective of this investigation is to determine the transfer and development length of 0.5-inch and 0.6-inch diameter prestressing strands.

The debonding, or blanketing of strands in an alternative to draping strands in order to control the maximum tensioned and compressions stresses at the ends of concrete beams. Debonding strands can simplify construction by allowing straight strand patterns. Draping strands is more difficult and more dangerous. Debonded strands likewise enjoy some economical advantages to draped strands.

A testing program was conducted that included measuring of transfer lengths, measuring of development lengths, and testing the behavior and performance of beams with debonded strands. A simple analytical model was developed that predicts behavior of pretensioned bond. Bond failure is predicted based upon the distress caused by cracks when they propagate through the anchorage zone of prestressing strands. Tests showed that the model accurately predicts strand anchorage, or conversely, bond failure.

Based on experimental data, it was determined that bond failure would be prevented if no cracking occurred in the anchorage zone of a pretensioned strand. Design recommendations are made for transfer length, development length, and the use of debonded strands.

IMPLEMENTATION

From this experimental program, design guidelines for transfer, development and debonding of pretensioned prestressing strands are developed. The experimentation demonstrated behavioral principles that are translated into design guidelines.

Two main conclusions are to be drawn from this research. First, 0.6-inch diameter strand is safe when used in pretensioned applications. Secondly, debonded strands can be employed safely when following the recommendations of this report.

TABLE OF CONTENTS

METRIC (SI*) CONVERSION FACTORS

APPROXIMATE CONVERSIONS TO SI UNITS

Symbol	When You Know	Multiply by	To Find	Symbol
		LENGTH		
in	inches	2.54	centimeters	cm
ft	feet	0.3048	meters	m
yd	yards	0.914	meters	m
mi	miles	1.61	kilometers	km
		AREA		
in^2	square inches	645.2	millimeters squared	mm^2
ft^2	square feet	0.0929	meters squared	m^2
yd^2	square yards	0.836	meters squared	m^2
mi^2	square miles	2.59	kilometers squared	km^2
ac	acres	0.395	hectares	ha
		MASS (weight)		
oz	ounces	28.35	grams	g
lb	pounds	0.454	kilograms	kg
T	short tons (2,000 lb)	0.907	megagrams	Mg
		VOLUME		
fl oz	fluid ounces	29.57	milliliters	mL
gal	gallons	3.785	liters	L
ft^3	cubic feet	0.0328	meters cubed	m^3
yd^3	cubic yards	0.0765	meters cubed	m^3

NOTE: Volumes greater than 1,000 L shall be shown in m^3.

		TEMPERATURE (exact)		
°F	Fahrenheit temperature	5/9 (after subtracting 32)	Celsius temperature	°C

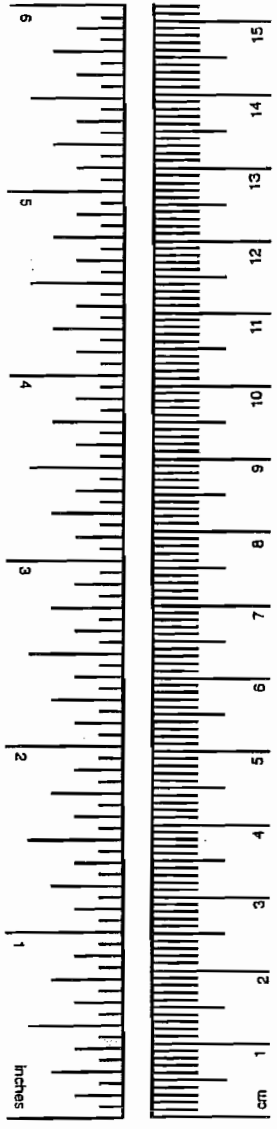

APPROXIMATE CONVERSIONS FROM SI UNITS

Symbol	When You Know	Multiply by	To Find	Symbol
		LENGTH		
mm	millimeters	0.039	inches	in
m	meters	3.28	feet	ft
m	meters	1.09	yards	yd
km	kilometers	0.621	miles	mi
		AREA		
mm^2	millimeters squared	0.0016	square inches	in^2
m^2	meters squared	10.764	square feet	ft^2
m^2	meters squared	1.20	square yards	yd^2
km^2	kilometers squared	0.39	square miles	mi^2
ha	hectares (10,000 m^2)	2.53	acres	ac
		MASS (weight)		
g	grams	0.0353	ounces	oz
kg	kilograms	2.205	pounds	lb
Mg	megagrams (1,000 kg)	1.103	short tons	T
		VOLUME		
mL	milliliters	0.034	fluid ounces	fl oz
L	liters	0.264	gallons	gal
m^3	meters cubed	35.315	cubic feet	ft^3
m^3	meters cubed	1.308	cubic yards	yd^3
		TEMPERATURE (exact)		
°C	Celsius temperature	9/5 (then add 32)	Fahrenheit temperature	°F

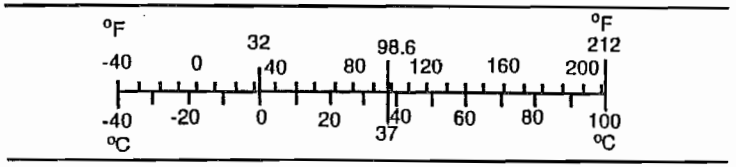

These factors conform to the requirement of FHWA Order 5190.1A.

* SI is the symbol for the International System of Measurements

CHAPTER 1
INTRODUCTION

In pretensioned concrete, bond between prestressing steel and concrete is an essential component to ensure the integrity of a pretensioned member. Bond is derived from mechanical interaction between concrete and steel. Bond controls many aspects of design. Specifically, the anchorage and development of the prestressing force are dependent exclusively on bond. This research investigates the bond between pretensioned steel and concrete by studying the behavior of prestressed concrete specimens under load and also at transfer of the prestressing force. Based on the observed behavior, design guidelines are developed for the transfer and development of pretensioned steel along with design guidelines for the use of debonded strands in pretensioned concrete beams.

1.1 Objectives of the Research

This research project has two specific objectives. The first objective is to determine the transfer length and the development length of both 0.5 inch and 0.6 inch prestressing strands. The second objective is to develop design guidelines for the use of debonded strands in pretensioned concrete. These specific objectives are included in the more generalized objective to develop a rational understanding of the bond mechanisms between concrete and prestressing steel. From these understandings, behavioral models can be employed to develop design guidelines.

1.2 Background

Research reported in this document was performed under Project 3-5-89-1210, entitled ***Influence of Debonding of Strands on Behavior of Composite Prestressed Concrete Bridge Girders***, and funded through the Texas Department of Transportation (TxDOT) and the Federal Highway Administration (FHWA). At its inception, the scope of the project was limited to the development of design guidelines for the use of debonded strands. In its second year, the project was augmented to include transfer length and development length research for both 0.5 inch diameter and 0.6 inch diameter prestressing strands. This modification contained a significant amount of testing and research that was separate from the research on the debonding of strands. As such, many tests were performed on specimens that contained only fully bonded strands.

However, as the project evolved, it became apparent that the two topics were inextricably linked. The behavioral characteristics of pretensioned bond were common to both fully bonded strands and debonded strands. Transfer length and development length test results became the building blocks for developing the testing program for beams with debonded strands. The common denominator to both sets of problems was the mechanisms that affect pretensioned bond. Understanding the behavior and the mechanics of pretensioned bond was essential to understanding the test results on both fully bonded and

debonded specimens and their impact on the overall structural behavior. In this document, test results are critically examined to determine the behavioral mechanisms that can be generally applied to the bond problem. The mechanisms of bond are developed and then applied to developing design guidelines.

1.2.1 Transfer and Development of Pretensioned Strand, And the 0.6 Inch Diameter Strand. On October 26, 1988, the FHWA issued a moratorium disallowing the use of 0.6 inch diameter prestressing strand in pretensioned applications. Additionally, the required development length for all other sizes of prestressing strand was increased to 1.6 times the current AASHTO and ACI requirements (AASHTO equation 9-32 and ACI Section 12.9). Recent studies had indicated that measured transfer lengths and development lengths exceeded current code requirements[39,53,54]. The restrictions were adopted as an interim measure until additional research results were available to either substantiate or restructure current code provisions.

The 0.6 inch diameter seven-wire strand has the advantage of 40% greater area and therefore a 40% greater capacity than an 0.5 inch diameter strand. This leads to improved efficiency of flexural members. Also, the use of 0.6 inch strand with high strength concrete has the added advantage of increasing span limits for standard cross sections. While the 0.6 inch strand has 40% greater area, it has only a 20% larger surface area. Considering that the bond forces act on an area only 20% larger in size while restraining a pretensioned force that is 40% larger, there is a natural concern that sufficient bond could be developed to transfer and develop the larger 0.6 inch diameter strand in pretensioned applications.

1.2.2 The Need and Use for Debonded Strands. The debonding (blanketing) of strand is an alternative to draping strands in order to control the maximum tensile and compressive stresses in the end regions of pretensioned beams. Debonding strands can simplify girder construction; draping strands is more difficult and more dangerous. Likewise, debonding strands may enjoy economical advantages over draping strands.

Rules governing the design of pretensioned girders with debonded strands have been based more on engineering judgements than experimental data or analytical reasoning. This research develops an analytical model, then compares the analysis with the experimental data. Current code provisions require that the development length for debonded strands be 2.0 times the development length for strands that are fully bonded (ACI Section 12.9.3 and AASHTO Section 9.27.3). While the current provisions are based primarily on three separate research studies[11,17,25], the specific results from these tests were generalized to include all design cases and do not adequately reflect the behavior of pretensioned structures.

1.3 Definitions

In this section, the definitions of transfer length and development length are given. Also, debonded strands are defined and described. Other important definitions can be found in the glossary in Appendix E.

1.3.1 Transfer Length. In pretensioned beams, transfer length is the distance required to transfer the fully effective prestressing force from the strand to the concrete. Stated another way, transfer length is the length of bond from the free end of the strand to the point where the prestressing force is fully effective. The transfer zone is defined as the region of concrete spanned by the transfer length. An idealization of steel stresses is shown in Figure 1.1. Stresses in the pretensioned steel vary from zero at the free end of the strand increasing throughout the transfer zone until the prestress force is fully effective. Increases in strand tension come about by bond stresses that restrain, or hold back, the strand. At the point of full transfer, the stress in the steel remains constant over the length. This is represented by the flat interior portion of the curve.

Concrete and steel forces must be in equilibrium at every point along the length. Tension in the steel is always balanced by equivalent and opposite compression in the concrete. Therefore, the variation of steel strains is mirrored by the variation in concrete strains. The idealization of Figure 1.1 is proven out by actual strain measurements from Test Specimen FCT350-3, shown in Figure 1.2. Note the increase in strains at each end of the specimen where the prestress force is transferred to the concrete. A transfer zone is found at each end of every pretensioned element, evidenced by the increasing strains in the concrete. The strain plateau in the interior of the specimen distinguishes the region where the prestress force is fully effective.

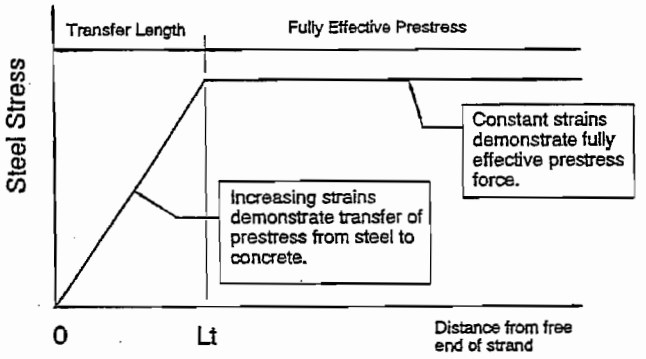

Figure 1.1 Idealized Steel Stress vs. Length for Pretensioned Concrete Member

1.3.2 Development Length. Development length is the bond length required to anchor the strand as it resists external loads on the member. As tension increases in the strand, additional bond stresses are created which resist movement of the strand. Consider a typical simply supported beam loaded in flexure. Tension in the strand increases to resist flexural moments imposed by external loads. As strand tension increases, bond strength must also increase. Strand equilibrium is maintained as additional bond stresses resist increases in strand tension. If bond stresses anchor the strand so that flexural failure results under increasing load, then strand tension has been adequately developed and that bond

length is sufficient. In these cases, the bonded length of strand equals or exceeds the development length. Conversely, if the strand slips through the concrete from the influence of external loads on the member, we say that bond or anchorage has failed and that the bonded length of the strand is less than the development length.

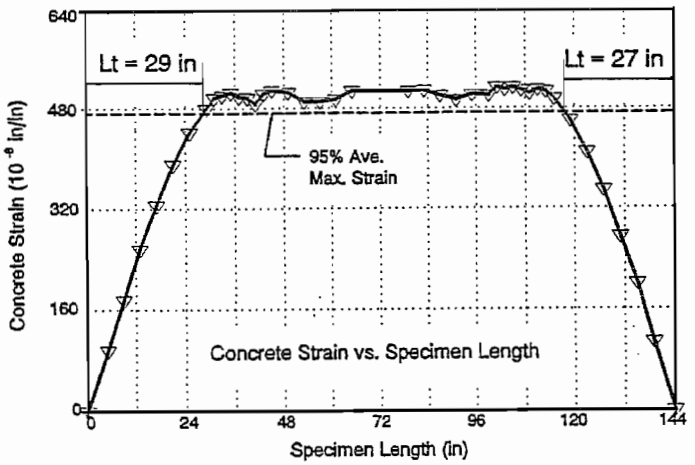

Figure 1.2 Strain Profile and Measured Transfer Length, FC350-2

1.3.3 Debonded Strands. Debonded strands are strands that have been coated or wrapped so that the strand will not bond to the concrete. Debonding can be accomplished by several methods. For example, coating the strand with grease or placing plastic tubing over the strands are effective methods for debonding strands. In regions of the beam where debonded strands is required to be fully active, the debonding is discontinued, and the strand is allowed to bond with the concrete. In this manner, debonding can be used to vary the prestress force and its eccentricity along the length of a pretensioned concrete element.

1.4 Current Code Provisions

AASHTO and ACI code requirements for transfer, development and debonding are nearly identical to one another. Current code provisions are included in other chapters within the text. The code treatment of transfer length is discussed in Section 3.3. Development length provisions are discussed in Section 4.3. Lastly, code requirements for debonded strands are discussed in Section 5.2.

1.5 The Testing Program

1.5.1 Transfer Length Testing. Transfer length measurements were taken on sixty-five specimens. Fifty of those tests were performed on rectangular prisms with either one, three, or five strands. Variables included the size of the strands, debonded strands, and confining reinforcement. Transfer lengths were also measured on AASHTO-type beams and the full sized Texas Type C girders. Transfer lengths from these specimens help to broaden the scope of the testing program beyond that of smaller transfer length prisms that have been historically tested. The transfer length testing program, procedures, results and discussion are found in Chapter 3.

1.5.2 Development Length Testing. A series of development length tests were performed on scale model AASHTO-type specimens that were designed to resemble a

composite pretensioned bridge girder. All of the strands in this series were fully bonded, in other words, bond began at the ends of the pretensioned beam and no debonding was employed. Development length was measured for both 0.5 inch strands and 0.6 inch strands. These tests and their results are presented and discussed in Chapter 4.

1.5.3 Tests on Beams with Debonded Strands, Static Tests. This series of beams contained some strands that were debonded. The beams are sometimes referred to as debonded beams. In the design of these beams, an analytical rationale was developed to predict the behavior of debonded beams, and whether or not a beam was in danger of failing in bond. The analytical rationale is based on the prediction of cracking in concrete. Flexural tests were performed on these beams to test their behavior, and particularly to examine their behavior in comparison to the predicted behavior. This testing program, an explanation of the prediction model, and the test results are presented and discussed in Chapter 5.

1.5.4 Tests on Beams with Debonded Strands, Repeated Load Tests. Beams tested in this series were companion beams to statically tested beams discussed in Section 1.5.3. The purpose of these tests was to investigate the possibility and the consequences of bond distress during repeated loading. Eight tests were performed on five beams. One of the beams contained fully bonded 0.6 inch strands. These tests are presented and discussed in Chapter 6.

1.5.5 Tests on Texas Type C Composite Girders. Three full-sized girders were manufactured at a nearby prestressing plant and brought to Ferguson Structural Engineering Laboratory (FSEL) where the composite slab was cast and the girders were tested. These tests were designed to demonstrate the behavioral patterns that were noted from earlier tests and also to demonstrate the design of pretensioned composite girders with debonded strands. One of the girders contained draped strands as a control specimen. The other two contained debonded strands. All other design parameters were essentially the same. The description of the design, fabrication, and testing of these specimens is found in Chapter 7 along with the presentation and discussion of the test results.

CHAPTER 2
ELEMENTS OF BOND

2.1 Elements of Bond: The Basis for Behavior

The bond between pretensioned strand and concrete has been treated empirically. Many formulae[1,2,5,8,15,22,39,52] have been presented throughout the literature to fit experimental results, but no comprehensive mathematical models based solely on the physical properties of the materials have been offered. Certainly, the bond problem is very difficult to model with any mathematical representation. Janney(1954)[1] showed that the tangential stresses in the concrete surrounding the strand exceeds the tensile capacity of the material, causing the concrete to crack locally and creating a material discontinuity. Another variable, friction, has been recognized as a major contributor to the transfer and development of prestressing force, but there have been very few efforts to quantify the frictional bond stresses between prestressing steel and concrete. On the contrary, many studies concluded that large variability exists in the frictional component. Additionally, seven wire strand contributes to bond stress by the mechanical interlocking from the helical patterns of the individual wires. This effect has been noted in the earliest research on seven wire strand, but again, very little effort has been made to quantify the contribution of mechanical interlocking or to even describe qualitatively how much influence that mechanical interlocking may have on bond.

Bond stresses are not easy to represent mathematically. Concrete cracks in the transfer zone. Strands slip relative to the concrete upon detensioning. The strands untwist to relieve their tension, but cannot regain their original shape. At the same time, the strands expand against the concrete causing large normal forces which in turn create frictional restraint. Friction defies prediction because of variability in surface conditions of the strand or concrete. In the transfer zone, friction from Hoyer's effect gradually restrains untwisting of the strand through the transfer zone. As twist restraint increases, bond stresses from mechanical interlocking also increase. All of these factors contribute to what would be a very complex mathematical expression for bond stresses.

Fortunately, it may not be too important to describe the bond stresses in exact mathematical language. In fact, a qualitative understanding of the mechanisms generating bond appears to sufficiently describe the anchorage and development of pretensioned strand. These bond mechanisms, or **elements of bond**, are presented here to provide a basis for understanding the bond behavior of pretensioned seven-wire strand. Using the elements of bond, the anchorage or anchorage failure of pretensioned strand can be predicted. Accordingly, the scope of this research does not include a mathematical model for bond stresses along the length of the pretensioned strand. Instead, the qualitative model for bond is presented as a means to predict bond behavior.

In this chapter, the fundamental mechanics of bond are investigated qualitatively. From the tests performed in this research and from a review of past and concurrent

research, specific elements of bond can be established. The qualitative bond models, correlate very well with actual test results, demonstrating the ability to predict bond failure. These **Elements of Bond** provide us with the essential mechanisms that contribute to bond of pretensioned strands. From these mechanical models, we can begin to understand and predict the behavior of pretensioned strands, the transfer of their prestress forces and the development of their strength under load.

2.2 Elements of Bond

There are three distinct and different elements of bond. They are:

1) Adhesion,
2) Hoyer's Effect, and
3) Mechanical Interlocking.

These three mechanisms combine to develop what is called "bond". "Bond" is derived from the action of any one or more of these mechanisms. Hoyer's effect is independent from the other two in that it is derived from the change in steel strain in the transfer zone. On the other hand, mechanical interlocking depends upon Hoyer's effect and/or adhesion to restrain the strand and prevent twist. Note that friction is not listed here as a separate mechanical process. However, friction is a component and contributor to both Hoyer's effect and mechanical interlocking. Without friction, the amount of bond from Hoyer's effect would be zero, and mechanical interlocking's effect would be reduced.

2.2.1 Adhesion. Adhesion is the glue between the concrete and the steel. By definition, the glue line is very thin and the resulting bond stress versus slip behavior is rigid-brittle. A representation of the behavior is shown in Figure 2.1. Adhesion effectively prevents displacement of the strand relative to the concrete until some critical stress is reached. At that critical stress, the glue fails and resistance provided by the glue reduces to zero. Failure of the glue is always brittle. In the case of a pretensioned strand, the bond lost from the failure of adhesion is often replaced by the other mechanisms. However, it is important to recognize that adhesion does not contribute to bond once slip has occurred.

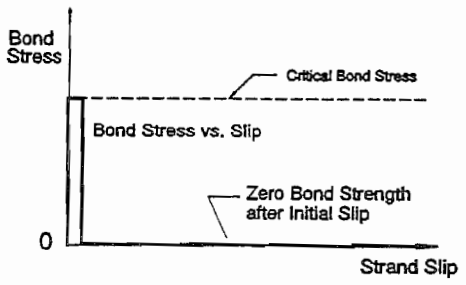

Figure 2.1 Adhesion: Rigid - Brittle Behavior

Because of this rigid-brittle behavior, adhesion contributes little or nothing to either prestress transfer bond or the bond developed to resist additional strand tension from applied loads. At transfer, the prestressing strands slip relative to the concrete. In fact, the transfer zone is characterized by strand slip. The transfer length is defined as the length

from the free end of the strand to the point where the change in strand strain resulting from the prestress transfer equals the change in concrete strain. This occurs at the point where there is no slip between the concrete and the strand.

At development bond failure, external loads increase the tension on the strand until it is pulled through the concrete. In development failures, the strands' bond strength is insufficient to resist the increase in strand tension. Slip of the strand at bond failure is an obvious result. In many of the flexural development length tests, the strands slipped on the order of 0.001 to 0.005 inches, yet the beams were able to achieve full flexural capacity. In these cases, the behavior resembles a hybrid between flexural failure and general bond failure. Small strand slips can occur without producing complete bond failure, and the beams fail in flexure. Therefore, adhesion does not make a primary contribution to bond of the pretensioned strand, in this case flexural or development bond.

2.2.2 Hoyer's Effect. Hoyer's Effect is named after E. Hoyer who performed early research on prestressed concrete. At that time, small diameter smooth piano wire was used as prestressing steel. There were no deformations on the steel to ensure transfer of the prestressing force to the concrete. In 1939, Hoyer investigated the mechanism that anchored the pretensioned force to the concrete. He identified the mechanism that bears his name.

When steel is pretensioned, the diameter of the strand or wire reduces by Poisson's ratio as it is elongated. Then concrete is cast surrounding the prestressing steel. Upon release of the prestressing force, the steel strands or wires lose their initial prestress and expand laterally, trying to regain their original form. When this lateral expansion is resisted by concrete surrounding the strand, a normal force is imposed at the boundary between concrete and steel. In turn, this normal force activates a frictional force between the concrete and steel. This friction opposes relative movement of the steel with respect to the concrete, thereby restraining the prestressing strand and holding it in tension. Hoyer's effect is illustrated in Figure 2.2. Hoyer's Effect is also known by a very descriptive name, wedge action.

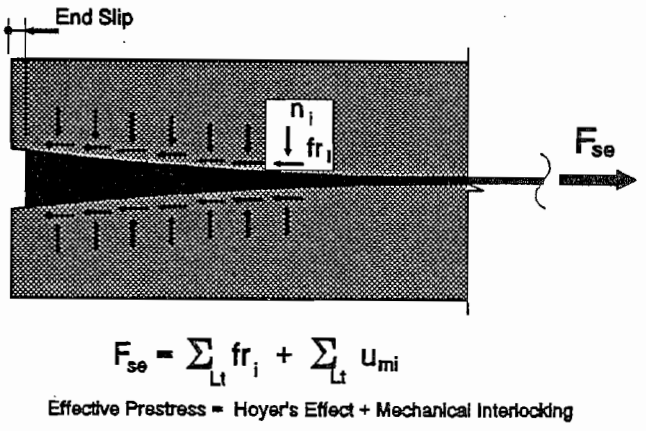

Figure 2.2 Wedge Action from Hoyer's Effect

Hoyer's effect is active almost exclusively in the transfer zone. When a pretensioned beam is loaded in flexure, strand tension increases with applied moment. Likewise, the diameter of the strand shrinks, and Hoyer's effect is reduced significantly. This idea led early researchers[1,5] to suggest that strand anchorage will fail if a strand's tensile stress

increased in the transfer zone. In 1959, Hanson and Kaar performed a series of development tests on rectangular beams. They theorized that as a beam is loaded, a wave of high bond stresses progress from the point of maximum moment towards the anchorage zone. If that wave of high bond stress should reach the transfer zone, further increases in strand tension would reduce the diameter of the strand, effectively destroying Hoyer's effect. Furthermore, anchorage failure would occur as the strand is freed to pull through the concrete.

This phenomenon was witnessed in the tests performed in this research. In reality, increases in strand tension occur at the crack locations. When a crack forms, the tension force that was shared by the concrete must now be carried by the strand alone. Local increases in strand tension in turn require increases in bond stress as the tension redistributes from the strand into the concrete on either side of a crack.

2.2.3 Mechanical Interlocking. When concrete is cast around a seven-wire strand, the concrete forms an envelope or sleeve surrounding the strand. The hardened concrete mimics the shape of the seven-wire strand. The concrete completely surrounds the strand, filling even the narrow crevices between individual wires, called the interstices of the strand. If the strand attempts to pull through the concrete without twisting, movement is resisted by the concrete ridges acting on the outside wires of the strand. This resistance is called mechanical interlocking.

In seven wire strand, six outside wires are wound around a single center wire in a helical pattern. The pitch of the outside wires varies between manufacturers, but the differences are small. For 0.5 inch strands used in this research, the pitch of an individual wire was about 7.5 inches which corresponds to an angle of about 9°. The helical windings provide the "humps" necessary to develop mechanical interlocking in pretensioned strand. When external loads apply additional tension to the strand, movement of the strand relative to the concrete is resisted by the interlocking of the outside wires reacting against matching deformations in the concrete. This effect is illustrated in Figure 2.3. The helical strand pattern is analogous to deformations in mild reinforcing steel. If twisting is restrained, bond between strand and concrete behaves somewhat like pullout of mild reinforcement. Mechanical interlocking bond stresses, u_{mi}, is a function of the normal force, f_i, the angle of pitch θ and the coefficient of friction μ.

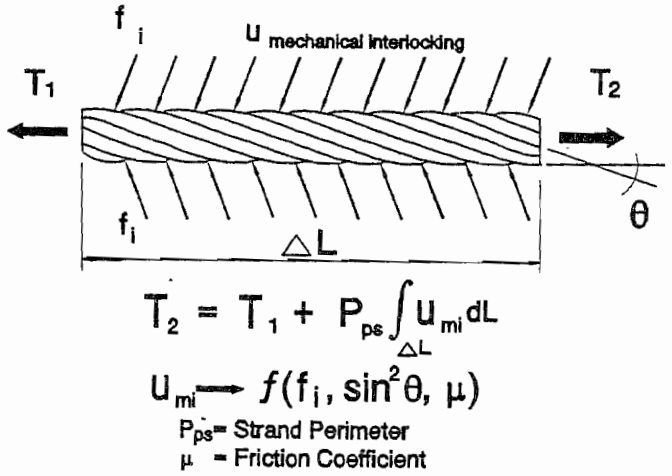

Figure 2.3 Mechanical Interlocking

Mechanical interlocking is the largest contributor to flexural bond, especially in cracked regions. As a flexural crack forms, strand slip must occur for some small finite distance on either side of the crack to preserve compatibility of the strand. When slip occurs, mechanical interlocking is activated by the reaction of the outside wires interlocking with the concrete envelope. Bond stresses from mechanical interlocking can be very large in the immediate vicinity of cracking. An idealization of high bond stresses immediately adjacent to the cracks is illustrated in Figure 2.4. Flexural bond stresses result from changes in stress in the steel. At the crack locations, increases in steel stresses demonstrate high absolute bond stresses. Note that bond stresses, u_b, are given by:

$$u_b \propto \frac{d}{dx} (\text{steel stress}).$$

Experimental evidence for this illustration is demonstrated by the well distributed crack patterns of the beams tested.

Mechanical interlocking is dependent on one very important condition, namely, strands must be restrained from twisting. If twist of the strand is not restrained, then the strand can simply untwist through the concrete, rendering mechanical interlocking completely ineffective. Strand twisting led early researchers to discount the effects of mechanical interlocking. This general philosophy is reflected in current ACI and AASHTO codes.

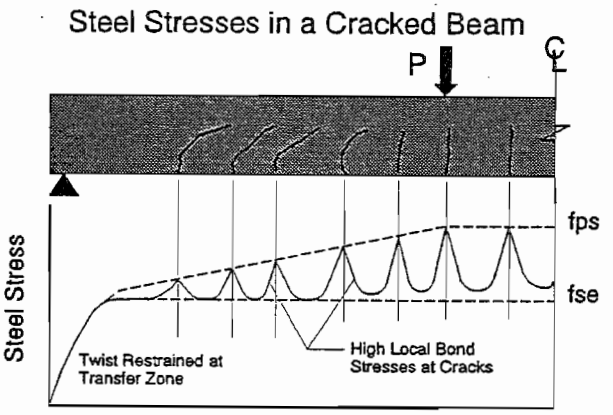

Figure 2.4 Pretensioned Steel Stresses in a Cracked Beam

At the University of Illinois, Stocker and Sozen[15] tested the bond mechanisms of prestressing strands. A series of pull-out tests were performed where the strands were restrained from twisting in some of the specimens but allowed to twist in others. The researchers expected that larger forces would be required to pull out the restrained strands. However, in comparing the pull-out strengths, very little difference was noted between the specimens where twist was restrained and the specimens where strands were free to twist. Current code provisions discount bond stresses derived from mechanical interlocking based, in part, on these results.

However, their test setup was responsible for this apparent paradox. In Stocker's test set-up, long lengths of free strand made the angle of twist per unit length much smaller than in an actual pretensioned beams adjacent to a crack. ("Free Strand" refers to strand that is not immediately confined by adjacent concrete.) The strand was restrained several inches

from the point where strand entered the concrete. Consequently, the torsional moment required to restrain twisting was much smaller in these tests than would be found in a real beam. This type of test set-up makes mechanical interlocking ineffective as is demonstrated by the test results.

In an actual pretensioned concrete member, the length of free strand is exactly equal to the width of the cracks, a very small distance. When a crack forms, the strand extends across the crack. Twisting is restrained by a combination of adhesion and interlocking acting on the strand immediately adjacent to the crack. Resulting bond stresses in real structures can be much higher than bond stresses determined from pull out tests.

2.3 Bond Mechanics in the Transfer Zone

Bond for the transfer of pretensioned force develops from a combination of Hoyer's effect and mechanical interlocking. The relative contribution of each is uncertain, but most of the transfer bond probably comes from Hoyer's effect because twist restraint has not yet developed for mechanical interlocking to be fully effective. Most of the earlier researchers attribute transfer bond to Hoyer's effect[1,2,5,7,15]. A representation of the relative contributions from these two elements of bond is shown in Figure 2.5. Note that mechanical interlocking is shown to contribute to bond towards the latter portion of the transfer zone. Increases in bond from mechanical interlocking develop as twist restraint is generated from Hoyer's effect, as shown in Figure 2.5.

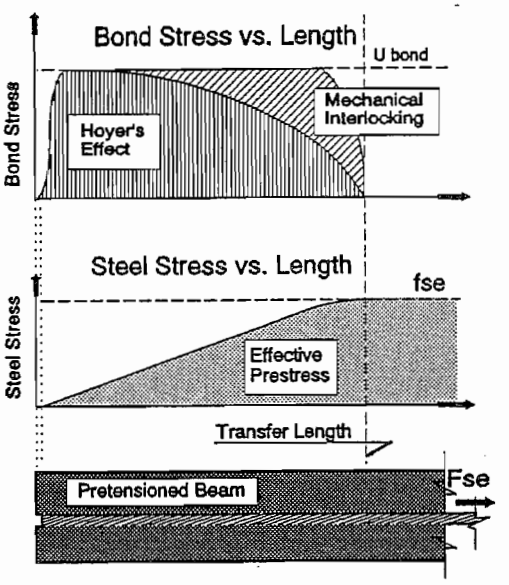

Figure 2.5 Idealization of Bond Mechanics in Transfer Zones

Mathematically, integration of the bond stresses over length must equal the steel stress. As a corollary, total bond stress is the derivative of steel stress. The individual contributions of Hoyer's effect versus mechanical interlocking are not known. However, transfer length testing shows that steel stresses increase approximately linearly through the transfer zone. Linear variation of steel stresses requires that bond stresses remain approximately constant through the transfer zone. A typical strain profile for a transfer length specimen is shown in Figure 2.6. (Transfer length testing is discussed in greater detail in the next chapter.)

Earlier experimental research supports the idealized bond stress distributions illustrated in Figure 2.5. Janney[1] performed transfer length experiments on smooth wire in 1954. In these tests mechanical interlocking could not contribute to bond because the wires were smooth, effectively isolating Hoyer's effect as the only bond mechanism. The stress profile from some of Janney's tests are shown in Figure 2.7. Interestingly, the shape of the

stress profile is parabolic through the transfer zone. If mechanical interlocking in Figure 2.5 were eliminated from the transfer bond, the resulting stress profile through the transfer zone would be parabolic. Similar stress profiles were measured in a more recent test series. Nanni[60] tested the transfer length of Fiberglass Reinforced Plastic (FRP) strand. Even though these strands are not completely smooth (some aramid fibers are wrapped around the strand like column ties), twist restraint did not affect bond stresses. In these tests, the strain profile was distinctively parabolic, not linear. These and Janney's tests suggest that Hoyer's effect alone yields a parabolic transfer, but that this effect in combination with mechanical interlocking creates a uniform bond stress through the transfer zone.

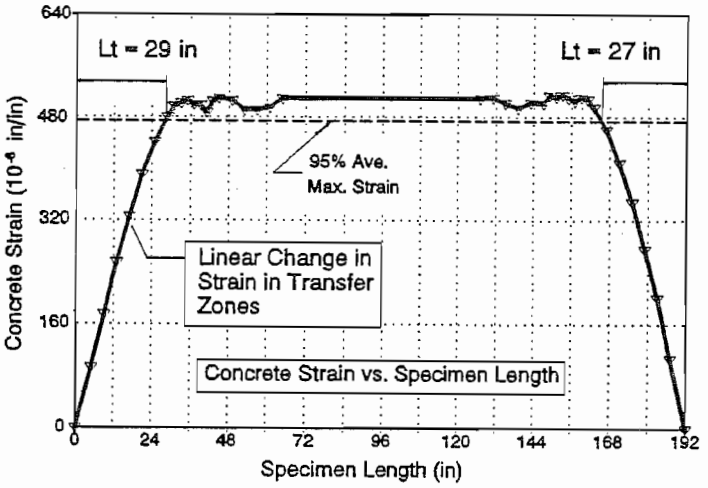

Figure 2.6 Typical Strain Profile From Transfer Length Specimen, FC350-2

2.4 Bond Mechanics, Resistance to External Load

When a pretensioned beam is loaded in flexure, tension in the strands must increase to resist the applied moments. As loads increase and concrete cracks, prestressing strands are required to carry even greater tension. Additional strand tension must be resisted by bond stresses. Bond stresses that resist external loads have generally been called "flexural bond stresses". This is somewhat of a misnomer because bond stresses are required to resist additional strand tension whether tension comes from flexural loads or shear loads. In the past, effects of shear have been largely ignored.

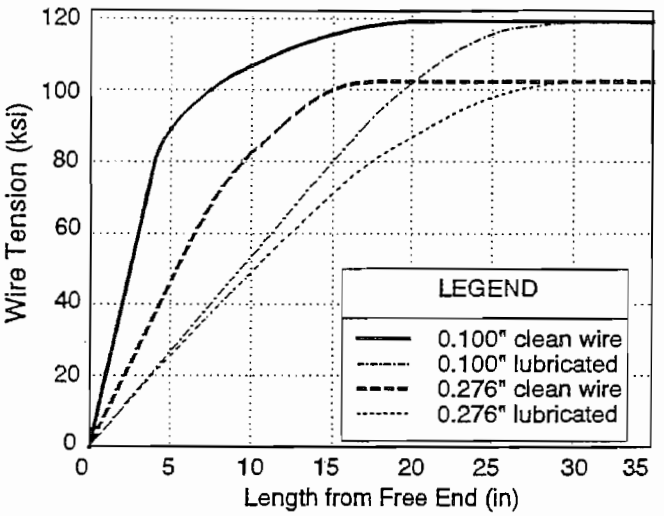

Figure 2.7 Stress Distributions From Clean and Lubricated Wire; Janney 1954

Figure 2.4 illustrates changes in steel stress along the length of a cracked beam. The illustration shows large increases in steel stress at the crack locations. Increases in steel stress must be developed by high bond stresses. Experimentation confirms the presence of very strong bonding forces.

Consider the common case of simply supported beam structures such as highway bridges. Pretensioned steel is placed in the bottom of the cross section to resist flexural moments from gravity loads. As moments increase, tension in the steel increases slightly, functioning as part of the composite section. When the concrete cracks, tension in the steel increases suddenly and abruptly. Large increases in strand tension must be matched by large increases in bond stresses adjacent to the crack as shown in Figure 2.4. These ideas were reported and confirmed by Hanson and Kaar[5].

When a crack forms in the concrete, the strands must slip for some finite distance on either side of the crack. The length of the slip is dependent on the value of the bond stresses adjacent to the crack and total strand slip must equal the width of the crack. The relative displacement, u_s, summed over the length of slip equals the crack width:

$$(\Sigma u_s \, dl)_{\text{both sides}} = \text{crack width.}$$

Mechanical Interlocking is developed upon cracking; the opening of the crack attempts to pull the strand through the concrete. Strand tension is resisted by the interlocking of the individual wires with the ridges in the concrete and is analogous to pull out of mild reinforcement.

When a crack forms in a pretensioned beam, tension in the steel increases dramatically at the crack location. That increase in strand tension must be restrained by interlocking bond stresses as illustrated in Figure 2.8. (Note that this example is taken from a region of constant moment, and that representations of stresses are qualitative.)

As bond stresses resist steel tension, they also induce tension into the concrete. As concrete tension increases between primary cracks, the tensile strength of concrete may be exceeded and a secondary crack may form. By investigating the relationships between concrete tension and crack spacing, an approximate value of the bond stresses that act to restrain the strand can be obtained.

The lower half of Figure 2.8 shows an assumed distribution of bond stresses. Bond stresses are highest immediately adjacent to the cracks and decrease with distance away from the cracks. Likewise, at the crack locations, concrete stress must be zero. When the secondary crack forms, the concrete tension must have reached the modulus of rupture, approximately $f_r = 7.5\sqrt{f'_c}$. Equilibrium between bond stress and concrete tension must be satisfied:

BondStress × *BondArea* = *ConcreteTension*

By assuming a distribution for bond stresses over length and by assuming an effective tensile area of concrete, the equilibrium equation can be solved to yield a value for the maximum bond stress derived from crack spacing. This procedure is outlined in Figure 2.9. Bond stresses are assumed to vary as a sine wave between crack locations. This distribution satisfies the boundary conditions and provides a continuous function between cracks. The area of concrete tension is taken as the area of the cross section immediately influenced by strands. More accurately the tension area would be taken as the height of the secondary cracks.

Equilibrium between bond stresses and concrete tension must be satisfied. Bond stresses can be integrated over the bonded length times the perimeter of all the strands, then set equal to concrete tension:

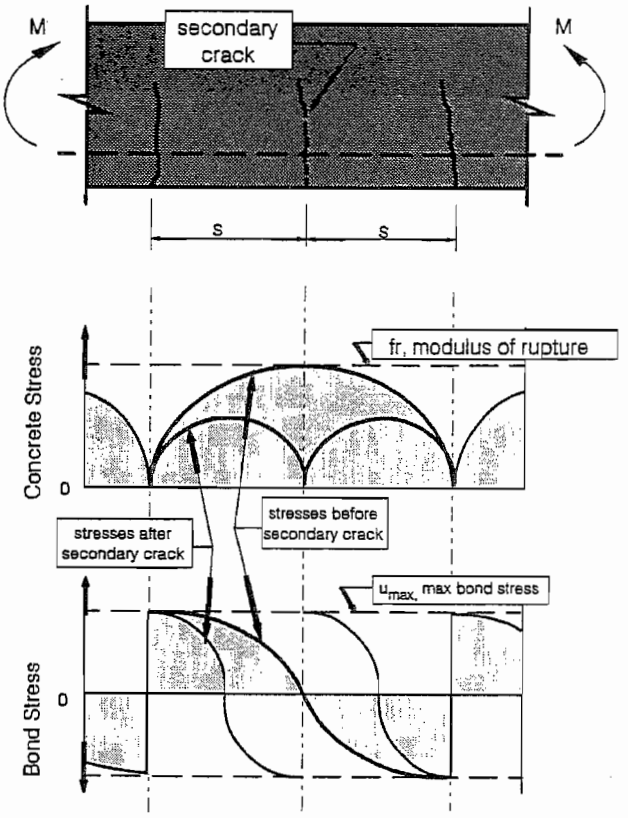

Figure 2.8 Idealization of Concrete Stresses and Bond Stresses at Cracks

$$NP_{ps}\int_0^S u_{max}\cos\frac{\pi}{2S}\,x\,dx = f_r A_c$$

where
- N = Number of strands,
- P_{ps} = Strand perimeter,
- S = Crack spacing,
- f_r = Modulus of rupture (581 psi for 6000 psi concrete),
- A_c = Area concrete that resists tension, and
- u_{max} = Maximum bond stress.

This equation is solved in Figure 2.9 for specimen DB850-F1A. The values of N, P_{ps}, S, f_r, and A_c are given in the figure. Solution of the equation yields a maximum bond stress, u_{max} equal to 617 psi, or 1.29 kips per linear inch of strand.

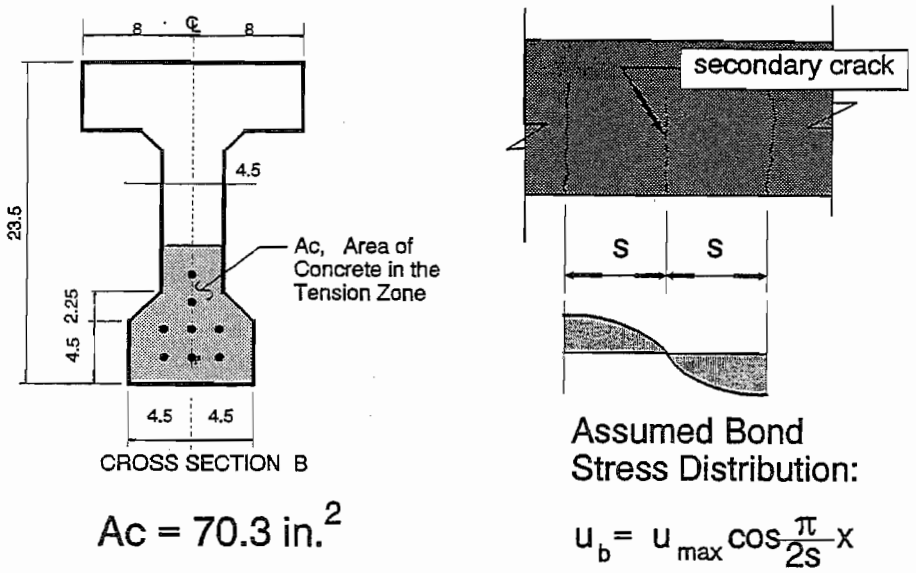

Bond Stress * Bond Area = Concrete Tension

$$N P_{ps} \int_0^s u_{max} \cos \frac{\pi}{2S} x \, dx < f_r Ac$$

P_{ps} = Strand Perimeter = 2.094 in

fr = Modulus of Rupture = 581 psi

From Test DB850-F1A:

Crack Spacing Average = 6.2 in.

U_{max} = 617 psi = 1.29 k / in

Figure 2.9 Calculation of Maximum Bond Stress From Average Crack Spacing

This procedure demonstrates that relatively large bond stresses may be developed from mechanical interlocking. In this case, bond stresses immediately adjacent to the crack were computed to be on the order of 1.29 kips per linear inch. One can see from this example that large increases in strand tension are resisted by similarly large increases in bond stresses, primarily due to mechanical interlocking in regions immediately adjacent to cracks in the concrete.

By contrast, current AASHTO and ACI code expressions assume that flexural bond stresses are approximately 300 pounds per linear inch, less than one fourth the value calculated from the procedure in Figure 2.9. This large difference is caused by assumptions made in the ACI code that assume bond stresses remain relatively constant over the flexural bond length. Instead, bond stresses vary considerably over length, caused by cracking in the concrete.

It should be noted that the preceding derivation was formulated based upon regions of constant moment. In those regions, tension in the strands remains theoretically constant at all crack locations. However, tension in the strand must decrease as distance from the crack increases, otherwise, no tension could be transferred back into the concrete. If strand tension were to remain constant throughout the constant moment region, then only one crack would form in this region, and the strands would behave as unbonded tendons. The presence of distributed cracking proves the presence of bond stresses in regions of flexural cracking.

In regions where moment varies over length, this theory is also useful to explain variations in strand stresses as well as bond stress distributions over length. Just as in regions of constant moment, strand stress must increase as the concrete cracks. (If strand stress does not increase as concrete cracks, strand slip would extend to the end of the beam and bond failure would be indicated.) As tension in the strand increases, it must be resisted by bond stresses on either side of the crack. In regions where moment varies, the bond stresses will not distribute antisymmetrically (as they do in regions of constant moment). Instead, the bond stresses in these regions must be qualitatively described as the summation of bond stresses as given by the constant moment derivation plus a bond stress component to account for changing moment. The bond stress distributions in these regions must closely resemble the bond stress distributions found in regions of constant moment, including bond stresses that act in opposing directions on either side of a crack.

2.5 Anatomy of Bond Failure

To understand the **Elements of Bond**, it is helpful to understand the mechanisms that can cause anchorage failure. Stated very simply, anchorage failure will occur when external loads require strand tension to increase within the transfer zone. Increases in strand tension cause the strand diameter to reduce slightly resulting in a loss of bond from Hoyer's effect. When bond from Hoyer's effect is destroyed, the strand also loses its twist restraint. As the strands are allowed to twist, bond stresses from mechanical interlocking begin to lose their effectiveness. The end result is complete bond failure and collapse of the pretensioned member.

A model for prediction of bond failure was given by Janney(1954)[1] and confirmed with tests on seven wire strand by Hanson and Kaar(1959)[5]. Hanson and Kaar performed tests that showed anchorage failure is caused by increasing strand tension within the transfer zone. They developed the theory that a wave of high bond stresses proceeds outward from the region of loading towards the anchorage zone. If this wave of high bond stress reaches the transfer zone, anchorage failure results.

Increases in strand tension are brought on by cracking of the concrete. Some increases in strand tension occur before cracking, however these increases are small compared to the increases that occur after cracking. (Bond stresses that are required by

action of an uncracked section may be resisted by adhesion between concrete and steel.) Until concrete cracks, strand tension remains relatively unchanged.

Hanson and Kaar never linked the importance of cracking with anchorage failure. To carry their theory one step further, one might say that if a crack propagates through the transfer zone of a strand, or immediately next to the transfer zone, then anchorage failure is imminent. This is the prediction model that is proven out by the extensive test program described in the remainder of this document. It is restated:

> **If cracks propagate through the anchorage zone of a strand, or immediately next to the transfer zone, then failure of the strand anchorage is imminent.**

This prediction model has successfully corroborated test results on pretensioned beams. It has proven accurate for beams with debonded strands as well as for beams where all of the strands are fully bonded to the ends of the member. This prediction model may prove to be very valuable in providing safe and economical pretensioned structures and improving the confidence of structural engineers designing and building in pretensioned products.

In the testing program, some exceptions to this rule have been noted, where the strands have slipped very small distances just prior to flexural failure, without anchorage failure. These special cases come about from an effort to test specimens bordering between anchorage failure and flexural failure.

2.6 Chapter Summary

In this chapter, the three elements of bond are described and discussed. These elements of bond include:

1) Adhesion,
2) Hoyer's Effect, and
3) Mechanical Interlocking.

The elements combine to anchor pretensioned strand in concrete. Transfer of the prestressing force to concrete is largely accomplished through the action of Hoyer's effect, with some contributions from mechanical interlocking. On the other hand, mechanical interlocking is largely responsible for developing strand tension required by externally applied loads. As demonstrated by example, mechanical interlocking can develop relatively large bond stresses.

For mechanical interlocking to be effective, the strand must not be allowed to twist through the concrete. If twist is unrestrained, mechanical interlocking will be ineffective. Twist restraint is provided by the strand anchorage zone, commonly called the transfer zone, where Hoyer's effect is the primary mechanism.

Adhesion makes little or no contribution to bond in any of the limit states. Strand slips occur at both the transfer of prestressing force and immediately preceding anchorage failure of the strands, without apparent reduction in anchorage capacity.

Lastly, anchorage failures can be linked directly to the incidence of cracking in the transfer zone of a pretensioned strand. As a crack propagates across the anchorage zone, strand tension must increase. Increases in strand tension cause the strand's diameter to reduce, decreasing the effectiveness of Hoyer's effect. The reduction in bond strength from Hoyer's effect allows the strand to be pulled through the concrete. Twist restraint is lost resulting in reduction of bond stresses from mechanical interlocking. These mechanisms eventually lead to bond failure.

CHAPTER 3
MEASUREMENT OF TRANSFER LENGTH ON PRETENSIONED CONCRETE SPECIMENS

3.1 Introduction

This chapter discusses transfer length, its definition, current code provisions, its importance and its use in current design practice. A large testing program was carried out measuring transfer length on a variety of specimens. The testing program is reviewed and summarized in this chapter. Other pertinent research is reviewed with special attention to its relationship to this research. Finally, the overall impact of this test program on design requirements and recommended transfer lengths is discussed.

3.1.1 Definition. Transfer length is the distance required to transfer the fully effective prestressing force from the strand to the concrete. The definition for transfer length is discussed in greater detail in Section 1.3.1 and illustrated in Figure 1.1. For beams that contain debonded strands (or blanketed strands), multiple transfer zones are present. In the case of debonded strands, bond begins where the debonding terminates. In all cases the effective prestress force is zero at the initial point of bond.

3.1.2 Current Code Provisions. Neither the ACI nor AASHTO codes provide a requirement for transfer length. However, both codes suggest a transfer length of 50 strand diameters[48,49] (ACI Section 11.4.4 and AASHTO Section 9.20.2.4). This recommendation is located in the shear provisions of the codes. The ACI Commentary to the Building Code, Section 12.9 on the development of prestressing reinforcement, provides a formula for transfer length based on the effective prestressing force and strand diameter. This formula is derived from the expression for development length. The suggested transfer length is given by:

$$L_t = \frac{f_{se}}{3} \times d_b$$

Figure 3.1 shows the ACI Commentary assumption for transfer and development of stress in the strand. Steel stress is plotted versus the "distance from the free end of strand". The transfer length is represented in the first and steeper portion of the curve.

Variations in steel stress are represented in two sections. In the second section, outside the transfer zone, the steel stress is shown to be increasing beyond f_{se}. This increase in stress results from applied load. The term, "flexural bond length," shown in Figure 3.1 is defined as the additional bond length required to develop the maximum stress in the strand. Summing the transfer length with the flexural bond length gives the AASHTO 9-32 and ACI 12.9.1 requirements for development length:

$$L_d = \frac{1}{3} f_{se} d_b + (f_{ps} - f_{se}) d_b = (f_{ps} - \frac{2}{3} f_{se}) d_b$$

Current codes for both the transfer length and development length are based on an assumed value for bond stresses. This value for bond stress is empirical and based on transfer length testing performed by Janney[7], Kaar, LaFraugh and Mass[8], Hanson and Kaar[5], and Kaar and Magura[11]. The assumed average bond stress in the ACI code is calculated by solving equilibrium on the strand:

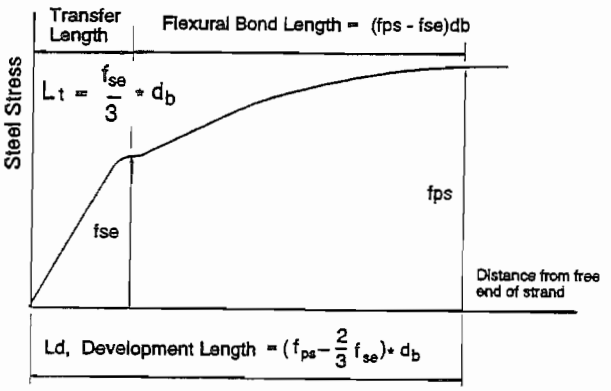

Figure 3.1 Steel Stress vs. Distance. ACI Commentary 12.9

$$L_t u_b P_{ps} = f_{se} A_{ps}$$

and substituting the ACI Commentary expression for transfer length:

$$L_t = \frac{f_{se}}{3} d_b = \frac{f_{se}\left(\frac{A_{ps}}{P_{ps}}\right)}{u_b}$$

where $A_{ps} = 7/36\ \pi d_b^2$ and $P_{ps} = 4/3\ \pi d_b$. Solving for the average bond stress, u_b:

$$u_b = 429 psi = 1000\ lbs/inch\ for\ 0.5\ inch\ strand.$$

Flexural bond is treated in the same manner, but its assumed average value is lower by a factor of three. Average flexural bond stresses were derived empirically from flexural bond tests[5]. Using a similar method to that described above, the empirical value for the average flexural bond stress, u_f:

$$u_f = 146\ psi$$

The average flexural bond stress is lower because flexural cracking occurs within the development length and disturbs bonding between steel and concrete, thereby reducing bond strength.

The ACI commentary acknowledges other factors that may affect transfer length such as low slump concrete and the strands' surface condition. Low slump concrete may cause longer transfer lengths if the concrete is not properly consolidated. Low slump concrete is typically used in the manufacture of precast hollow core slabs. Additionally, the importance of surface condition is recognized. Strands that are slightly rusted have been shown to have shorter transfer lengths[1,7,12,15]. Conversely, strands that are lubricated demonstrate

significantly longer transfer lengths. In fact, surface condition of the strand has been shown to be the single biggest variable in estimating the transfer length of pretensioned strand. As such, it should be the biggest concern for designs when transfer length is critical to structural performance.

Concrete strength is not reported as a factor in transfer length under current design codes. Tests performed by Kaar, LaFraugh and Mass[8] indicated that concrete strength did not affect the transfer length. However, more recent research suggests that concrete strengths do affect transfer lengths. These tests[44] indicate that stronger concrete results in shorter transfer lengths.

3.2 Transfer Length: Its Importance and Use

Transfer length is a structural requirement only as the transfer of prestressing force must be sufficient to maintain the integrity of the structure. Significant variations in transfer length will not normally control the design or performance of pretensioned structures. Therefore, when discussing the measurement of transfer length, the importance of transfer length should not be overestimated. Consequently, an exact value for transfer length may not be necessary to design and build safe concrete structures.

On the other hand, transfer length can significantly impact structural behavior in some design cases. The impact that the transfer length has on cracking loads is the most important factor in structural performance. At the point where bond begins, the effective prestress is zero. At the end of the transfer zone, the prestress is fully effective. In between, the effective prestress force is less than fully effective, which affects the elastic properties of the member. Most importantly, a pretensioned structure has less resistance to cracking within the transfer zone of the pretensioned strands. Therefore, it is important to understand the design cases where transfer length may be a controlling factor, and to adjust design procedures accordingly.

As stated earlier, AASHTO and ACI suggest a transfer length of 50 strand diameters. They also recommend the assumption that the effective prestress force varies linearly from zero at the free end of the strand to the maximum prestress force over the transfer length. These suggestions are provided so that the designer can calculate the concrete's contribution to shear strength, V_c, which is, in current design, either the web cracking shear (V_{cw}) or inclined cracking shear (V_{ci}).

One problem with this approach is that shear cracking can cause anchorage failure of the strand. Flexural tests demonstrate that when anchorage failure occurs, not only is the concrete contribution to shear strength lost, but the tension required from prestressing strand is also lost. A simple truss model for shear demonstrates that loss of the bottom tension chord will result in shear failure of the structure. Consequently, code provisions for shear may not preclude bond/shear failures in some pretensioned members. This behavior is discussed in greater detail in Chapter 4.

Tests performed in this research indicate that transfer length is very important in the prediction of development failure. In the ultimate limit state for highway girders, both the flexural capacity and the shear capacity are affected by the transfer length. These tests show that if a crack propagates across the transfer zone of a strand, then that strand can be expected to fail in bond. Because either flexural cracking or shear cracking can occur in the transfer zone of a strand, preventing or predicting both types of cracks is important to development of the strength of the member. Therefore, the transfer length is important to enable calculation of the cracking loads; and it is important to know the transfer lengths so that we can know which cracks will affect the development of the strand.

3.3 Transfer Length Tests

3.3.1 Variables. Transfer lengths were measured on a wide variety of research variables and on different sizes and types of cross sections. The variables included:

1) Number of strands (1, 3, 4, 5, 8, and 24),
2) Size of strand (0.5 inch and 0.6 inch),
3) Debonding (fully bonded or debonded strands),
4) Confining reinforcement (with or without),
5) Size and shape of the cross section.

The number of specimens and the variables included represent one of the largest bodies of transfer length data taken from a single research project.

3.3.2 Scope. Altogether, transfer lengths were measured on 65 specimens. Of these, 26 had a single strand, 18 had three strands, 6 were five strand specimens, 12 were scale model AASHTO-type beams with four, five, or eight strands, and finally; transfer lengths were also measured on three full sized Texas Type C girders with 24 strands each.

Figures 3.2, 3.3, 3.4, 3.5 and 3.6 show the various specimens in the testing program. Details of Texas Type "C" girders are shown in Figure 7.1. These figures also identify the characteristics of each specimen. Each specimen is identified by a numbering system containing a code to help identify the characteristics of that specimen. The specimen numbering system is explained by the example is given in Table 3.1. (SS specimens were the earliest single strand specimens. They are not included in Table 3.1, but are identical in design to the FC specimens.)

3.3.3 Instrumentation. Measurement of the transfer length was performed by measuring strains in the concrete and the steel along the length of the specimen. As described above, the prestress force is fully effective when there is no change in strain with respect to the length. By measuring the concrete strains and plotting the strains with respect to length, transfer length can be determined from the resulting strain profile. These data were collected:

1) Strains on the outside surface of the concrete,
2) Electrical strain gages on the strand,
3) End slips, and
4) Visual inspection.

Measurement of the strains on the outside surface of the concrete proved to be the most reliable data. Concrete strains were measured with detachable mechanical strain gages (DEMEC gages). The DEMEC gages are used in conjunction with DEMEC points. The DEMEC points, or targets, are stainless steel discs with a machined hole in the center. The DEMEC gage is received by the holes in the center of the targets, and the change in length is measured between targets.

Table 3.1

Key to the Specimen Numbering System

EXAMPLE: FCT360-4

F =	Fully Bonded (D = Some strands are debonded)
C =	Rectangular Cross Section
	(A = 22 inch deep AASHTO-type beam
	B = 23.5 inch deep AASHTO-type beam
	R = 16 inch deep Rectangular beam
	Z = Texas Type C girder)
T =	Transverse Reinforcement is included (if transverse reinforcement is not included, T does not appear)
3 =	Number of Prestressing Strands
6 =	0.6 inch Diameter Strands (5 = 0.5 inch Diameter Strands)
0 =	2 inch Strand Spacing (2 = 2.25 inch Strand Spacing)
4 =	The number of the specimen in a particular series

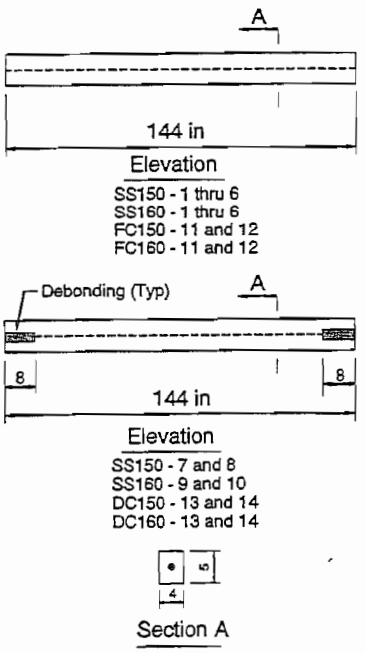

Figure 3.2 Details of Single Strand Specimens

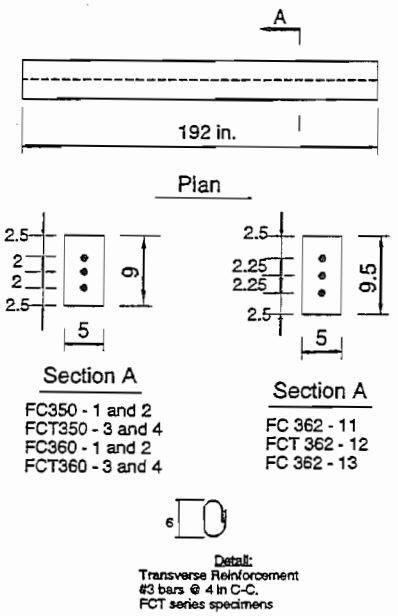

Figure 3.3 Details of Fully Bonded, Three Strand Specimens

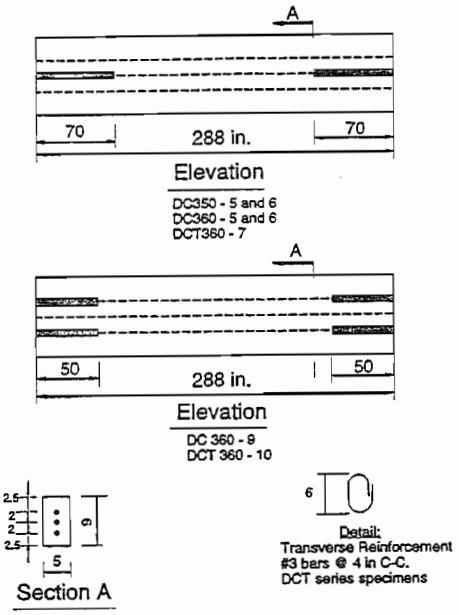

Figure 3.4 Details of Debonded, Three Strand Specimens

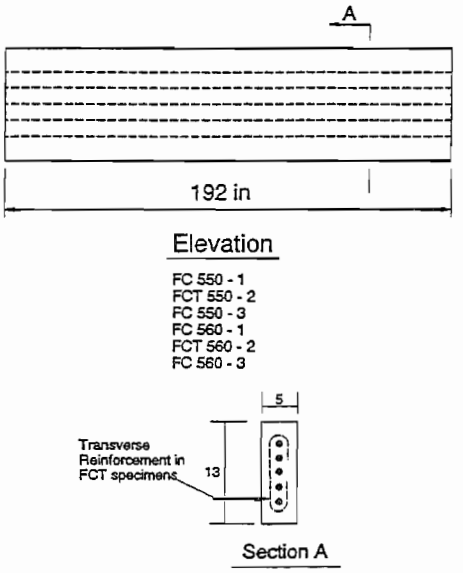

Figure 3.5 Details of Five Strand Transfer Length Specimens

The DEMEC gage and targets are shown in Figure 3.7. The gages used in this research were manufactured by Hayes Manufacturing Company in England. The "DEMEC gages" proved to be reasonably accurate, within 20 to 30 microstrains (± 20 to $\pm 30 \times 10^{-6}$ in/in). For the rectangular specimens, DEMEC targets were located at mid-height, which also corresponded to the centroid of the prestressing steel. In the AASHTO-type specimens (FA550, FA460 and DB850's) and on the Texas Type "C" specimens, DEMEC gages were located approximately 1.5 inches up from the bottom flanges.

Gage length of the DEMEC gage was 200 mm, which is approximately an eight inch gage length. For some of the earlier tests, a two inch gage was used. However, results with the two inch gage proved unsatisfactory. The absolute error of the system appears

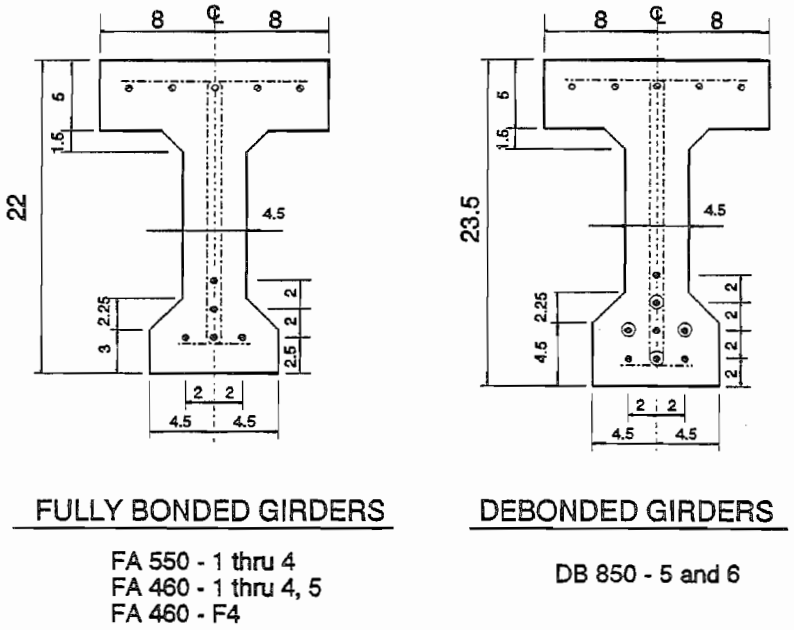

Figure 3.6 AASHTO-Type Girder Cross Sections

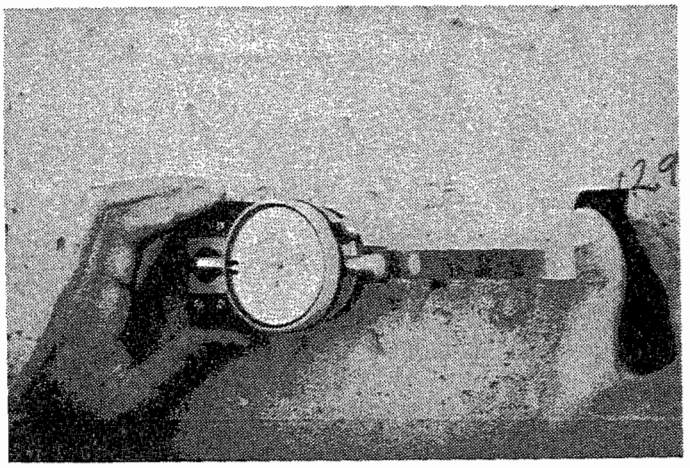

Figure 3.7 Photograph of DEMEC Gage; Measurement of Concrete Strains

to be nearly the same for all lengths of DEMEC gages, therefore the relative error is less for longer gages compared to shorter gages.

Electrical Resistance Strain Gages (ERSG's) were mounted on the prestressing strands before concrete was cast. Ideally, the change in strain over the strand's length would measure transfer length. However, the ERSG's proved to be unreliable for several reasons. First of all, each wire of the seven wire strand experiences a slightly different strain condition[44]. As the strand is detensioned and relative displacements between strand and concrete take place, relative displacements between wires is also probable. Secondly, a large percentage of the gages in the transfer zone are destroyed at transfer. Either the changes in strain exceeded the capacity of the ERSG or the relative displacement between the steel and concrete destroyed the gage. Thirdly, the ERSG's presence on the strand interfered with bond, at least locally. The adverse effect of too many ERSG's mounted on a strand would prejudice the test result. Lastly, the gages are difficult to protect during casting. They are susceptible to damage from vibrators or damage by moisture while casting the concrete. All of these factors compound to render ERSG's ineffective in measuring transfer length of pretensioned strand.

End slips were also measured. In the early tests on "SS" specimens, a dial gage was clamped to the strand at the end of the specimen to measure the amount of strand that slipped into the concrete upon release of the pretensioning force. However, release of the strands proved to be too violent and several dial gages were damaged. Also, the results showed large amounts of scatter. These results were discounted as unreliable. End slips were then measured by placing a tape marker on the strand, and measuring the distance the tape slipped toward the concrete upon release of the strand. Measurements with this method are accurate to about 0.03 inches (1/32 inches). End slips and their relation to transfer lengths are discussed in Section 4.6.4.

3.3.4 Test Procedure. Test procedures were chosen to mimic actual pretensioned concrete plant construction as much as possible. Accordingly, procedures for the fabrication

of the specimens followed standards for plant construction. The procedures for fabrication and testing can be summarized by a few simple steps:

1) Stress the prestressing steel
2) Place the mild reinforcement
3) Set the forms
4) Cast the concrete
5) Cure the concrete (usually two days)
6) Remove the formwork
7) Take initial measurements
8) Detension the strands (usually by flame cutting)
9) Take final measurements

The difference between initial and final measurements yielded the concrete strains which are plotted along the length of each specimen. From these strain plots the transfer length is established.

Strands were tensioned using a hydraulic actuator and an electric pump. Hydraulic pressure was continuously monitored as a measure of strand tension. Strands were initially tensioned to approximately 1600 pounds of tension so that the geometry of the strand would be established relative to the specimens. Electrical resistance gages were then attached to the strands. Strands were then tensioned incrementally until the initial prestress was reached. Each of the strands was tensioned to 75% f_{pu}, or 202.5 KSI. Strand elongation was also measured for all strands as a check against the hydraulic pressure. Some small variations in initial strand tension, on the order of $\pm$5 KSI, were noted. However, differences in strand tension do not significantly impact the test results. The total error of 5 KSI represents only $2^1/_2$% error in the total tensile force. The scatter in the data exceeds the possible resulting differences from variance in pretension.

After strands were tensioned, mild reinforcing was set in place. Debonding material, if required, was applied to the strands. Concrete was cast into plywood forms. During casting, care was taken to insure proper consolidation of the concrete by vibrating.

Concrete curing was performed by covering the specimens with plastic sheeting. The plastic remained on the concrete until form removal, just before initial DEMEC readings were taken and prestressing was detensioned. The curing period for most specimens was 48 hours. No curing was performed after form removal.

In the pretensioned industry, strands are usually detensioned within 18 to 24 hours of casting the concrete. These quick turnarounds are driven by an extremely competitive marketplace. Therefore, the most important concrete parameter is the strength at release. Conversely, concrete strengths at 28 days are not usually critical. In this project, release was specified after two days. Other factors such as student work schedules precluded a one day release of prestressing. In almost every case, release was performed on the second day,

approximately 48 hours after casting. In only two cases, release was performed on the third day because of very low concrete strength. Concrete strengths at release are given in Table 3.12. Concrete mix proportions are given in Table 4.1.

Before release, initial measurements were taken. The initial measurements included electrical resistance strain gages (ERSG's), initial DEMEC readings on the external faces of the concrete, and measurement of the initial end slip reading. After release, these measurements were repeated. Strains in the concrete and steel are given by the difference between initial and final readings from the DEMEC data. End slip is also given by the difference between the initial and final readings.

Measurement of concrete strains with the DEMEC gages proved to be an effective and reliable way to measure transfer length. These measurements were taken on the outside surface of the concrete along both sides of the specimen. By taking strain readings from both sides of the specimen, effects from eccentric prestressing were alleviated. Also, by averaging strains from the two sides, a more accurate overall result can be expected. Over many trials, the DEMEC gages proved to be very accurate compared to any other data that was available. The accuracy of the DEMEC gage reading proved to be about $\pm 25 \times 10^{-6}$ in/in. This level of accuracy is borne out over many different tests with many different researchers. Even so, the error represents 5% to 10% of the measured strains.

Two different cutting methods were used to detension the strands. In the first method, the strands were flame cut at full tension in order to recreate a worst case for release of the prestressed force. Several past researchers had noted that transfer lengths on the "cut" end were much longer than transfer lengths on the "dead" end[8,11,39]. However, when the first single strand specimens were flame cut at full tension, moderate damage was inflicted on some of the specimens. Additionally, the data showed considerable scatter, raising doubts about the procedure. This procedure was used on the original 18 single strand specimens. These specimens have been relabeled as "SS" in order to distinguish them from other specimens.

With the testing of the multiple strand specimens, a slight variation was adopted in the detensioning procedure. Instead of flame cutting at full tension, the strands were detensioned gradually to about 70% of their full pretension, and then flame cut. This method resulted in transfer lengths that matched more closely the transfer lengths that were measured on larger specimens where strands were cut at 100% tension.

Justification for the moderated method is that the energy released from cutting a strand represents a larger shock to a small cross section than to a large cross section. A large cross section, usually with multiple strands, has a larger mass to absorb and distribute the energy at release, plus it contains additional reinforcement from the other strands. Furthermore, strands must be flame cut one at a time, so as each additional strand is cut the cross section enjoys greater precompression. The specimens that were detensioned using this method are the FC3, DC3 and FC5 series.

The larger cross sections, including the AASHTO-type beams and the Texas Type C girders, were flame cut at 100% tension. The specimens that were flame cut at 100% tension include the FA550, FA460, FR350, FR360, and DZ/FZ2450 series specimens. The data indicate that transfer lengths measured on the small specimens with the moderated flame cutting method correlate closely with the larger specimens cut at full tension.

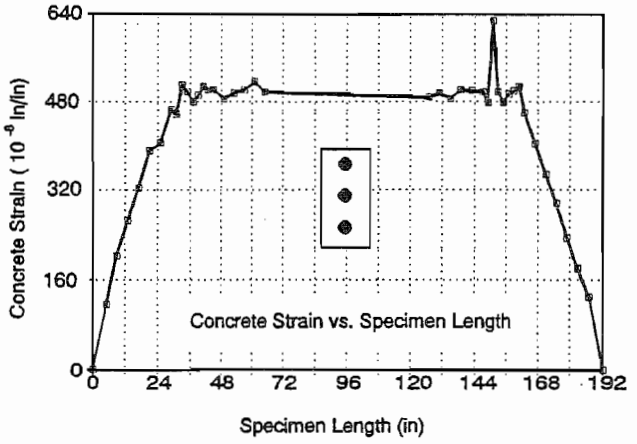

Figure 3.8 Strain Profile of "Bare" Strains, FCT350-3

3.4 Method of Data Analysis

3.4.1 Measurement Technique and Data Smoothing. The strain profile taken from FCT350-3 is illustrated in Figure 3.8. Measured concrete strains are plotted versus the length of the specimen. The typical strain increase from the ends of the specimen demonstrates the transfer of prestress from the steel to the concrete.

Strain measurements were taken with the DEMEC gages. Concrete strain at transfer was determined from the numerical difference between the initial reading and the final reading. In order to minimize errors, a specific procedure for obtaining measurements was adopted. All DEMEC readings were taken by teams of two persons. Each person would take measurements independently of the other. Once the measurements were taken,

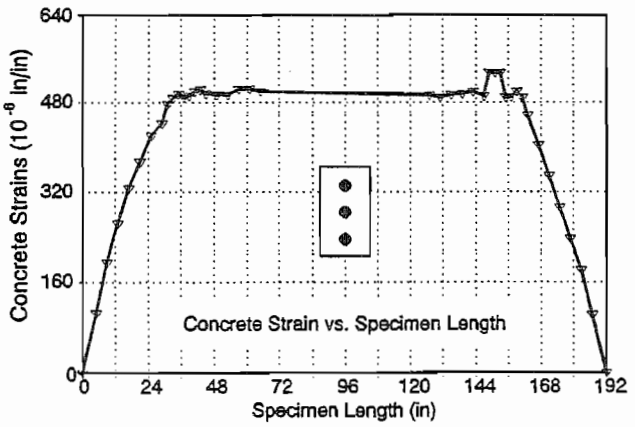

Figure 3.9 Strain Profile of "Smoothed" Strains, FCT350-3

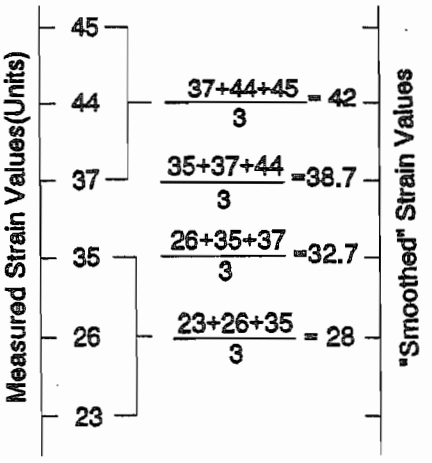

Figure 3.10 Illustration of "Smoothing"

readings were compared. If the readings from the two individuals differed by greater than 0.000032 in/in, measurements were retaken until the difference was resolved. Strain measurements from the two individuals were then averaged together with the average measurements from the other side of the specimen. In effect, the "bare" strain measurements are actually the average of four sets of readings, collected by two individuals from both sides of the specimens.

In order to further reduce anomalies in the data, the "bare" strain profiles were smoothed by averaging the data over three gage lengths. Figure 3.9 illustrates the same strain profile of Figure 3.8, but with smoothed values. The smoothing technique is illustrated numerically in Figure 3.10. The smoothing technique can be summarized by the following equation:

$$(STRAIN)_X = \frac{(STRAIN)_{X-1}+(STRAIN)_X+(STRAIN)_{X+1}}{3}$$

3.4.2 Determination of the Transfer Length: The 95% Average Maximum Strain Method. Transfer lengths for each specimen were determined from evaluation of the strain profiles. The method used is called the "95% Average Maximum Strain" method and was conceived from this research project. Its execution is very simple:

1) Plot the "smoothed" strain profile.

2) Determine the "Average Maximum Strain" for the specimen by computing the numerical average of all the strains contained within the strain plateau of the fully effective prestress force.

3) Take 95% of the "Average Maximum Strain" and construct a line corresponding to this value.

4) Transfer length is determined by the intersection of the 95% line with the "smoothed" strain profile.

This procedure is illustrated in Figure 3.11 for test specimen FC350-2. The average maximum strain is the average of all the strains contained on or near the plateau of the fully effective prestress force. It may include all of the points above the 95% line, but generally, only the points clearly upon the strain plateau are included in the average. This method results in a value that is relatively free from arbitrary interpretation, which is the major advantage from using this method. Current variations in analysis methods leaves data open to arbitrary interpretation. Another advantage of this method is that the value of the "Average Maximum Strain" will not change significantly if one or two data points are either included or excluded from the average in error.

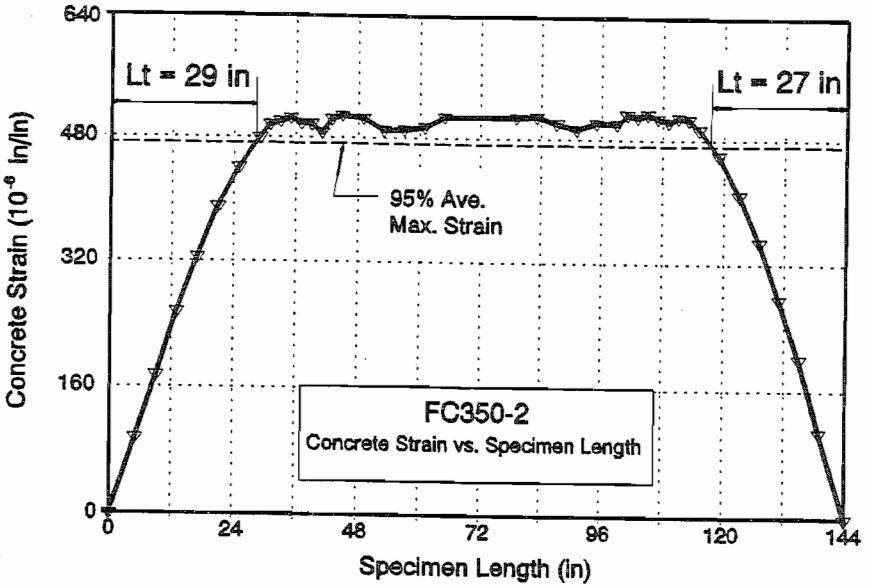

Figure 3.11 95% Average Maximum Strain Method to Determine Measured Transfer Length

On the other hand, this method has drawn criticism because it does not use the fully effective concrete strain to determine the transfer length. Instead, the transfer length is determined by the intersection of the concrete strain curve with a flat line drawn at 95% of the average maximum strain. Precedent does exist for using 95% of the maximum stress or strain. Hanson and Kaar used 95% of the maximum strain in their transfer length study[5].

The 95% Average Maximum Strain method represents an accurate value for determining the transfer length. If, on one hand, the reported transfer lengths are too short because only 95% of the maximum strain is used to define transfer length, then it must also be stated that smoothing effects inherent in this method cause the measured transfer length to be artificially lengthened. Smoothing effects are discussed in the next section.

3.4.3 Effects of Averaging. Smoothing of the data actually comes from two different sources; the smoothing technique described in Section 3.4.2, and a second source; smoothing introduced by the DEMEC gage. Figure 3.12 demonstrates both effects. In truth, the DEMEC gage measures an average strain over the length of the gage. As the drawing shows, this has a rounding effect on the strains at the transfer length. In the figure, an idealized strain profile is assumed. The assumed strain profile is bilinear with a sharp break at the transfer length. On the other hand, the "bare" strains measured with the DEMEC gage indicate a slight rounding of the strain profile at the transfer length. As the strains are further smoothed by the averaging technique, the strain profile becomes even more rounded.

For the idealized strain profile, the prestress force is fully effective 24 inches from the free end of the strand. On the other hand, if one considers only the "bare" data, the

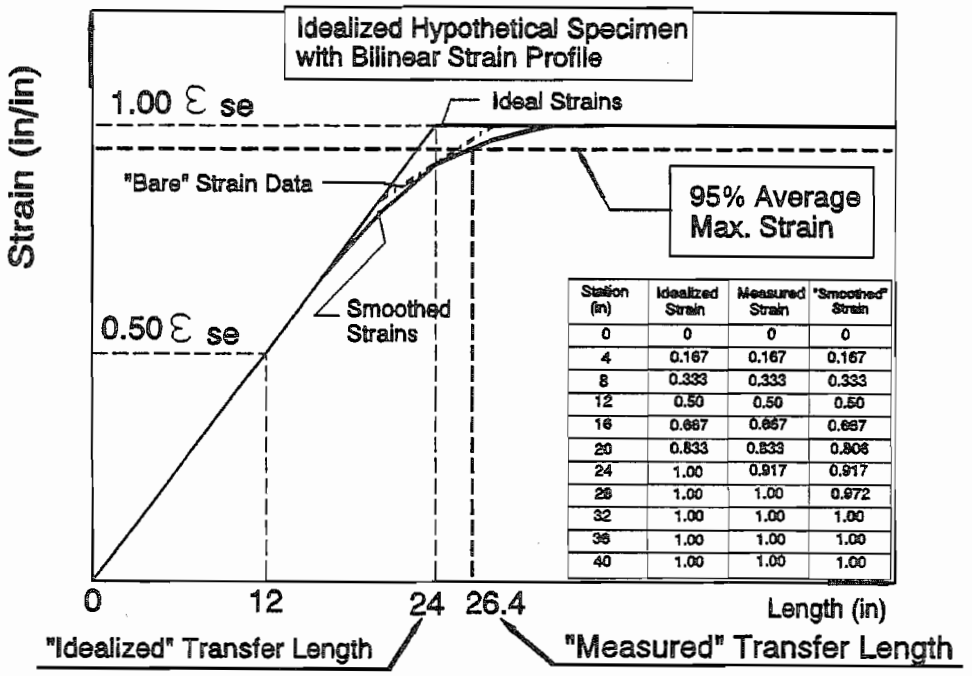

Figure 3.12 Effects of Smoothing on Measured Transfer Length

transfer length would be 28 inches. Furthermore, if transfer length is determined from 100% strain of the "smoothed" strain profile, the transfer length would be 32 inches, another 33% longer than the "idealized" transfer length. This demonstrates that the smoothed curves, using the procedure of Section 3.4.2, give a conservative result. In fact, this is always true because the strain profiles always have decreasing slope in the close vicinity of the transfer length.

Now consider the values of transfer length obtained by the 95% Average Maximum Strain Method. The smoothed curve intersects the 95% Average Maximum Strain line at a length equal to 26.4 inches (Figure 3.12). The result is conservative compared to the 24 inch idealized transfer length. One would need to use a 90% Average Maximum Strain to obtain a value approximately equal to the idealized transfer length. Therefore, for this idealized strain profile, the 95% Average Maximum Strain Method is conservative by about 10%.

One must also consider the effects that averaging has on the actual transfer length specimens. Variation in real strain through the transfer zone is probably not bilinear as in the preceding example. An example is shown in Figure 3.13 of a strain profile from transfer length tests performed by the Florida Department of Transportation (FDOT). Strain measurements were taken from ERSG's mounted to the outside face of the concrete and exhibit more of a parabolic shape as the strain profile nears the maximum strain plateau.

Given a parabolic strain profile, averaging or smoothing the data does not affect the resulting transfer length measurement as dramatically as if the strain profile were bilinear, however, smoothing the data will still result in a conservative value.

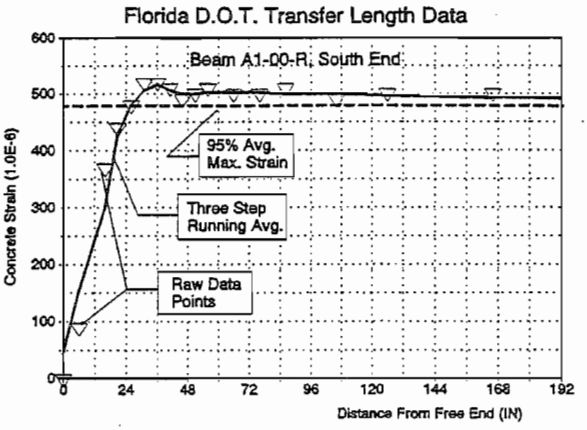

Figure 3.13 Strain Profile from FDOT Type II Girder

In a parabolic strain profile, the strains approach the plateau asymptotically. In theory, an exact value for the transfer length of a parabolic strain profile does not exist. The intersection of the strain profile with a plateau is almost impossible to define. Furthermore, attempting to define that intersection would introduce the possibility of large errors into the procedure. On the other hand, the 95% Average Maximum Strain Method forms a definite intersection with the strain profile, resulting in transfer lengths that are both reliable and accurate.

3.5 Measured Transfer Lengths

Measured transfer lengths are reported in Tables 3.2 through 3.10. All reported measured transfer lengths were obtained with the 95% Average Maximum Strain method. Transfer lengths were measured immediately after release. Tables 3.2 and 3.4 report the measured transfer length for 0.5 inch strands, fully bonded from the end of the specimen. Table 3.2 reports the measured transfer lengths for specimens designated "SS." This designation refers to the original 18 single strand specimens where strands were flame cut at 100% tension.

TABLE 3.2

MEASURED TRANSFER LENGTHS "SS" SINGLE STRAND SPECIMENS 0.5 INCH STRANDS

SPECIMEN	CUT END	DEAD END
SS150-1	-	-
SS150-2	-	-
SS150-3	28	25
SS150-4	28	24
SS150-5	46	30
SS150-6	52	35
AVERAGE	**38.5**	**28.5**

The transfer length of specimens SS150-1 and SS150-2 exceeded half the length of the specimen. SS150-1 had poor concrete strength.

Table 3.4 reports data for all other 0.5 inch strands that were fully bonded. These include all specimens that were detensioned to 70% of pretensioning stress before the strands were flame cut. Table 3.4 also includes data from the FA550 and DB850 AASHTO-type beams whose strands were flame cut at 100% tension. For specimens labeled "DC", these data refer to measured transfer lengths on the fully bonded strands, even though the specimen may have contained one or more debonded strands.

Measured transfer lengths for 0.6 inch strands are reported in Tables 3.3, 3.5, and 3.7. Again, the "SS" designation in Table 3.3 refers to single strand specimens that were cut at full tension. Transfer lengths for fully bonded 0.6 inch strands are reported in Table 3.5. Transfer lengths reported in Table 3.5 include specimens where the strands were detensioned to 70% of their pretensioning before they were flame cut. Table 3.5 also includes the transfer lengths for specimens in the FA460 AASHTO-type beam series that were flame cut at 100% tension.

Tables 3.6 and 3.7 report the transfer lengths measured for strands that were debonded, or blanketed. These strands were debonded a distance of 8 inches in the DC150 and DC160 series, 70 inches or 50 inches in the DC350 or DC360 series, and 78 inches in the DB850 series.

TABLE 3.3

MEASURED TRANSFER LENGTHS "SS" SINGLE STRAND SPECIMENS 0.6 INCH DIAMETER STRANDS

SPECIMEN	CUT END	DEAD END
SS160-1	49	-[1]
SS160-2	-[1]	44
SS160-3	-[1]	48
SS160-4	56	45
SS160-5	52	32
SS160-6	30	38
SS160-7	37	36
SS160-8	28	32
AVERAGE	**42.0**	**38.5**

1. These specimens were damaged at prestress release. Transfer length measurements were not possible.

Figure 3.14 illustrates the strain profile for specimen FCT350-3, which is typical for a fully bonded specimen with 0.5 inch strands. Figure 3.15 is the strain profile for specimen

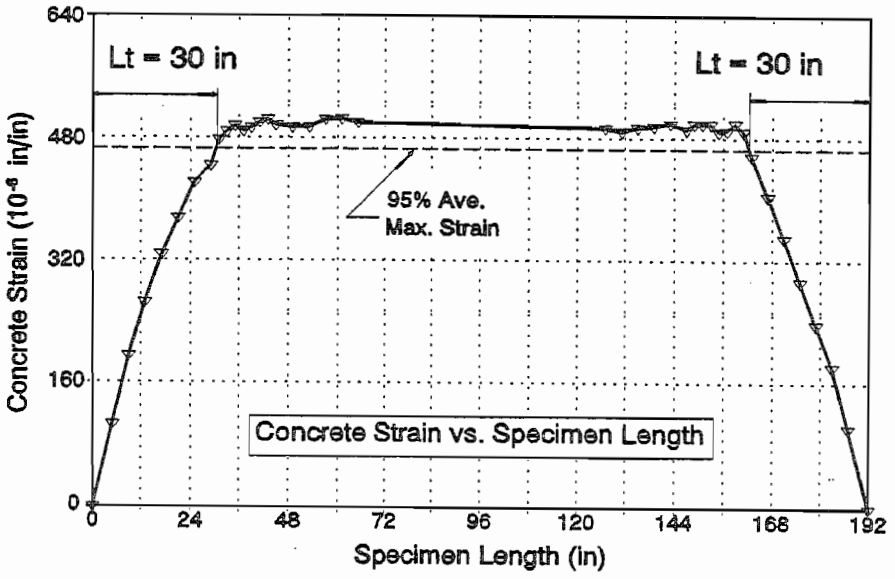

Figure 3.14 FCT350-3, Transfer Length

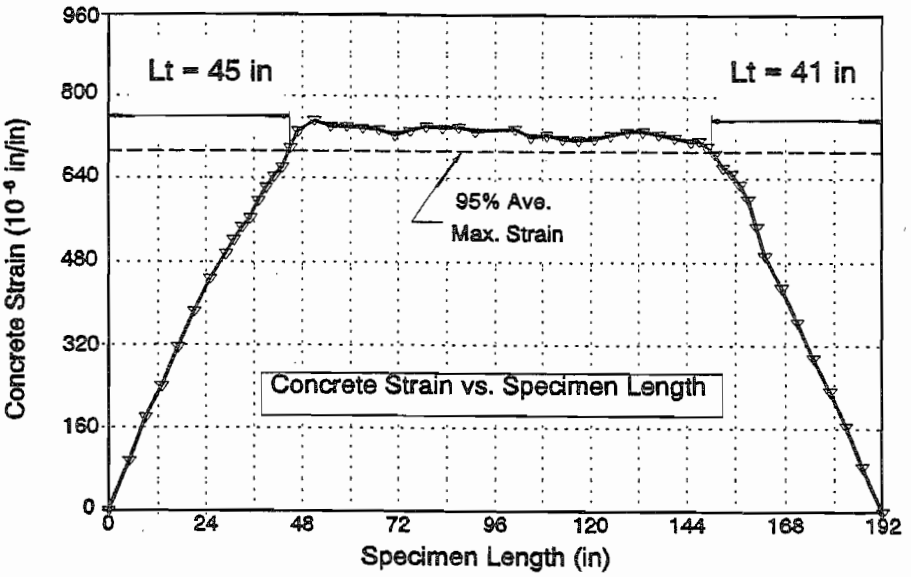

Figure 3.15 FC362-13, Transfer Length

FC362-13, which is typical for a fully bonded specimen with 0.6 inch strands. For specimens with fully bonded strands, the transfer length at each end of the specimen is evidenced by the ascending and descending portions of the strain profile. Strain profiles for all of the specimens are included in Appendix A.

Figure 3.16 is a strain profile taken from a specimen that contained three strands, one of which was debonded for a distance of 70 inches. Several significant observations can be made from this figure. An intermediate plateau occurs between the transfer zone of the

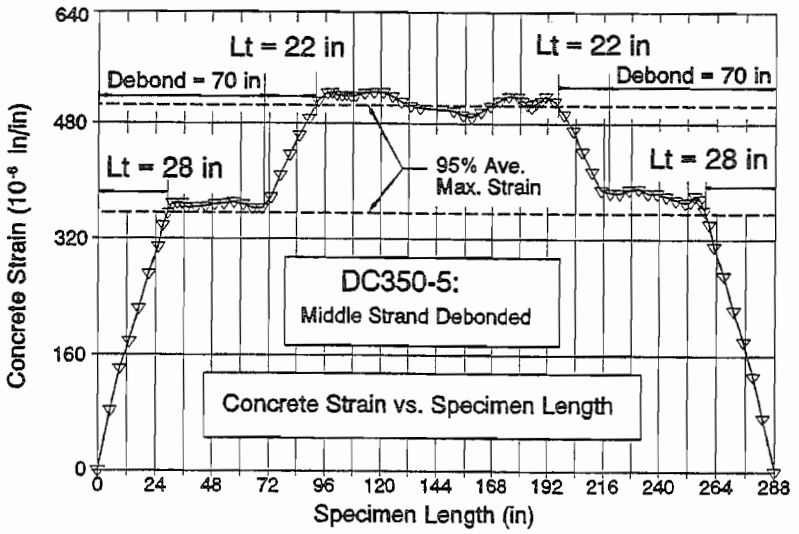

Figure 3.16 Strain Profile for Specimen DC350-5, With Debonded Strand

two fully bonded strands and the transfer zone of the single debonded strand. This clearly demonstrates that blanketing effectively eliminated bond between the prestressing strand and the concrete. Lastly, note the differences in slope for the strain profile between the transfer zone of the two fully bonded strands and the transfer zone for the single debonded strand. The slope of the strain profile at the beam's end transfer zone is approximately twice that of the intermediate transfer zone.

TABLE 3.4

MEASURED TRANSFER LENGTHS
0.5 INCH DIAMETER, FULLY BONDED STRANDS

SPECIMEN	NORTH END	SOUTH END
FC150-11	29	35
FC150-12	31	31
FC350-1	35	28
FC350-2	29	27
FCT350-3	30	30
FCT350-4	29	31
DC350-5	28	28
DC350-6	30	33
FC550-1[a]	38	37
FCT550-2[a]	37	37
FC550-3[a]	33	47
FA550-1[b]	17	17
FA550-2[b]	25	21
FA550-3[b]	20	17
FA550-4[b]	21	21
DB850-5[b]	31	43
DB850-6[b]	41	33
AVERAGE	29.6	30.4
Standard Deviation = 7.2 inches		

a. Low concrete strengths, f'_c = 3853. Omitted from average.
b. AASHTO-type beams

3.6 Measurement of Transfer Length on Texas Type C Girders

Transfer lengths were measured on three full sized highway girders. These girders were tested primarily in flexure under repeated loads as the final part of this research project studying the influence on debonded strands. However, measurement of transfer lengths on actual field constructed specimens is important to understanding results from smaller specimens, so transfer length data was collected. Results from these tests are somewhat surprising in that they do not appear to continue the previous trend that larger cross sections enjoy shorter transfer lengths. Instead, they may confirm suspicions that transfer length is largely dependent on surface condition and/or other variables that contribut to large degrees of variability. The resulting transfer lengths reflect that variation.

Transfer length strain profiles for the three beams are shown in Figures 3.17, 3.18, and 3.19. Girders DZ2450-1 and DZ2450-2 contain some debonded strand (8 out of 24), so the strain profile will not exhibit a true plateau. Instead of using the 95% Average Maximum Strain method, the transfer lengths were obtained by visually inspecting the strain profile. All the strands in FZ2450-3 are fully bonded, however, a strain gradient must exist because strands are draped (6 out of 24). Qualitatively, the effects of draping alter the strain profile corresponding to the effects of a changing eccentricity. In these beams, the effects are negligible. The transfer lengths are shown in the figures.

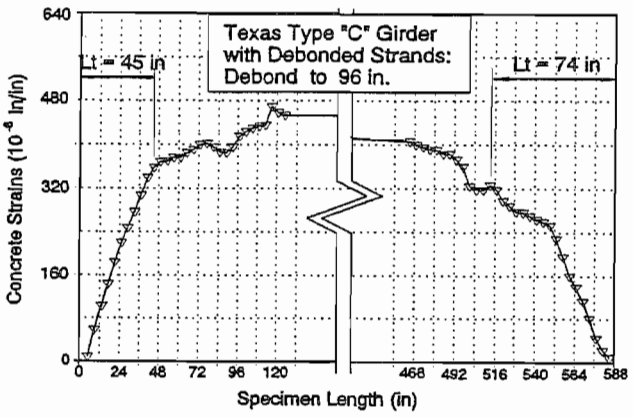

Figure 3.17 Strain Profile for DZ2450-1

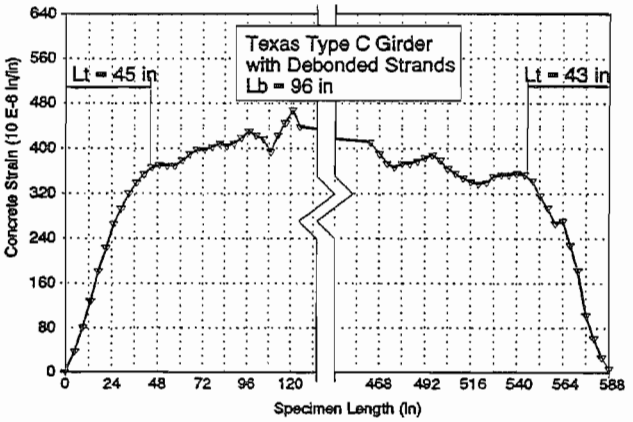

Figure 3.18 Strain Profile for DZ2450-2

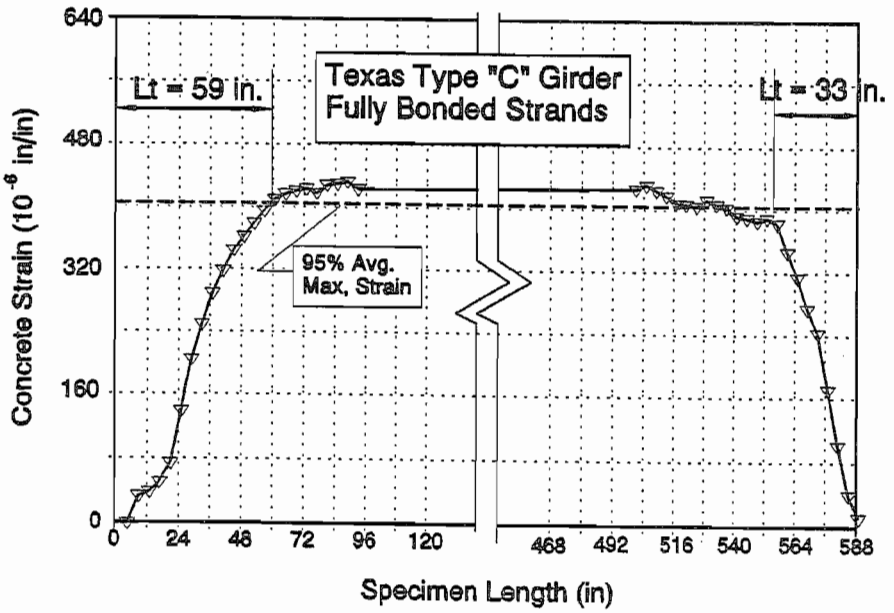

Figure 3.19 Strain Profile for FZ2450-3

TABLE 3.5

MEASURED TRANSFER LENGTHS
0.6 INCH DIAMETER, FULLY BONDED STRANDS

SPECIMEN	NORTH END	SOUTH END
FC160-11[a]	-	-
FC160-12[a]	51	41
FC360-1	39	44
FC360-2	37	51
FCT360-3	43	58
FCT360-4	51	42
FC362-11	46	46
FCT362-12	44	43
FC362-13	45	41
DC360-5	41	33
DC360-6	35	43
DCT360-7	-	-
DC360-9	-	-
DC360-10	-	-
FC560-1[b]	45	51
FCT560-2[b]	47	55
FC560-3[b]	48	48
FA460-1[c]	24	44
FA460-2[c]	33	34
FA460-3[c]	32	33
FA460-F4[c]	25	30
FA460-5[c]	33	37
FA460-6[c]	33	30
AVERAGE	**39.6**	**42.3**
Standard Deviation = 8.0 inches		

a. Low concrete strength, f'_c = 3853 psi.
b. Concrete stress exdeeded the allowable stress at transfer: f_{ce} = 3090 > 0.6 f'_{ci} = 2690.
c. AASHTO-type beams

It is possible that differences in test methods are responsible for the apparent discrepancies. Transfer lengths were measured using the same procedure as before. DEMEC gage readings were taken before detensioning and again after detensioning. The strands were flame cut at 100% tension, however, the beams were not visibly affected by strand cutting. One difference in procedure is that measurements were taken only on one side of the beams. It is possible that measurements could be affected by slight eccentricities in prestressing. Also, measurements were taken outside at the pretensioning plant. Differences in ambient temperatures could have affected the results. Nevertheless, it is difficult to fault the test procedure as significantly different than before.

Instead, these measurements should serve as evidence that wide variation exists in transfer length from one specimen to another. This possibility of variation should be reflected in the design and fabrication of pretensioned structures. For elements whose transfer length may be critical, special treatment of the strand may be needed to provide reliability of anchorage.

The Florida Department of Transportation tested transfer lengths of AASHTO Type II girders in a pretensioning plant[55,59]. These specimens did not show longer than normal transfer lengths. Either contamination of the strands' surface or difficulties in measurement could cause these longer field measurements. In light of the procedure to oil forms, it seems most likely that the strand surfaces became contaminated with form oil.

TABLE 3.6

MEASURED TRANSFER LENGTHS, INCHES
0.5 INCH DIAMETER, DEBONDED STRANDS

SPECIMEN	NORTH END	SOUTH END
DC150-13	24 inches	25 inches
DC150-14	28 inches	20 inches
DC350-5	22 inches	22 inches
DC350-6	30 inches	29 inches
DB850-5[a]	39 inches	35 inches
DB850-6[a]	31 inches	35 inches
AVERAGE	**29.0 inches**	**27.7 inches**
Average = 28.3 inches Standard Deviation = 6.0 inches		

a. AASHTO-type beams

TABLE 3.7

MEASURED TRANSFER LENGTHS, INCHES
0.6 INCH DIAMETER, DEBONDED STRANDS

SPECIMEN	NORTH END	SOUTH END
DC160-13[a]	-	-
DC160-14[a]	-	-
DC360-5	32 inches	20 inches
DC360-6	25 inches	28 inches
DCT360-7	27 inches	29 inches
DC360-9	31 inches	26 inches
DCT360-10	45 inches	55 inches
AVERAGE	**32.0 inches**	**31.6 inches**
Average = 31.8 inches Standard Deviation = 10.4 inches		

a. Low concrete strength, f'_c = 3853 psi. Omitted from average.

TABLE 3.8

COMPARISON OF TRANSFER LENGTHS AND STRAND GEOMETRY: 0.5 INCH VS. 0.6 INCH

STRAND PROPERTIES		
	0.5 INCH STRAND	**0.6 INCH STRAND**
AREA	0.153 inch^2	0.217 inch^2
PERIMETER	2.09 inches	2.51 inches
AVERAGE TRANSFER LENGTHS		
TEST SERIES	**0.5 INCH STRAND (No. Ends Tested)**	**0.6 INCH STRAND (No. Ends Tested)**
FC1	31.5 (4)	46.0[a] (2)
FC3	29.8 (12)	43.4 (18)
FC5	38.2[a] (6)	49.0[b] (6)
FA550 & DB850 /FA460	25.6 (12)	32.3 (12)
AVERAGE	**30.0 inches**	**40.9 inches**
STD. DVN.	7.2 inches	8.0 inches

a. Low concrete strength, f'_c = 3853 psi.
b. Concrete stress exceeded the allowable stress: f_{ce} = 3090 > 0.6 f'_{ci} = 2690.

3.7 Effect of Variables

Transfer length is affected by many factors. Variables such as strand weathering and strand size have demonstrated their impact on prestress transfer over many research projects[1,2,5,8,11,12] From these data, the influence of several different variables can be observed. The discussion will include:

1) Strand diameter
2) Strand spacing
3) The transfer length of debonded strands
4) Size of the cross section
5) The effect of confining reinforcement

3.7.1 Strand Diameter. Table 3.8 compares transfer lengths for the two different sizes of strands. Clearly, the measured transfer lengths for 0.6 inch strand are longer than those for 0.5 inch strand. Average values for these series are 30.0 inches for 0.5 inch strand and 40.9 inches for 0.6 inch strand. Standard deviations for the data are 7.2 inches and 8.0 inches, respectively. Results from "SS" specimens are not included in this comparison because the nature of the single strand specimens combined with the effects of the sudden release would skew the results.

The average transfer length for the 0.6 inch strand is approximately 30% greater than the average transfer length of 0.5 inch strands. These data reinforce transfer length as a function of strand diameter. The code expressions for transfer length, both 50 d_b and $^{fse}/_{3}$ d_b, suggest that the transfer length varies linearly with the strand diameter. The ratio of the strand diameters would predict only a 20% increase from 0.5 inch to 0.6 inch strands. This assumes linear behavior and uniform bond stress for all sizes of strands. Currently, there is some discussion between researchers that transfer length does not vary linearly with strand diameter. However, from this data, such comparisons are difficult to justify.

3.7.2 Strand Spacing. Current practice dictates that center to center spacing of strands should be at least 4 times the strand diameter. Although this rule of thumb is based on very little experimental data, it has served the industry well, especially because the industry standard was 0.5 inch strands at two inch spacings. With the possibility of using 0.6 inch strands, this rule of thumb has been questioned. In fact, the structural efficiency of the 0.6 inch strand would be lost if 2.4 inch spacings were required. Consequently, tests were performed to determine what effects strand spacing would have, if any, on transfer lengths.

The data for transfer lengths of 0.6 inch strand with 2.0 inch and 2.25 inch spacings are compared in Table 3.9. The average transfer length for all 0.6 inch strands was 43.4 inches. This value is slightly less than the average transfer length for 0.6 inch strands with 2.25 inch spacings, which was 44.2 inches. These data indicate that strands with 2.25 inch

spacings have nearly identical transfer lengths than strands with 2 inch spacings. The need for wider spacings to accommodate 0.6 inch strands is not demonstrated.

TABLE 3.9

EFFECT OF STRAND SPACING ON MEASURED TRANSFER LENGTH: 2 INCH SPACING VS. 2.25 INCH SPACING FOR 0.6 INCH DIAMETER STRAND

SPECIMEN	NORTH END	SOUTH END
FC362-11	46 inches	46 inches
FCT362-12	44 inches	43 inches
FC362-13	45 inches	41 inches
AVERAGE, SPECIMENS WITH 2.25 INCH SPACINGS = **44.2 inches** Standard Deviation = 1.9 inches		
AVERAGE, ALL SPECIMENS WITH 0.6 INCH STRAND = **43.4 inches** Standard Deviation = 5.9 inches		

The table correctly compares 3-strand specimens with 0.6 inch strand on 2.25 inch spacing with all 3-strand specimens with 0.6 inch strand on 2 inch spacing.

In a related issue, 0.6 inch strand is more likely to cause splitting upon pretensioning release because its larger size will cause larger bursting stresses. Current standard box girder shapes in the State of Texas have 5 inch thick bottom flanges and 6 inch wide webs. Tests were performed to study the reliability of transferring fully bonded 0.6 inch strands on 2 inch spacings in a 5 inch wide concrete member. Six specimens were fabricated 5 inches wide and 13 inches deep with 5 strands each, FC(T)550-1, 2 and 3 and FC(T)560-1, 2, and 3. These specimens were inspected for splitting cracks and measured for transfer length. No signs of splitting were detected. Furthermore, transfer lengths for these specimens were within normal ranges. These tests confirm that 2.0 inch spacing is sufficient for 0.6 inch strands for all cross sections.

3.7.3 Transfer Length for Debonded Strands. Table 3.10 compares the measured transfer lengths for debonded strands with transfer lengths from fully bonded strands. Measured transfer lengths of debonded strands are consistently shorter than those of fully bonded strands. Debonded 0.5 inch strands were transferred in an average of 28.3 inches while their fully bonded counterparts were transferred in 30.0 inches. Differences were even greater for 0.6 inch strands. Measured transfer lengths of debonded strands were 31.8 inches compared to 40.9 inches for fully bonded strands.

TABLE 3.10

COMPARISON OF MEASURED TRANSFER LENGTHS: DEBONDED STRANDS VS. FULLY BONDED STRANDS

Averages of Measured Transfer Lengths

	0.5 INCH STRAND (Std.Dvn.)	0.6 INCH STRAND (Std.Dvn.)
FULLY BONDED STRANDS	**30.0 inches** (7.2)	**40.9 inches** (8.0)
DEBONDED STRANDS	**28.3 inches** (6.0)	**31.8 inches** (10.4)

The transfer zone of a debonded strand is positioned in regions of the specimen that enjoy precompression from strands that are fully bonded. While the difference in transfer lengths is significant, the differences do not appear large enough to warrant special

provisions for the transfer length of debonded strands. Again, scatter in the test data causes greater variation in the results than the observed differences in transfer length.

3.7.4 Size Effects of Cross Section on Transfer Length. The larger AASHTO-type cross sections were designed to be used for development length tests. These specimens were also tested for transfer length and their results are reported in Tables 3.4 and 3.5. In the literature, most transfer length research has been performed on rectangular prisms with a single strand.[53,44,8,2,1] Very few transfer length measurements have been taken on multi-strand specimens such as the three and five strand specimens tested here. Naturally, data from larger beams should match more closely the transfer lengths of actual pretensioned girders in the field.

Figures 3.20 and 3.21 compare the transfer lengths versus the specimen series. Generally, the larger the specimen, the shorter the transfer lengths. Considering specimens with 0.5 inch strands, the transfer lengths for the AASHTO-type beams are very low, almost 40% lower than the FC3 series. The FC5 series results could be slightly skewed because of low concrete strength, Table 3.12 and a concrete stress at transfer that exceeds $0.6f'_c$. This result is made more remarkable by the cutting techniques. The FC1, FC3, DC3, and the FC5 series were flame cut after slight detensioning whereas the AASHTO-type beams were flame cut at 100% pretension. The "SS" series is the initial single strand test series where the strands were cut at full tension, which resulted in more scatter than with other test series.

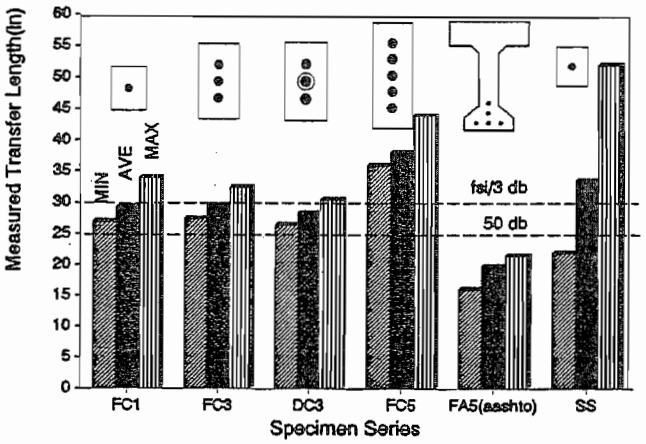

Figure 3.20 Transfer Lengths, 0.5 Inch Strands. Summary by Specimen Series, Fully Bonded

It is possible to develop a rationale relating larger cross sections to shorter transfer lengths. First of all, the greater mass of concrete is probably less susceptible to damage from sudden release of energy by sequentially flame cutting individual pretensioned strands. Secondly, the greater number of strands could be acting as reinforcement to the cross section, helping to distribute the energy and stress from the release of a single strand. Lastly, with each successive cut, the cross section becomes increasingly precompressed. The strands that are cut last transfer their pretensioned force into a cross section with increasingly greater precompression.

The same trend is demonstrated with 0.6 inch strands in Figure 3.21. These data clearly show that test specimens with larger cross sections and multiple strands possess significantly shorter transfer lengths. Tests on the different series were all performed with

consistent procedures and with the same strand, under the same laboratory conditions. These results are significant because much of the transfer length research has been done on single strand specimens with relatively small cross sections.

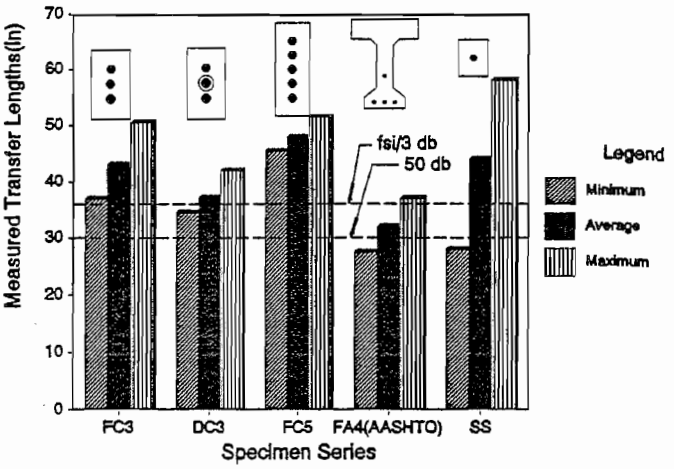

Figure 3.21 Transfer Lengths, 0.6 Inch Strand. Summary by Specimen Series

3.7.5 Confining Reinforcement. Confining reinforcement is analogous to hoop ties in a column. In a column, the hoop ties prevent the longitudinal reinforcement from buckling outward. The ties confine the concrete within the core by resisting lateral deformations. In the transfer zone, transfer of pretensioned strands causes bursting stresses in the surrounding concrete. Presumably, confining reinforcement surrounding the concrete and pretensioned strand would shorten the transfer length. However, these data do not support this idea. Data presented in Table 3.11 show similar transfer lengths with or without transverse reinforcement. Clearly, transverse reinforcement does not participate significantly in prestress transfer, as shown in these tests.

These tests demonstrate that confining reinforcement will not contribute significantly until concrete is subjected to large lateral strains. Even though confining reinforcement must increase the elastic stiffness in the circumferential direction, this effect is apparently small compared to the elastic stiffness of concrete.

On the other hand, in cases where splitting occurs at transfer, confining reinforcements are the only elements that maintain integrity of the concrete if splitting cracks should occur. Therefore, transverse reinforcement should not be eliminated from standard detailing.

3.7.6 Concrete Strength. At the beginning of this project, concrete strength was not selected as a variable. Tests performed by Kaar, LaFraugh, and Mass[8] measured transfer lengths of different sizes of strand while

TABLE 3.11

EFFECT OF CONFINING REINFORCEMENT ON THE MEASURED TRANSFER LENGTH

Averages of Measured Transfer Lengths Fully Bonded Strands

	0.5 INCH STRAND	0.6 INCH STRAND
FCT350-3	30.0	
FCT350-4	30.0	
FCT360-3		50.5
FCT360-4		46.5
FCT362-12		43.5
AVERAGE TRANSFER LENGTHS FOR STRANDS CONFINED BY REINFORCEMENT	30.0	46.8
AVERAGE TRANSER LENGTHS FOR ALL SPECIMENS	30.0	40.9

varying concrete strengths. They concluded that concrete strength did not affect the transfer length of pretensioned strands. Therefore, concrete strength has been discounted as a factor in transfer length. The code expressions do not contain concrete strength as a variable affecting transfer length.

In 1988, Castrodale, Kreger and Burns[44] performed limited testing of transfer length as a function of concrete strength. In their tests, transfer lengths were shorter for higher strength concretes. Concurrently, some research projects are testing transfer length as a function of concrete strength. Preliminary data seem to indicate that high strength concrete will shorten the transfer length. However, these projects have not concluded and the results have not been published.

In this research, some specimens had concrete with lower than specified strengths. Consistently, in those cases, measured transfer lengths were longer than in companion specimens. Concrete strengths are reported in Table 3.12 along with the measured transfer lengths. Low concrete strengths affected specimens FC550-1, 2, and 3, and FC160-11 and 12. In these specimens, longer than average transfer lengths were measured. However, these data are not conclusive.

TABLE 3.12

CONCRETE STRENGTHS VS. TRANSFER LENGTHS

SPECIMEN	TRANSFER LENGTH		f'_{ci}	f'_c
	NORTH END	SOUTH END		
FC150-11	27	34	4481	6710
FC150-12	29	28	4481	6710
FC350-1	33	28	4315	6630
FC350-2	28	28	4315	6630
FCT350-3	31	30	4315	6630
FCT350-4	29	32	4315	6630
DC350-5	27	28	4201	6250
DC350-6	29	31	4201	6250
FC550-1	40	37	3853	5402
FCT550-2	36	40	3853	5402
FC550-3	33	44	3853	5402
FC160-11	-	-	3853	5402
FC160-12	48	46	3853	5402
FC360-1	42	41	4201	6250
FC360-2	37	48	4201	6250
FCT360-3	40	46	4201	6250
FCT360-4	51	42	4792	7298
DC360-5	42	36	4792	7298
DC360-6	35	41	4792	7298
DCT360-7	41	35	4792	7298
DC360-9	37	35	4759	7525
DCT360-10	35	37	4759	7525
FC362-11	46	44	4759	7525
FCT362-12	44	42	4759	7525
FC362-13	42	40	4759	7525
FC560-1	46	37	4481	6603
FCT560-2	48	47	4481	6603
FC560-3	48	52	4481	6603

3.7.7 Strand Surface Condition. The impact of strand surface condition on transfer length has been established by many researchers[1,5,8,12,15,18].

Strand that is rusted or weathered in some way generally has a shorter transfer length than bare, bright strand. A coating of light rust improves the frictional restraint between concrete and strand. Conversely, transfer lengths can become very long if the strand is lubricated or otherwise contaminated with oil. In this research, bare, bright clean strand was tested. No oils were used near the strand at any stage of fabrication. Care should always be taken in the fabrication of pretensioned members to prevent oil from getting on the strand.

In the fabrication of highway bridge girders, normal plant procedures call for the lubrication of formwork to extend the life of the forms. This practice risks damaging the bond between concrete and strand by contaminating the strands' surface with oil. In fabrication of specimens DZ2450-1, DZ2450-2 and FZ2450-3, oil was used to lubricate the forms using a procedure that endangers an effective bond.

The bottom form, or soffit, was oiled after the strands were in place and tensioned. Only 1.75 inches separate the sofit and the bottom row of strands. During the oiling of the sofit, an oily rag wrapped around a paddle (See Figure 3.22) is passed along the bottom form. The probability that oil contacted the strands is very high, increasing the likelihood that transfer lengths for full sized pretensioned girders are longer than first expected. On the other hand, the strands in plant conditions tend to developed some light rusting from exposure to the weather. This may counter the effects of oil.

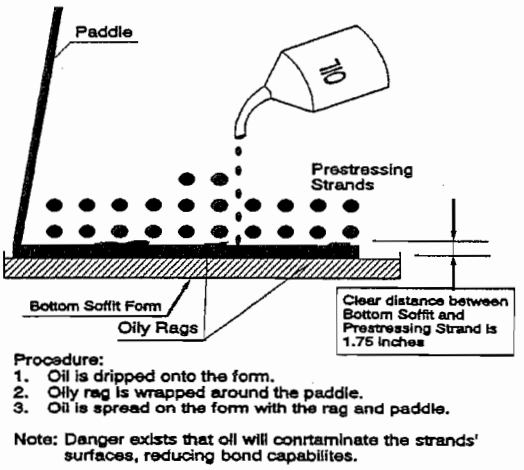

Figure 3.22 Form Oil Applied to Bottom Soffit Form in Pretensioning Plant

At best, strand surface condition is extremely variable. Some strands may be significantly weathered by the time they are used in fabrication of a pretensioned member. Some plants may protect their strand from the elements; others may not. Also, the industry has recently noted an unusually high incidence of pullout failures for strand in a variety of applications. Some fault has been placed on the lubricants used in the manufacture of high strength strand. The lubricants are generally described as soaps, more accurately termed stearates. Variability in these lubricants may also influence pretensioned bond.

To summarize, strand surface condition is probably the most important variable affecting transfer length of strand, yet it is the least predictable. No quality assurance procedures exist to qualify strand surface conditions. Large degrees of scatter in the data exist not only from researcher to researcher, but within an individual research project, as

exhibited here. Strand surface condition could be the cause of a significant portion of these differences.

It should be noted that strand used in this study was furnished with mill condition surface. It was protected from corrosion during the period of its use in constructing test specimens. For specimens fabricated at FSEL, the effects of strand surface condition were minimized as a variable by maintaining consistent use of the strand material and handling it carefully to avoid surface contamination. However, the strands used in the fabrication of the Texas Type C girders were beyond the control of the research project. Although these strands did possess some surface slight surface rust, it is likely that their surfaces were contaminated with oil.

3.8 Summary of Transfer Length Measurements

Sixty-five transfer length tests were performed at FSEL. The average transfer length of those specimens was 30.0 inches for 0.5 inch strands and 40.9 inches for 0.6 inch strands. The standard deviation was 7.2 inches and 8.0 inches respectively. Transfer lengths were measured on three full-sized girder specimens at a prestressing plant. Results from these specimens indicated large amounts of scatter with significantly longer transfer lengths when compared to the specimens tested in the laboratory. Differences are accounted from outdoor conditions and slight variations in test procedure. However, the largest differences appear to occur because of strand surface contamination with form oils.

CHAPTER 4
DEVELOPMENT OF PRETENSIONED STRAND

4.1 Introduction

When external loads act upon a pretensioned beam, tension in the strands increases beyond the effective prestress force due to moments resulting from externally applied loads. As tension in the strands increases, the resistance offered by the various bond mechanisms that anchor the strand must also increase. Traditionally, bond strength to resist additional tension has been termed the "development" of the strand. Tension in the strand is resisted, or "developed" by bond acting between the strand and concrete. The required bond strength is developed by lengthening the anchorage zone of the strand beyond the prestress transfer zone to include the "flexural bond length". "Flexural bond" is the additional bond stress activated by increases in strand tension from application of external loads. In the ACI Commentary, development length equals the sum of the transfer length plus the flexural bond length. Therefore, "development length" is defined as the total anchorage length required to resist tension from both the prestress transfer and external loads.

The development length of prestressing strand is discussed in this chapter, including its definition, current code provisions, its importance and its use in current design practice. Factors affecting development length are discussed including strand size and the shape of the cross section. Tests were performed on specimens with 0.5 inch strands and specimens with 0.6 inch strands. The cross section was varied to include I-shaped beams resembling an AASHTO-type composite cross section and beams with rectangular cross sections.

Tests were performed to measure development lengths of prestressing strands. Variables included strand size and the beam cross section. Development lengths were measured in both beams with I-shaped cross-sections and beams with rectangular cross section. Variations in cross section are found to affect the web shear cracking loads and, by consequence, development of the prestressing strand. The occurrence of strand slip is correlated to web shear cracking, and measured web cracking loads are compared to calculated values. Results from the tests indicate that, under certain conditions, current AASHTO and ACI codes are inadequate. Conversely, in other tests, current code provisions require longer development lengths than necessary.

4.1.1 Definitions. In this section, three terms are defined and discussed; development length, embedment length, and critical section. Development length is the bond length required to anchor the strand as it resists external loads on the member. The definition is discussed in Section 1.2.2 and is not repeated here.

Embedment length is a property of the loading case and/or geometry of the beam or structure. It is distinguished from development length which is a function of material properties. Simply stated, embedment length is the bonded length of the strand from the

beginning of bond to the ***critical section***. The embedment length was varied for each test. Embedment length begins with bond, usually at the ends of a beam, and extends to the ***critical section***. Strands bonded from the ends of a member are called "fully bonded." In cases of debonded strands, the embedment length begins where the debonding ends.

In most design applications, and in the literature, the ***critical section*** is interpreted as the point of maximum moment. This is the definition that is used in this chapter. However, as will be shown, the critical section for bond and development may be disparate from flexural behavior. In fact, one may consider each section of the beam to be critical for bond and perform a check at each section for required development length. However, for purposes of discussion in this chapter, the ***critical section*** is defined as the point of maximum moment and the ***embedment length*** is the distance from the end of the beams to the load point.

4.1.2 AASHTO and ACI Code Provisions. AASHTO and ACI codes are nearly identical with regard to development length. ACI development length provisions are repeated here for discussion:

> *12.9.1 Three- or seven-wire pretensioning strand shall be bonded beyond the* ***critical section*** *for a development length, in inches, not less than*
>
> $$(f_{ps} - \frac{2}{3} f_{se})\, d_b$$
>
> *where d_b is strand diameter in inches, and f_{ps} and f_{se} are expressed in kips per square inch.*
>
> *12.9.2 Investigation may be limited to cross sections nearest each end of the member that are required to develop full design strength under specified ultimate loads.*

These provisions, when interpreted broadly, can account for a variety of load conditions. Implicit in these provisions are requirements to develop strand to the critical section for shear. In keeping with a broad interpretation for development length, Section 12.9.2 encourages the engineer to investigate the end regions of the beam. However, in practice, strand development is checked only for flexural capacity because of the treatment of strand stresses.

In the code provisions listed above, development length varies as a function of strand tension at the nominal flexural capacity, f_{ps} (f^*_{su}). Both codes contain formulae relating f^*_{su} and f_{ps} to the strand stress at nominal flexural capacity. It is only natural that development then be treated primarily as a requirement of flexural loads. Even though f_{su} and f_{ps} may be treated in more general terms by using a more discriminating analysis, the code misleads the user in prescribing development length as a requirement for flexural resistance.

Even so, examining development, or bond failure, as an antithesis to flexural failure helps to understand the general idea of strand anchorage and development. If embedment length is greater than the required development length (Le > Ld), then the beam fails in flexure. Conversely, if embedment length is less than the required development length (Le < Ld), then the beam fails in bond.

However, other behavioral mechanisms impose additional requirements on strand development. Tests reported in this and other research consistently demonstrate web shear cracking to precipitate anchorage failures[32,35,43,40,51,55]. Typically, when shear cracks form near the ends of a specimen, pretensioned strands must carry additional tension. Using a truss analogy, when web cracks form, the concrete loses its tensile capacity and the prestressing steel must carry the tension required of the bottom chord. In many of the tests, when web shear cracks formed at the ends of a beam, the embedment length of the strands was insufficient to develop tension required to sustain the shear capacity, and the strands failed in bond. Laboratory tests[32,43] on pretensioned beams demonstrate the tendency of beams to collapse in shear upon the formation of web shear cracks.

Anchorage failures from shear cracking suggest the existence of a critical section which does not coincide with the region of maximum moment. In truth, neither AASHTO nor ACI can ever define the ***critical section.*** Instead the ***critical section*** must be defined by any and all possible failure mechanisms. Engineers must be aware of sections that might be susceptible to anchorage failures, which include more possibilities than just the anchorage required for flexural bond and development.

4.2 Development Length Tests

Nineteen tests were performed on beams that were I-shaped to resemble AASHTO-type composite sections. Additionally, nine tests were performed on rectangular beams. Of the AASHTO-type specimens, nine tests were performed on specimens with 0.5 inch strands and ten tests were performed on specimens with 0.6 inch strands. Five tests were performed on beams with 0.5 inch strands while four tests were conducted on rectangular beams with 0.6 inch strands. Details of the cross sections and specimen numbers are given in Figures 4.1 and‘ 4.2. In all, a total of 28 tests were performed on 13 beams. Most of the specimens were tested twice, once at each end. The specimen numbering system, given in Table 3.1, is coded to distinguish the characteristics of each specimen.

Some additional details of the testing program were reported in a Master's Thesis by Bruce Lutz, *Measurement of Development Length of 0.5 inch and 0.6 inch Diameter Prestressing Strand in Fully Bonded Concrete Beams.*[61]

4.2.1 Specimen Fabrication. All of the specimens were built in the Ferguson Structural Engineering Laboratory (FSEL) at The University of Texas at Austin. Specimens were fabricated following a consistent sequence of procedures:

1) Stress strand to 75% f_{pu} (202.5 ksi)
2) Placement of mild reinforcement
3) Placement of formwork
4) Casting of concrete
5) Curing of concrete in place (two days)
6) Release of pretensioning

The specimens were tested in sequence, but not before concrete had gained design strength for testing.

The strands were stressed individually using a hydraulic double headed actuator. The actuator is made specially for pretensioned applications and contains a nose piece that seats the teeth of the chuck into the strand before releasing the prestress force. Elongations were also measured to ensure that correct tension was applied to the strand.

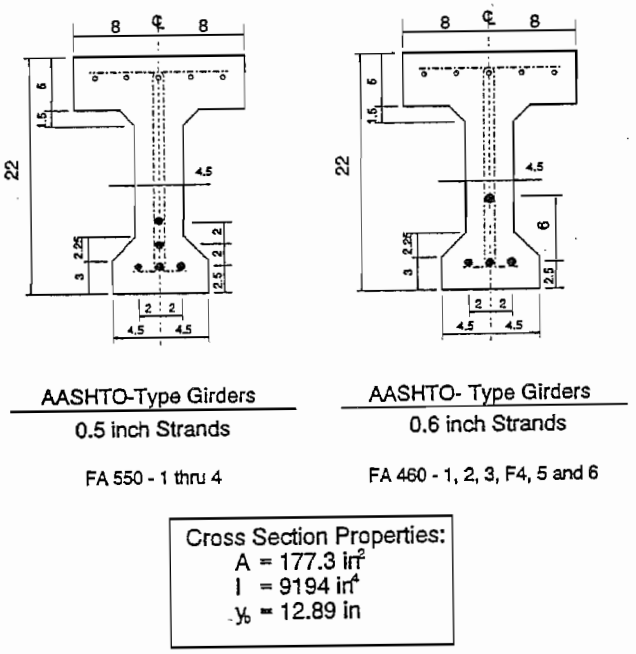

Figure 4.1 AASHTO-Type Girder Cross Sections

Mild reinforcement consisted of longitudinal top steel and vertical shear stirrups. No mild steel was placed longitudinally in the bottom of the cross section. The cross section details of Figures 4.1 and 4.2 show the mild reinforcement. Shear reinforcement was designed in accordance with AASHTO and ACI provisions. The photograph in Figure 4.3 shows the fabrication area, and includes a reinforcement cage, the prestressing bed and the formwork for casting concrete.

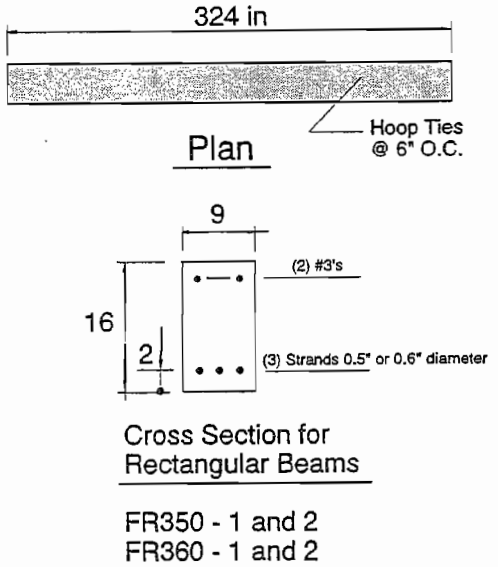

Figure 4.2 Rectangular Beam Details

Tension in the strands was released by flame cutting. The strands were cut at 100% of pretension without any gradual lessening of tension before cutting. Strands were cut in a sequence that alternated between opposite ends of the prestressing bed.

4.2.2 Material Properties. The strand's ultimate strength was specified at 270 ksi. The seven-wire, low relaxation prestressing strand used in these tests is the current industry standard for prestressed applications. The ultimate strength of the strands was tested at Ferguson Lab. The strands' ultimate strength was 281 ksi for the 0.5 inch strand and 276 for the 0.6 inch strand. FR350 beams contained strands with an ultimate strength of 283 ksi. Stress versus Strain data were provided by the strand manufacturer and are shown in Appendix A, Figures A1, A2 and A3.

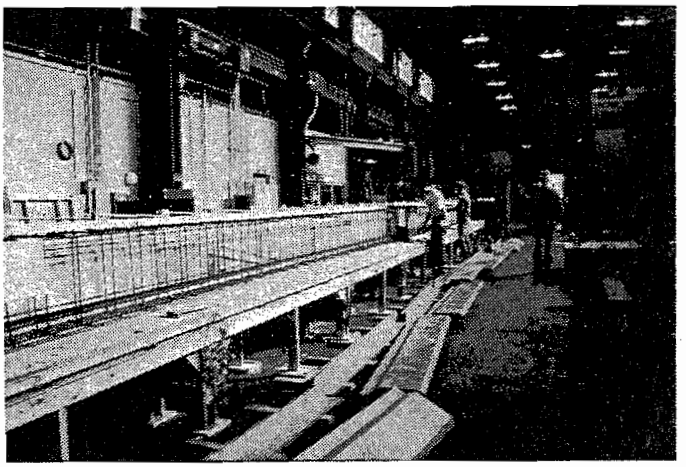

Figure 4.3 Fabrication of AASHTO-Type Beams

The concrete strengths were originally designed to be 4500 psi at release and 6000 psi for 28 day strength. Concrete proportions are given in Table 4.1. The original mix design specified nominal 3/8 inch maximum sized coarse aggregate. However, problems casting the first beams in the series, beams FA550-1 and FA550-2, forced a change in aggregate size. In these first two beams, initial set occurred before the concrete could be properly consolidated and some honeycombing resulted. For subsequent casts, the mix design was changed, substituting 5/8 inch course aggregate for the 3/8 inch aggregate. Higher concrete strengths resulted. Concrete strengths are given in Table 4.2.

4.2.3 Testing Apparatus. The testing apparatus is shown in the photograph in Figure 4.4. The apparatus included a loading frame, a hydraulic actuator, a spreader beam to create a constant moment region, and support beams which allowed the support locations to be varied from test to test. Development length testing requires that embedment length be varied from test to test. Results from previous tests are used to determine the embedment length for future tests. By varying the support locations, embedment lengths could also be varied accordingly.

Figure 4.5 illustrates a typical loading condition. Embedment length and span were varied from test to test. These dimensions are shown with the load deflection curves for each beam. For each test, the applied moment between the load points was kept constant. This was done by varying the location of the load point atop the spreader beam. The distance between the load points of the spreader beam onto the test specimen were kept constant at 24 inches.

TABLE 4.1

CONCRETE MIX PROPORTIONS AASHTO-TYPE BEAMS AND RECTANGULAR BEAMS

MATERIALS	WEIGHT PER CUBIC YARD
Type I Cement	611 LBS.
Water	290 LBS.
Coarse Aggregate[1] (5/8 inch Gravel)	1680 LBS.
Fine Aggregate(Sand)	1355 LBS.
Water Reducer[2] (M.B. 761-N)	37 fluid oz.

1. 3/8" aggregate was specified for FA550-1 and 2. Concrete for all other beams contained 5/8" aggregate.
2. Quantity and type of water reducer varied somewhat from cast to cast. However, all water reducers were low range water reducers.

TABLE 4.2

CONCRETE STRENGTHS AT FLEXURAL TESTING

BEAMS WITH 0.5" STRANDS		BEAMS WITH 0.6" STRANDS	
BEAM	CONCRETE STRENGTH (PSI)	BEAM	CONCRETE STRENGTH (PSI)
FA550-1	5110	FA460-1	6360
FA550-2	5110	FA460-2	6850
FA550-3	5430	FA460-3	6850
FA550-4	5850	FA460-5	7400
		FA460-6	7440
FR350-1	6790	FR360-1	7020
FR350-2	6790	FR360-2	7020

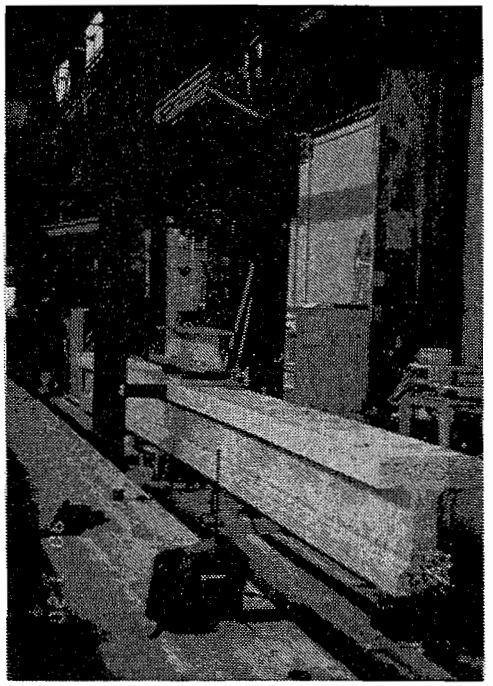

Figure 4.4 Testing Apparatus

4.2.4 Instrumentation. Instrumentation measured load applied, beam deflection and strand end slip. Other data measured electronically included hydraulic pressure and electrical resistance strain gages (ERSG's) applied to strands. Figure 4.6 illustrates the instrumentation and locations where measurements were taken.

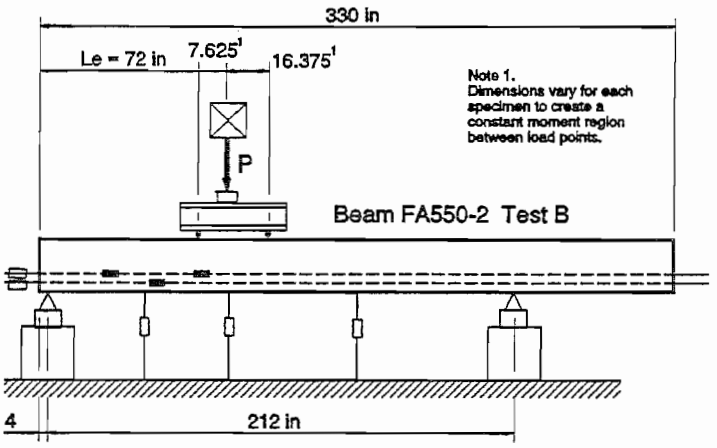

Figure 4.5 Typical Dimensions of Test Setup for Development Length Tests

Load was measured using an electronic load cell at the hydraulic actuator. Deflection and end slips were measured by linear potentiometers. All of the electronic instruments were calibrated prior to testing. End slip measurements are accurate to $\pm$0.001 inches, thus even very small end slips were detected for each individual strand.

Figure 4.5 illustrates a typical loading condition. Embedment length and span were varied from test to test. These dimensions are shown with the load deflection curves for each beam. For each test, the applied moment between the load points was kept constant. This was done by varying the location of the load point atop the spreader beam. The distance between the load points of the spreader beam onto the test specimen were kept constant at 24 inches.

Figure 4.5 illustrates a typical loading condition. Embedment length and span were varied from test to test. These dimensions are shown with the load deflection curves for each beam. For each test, the applied moment between the load points was kept constant. This was done by varying the location of the load point atop the spreader beam. The distance between the load points of the spreader beam onto the test specimen were kept constant at 24 inches. Concrete strains were measured on top of the beam in the constant moment region of each test. Measurements were taken at each load increment with the DEMEC gage system discussed in Chapter 3. Two pairs of DEMEC gage points were located on the top of the compression flange on opposite sides.

4.2.5 Test Procedure. Beams were loaded statically until failure. Load was increased at regular increments of approximately 2.0 to 5.0 kips until first cracking. Measurements were recorded at each load increment. Cracking loads and crack locations were noted and recorded. After cracking, load was increased in smaller increments. Any special behavior was noted and crack patterns were marked on the specimen. Web shear cracking loads were noted and recorded as were any significant strand end slips. Failure

was defined as the beam's inability to resist increased load. Flexural failures resulted in compression failure of the top flange of the beam. Anchorage failures resulted in general slip of the strand relative to the concrete and a sudden loss of beam capacity.

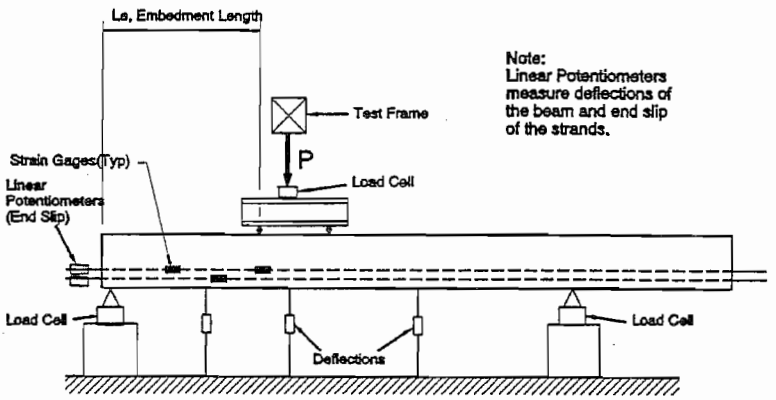

Figure 4.6 Instrumentation for Development Length Tests

Development length cannot be tested directly, meaning that one cannot determine the required development length by performing a single test. In this research, development length is obtained by a progression of tests where the result from each individual test becomes a single data point for the whole development length test series. In a succession of tests, embedment length is varied from test to test. Failure mode is considered before the embedment length for the next test is chosen. If, in the sequence of tests, bond failure occurs at the tested embedment length, then the next test can contain longer embedment in hopes of obtaining a flexural failure. In this manner, the two possible failure modes can be spanned by different embedment lengths. Longer embedment lengths are more likely to produce flexural failure and shorter embedment lengths are more prone to bond failure. As the test series progresses, the division between failure modes becomes more and more distinct. In this series, many tests were performed at or near the "borderline" between flexural failure and bond failure.

Each beam specimen was tested at least twice, once at each end. The first test on a specimen is designated Test "A" while the second test is designated Test "B". This procedure was possible because individual anchorage zones exist at each end of each pretensioned beam. Normally, the second anchorage zone was undisturbed from the first test, so the second test yielded a valid test. The only noticeable effect of testing beams twice was that flexural cracking from the first test sometimes influenced the initial stiffness of the beam in the second test. Two beams, Specimen FA550-1 and Specimen FR350-1 were tested three times. Tests FA550-1A, FA550-1B, and FA550-1C are all tests performed on the same beam. The load deflection curve of Test FA550-1C did not indicate a definite cracking point because the beam was already cracked from tests FA550-1A and FA550-1B.

4.3 Development Length Test Results

4.3.1 Test Results, AASHTO-Type Beams. In this section, results are reported from beam tests on the AASHTO-type series FA550 and FA460. Again, all of these specimens contain fully bonded strands with the strand arrangement shown in Figure 4.1. The FA550

series beams each contained five 0.5 inch strands. The FA460 series beams each contained four 0.6 inch strands. Behavior of both series of beams is remarkably similar.

Two types of failures were observed in this test series, flexural failure and shear/bond failure. Flexural failure is evidenced by crushing of the concrete after yielding of the strand. Two criteria, capacity and ductility, must be met to classify a failure as flexural. First, the ultimate flexural capacity of the section must be developed; and second, the beam must experience large deformations past the yield point (ductility). Ductility is a requirement in these test series and in current design standards for flexural members, because beams are underreinforced. By meeting the criteria of capacity and ductility, a beam demonstrates a predictable load capacity with reasonable warning before collapse. Flexural failures are desirable because they achieve an easily predicted limit state while providing warning before collapse. Without these two criteria for capacity and ductility, a failure cannot be classified as a flexural failure.

Failure mode versus embedment length is plotted from 0.5 inch strand specimens in Figure 4.7. For specimens with 0.6 inch strands, Figure 4.8 plots the failure mode versus embedment length. Development length is defined by the borderline between failure modes. For 0.5 inch strands the required development length was 72 inches and for 0.6 inch strands it was 84 inches. These measured development lengths are indicated on the plots.

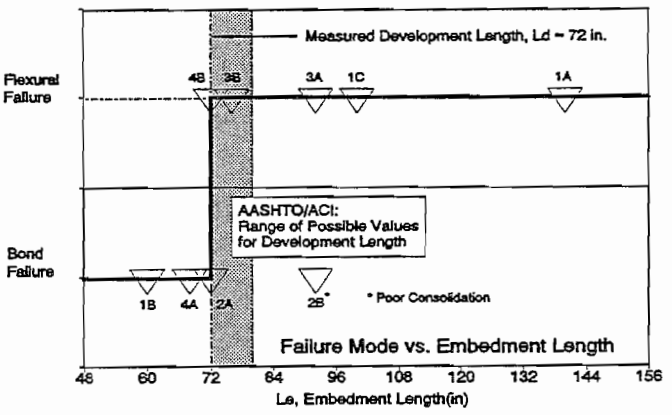

Figure 4.7 Development Length Tests: 0.5 Inch Strands in AASHTO-Type Beams

The range of calculated development lengths are also indicated on the plots by the shaded areas labeled "AASHTO/ACI..." These values were calculated using AASHTO equation 9-32. Using the values for strand stresses, f_{su} = 260 ksi and f_{se} = 150 ksi, the calculated development lengths are L_d = 80 inches for 0.5 inch strand, and L_d = 96 inches for 0.6 inch strand. Even though the measured development lengths show the calculated code values to be slightly conservative, the measured development lengths do fall within the range of possible calculated values from AASHTO 9-32. If f_{su} = 250 ksi and f_{se} = 160 ksi, then the calculated development lengths would be 72 inches for 0.5 inch strands and 84 inches for 0.6 inch strands.

Results from the AASHTO-type beam tests are presented in Table 4.3. The table gives the embedment length and the mode of failure. The measured value of the ultimate moment is listed and compared to the calculated value for nominal flexural capacity. M_n(calc) is calculated from strain compatibility principles and corresponds to a concrete

strain of 0.003 in/in. M_n(calc) is 3541 k-in for the FA550 beams and 3940 k-in for FA460 beams. Concrete strain at the ultimate load is listed for each test. These strains were measured in the region of maximum moment on the top fiber of each beam. Concrete strain is a good indicator of the failure mode. Generally, if the concrete strain reached or exceeded 0.003 in/in, then the failure was probably flexural. Conversely, beams that failed in bond generally did not develop ultimate concrete strain because the strand anchorages failed before large deformations could occur.

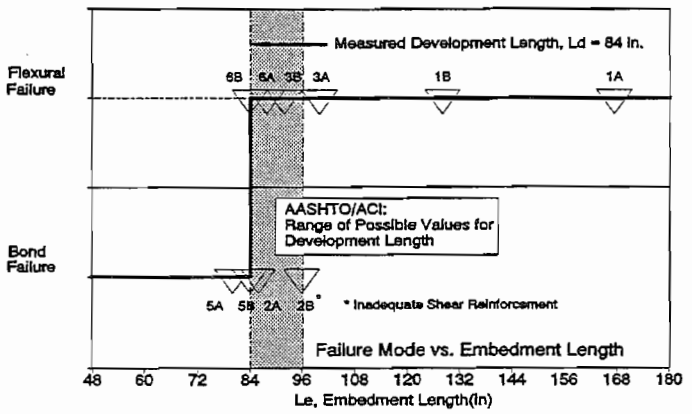

Figure 4.8 Development Length Tests: 0.6 Inch Strands in AASHTO-Type Beams

A flexural failure is demonstrated by Test A on Specimen FA550-3. The calculated ultimate flexural capacity of 3541 k-in was exceeded by the ultimate moment during the test by 3.4%. Flexural failure occurred at a load of 77 kips. Concrete fibers at the top of the beam crushed at a strain of 0.004148 in/in. Maximum beam deflection was measured at 1.90 inches at the ultimate load and failure. Load versus deflection is plotted in Figure 4.9 along with end slips. If yield is defined as 90% of ultimate load, then the deflection at yield is approximately 0.75 inches. Dividing 1.90 inches by 0.75 inches gives a ductility ratio of about 2.5. Note that no strand slip was detected. The photograph in Figure 4.10 illustrates a typical flexural cracking pattern, taken from Test FA550-3A.

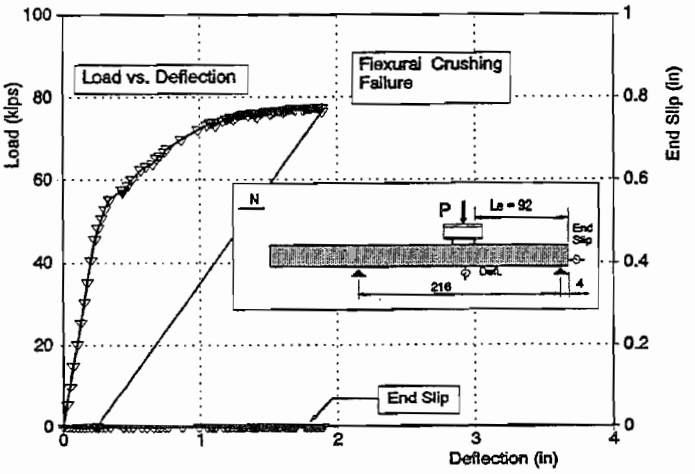

Figure 4.9 Beam FA550-3 Test A: Typical Flexural Failure

Bond failure denotes the complete or nearly complete loss of bond strength. Bond failures are characterized by gross displacements of the strands relative to the concrete, and strand end slips into the concrete are noted. Many times, beams failing in bond do not develop the full flexural capacity of the section, or if they do, they cannot sustain load capacity through large deformations. Bond failures were typically more sudden and explosive than flexural failures. In these tests, bond failures were generally accompanied

TABLE 4.3

SUMMARY OF DEVELOPMENT LENGTH TESTS
AASHTO-TYPE BEAMS

Test No.	L_e (in)	M_U(test) (k-in)	Mu/Mn	Concrete Strain at Ultimate	Failure Mode
FA550-1A	140	3645	1.03	4424	FLEXURAL
FA550-1B	60	3730	1.05	2146	SHEAR/BOND
FA550-1C	100	3617	1.02	2756	FLEXURAL
FA550-2A	72	3222	0.91	1938	SHEAR/BOND
FA550-2B	92	3683	1.04	2382	SHEAR/BOND[2]
FA550-3A	92	3663	1.03	4148	FLEXURAL
FA550-3B	76	3675	1.04	3724	FLEXURAL
FA550-4A	68	3576	1.01	1731	SHEAR/BOND
FA550-4B	72	3796	1.07	3142	FLEXURAL
FA460-1A	167.5	3798	0.96	3016	FLEXURAL
FA460-1B	128	4129	1.05	3113	FLEXURAL
FA460-2A	86	4059	1.03	3538	FLEXURAL[3]
FA460-2B	96	3843	0.98	2228	SHEAR/BOND[4]
FA460-3A	100	4020	1.02	3192	FLEXURAL
FA460-3B	92	4048	1.03	3454	FLEXURAL
FA460-5A	80	3582	0.91	1646	SHEAR/BOND
FA460-5B	84	3562	0.90	1488	SHEAR/BOND
FA460-6A	88	4037	1.02	3198	FLEXURAL
FA460-6B	84	3910	0.99	3106	FLEXURAL

1. M_n(calc) = 3541 k-in for FA550's; M_n(calc) = 3940 k-ft for FA460's
2. Poor consolidation
3. Flexural failure w/ 0.15 inches End Slip
4. Stirrup spacing too large

by shear failures. These are called "shear/bond" failures in Table 4.3.

A typical shear/bond failure resulted in Test A on Specimen FA550-4. Even though failure was not flexural, the maximum moment during testing reached the calculated nominal moment. However, the beam did not possess any ductility because bond failed before any large deformations could take place. Failure was classified as a bond failure. Load versus deflection and end slip is plotted in Figure 4.11. Note that the first end slip

corresponds to the first web shear crack. This result is repeated in all of the tests in this series. The first end slip occurred with the formation of web shear cracks. There are a few exceptions, but generally, the strands slipped when web shear cracks formed. In Test FA550-4A, shear loads cracked the web at a total load of 69.9 kips. The shear in the shear span was 56.3 kips. The photograph in Figure 4.12 shows that several web shear cracks formed simultaneously, marked by the total load "70." As loading was continued, the beam's resistance also increased. However, note the web crack which formed at 80 kips, marked "80" in Figure 4.12. This crack formed through the transfer zone of the strands. Complete anchorage failure followed formation of this crack.

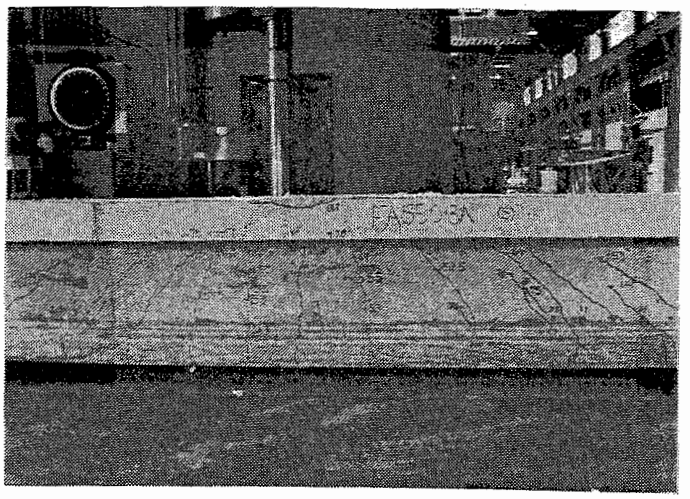

Figure 4.10 Test FA550-3A: Typical Flexural Cracking

The load versus deflection curves for all of the tests in the FA550 and FA460 series are plotted in Appendix C. By examining these plots, a correlation can be established between first web cracking and first end slip. Also, the effect that end slips have on load capacity is illustrated quite dramatically. In almost every case, large end slips are accompanied by large losses in load. Table 4.4 lists the cracking loads for the FA550 and FA460 test series beams including both the flexural cracking load and the web shear cracking load.

4.3.2 Influence of Web Shear Cracking on Development. In general, when a crack, either flexural or shear, extends across a strand, then that strand must slip within a finite distance adjacent to and on either side of the crack. Bond stresses increase adjacent to the crack to develop additional strand tension due to cracking. In the case of flexural cracks which form towards the middle of a span, long bonded lengths of strand are available to develop strand anchorage. On the other hand, web shear cracks are not limited to the mid-regions of a span. In fact, they are more likely to develop towards the supports in cases of simply supported beams or in beams with debonded strands.

When a web shear crack propagates across a strand, the strand must slip some finite distance. Bond stresses are activated to develop additional strand tension. However, if the shear crack extends through or near the anchorage zone of the strand, strand slip is likely to occur. In the anchorage zone, bond is primarily the result of Hoyer's effect, derived from Poisson's ratio causing expansion of the strand upon its release (transfer). Increases in

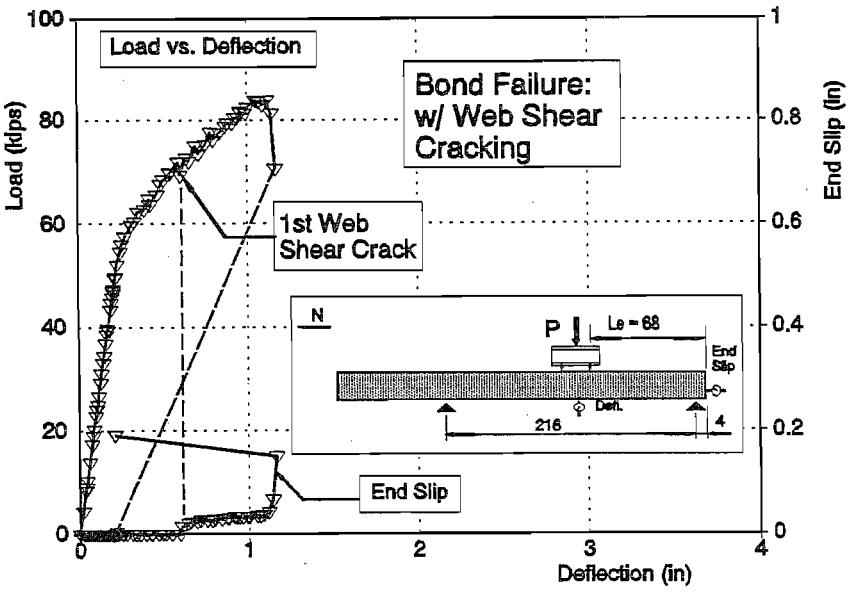

Figure 4.11 Beam FA550-4 Test A: Typical Shear/Bond Failure

strand tension at the crack location cause Hoyer's Effect to be lost, at least locally. In turn, strand slip is probable. Furthermore, when the strand slips, precompression in the concrete decreases, and the shear loads increase the tension requirements on the strand. At some point, pretensioned strand can no longer resist tension required by shear loads, and the beam fails. Some beams that failed in this fashion did so with very violent and explosive failures. Examples of this behavior are Tests FA550-1B, 2A, and 2B. Large concrete chunks were torn from the bottom of the beams accompanying loud and dangerous failures. In Figure 4.13, photographs of Test FA550-2A illustrate dramatic shear/bond failures. Load versus deflection and end slip for FA550-2A are shown in Figure 4.14. Later tests were loaded more cautiously when shear failure was imminent so that sudden collapses were avoided.

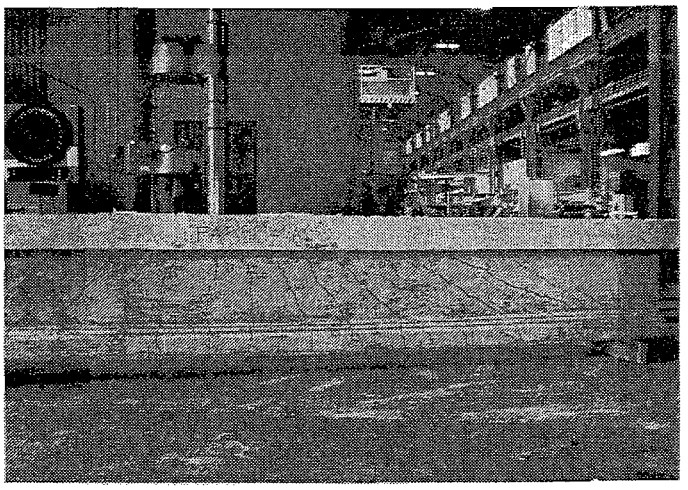

Figure 4.12 Beam FA550-4A: Typical Shear/Bond Failure

Interestingly, test specimen FA550-4A was able to resist increased loads beyond the initial web cracks and end slips. Strands in several of the tests experienced small amounts of slip without general bond failure. This demonstrates the presence of reserve bond strength beyond initial strand slip. A closer look at the photograph in Figure 4.12 reveals that the initial web shear cracks, marked "70" extend only to a distance approximately 20 inches from the ends. Transfer lengths for these specimens were measured to be quite short, 21 inches (Table 3.4), and the initial web shear cracks may not extend through the transfer zone. This may explain the presence of web shear cracks and small end slips without general bond failure. If the strand is anchored in the concrete in regions unaffected by the web shear crack, then the strand should be able to develop additional tension to carry shear loads.

Figure 4.13 Photograph of FA550-2A Explosive Shear Failure

Another important point is that bond integrity of the lower strands may be preserved even with web shear cracking. In the FA550 and FA460 specimens, four 0.5 inch strands or three 0.6 inch strands are contained well within the bottom flange of the cross section. Web cracks do not propagate through the bottom flange as readily as through the web because shear stresses are smaller. Using the truss analogy, the tension chord is composed of the precompressed concrete plus the pretensioned strand. Theoretically, before web cracks can extend through the bottom flange, tension in the bottom chord due to shear loads would have to overcome the precompression stresses in the concrete.

Initial web shear cracking occurred at a load of 69.4 kips with shear of 46.2 kips. If the shear was resisted entirely by the truss mechanism, then the bottom tension chord must carry 80 kips of tension, less than the 97 kips of precompression that is found in the bottom flange, Figure 4.15. After initial web cracking, the beam, FA550-4A, possessed additional capacity. Load was increased until failure occurred at a total load of 83.8 kips with a shear of 55.9 kips. In Figure 4.15, a representation of the truss model depicts the load case of Test Specimen FA550-4A at its failure load. In specimen FA550-4A, total precompression force from the four bottom strands equaled:

$$4\ strands \times 0.153\ in^2 \times 160\ ksi = 97\ kips$$

Again, if shear is resisted entirely by the truss mechanism, then the tension chord must resist about 97 kips of tension. As tension in the bottom chord approaches the total amount of precompression, the crack propagates through the bottom flange and general bond failure of all the strands causes complete beam failure. In the photograph, Figure 4.12, web shear cracks marked "70" remain in the web. Conversely, the web cracks marked "80" extend through the bottom flange. These cracks occurred at a total load of approximately 80 kips, and the beam failed very soon after these cracks formed. This test demonstrates that web shear cracks do not necessarily extend through the bottom flange upon first cracking, and that additional beam strength exists beyond web cracking, even though strands have slipped. However, under increasing load, cracks are likely to propagate through the bottom flange and cause general bond failure.

First incidence of web cracking is reported in Table 4.4. When web cracking shear is compared to the calculated values for predicting web shear cracking, reasonably good correlation is found. The web shear crack is calculated to occur at a principal inclined tensile stress equal to $4\sqrt{f'c}$ as given by an elastic analysis. The calculation for web shear cracking considers the transformation of stress at three different possible first cracking locations. The calculation for web shear cracking is described in Figure 4.16. Point A falls within the transfer zone from the end of the beam and the effective prestress is reduced by the proportion of $^{13.09}/_{25.0}$, where 13.09 inches is the distance of Point A from the beam's end and 25 inches is approximately one transfer length.

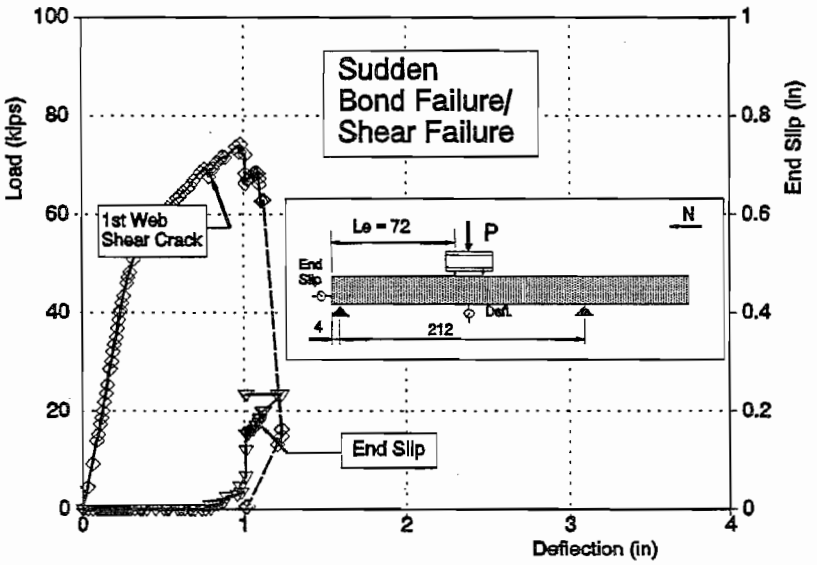

Figure 4.14 Beam FA550-2 Test B: Sudden Collapse Simultaneous Bond Failure and Shear Failure

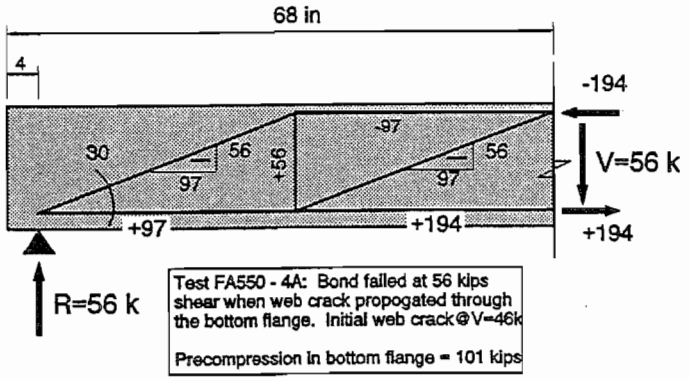

Figure 4.15 Truss Model of Shear Load at Failure Test FA550-4A

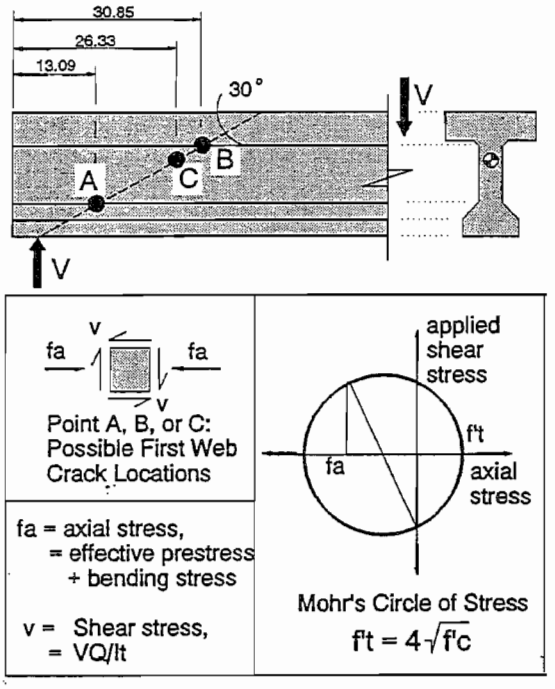

Figure 4.16 Calculation of Initial Web Shear Crack

If the web cracking shear is known, a simple calculation gives an approximation for the measured development length:

$$\left(\frac{M_u(test)}{V_{cw}(test)}\right)_{avg} = \frac{3679k''}{44.97k} = 81.8inches$$

While 82 inches is slightly longer than the measured development length of 72 inches for 0.5 inch strands, this method can still become a powerful predictor of development length failures for any given cross section. For 0.6 inch strands, the same expression is given as follows:

$$\left(\frac{M_u(test)}{V_{cw}(test)}\right)_{avg} = \frac{4001k''}{45.06k} = 88.8inches$$

and 89 inches compares favorably to the 84 inches measured. While, these calculations reflect that complete bond failure did not occur with web cracking in every case, the

calculation is easily performed and it provides a reasonable and slightly conservative predictor of anchorage failure.

TABLE 4.4

SUMMARY OF FLEXURAL AND WEB SHEAR CRACKING AASHTO-TYPE BEAMS

Test No.	Flexural Cracking		Web Shear		Init Slip	Fail Mode
	P_{cr}	M_{cr}[1]	P_{cw}	V_{cw}[2]		
FA550-1A	38.03	2241	-	-	-	FLEX
FA550-1B	50.24	1876[3]	68.75	45.83	V_{cw}	BOND
FA550-1C	N/A	N/A	None	None	-	FLEX
FA550-2A	50.98	2213	67.70	43.21	V_{cw}	BOND
FA550-2B	50.04	2385	77.25	41.85	V_{cw}	BOND
FA550-3A	50.76	2420	76.66	41.52	-	FLEX
FA550-3B	51.26	2335	72.79	46.05	-	FLEX
FA550-4A	54.59	2329	69.39	46.26	V_{cw}	BOND
FA550-4B	50.45	2190	78.43	50.06	V_{cw}	FLEX
FA460-1A	31.30	2436	-	-	-	FLEX
FA460-1B	41.52	2574	-	-	-	FLEX
FA460-2A	53.84	2529	81.48	46.68	P=74.1	FLEX
FA460-2B	55.72	2563	83.55	41.78	V_{cw}	BOND
FA460-3A	52.41	2516	-	-	-	FLEX
FA460-3B	59.73	2628	-	-	-	FLEX
FA460-5A	56.46	2592	76.26	46.08	V_{cw}	BOND
FA460-5B	54.62	2549	74.32	43.36	V_{cw}	BOND
FA460-6A	54.25	2563	80.82	45.46	V_{cw}	FLEX
FA460-6B	54.36	2537	80.55	46.99	V_{cw}	FLEX

1. M_{cr}(calc) = 2222 k-in for FA550's; M_{cr}(calc) = 2435 k-in for FA460's
2. V_{cw}(calc) = 40.2 kips for FA550's; V_{cw}(calc) = 42.0 kips for FA460's
3. Honeycomb

In conclusion, these tests demonstrate that web shear cracking precipitates initial bond slip. Even though total bond failure does not always coincide with web cracking and initial bond slip, web cracking does precipitate strand slip. In turn, strand slip increases with

additional load and bond failure will occur. Perhaps, a simpler model for bond failure is given in this statement:

> In tests where web cracking did not occur, bond did not fail; strand anchorage proved to be sufficient to resist external loads and the strand was adequately developed.

4.3.3 Test Results, Rectangular Beams. The rectangular beams were designed and tested to study how different cross sections affect strand development. Specifically, because web shear cracks could not form in these rectangular cross sections, the development lengths could be measured without influence from web shear cracking. Four beams were cast, each had three strands as shown in Figure 4.2, and a total of nine tests were performed on the four beams. Two of the beams contained 0.5 inch strands and two of the beams contained 0.6 inch strands. Test results are reported in Table 4.5. The end slip recorded in plots for these tests and shown in Appendix C is the strand that had the largest slip of the three strands.

TABLE 4.5

SUMMARY OF DEVELOPMENT LENGTH TESTS
RECTANGULAR BEAMS

Test No.	L_e (IN)	M_n(test) K-IN	Mu(test)/ Mn(calc)	Concrete Strain at Ultimate	Failure Mode
FR350-1A	60	1044	0.64	680	BOND
FR350-1B	72	1087	0.67	1408	BOND
FR350-1C	150	1675	1.03	1588	FLEXURAL
FR350-2A	84	1461	0.90	2880	BOND/FLEX
FR350-2B	96	1604	0.98	3100	FLEX/BOND
FR360-1A	96	2010	0.98	3872	FLEXURAL
FR360-1B	96	2015	0:98	3704	FLEXURAL
FR360-2A	84	2039	0.99	4652	FLEXURAL
FR360-2B	78	2111	1.03	4100	FLEXURAL

1. M_n(calc) = 1629 k-in for FR350 series beams. Calculated by strain compatability.
2. M_n(calc) = 2056 k-in for FR360 series beams. Calculated by ACI (18-3).

The first test of the series, FR350-1A, gave a surprising result. Embedment length for the first test was chosen at 60 inches. Flexural failure was expected even though this length was shorter than the 72 inches measured for development length of the AASHTO-

type beams. Because web shear cracking was not a factor for the rectangular beams, 72 inches could be considered an upper limit for the rectangular beams given that test conditions and materials were similar to the AASHTO-type beams. However, the result of test FR350-1A was a bond failure. Interestingly, this was the first bond failure from pure flexural behavior in all of the tests. Additional tension in the strand was imposed from flexural loads only. No increase in tension was required to resist shear cracking as was the case in the FA series. Load versus deflection and end slip is illustrated in Figure 4.17. In this test, bond slip and subsequent bond failure was initiated by a flexural crack at a distance 38 inches from the end of the beam, as noted in the figure. The crack and the slip occurred at the same load increment and it is not possible to determine whether the strand slipped before the concrete cracked or vice versa.

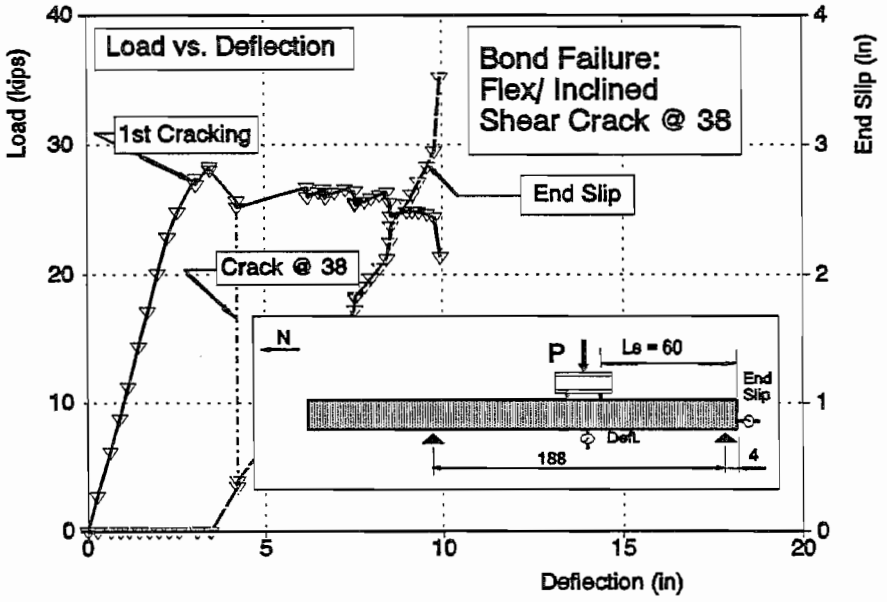

Figure 4.17 Beam FR350-1 Test A: Bond Failure of Rectangular Beam with 0.5 Inch Strands

Interestingly, this crack formed at an applied moment that was less than the cracking moment. The first flexural cracks formed at a load of 27.4 kips in the region near the maximum moment at crack locations 56 inches, 67 inches, and 87 inches from the end of the beam. The moment at first cracking was calculated from statics to be 1010 k-in. The crack at station 38 inches formed at a total load of only 28.3 kips and an applied moment of 634 k-in, less than two thirds of the expected cracking moment. This suggests that the beam suffered from lower precompression in this region. However, if the transfer length was 25 inches or less as it had been in the case of the AASHTO-type beams, the section 38 inches from the end should enjoy full precompression. A photograph of Test FR350-1A is shown in Figure 4.18.

After the second test, FA550-1B, also failed in bond at an embedment length of 72 inches, a third test was performed on beam FA550-1 to determine if flexural failure could be achieved. The third test was to determine ultimate flexural moment, and to study the cracking patterns of a flexural failure. The beam was loaded in the center so the embedment length was 150 inches in either direction. Of course, the beam was cracked from the two previous tests. From the load versus deflection and end slip plotted in Figure 4.19, the beam failed in flexure at the calculated nominal capacity. However, the most interesting result of this test was the cracking pattern, and particularly the crack spacings. For this test, only four flexural cracks were formed, at 58 inches, 64 inches, 81 inches, and 89 inches, measured from the south support. The average crack spacing for this beam was 10.33 inches.

Figure 4.18 Photograph of Cracking at Failure Beam FR350-1 Test A: Bond Failure

Crack spacing is an important indication for determining relative bond strength. Strong bond between concrete and steel results in close crack spacing and a greater number of cracks. Weak bond results in fewer cracks spaced further apart. In beams where smooth wire or unbonded tendons are used for prestressing, only one or two cracks will form. A hinge forms at the crack location and steel tension is not redistributed to adjacent concrete. In beams with stronger bond, the bond stresses relieve the strand tension by redistributing tension into the concrete. This results in more concrete cracks at narrower spacings.

Table 4.6 lists the average measured crack spacings for AASHTO-type and rectangular beams. In the rectangular beams (FR350's and FR360's), crack spacings were larger with 0.5 inch strands than with 0.6 inch strands. Beams with 0.6 inch strand had cracks spaced at only 6.85 inches whereas the beams with 0.5 inch strand had cracks spaced at 11.94 inches, almost twice as much. This is a very strong indication that bond of the 0.5 inch strands was weakened.

In the remaining tests of the FR350 series, embedment length was increased with each test. In the final test, FR350-2B, at an embedment length of 96 inches, the beam failed in flexure. Load versus deflection and end slip is plotted in Figure 4.20. Even in this test,

TABLE 4.6

AVERAGE CRACK SPACINGS DISTANCE BETWEEN FLEXURAL CRACKS
TESTS ON AASHTO-TYPE BEAMS AND RECTANGULAR BEAMS

BEAMS WITH 0.5" STRANDS		BEAMS WITH 0.6" STRANDS	
TEST	CRACK SPACING (IN)	TEST	CRACK SPACING (IN)
FA550-1A	N/A	FA460-1A	N/A
FA550-1B	N/A	FA460-1B	N/A
FA550-1C	N/A	FA460-2A	16.0
FA550-2A	6.6	FA460-2B	11.7
FA550-2B	6.6	FA460-3A	15.5
FA550-3A	10.4	FA460-3B	16.0
FA550-3B	7.3	FA460-5A	12.3
FA550-4A	7.5	FA460-5B	15.0
FA550-4B	8.15	FA460-6A	14.5
		FA460-6B	8.9
FR350-1A	12.3	FR360-1A	6.5
FR350-1B	14.0	FR360-1B	7.1
FR350-1C	10.3	FR360-2A	6.6
FR350-2A	11.7	FR360-2B	7.2
FR350-2B	11.4		
AVG. FR350	11.9	AVG. FR360	6.9

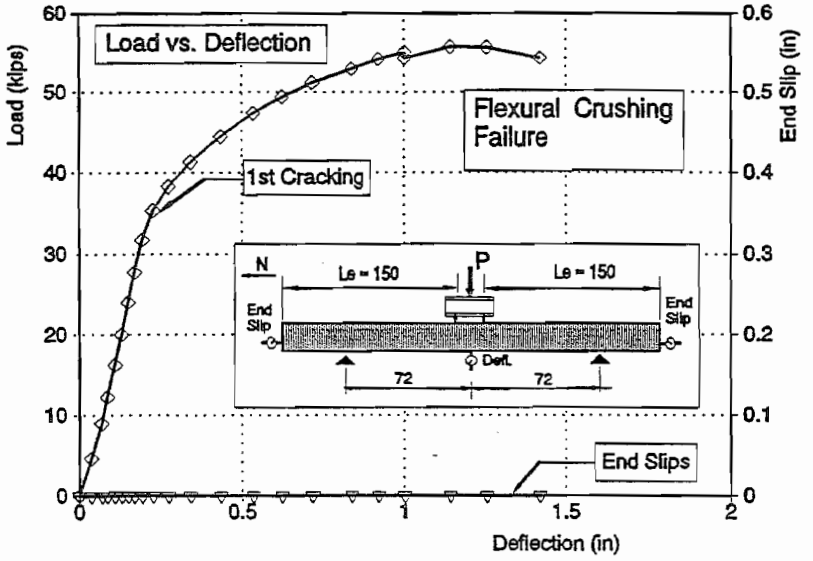

Figure 4.19 Beam FR350-1 Test C: Forced Flexural Failure

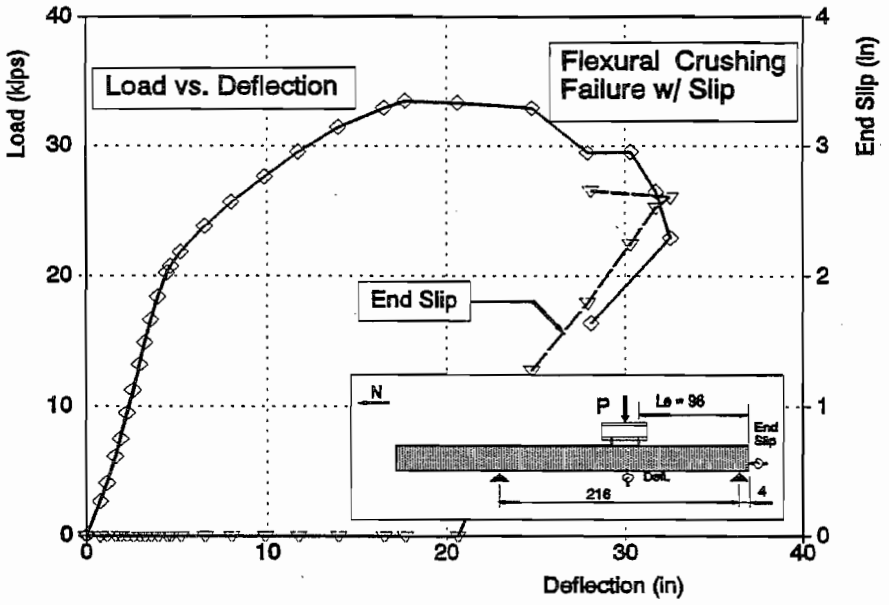

Figure 4.20 Beam FR350-2 Test B: Flexural Failure With End Slip

end slips to 0.25 inches were noted as the beam deformed at ultimate capacity. In fact this test was best be described as a borderline failure because ductility was limited at the ultimate capacity before bond failure occurred. Figure 4.21 is a photograph showing this failure.

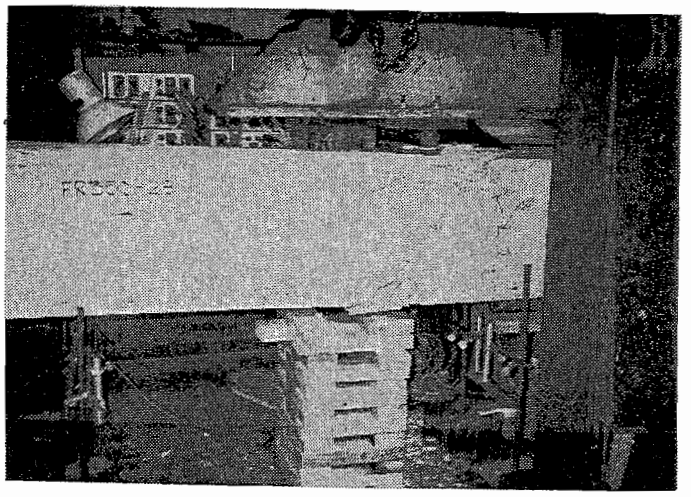

Figure 4.21 Photograph of Beam FR350-2 Test B: Flexural Failure With End Slip

The rectangular beams with 0.6 inch strands (FR360's) behaved similarly to the AASHTO-type girders except, of course, without web shear cracking. Because of the experience from the FR350 series, with 0.5 inch strands, embedment lengths were lengthened for the initial tests. Beam FA360-1A was tested at an embedment length of 96

inches. This corresponds to approximately 1.0 L_d as given by the code equations. Also, this was the required development length from the FR350 series. Test FR360-1A failed in flexure with no end slip. In Table 4.5, the concrete strain at failure was 0.003872 in/in and the moment reached 98% of the calculated capacity. The load versus deflection curve shown in Figure 4.22 has the form of a typical flexural failure for a pretensioned beam.

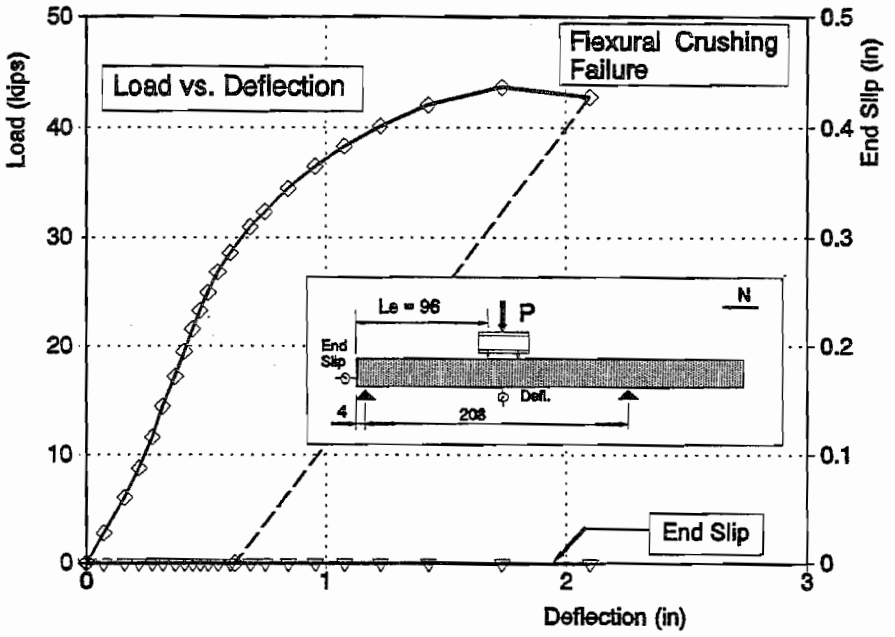

Figure 4.22 Beam FR360-1 Test A: Typical Flexural Failure Rectangular Beams With 0.6 Inch Strands

In test FA360-1B, the same embedment length was tested again because of concern over a splitting crack that had formed upon transfer of the strands' tension. This crack, shown in the photograph of Figure 4.23, formed along the bottom of the beam for a short distance, corresponding to the center strand location. Figure 4.24 plots the load-deflection curve for Test FA360-1B. When this curve is compared to the curve from Test FA350-1A, the curves appear identical for the first 2 inches of deflection. In fact, behavior was exactly the same and no detrimental effects can be attributed to the splitting crack. In Test 1B, loading was continued past concrete crushing, and capacity of the beam was reduced with increased deflection.

For the remaining two tests in the FR360 series, embedment lengths were reduced for each test in an effort to define an embedment length that would cause bond failure. However, both of the remaining tests resulted in flexural failures, meaning that a lower limit for development length was not found. However, it can be said that length of bond required to develop strand tension, at least for this test series, was less than 78 inches. Load versus deflection responses and end slips for the last two tests are plotted in Figures 4.25 and 4.26.

From the AASHTO-type beams, development length for 0.6 inch strands was found to be 84 inches, but for FR360 beams, L_d is less than 78 inches. This demonstrates that the required development length is dependent on properties of the cross section. More specifically, narrower cross sections that are susceptible to web shear cracking require longer development lengths than cross sections that have thicker webs (or no web in the case of rectangular beams).

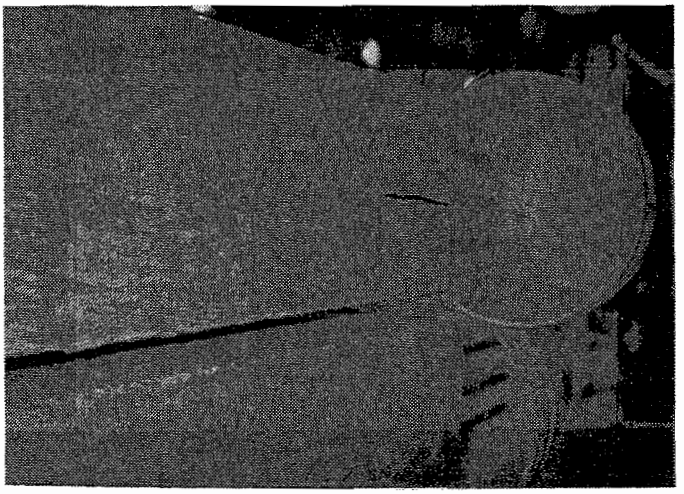

Figure 4.23 Photograph of Splitting Crack, Beam FR360-1A, Before Testing

The tests on rectangular beams are summarized in the graphs in Figures 4.27 and 4.28. The graphs plot failure mode versus embedment length. For the FR350 beams, rectangular cross section with 0.5 inch strands, the required development length was about 96 inches. However, if the bond conditions had been similar to the FA550 series, then the development length could have been much shorter.

For the rectangular beams with 0.6 inch strands, the development length was less than 78 inches. The plots FR360-1A and FR360-1B show very small amounts of end slip, less than 0.01 inches. Greater strand slips were measured in many other tests, even resulting in flexural failure. On the other hand, the presence of some strand slip is significant because it indicates that bond stresses are active along the entire bonded embedment length. Complete bond failure is likely at embedment lengths not much shorter than 78 inches.

4.3.4 Measured End Slips Compared to Transfer Length. The end slip data provides evidence that the bond of the 0.5 inch strands in the FR350 series beams was poor. End slip data measured the amount that a strand slips into the concrete upon release of the pretensioning. End slip has been suggested as an alternative method to measure transfer length. End slip measurements correlate with transfer length; the more a strand slips into the concrete, the longer the transfer length must be. However, these measurements are only indirectly related to transfer length and results cannot be considered as accurate as direct measurements. Because transfer lengths were not measured directly on the rectangular beams, end slips provide the only data to establish the transfer lengths on these specimens.

Figure 4.29 illustrates the relationship between end slip and transfer length. After tensioning and before release, stress in the steel begins at f_{si}. When pretensioning is

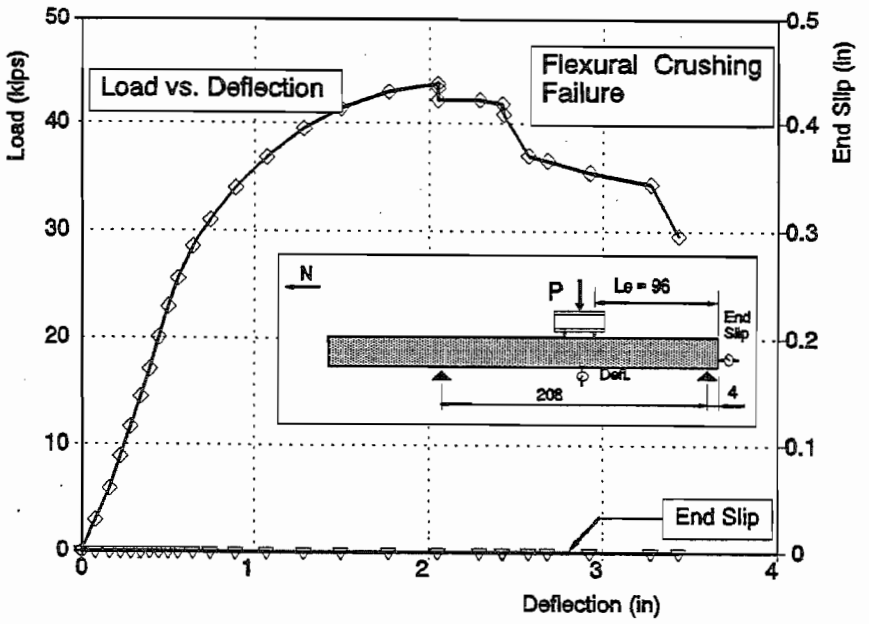

Figure 4.24 Beam FR360-1 Test A: Flexural Failure With Transfer Splitting Crack

released, the steel stress at the end of the concrete is reduced to zero because there is no restraint on the strand at its free end. Through the transfer zone, stress in the prestressing steel, f_{ps}, and stress in the concrete, f_{cc}, increase proportionately. At the end of the transfer zone, L_t from the beam end, there is no slip between the concrete and the steel. Figure 4.29 expresses these concepts in terms of strain which may be easier to understand. Total shortening of the steel is given by the expression:

$$\Delta_{ps} = \int_0^{L_t} \frac{f_{si} - f_s(x)}{E_{ps}} dx$$

and total shortening of the concrete is given by:

$$\Delta_c = \int_0^{L_t} \frac{f_c(x)}{E_c} dx$$

The stress f_c is the concrete stress at the steel centroid.

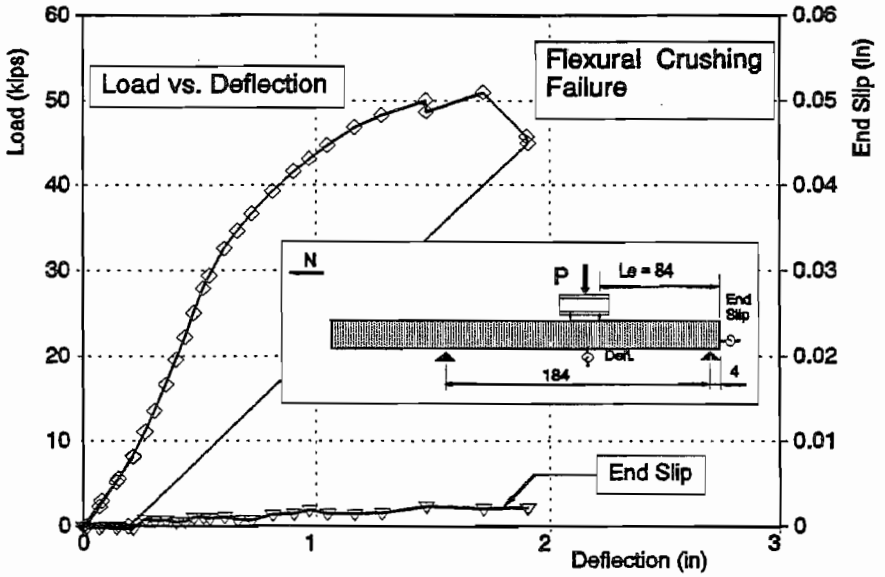

Figure 4.25 Beam FR350-2 Test A: Flexural Failure With Small Strand Slip

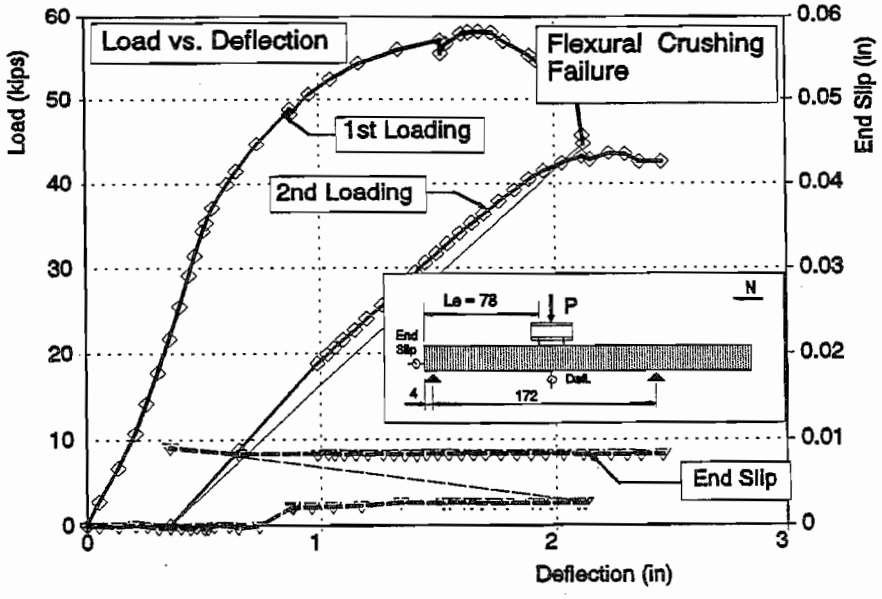

Figure 4.26 Beam FR360-2 Test B: Flexural Failure at Short Embedment With Multiple Loadings

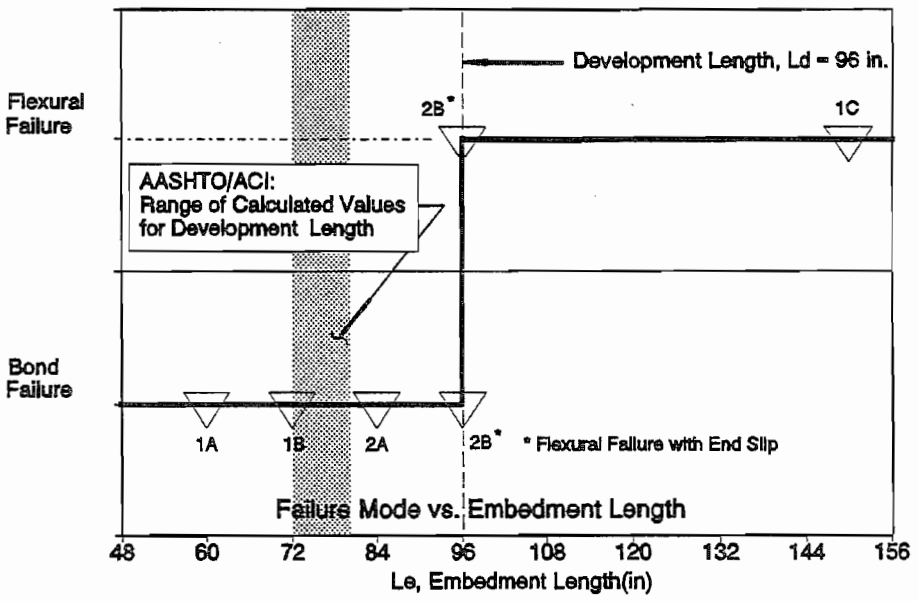

Figure 4.27 Development Length Tests: 0.5 Inch Strands in Rectangular Beams

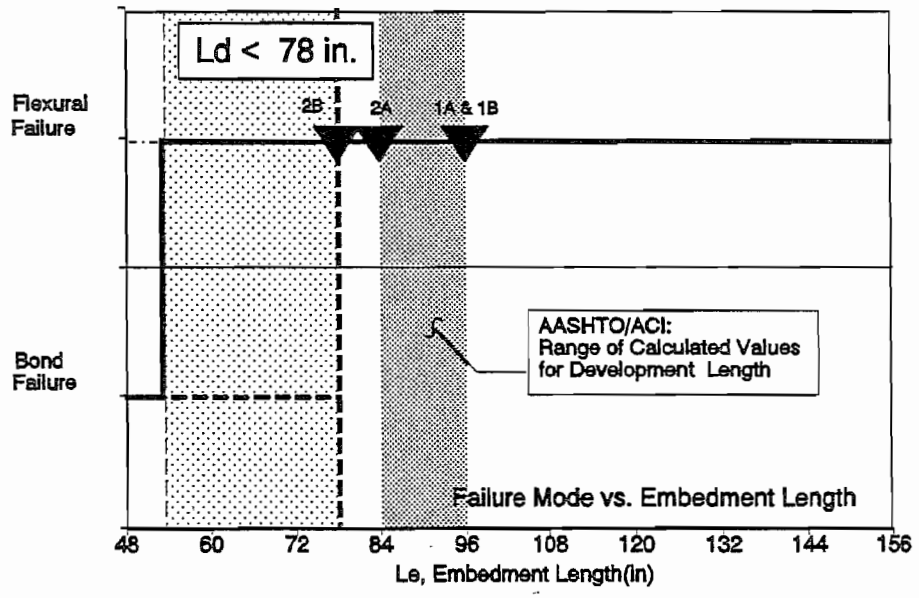

Figure 4.28 Development Length Tests: 0.6 Inch Strands in Rectangular Beams

End slips are approximate measures of transfer length because the concrete and steel stresses as a function of length are not precisely known. However, by reviewing the transfer length data, most of the data approximates linear shapes over large portions of the transfer length. Therefore, the variation of stresses can be taken as linear with respect to length:

$$f_{ps}(x) = \frac{x}{L_t} f_{se} \quad ; \quad f_c(x) = \frac{x}{L_t} f_{ce}$$

If steel stress varies linearly, the concrete stress becomes a simple linear variation of the difference between steel stresses:

$$f_c(x) = \frac{(f_{si} - f_{se})}{E_{ps}} \times \frac{x}{L_t}$$

End slip is the difference between strand shortening and concrete shortening. The end slip is taken as:

$$Slip = \Delta_{ps} - \Delta_c$$

and the relationship between Slip and Transfer Length, L_t can be established:

$$L_t = Slip \times \left(\frac{2 \times E_{ps}}{f_{si}} \right)$$

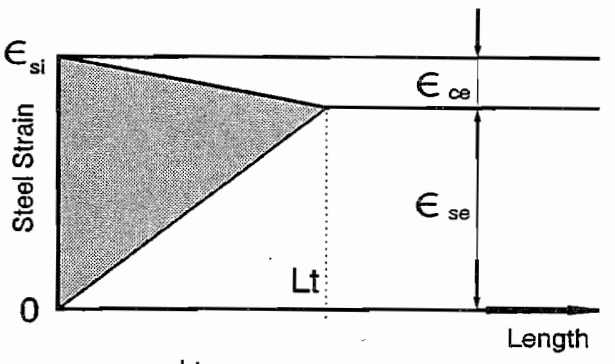

$$\Delta_{ps} = \int_0^{Lt} (\epsilon_{si} - \epsilon_s(x))\, dx$$

$$\Delta_c = \int_0^{Lt} (\epsilon_c(x))\, dx$$

$$\epsilon_c(x) = (\epsilon_{si} - \epsilon_{se}) \frac{x}{Lt}$$

$$Slip = \Delta_{ps} - \Delta_c = \text{Shaded Area}$$

$$Lt = Slip \left(\frac{2\ Eps}{fsi} \right)$$

This figure is reproduced, with some changes, from Reference 51.

Figure 4.29 Transfer Length as a Function of End Slip

Average end slips for each specimen are given in Table 4.7. Also included are the transfer lengths calculated from end slips and the measured transfer lengths reported in Chapter 3.

From Table 4.7, two facts stand out. First of all, the end slips measured on the rectangular beams with 0.5 inch strand, FR350 beams, are much longer than end slips measured on the AASHTO-type girders. The average end slip for the rectangular, FR350, beams was 0.193 inches. For the AASHTO-type girders, FA550, the average end slip was 0.095 inches, less than one half the end slips in the rectangular beams. Secondly, the transfer lengths calculated from the end slips are well over 50 inches. The two beams, FR350-1 and 2 have transfer lengths in the range of 55 inches whereas the AASHTO-type girders have measured transfer lengths of approximately 20 inches.

TABLE 4.7

SUMMARY OF END SLIP DATA AND COMPARISON WITH MEASURED TRANSFER LENGTHS

BEAM	AVERAGE MEASURED END SLIPS (IN)		MEASURED TRANSFER LENGTHS (IN)		CALCULATED TRANSFER LENGTH[2] (IN)	
	NORTH	SOUTH	NORTH	SOUTH	NORTH	SOUTH
FA550-1	0.075	N/A	18	16	21.6	-
FA550-2	N/A	0.088	21	21	-	25.3
FA550-3	0.081[1]	0.100	22	22	23.3	28.8
FA550-4	0.094	0.131[1]	21	21	27.1	37.7
FR350-1	0.188[1]	0.177	N/A	N/A	**55.1**	**51.8**
FR350-2	0.188	0.219[1]	N/A	N/A	**55.1**	**64.2**
FA460-1	0.102[1]	0.094	30	37	29.7	27.3
FA460-2	N/A	N/A	34	37	-	-
FA460-3	N/A	N/A	33	33	-	-
FA460-F4	0.125[1]	0.133	28	29	36.4	38.7
FA460-5	0.125[1]	0.133	32	31	36.4	38.7
FA460-6	0.117	0.086[1]	32	31	34.0	25.0
FR360-1	N/A	N/A	N/A	N/A	-	-
FR360-2	N/A	N/A	N/A	N/A	-	-

1. Ends directly exposed to flame cutting.
2. Transfer Length is calculated from End Slips:
   E_{ps} = Modulus of Prestressing Strand.
   f_{si} = 196 ksi for all of these beams except FR360-1 and 2.

Because the transfer lengths for specimens FR350-1 and FR350-2 extend to over 20 inches, the theory presented in the Section 2.7 from the chapter on Elements of Bond is reinforced. When the rectangular beam cracked at a distance 38 inches from the end of the specimen, that crack propagated across the transfer zone of the strand. When additional tension was required in the strand by the crack, a decrease in strand diameter resulted and Hoyer's Effect was lost. In turn, the loss of Hoyer's Effect caused general bond failure. At this point, the strand slipped through the concrete and the beam failed.

Furthermore, the flexural crack 38 inches from the end of the beam was caused by a moment approximately 2/3 the cracking moment for the fully prestressed beam. The average first cracking moment was 1002 k-in from the three tests on beam FR350-1, yet this crack at station 38 formed at a moment of 634 k-in. Consider the proportions of the two cracking moments compared to the crack location divided by the transfer length.

$$\frac{634\ k''}{1002\ k''} = 0.63 \quad ; \qquad \frac{38''}{55''} = 0.69$$

While these two proportions are not exactly equal, they do demonstrate the relationship between transfer length and cracking moment. In fact, while cracking moment is a linear function of the prestress force, its abscissa is not zero because the unreinforced concrete possesses some tensile strength. In general, resistance to flexural cracking is reduced in the transfer zone of the strands. The cracking moment is a function of the prestress force. If the prestress force is not fully transferred, then the moment that causes first cracking is also reduced and the pretensioned member has less resistance to flexural cracking in the transfer zone than in the regions where prestressed forces are fully effective.

For the 0.5 inch strands, it is clear that the bond was weakened between prestressing steel and concrete. The most reasonable explanation for poor bond performance is that the strand's surface condition must have become contaminated in some manner. Both of the materials used, the concrete and the prestressing steel, were tested and proven through other tests, leaving only the surface condition of the strand to explain the abnormal results. Hoyer's effect is entirely dependent on friction, and to a lesser degree, so is mechanical interlocking. If the coefficient of friction is reduced significantly, then bond stresses will also be reduced.

In the fabrication of all of the test specimens used in this research, no oils were used anywhere near the prestressing bed, just to avoid possible contamination of strand surface. Results from other researchers had sometimes been questioned because oil had been used to oil the concrete forms. If results were unconservative compared to code provisions, then these results were discounted because oil was used on the project.

In the case of specimens FR350-1 and 2, there is some evidence that the strands could have been contaminated with oil or other materials from the laboratory. As stated above, the use of oil was prohibited in the fabrication area of this project. The lone exception came when fabrication of the debonded beams was completed in November of 1990. At that time, a clear lightweight oil was applied to the plexiglass table tops in order to remove concrete laitance. This was done before the project was extended to its fourth year and before the rectangular beams were planned. After approval for additional research was obtained, the strands used in the FR350 beams were placed in the prestressing bed in April of 1991. Although the table tops were wiped clean, no cleaning solvents were used. Some oil could have remained to contaminate the strands. The strands were used in tests on April 24, 1991 to determine the stiffness of the prestressing bed. The strands remained

in place in the prestressing bed until strand tensioning on May 21, 1991 in preparation for casting beams FR350-1 and FR350-2 on May 22. These three strands remained in the prestressing bed for about one month between the testing on April 24 and casting on May 22. In this length of time, it is possible some foreign substances contaminated the strands.

In view of the end slip data, crack spacing and the history of the prestressing bed prior to casting the two FR350 beams, it appears very likely that the strands' surface condition was contaminated in some manner, probably with the oil used to clean the plexiglass; and that this contamination reduced the friction between strand and concrete, significantly affecting the test results. While it is lamentable that these test results are inconsistent with other data, some extremely important facts are dramatized by this accident. Specifically, it should be recognized that form oil is commonly used in the pretensioning plants to preserve the life of the forms. And in the plant production conditions, strand surface contamination seems probable. These test results demonstrate the potential danger to beam performance and strength compared to that expected with clean, fully bonded strands.

4.4 Summary

Altogether, 28 development length tests were performed. Tests included beams with AASHTO-type I-shaped cross sections and also rectangular cross sections. Beams of both cross sections were tested with 0.5 inch diameter strands as well as with 0.6 inch diameter strands. The embedment length was varied for each test. In each test, two types of failure were possible, flexural failure or bond failure. If bond failed at a certain embedment length, then the embedment length was said to be less than the required development length. Conversely, if the beam failed in flexure, then the embedment length was said to be greater than the required development length. Consequently, development length is defined as the embedment length that borders between flexural failure and bond failure.

The development length for 0.5 inch strands in the AASHTO-type beams was determined to be 72 inches. For 0.6 inch strands, the measured development length was 84 inches. Test results are summarized in Figures 4.7 and 4.8 plotting failure mode opposite the embedment length.

In I-shaped sections, web shear cracking was found to precipitate bond failure. Because web shear cracking is discouraged by rectangular cross sections, the rectangular beams with 0.6 inch strands exhibited shorter development length requirements than their I-shaped companions. The development length for 0.6 inch strands in rectangular beams was found to beless than 78 inches. These results are illustrated in Figure 4.28.

In tests performed on rectangular beams with 0.5 inch strands, results did not conform to results from other beam series. In these specimens, the development length requirements were found to be much longer than anticipated. Failure modes versus embedment lengths are plotted in Figure 4.27. However, some other very important

conclusions can be drawn from these tests. Evidence developed from cracking patterns and end slip measurements suggested that these specimens suffered from poor bond. Longer transfer lengths resulted directly in the longer development length requirements.

Finally, these beam tests conformed to the theories put forth in the discussion on elements of bond. In every case, bond failure occurred only after cracks formed in or very near the transfer zone. Once strand anchorage had been disturbed, general bond slip was followed by eventual bond failure. In a few tests, small strand slips were detected without complete bond failure. In those cases, the embedment length was very near the required development length. These small slips are important, however, because they demonstrate that additional bond stresses can be developed beyond initial strand slip and that small strand slips are not always followed by complete anchorage failure.

Distribution of cracking is evidence of mechanical interlocking. As strand tension increases across the concrete crack, mechanical interlocking provides the bond mechanism to resist increases in strand tension. Mechanical Interlocking is highly dependent on friction as evidenced by the abnormally large crack spacings in the FR350 tests. If friction was only a small part of mechanical interlocking, then crack spacing would resemble the other tests more closely.

To summarize development failures, cracking must occur at or near the prestress transfer zone. In the AASHTO-type beams, flexural cracking did not occur near the transfer zones. However, these beams were susceptible to web shear cracking. When web shear cracking propagated through the transfer zone of a strand, that strand slipped through the concrete. In many cases, general development failure resulted. In beams where the web did not crack, these beams invariably failed in flexure.

In rectangular beams, flexural cracking is the only type of cracking likely to occur. Shear cracking is limited to inclined shear cracks originating from flexural cracks. Again, anchorage failures were limited to cases where cracking occurred in the transfer zones of the strands. The rectangular beams with 0.5 inch strands point this out very dramatically. Because the transfer zone was longer than for previous beams, flexural cracking occurred within the transfer zone. Upon the initial flexural crack, bond failure and beam collapse was the result.

Data from these tests, if considered independently, indicated that current code provisions accurately predict the required development length. However, the code provisions do not model the development of strand tension nor overall structural behavior. Code expressions and discussions on strand anchorage are misleading and do not accurately portray the beam behavior noted in these tests. Research at Florida Department of Transportation (FDOT) has demonstrated that bond failures may occur at embedment lengths much greater than the code required development length, given narrower cross sections and/or different loading patterns. From the tests on rectangular beams, new aspects on the development of bond are presented. The 0.5 inch strands contained in the

rectangular beam tests slipped even at lengths exceeding required development length. Conversely, the code provisions are proven conservative when compared to results from the tests on rectangular beams with 0.6 inch strands.

CHAPTER 5
PRETENSIONED BEAMS CONTAINING DEBONDED STRANDS: PREDICTION AND BEHAVIOR

5.1 Introduction

In the construction of pretensioned beams, prestressing strands are concentrated in the bottom of the cross section to provide maximum efficiency to resist flexural loads. Because of the concentration of prestressing forces in the bottom of the cross section, the allowable tensile and/or compressive stresses can be exceeded in the end regions of a beam. In the middle regions of a beam away from the ends, pretensioned stresses are balanced by the dead weight of the member. The traditional method to relieve overstresses in the end regions has been to drape strands upward towards the ends of a pretensioned beam, changing the strands' center of gravity, and effectively reducing concrete stresses in these cross sections.

The debonding, or blanketing of strands is an alternative to draping strands in an effort to control the maximum tensile and compressive stresses in pretensioned concrete highway girders. Debonding, by definition is the intentional breaking of bond between prestressing strand and concrete. This can be done by applying grease to the strands in the regions requiring debonding, however, the most common practice is to wrap specially made split plastic tubing which can snap around the strand, and prevent bond of the strand to the concrete. Debonding strands can simplify girder construction; draping of strands is more difficult and more dangerous. Debonded strands likewise enjoy economic advantages compared to draped strands.

Rules governing the use of debonded strands have been established more on the basis of engineering judgement than on experimental data. Under current code provisions, the required development length for debonded strand is twice the basic development length, except when zero concrete tension is allowed under service load conditions. These provisions are to prevent beam failure due to special behavior associated with debonded strand, most notably the possibility of bond failure and subsequent reduction in strength of the member.

A series of static flexural tests were performed on beams containing debonded pretensioned strands. An analytical model was developed that predicts anchorage failure based on the propagation of cracks in the transfer zone of the debonded strands. Test results demonstrate remarkable correlation with the predicted behavior. From the tests discussed in this study and further development of the models predicting bond failure, design of pretensioned beams with debonded strands should prove to be both economical and safe.

5.2 Current AASHTO and ACI Code Requirements

Current code provisions of ACI and AASHTO governing the use of debonded strands are again nearly identical. The code provision is repeated here:

> *ACI Section 12.9.3 - Where bonding of a strand does not extend to end of member, and design includes tension at service load in precompressed tensile zone, as permitted by Section 18.4.2., development length specified in Section 12.9.1 shall be doubled.*

Note: The basic development length is given in section 12.9.1 as:

$$L_d = (f_{ps} - \frac{2}{3} f_{se}) d_b$$

Therefore 1.0 $L_d \approx$ 80 in. and 2.0 $L_d \approx$ 160 in. for 0.5 inch strands.

This provision requires that debonded strands must be bonded for a length equal to twice the required development length for fully bonded strands. An exception is made if the beam is designed so that no bottom fiber tension is allowed at service load.

The code provisions reflect the behavioral uncertainty that surrounds debonded strands. Even though AASHTO specifications allow debonded strands, many states do not allow their use because they fear that debonding strands significantly weakens the pretensioned beam. The State of Texas currently does not allow debonded strands as an alternative to draping for I-shaped girders, but does employ debonded strands in box shapes and other cross sections.

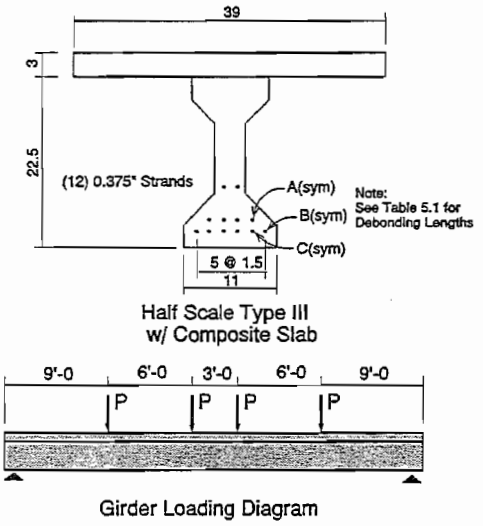

Figure 5.1 Tests on Beams With Debonded Strands; Kaar and Magura (1965)

5.3 Review of Related Research

Current standards for the development of debonded strands grew from the results of three research projects conducted over a fifteen year period from 1965 to 1979.

5.3.1 Kaar and Magura, 1965.[11] Kaar and Magura[11] tested three half scale AASHTO Type III girders to study flexural behavior. The beams contained 3/8 inch diameter strand. Cross sectional properties and loading arrangement is shown in Figure 5.1. Construction was composite as the deck slab was cast upon a precast pretensioned girder.

TABLE 5.1

SUMMARY OF TEST RESULTS
ON
BEAMS WITH DEBONDED AND FULLY BONDED STRANDS

KAAR AND MAGURA (1965)

BEAM	LOAD CYCLES	DEBOND PATTERN	FAILURE MODE
BEAM 1	5,000,000	FULLY BONDED	FLEXURE
BEAM 2	5,000,000	PARTIALLY BLANKETED	FLEX/SLIP
BEAM 3	5,000,000	FULLY BLANKETED	BOND
BEAM 4	1	FULLY BONDED	HOR. SHEAR
BEAM 5	1	PARTIALLY BLANKETED	FLEXURE

DEBONDING PATTERNS
DEBOND LENGTHS OF DEBONDED STRANDS

	STRAND A	STRAND B	STRAND C	Embedment % L_d
FULLY BLANKETED GIRDER	3'-11	6'-11	10'-11	1.0
PARTIALLY BLANKETED GIRDER	-	2'-4	6'-4	2.0
FULLY BONDED GIRDER	-	-	-	2.5

The first girder functioned as a control girder and all strands were fully bonded from the ends of the beam. The second girder was termed "partially debonded" by the authors. Strands in this girder were embedded a distance twice the required development length, or 2.0 L_d from the point of maximum moment. In the third girder, the strands were "fully debonded" meaning that the embedment of debonded strands was equal to one times the required development length, or 1.0 L_d from the point of maximum moment region. Table 5.1 provides the debonded lengths for the different test cases. Ultimate strength of the strands was 250 ksi. Strand stress after tensioning was 175 ksi. The effective prestress was assumed to be 140 ksi.

All three girders were loaded to the design live load for 5 million cycles and then tested statically until failure. Design live load was defined by the allowable tension stress of $3\sqrt{f'_c}$ allowed by the 1961 AASHTO Specifications for Highway Bridges. Load versus deflection was nearly identical for all three beams throughout fatigue loading. No end slips were detected under the fatigue loading in any of the tests. However, in the static tests to ultimate, the beams behaved quite differently. In the first beam with fully bonded strands, the beam was loaded until it failed in flexure by rupturing of the strands. No end slips were detected. The second beam, with partially debonded strands, also failed in flexure by rupturing of all prestressing strands. However, very small slips were measured on the debonded strands. In the third beam, anchorage of the debonded strands failed completely, as evidenced by the pulling of the strands through the concrete at failure. These results are summarized in Table 5.1.

In all three beams, behavior was similar until flexural cracking. Upon cracking, however, the debonded strands slipped through the concrete by various amounts. In the third beam, the debonded region of the strands extended into the cracked regions of the beam, and anchorage failure could be expected.

Two additional tests were performed with varying amounts of shear reinforcement, but with identical longitudinal reinforcement as the first three beams. The purpose of these tests was to assess the impact of debonding on shear capacity. Beam 4 contained fully bonded strand and beam 5 contained partially bonded strand, or strand with an embedment length twice the required development length, $L_e = 2.0\ L_d$. Vertical shear reinforcement for these two girders was reduced. In all of the beams, stirrup spacing was 50% greater than the requirement from AASHTO codes, so these beams were under-reinforced when compared to code requirements. Interestingly, beam 5 had slightly more shear reinforcement than beam 4 because of differences in pretensioned force. Beam 4, the fully bonded beam, failed in horizontal shear failure at the intersection between the beam's bottom flange and the beam's web. Beam 5 failed in flexure by fracture of the strands.

The beam with debonded strands whose bonded length was twice the required development length performed as well or better than the beam with fully bonded strands. Based on these tests, the AASHTO and ACI codes currently allow the use of debonded strands, but doubled the required development length for debonded strands. These tests demonstrated that debonded strands could be safely incorporated into the design of pretensioned beams. However, the conditions of the test were very specific and no general conclusions could be made about factors governing behavior of beams made with debonded strands.

5.3.2 Dane and Bruce, 1975.[17] Dane and Bruce performed a series of flexural tests on nine pretensioned beams. Six of the beams were composite half scale AASHTO Type III girders while the remaining three were full sized composite AASHTO Type II girders. The half scale girders contained 3/8 inch strand and the Type II girders contained 7/16 inch strands. In the series of six half sized Type III beams, the first pair of beams contained

draped strands to provide control for the experimentation. In the next pair of beams, 17% or two out of twelve strands were debonded. In the last pair of beams, an anchor plate was secured to debonded strands to aid in strand anchorage.

TABLE 5.2

FLEXURAL TESTS ON GIRDERS WITH DEBONDED STRANDS

DANE AND BRUCE(1975)

Girder	Type[1]	Span, L (ft-in)	Strand Size (in)	Debonding		Le[2] (ft-in)	Web Shear	Max. Slip @ Failure (in)
				Number	L_b (ft-in)			
G1	III	33'-0	3/8	None	Draped	11'-6	No	0
G2	III	33'-0	3/8	None	Draped	11'-6	No	0
G3[3]	III	33'-0	3/8	2 of 12	9'-8 1/2	1'-9 1/2	Yes	1.44
G4[3]	III	33'-0	3/8	2 of 12	9'-8 1/2	1'-9 1/2	Yes	1.70
G5	III	33'-0	3/8	2 of 12	9'-8 1/2	1'-9 1/2	Yes	0.88
G6	III	33'-0	3/8	2 of 12	9'-8 1/2	1'-9 1/2	Yes	1.05
G7	II	48'-0	7/16	4 of 22	Draped	5'-0	No	0
G8	II	48'-0	7/16	4 of 22	12'-0	5'-0	Yes	0.193
G9	II	48'-0	7/16	4 of 22	12'-0	5'-0	Yes	0.234

1. Type III girders were half sized. Type II girders were full sized.
2. Le = 21.5 inches is also the calculated ***transfer*** length for 3/8" strands.
   Le = 60 inches is the calculated ***development*** length for 7/16" strands.
3. Anchor plates attached to the debonded strands.

In the three Type III specimens, one beam contained fully bonded strands while the remaining two contained debonded strands. These beams each contained 22, $^7/_{16}$ inch diameter strands. Of those, 4 strands were debonded. Table 5.2 gives a general description of the test variables for each specimen. Figure 5.2 shows the test setup. Note that the embedment lengths, L_e, are inconsistent. For the 3/8 inch strands used in the half sized Type III girders, the embedment length actually equaled the calculated transfer length, L_e = 21.5 inches. For the Type II girders with $^7/_{16}$ inch strands, the embedment length equaled the calculated development length from the code equation, L_e = 60 inches = 1.0 L_d.

The girders were loaded statically until failure. All of the beams failed in flexure by crushing the concrete in compression. Significant end slips were measured on each of the debonded strands. End slips ranged from 0.1 inches to 0.88 inches. These are relatively large end slips and were caused by flexural cracking in the region where the debonded strands were being anchored and transferred. In spite of these measured strand slips, each specimen achieved its nominal capacity and each specimen maintained its resistance to load

through large deformations. As such, the failures must be considered flexural failures. However, a relatively low percentage (17% or 18%) of strands in these beams were debonded. If more strands had been debonded, anchorage failure of the strands is more probable.

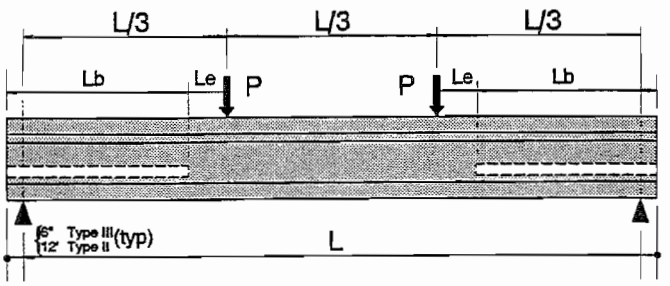

Figure 5.2 Flexural Tests on Composite Girders With Debonded and Draped Strands; Dane and Bruce (1975)

Again, these tests demonstrate that debonded strands can be safely incorporated into design of pretensioned beams. However, these tests are also quite specific and results from these tests cannot be generalized into broader design applications.

5.3.3 Rabbat, Kaar, Russell and Bruce, 1979.[23,25] In 1979, the Precast/Prestressed Concrete Institute (PCI) sponsored a series of tests on six full sized AASHTO Type II girders, each 50 feet long. Two of the girders contained draped strands while the other four had blanketed strands. Strands were 7/16 inch grade 250 ksi, stress relieved and with brown surface rust. Specimens were fatigue loaded with 5 million cycles at the full dead load plus live load. At the conclusion of 5 million cycles, specimens were loaded statically until failure.

The test series compared performance of specimens with debonded strands to those with draped strands. Additional variables included the embedment length of the debonded strands and the bottom fiber tension at service loads. Table 5.3 outlines the variables for each of the six specimens. The first group of three beams were fatigue loaded at the equivalent service load to give a maximum tensile stress equal to $6\sqrt{f'c}$ at the bottom fiber. All of these tests resulted in fatigue failure of the strands. The measured stress ranges (measured by strain gages attached to strand) in these three specimens ranged from 14 to 20 ksi.

Specimen G11 had an embedment length equal to only 1.0 L_d whereas specimen G13 was provided with twice the embedment length, equal to 2.0 L_d. Initial strand slip in G11 was larger than strand slip in G13. Researchers also noted that strand slips in G11 progressively increased through repeated load cycles. On the other hand, strand slips in G13 were relatively stable through the repeated load cycles. From these results, researchers concluded that an embedment length of 2.0 L_d was sufficient whereas an embedment length of 1.0 L_d was insufficient. However, it is difficult to draw any conclusions from these data. End slips from both specimens G11 and G13 were relatively small and should not overshadow the true cause of failure which is strand fatigue.

TABLE 5.3

SUMMARY OF FATIGUE TESTS
ON GIRDERS WITH DEBONDED STRANDS

RABBAT, KAAR, RUSSELL, AND BRUCE (1979)

Specimen Number	Maximum Tensile Stress[1]	Embedment Length % L_d[2]	Confining Reinforcement	Number of Cycles (10^6)	Failure Mode	Maximum Stress Range[4]	Maximum Strand Slip
G11	$6\sqrt{f'_c}$	1.0	No	3.78	Strand	18.2	0.026
G13	$6\sqrt{f'_c}$	2.0	No	3.20	Fatigue	20.1	0.006
G10	$6\sqrt{f'_c}$	Draped	No	3.63	Strand Fatigue Strand Fatigue	19.0	-
G14[3]	0	1.0	Yes	5.00	Flexure	13.4	0.005
G12[3]	0	1.0	No	5.00	Flexure	15.5	0.015
G10-A[3]	0	Draped	No	5.00	Flexure	-	-

1. Computed on the uncracked section.
2. 1.0 L_d = 66 inches (f_{ps} = 243 ksi and f_{se} = 140 ksi; d_b = 7/16")
3. Specimens were precracked before fatigue loading.
4. Stress ranges were measured with Electrical Resistance Strain Gages.

By comparison, tests G12 and G14 provided sufficient achorage to develop the strand under repeated loadings. These two specimens also had an embedment length equal to one development length, L_e = 1.0 L_d, however, the maximum load was smaller and produced zero tension on the bottom fiber. In these tests, small end slips less than 0.015 inches were observed under repeated loading as reported in Table 5.3. However, in the ultimate load test to failure, significant strand slips occurred. Debonded strands slipped more than 0.5 inches. In spite of strand slip, the beams failed by flexure at the beams' nominal capacity, so these tests must be ruled as flexural failures.

Figure 5.3 illustrates the loading arrangement in elevation, the location of crack formers, and the extent of debonding for the reference test series. The required development length for these strands was calculated to be 66 inches. The embedment length for the debonded strands is 66 inches, provided from the point of maximum moment. With debonding extending to this location, flexural cracking occurred in the transfer zones for the debonded strands. The measured end slips on specimens G12 and G14 were caused by cracking in the debonded strands' anchorage

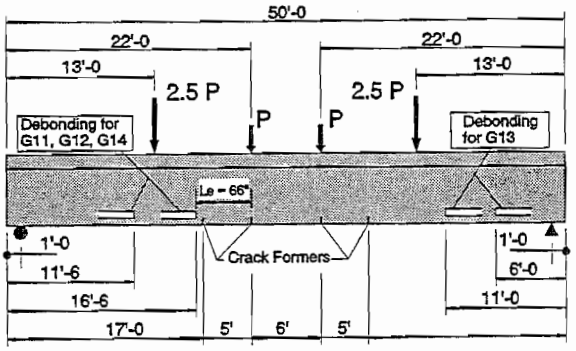

Figure 5.3 Fatigue Tests on Debonded Girders; Rabbat, Kaar, Russell and Bruce (1979)

zones. The large reported end slips at ultimate are an indication of impending bond failure of the debonded strands.

From these tests, code provisions were relaxed to allow the required development length for debonded strands to be reduced to 1.0 times the required development length if tension is not allowed in the cross section. The tests demonstrated that the requirement to double development length may be too excessive under very specific conditions. However, it is interesting that the code provisions were relaxed based on these somewhat confusing results. In comparing G11 and G13, end slips were small for both specimens. The true of failure in both specimens was strand fatigue. Also, even though flexural failures did occur on specimens G12 and G14, large end slips indicate that these results too are somewhat inconclusive, and that bond failure may occur in similar tests under different conditions.

5.4 Theoretical Development

The original purpose of this research was to develop design guidelines governing the use of debonded strands in pretensioned beams. In developing this portion of the research program, the first step was to characterize the behavior that distinguishes debonded beams from fully bonded beams. Certain mechanisms can be expected to affect the behavior of debonded beams more than fully bonded beams. The special provisions in the code have grown out of the recognition that beams containing debonded strands behave differently than beams with fully bonded strands.

In beams with debonded strands, the effective prestressing force is reduced in the end regions of the beams. This characterizes debonded beams and forms part of the basis for a rational model that predicts the behavior of beams with debonded strands. Additionally, it must be recognized that the formation of cracks through a strand's anchorage zone causes that strand to slip with the distinct possibility of complete bond failure. The relationship between cracking and bond slip is an important consideration in developing a rational theory of expected behavior.

A theory was developed that predicts the type of failure a pretensioned element is likely to experience, flexural failure, bond failure, or shear failure. The model that grew from the analytical development is easily understood because it is based on common and well understood behavioral principles. Tests performed in this test series substantiate the model. The behavioral mechanisms that led to development of a simple analytical model to predict anchorage failures are contained in the next several paragraphs.

The model was also used to design the beams for this test series. The purpose of this portion of the research was to develop design guidelines for the use of debonded strands in pretensioned girders. To accomplish this goal, the tests were planned with the intention that all the potential behavioral and failure mechanisms that might characterize beams with debonded strand would be demonstrated. By observing the full range of behavior during testing, it was hoped that any design guidelines developed in this research would be

comprehensive in nature, and that these design guidelines would be applicable to the wide variabilities that distinguish actual design situations.

5.4.1 Influence of Cracking on Bond. When a crack forms in concrete, tension in the pretensioned steel increases to resist the tensile forces. Local bond slip of the strand must occur over some finite distance immediately adjacent to the crack. Furthermore, the total amount of slip between concrete and steel, summing slip from both sides of the crack, must approximate the crack width. At the crack location, tension in steel increases while stress in the concrete is relieved. The additional tension in the steel is restrained by bond stresses between the concrete and the steel. The length of bond slip is equal to the length over which the increased tension in the steel is equilibrated by bond stresses.

In pretensioned beams, anchorage failure will occur when a crack forms within or very near the transfer zone of a strand. As the concrete cracks, tension in the strand across that crack must increase. As strand tension increases, strand diameter decreases. The strand's lateral expansion that occurred at transfer is negated, and the transfer bond from Hoyer's effect is lost, at least locally, as discussed in Chapter 2. As Hoyer's effect disappears, the strand will slip through the concrete. Upon increased loading, the anchorage can be expected to fail completely. This relationship between cracking, bond slip, and failure is established in the series of development length tests on fully bonded beams, discussed in Chapter 4. Additionally, the research discussed earlier in this chapter reports strand end slips at the onset of cracking in the anchorage zone of the debonded strand.

Therefore, the model for bond failure of debonded prestressing strands is directly related to a prediction for cracking in the debond/transfer zone of prestress concrete girders. Because cracking in concrete can be reliably predicted, bond failure of the prestressing strand can also be predicted.

5.4.2 Debonding: Lower Effective Prestress Force. When some of the strands are debonded, the effective prestress force is smaller in the end regions of a beam compared to the middle regions of a beam. This is demonstrated in Figure 5.4, where the effective prestress force is plotted along the length of the beam. For easier explanation, the example is taken from specimens designed for this test series. Each of the beams contained a total of eight strands, four of which were debonded. The length of debonding (L_b) is 78 inches. The effective prestress force at the end of the beams is zero. Over the first 25 inches, the prestress force increases from zero to 98 kips. This increase represents the transfer of the four fully bonded strands. The effective

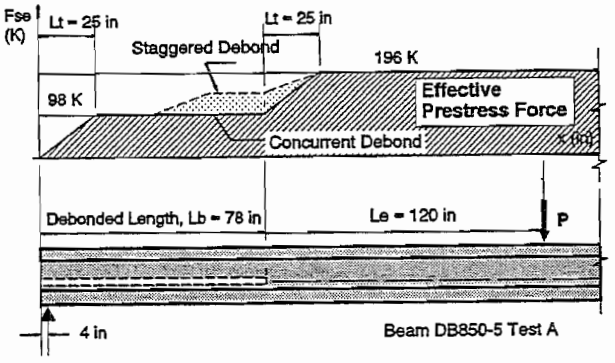

Figure 5.4 Effective Prestress Force (Beams With Debonded Strands)

prestress is about 160 ksi, and each 0.5 inch strand carries about 24.5 kips of tension. From 25 inches to 78 inches, the prestress force remains constant at 98 kips.

At the point where debonding terminates, 78 inches from the end, the debonded strands begin to transfer their prestressing force into the concrete. This is evidenced by the second transfer zone illustrated by an increase in prestress force from 98 kips to 196 kips. The second transfer zone is also shown to be 25 inches long, beginning at 78 inches and extending to 103 inches from the end of the beam. The transfer length assumed for these models is 25 inches, an approximate average of the measured transfer lengths discussed in Chapter 3. For the AASHTO-type beams, the measured transfer length was actually less than 25 inches in some cases, but much greater in others. It should be noted that longer transfer lengths could adversely affect a beam's behavior because the region of reduced prestress is extended towards the middle of the beam.

In the figure, a dashed line is shown indicated by "Staggered Debond." The solid line is denoted by "Concurrent Debond." In beams with staggered debonding, the termination point of various strands are "staggered," meaning that the debonded length varies from strand to strand. In concurrently debonded beams, the termination point is the same for all of the debonded strands. Staggered debonding is recommended based on tests performed in this research because the beam's behavior is significantly improved over concurrent debonding.

For example, Test Specimen DB850-5 has concurrently debonded strands. In this specimen, all of the debonded strands are debonded the same length, L_b = 78 in. Debonding on all four debonded strands is terminated concurrently at 78 inches from the end. On the other hand, Test Specimen DB850-4 has debonded strands that are staggered. In this specimen, two of the debonded strands are debonded a length of 39 inches whereas two of the strands are debonded a length of 78 inches. The debond length, L_b is listed as 78 inches for both specimens; however, the behavior of concurrently debonded specimens is quite different from specimens with staggered debonding. For the purposes of these tests, they illustrate some of the special problems inherent with concurrently debonded specimens.

5.4.3 Debonded Strand: Effects on Flexural Cracking Moment. The impact of debonding is shown in Figure 5.5. Applied moment is compared to the beam's cracking moment, M_{cr}. As shown in the figure, the cracking moment varies with the effective prestress force. The cracking moment is defined as the applied moment that is required to crack the bottom tension fiber of the cross section in flexure. It is a property of the beam and is dependent on the cross section properties and the effective prestress force. Cracking moment varies with prestressing force along the member length. The cracking moment is reduced in the debond/transfer zone in proportion to the effective prestress force. Note again the difference between the "concurrently debonded" specimens and the "staggered debonded" specimens.

At the end of the beam, the effective prestress force is zero and the cracking moment is given by the section modulus times the modulus of rupture; $M_{cr} = S_b \times 7.5\sqrt{f'_c}$. Outside the initial transfer zone, M_{cr} remains approximately constant until the debonded strands become bonded and additional prestressing force is transferred to the concrete. At the end of the second transfer zone, the beam enjoys the fully effective prestress force from all its strands. Not until this point does the beam's resistance to flexural cracking reach its full potential.

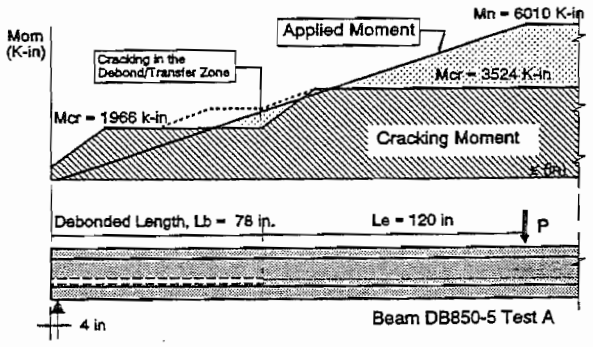

Figure 5.5 Applied Moment vs. Cracking Moment (Beams With Debonded Strand)

As load is applied to the beam, the moment varies linearly from the support to the load point (dead load moment is neglected.). As the load increases the moment also increases. Flexural cracking can be expected wherever the applied moment exceeds the cracking moment. From Figure 5.5, cracking will occur first in the regions of the largest applied moment, near the load point. As load increases, the region of flexural cracking expands with the region where moment exceeds M_{cr}. The region of the beam with flexural cracking moves towards the support as load is increased.

In a beam with fully bonded strands, only one region of flexural cracking would be expected. However, in beams with debonded strands, concrete in the debond/transfer zone could also suffer flexural cracking because the beam's resistance to flexural cracking is reduced. With additional increase in load and applied moment, the next region where flexural cracking could be expected is at the point where the debonding is terminated. In this example, the cracking moment for the debond/transfer zone is exceeded before the nominal flexural capacity of the section is achieved. Cracking in the transfer zone of the debonded strand will cause the debonded strands to slip and bond failure is probable. According to the model, bond failure of the debonded strand will occur.

The dashed line for cracking moments with staggered debonding is also shown in Figure 5.5. It should be noted that staggered debonding avoids cracking in the debond/transfer zone for the example shown.

5.4.4 Effects of Debonding on Web Cracking Shear. Just as the M_{cr} is reduced in the debond/transfer zone, the resistance to web shear cracking is also reduced. Prestressed concrete beams derive much of their resistance to web shear from the precompression of the concrete. Because web shear cracks result from exceeding the tensile strength of the concrete on an inclined plane, precompressing the concrete increases resistance to inclined tensile cracking. Similarly, debonding prestressing strands reduce a beam's resistance to web shear cracking in the debond/transfer zone because the effective prestress force has been

reduced. Therefore, beams with debonded strands are more susceptible to web shear cracking and consequently more susceptible to bond failure.

In Figure 5.6, applied shear is compared to the beam's resistance to web shear cracking, V_{cw}. In the debond/transfer zone, the reduced effective prestress likewise reduces the beam's resistance to web shear cracking. V_{cw}, like a beam's resistance to flexural cracking, is a property of the beam and is dependent on the beam's cross section and the effective prestress force. The applied shear, V_u, is constant from the load point to the support. If the applied shear exceeds V_{cw} then web shear cracking can be expected. Because applied shear is approximately constant over the shear span, any web shear cracking will most certainly affect the transfer zone of debonded strands.

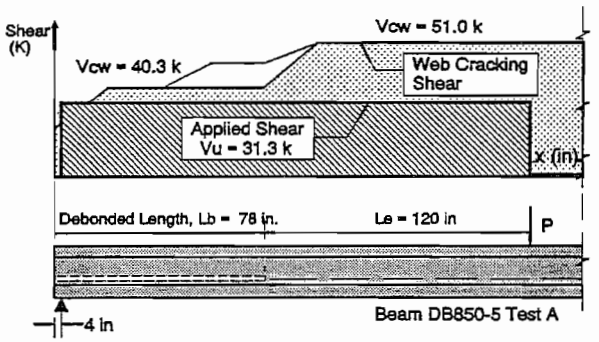

Figure 5.6 Applied Shear vs. Web Cracking Shear (Beams With Debonded Strand)

In the fully bonded development length tests, anchorage failures were caused, in large part, by web shear cracks propagating through the transfer zone of prestressing strand. In debonded beams, web shear cracking will have the same effect, and web shear cracking through the transfer zone of a strand will cause bond failure.

5.4.5 Bond Failure Prediction Model. From the preceding sections, it is shown that the effective prestress force reduces a beam's resistance to both flexural cracking and web shear cracking. In turn, any cracking in the transfer zone of a strand will cause that strand to slip or bond to fail. It follows that if these principles are applied to design, bond failures can be prevented. To prevent bond failure, the member can be designed so that it does not crack in the anchorage zone of debonded strands.

In Figures 5.7a through 5.7d, the model for prediction of cracking and bond failure is depicted. Embedment length is plotted versus the debonded length. The lines intersecting the plot are boundary lines separating different zones of behavior. The boundary lines are derived from behavioral models. For presentation of the prediction model, beam cracking strengths and ultimate strength are taken from the test series. Those properties are listed here:

M_{ult} = 6010 k-in
M_{cr} = 3524 k-in
M_{cr4} = 1966 k-in
V_{cw} = 51.0 kips
V_{cw4} = 40.7 kips

Note: M_{cr4} and V_{cw4} are values for the debonded regions where only four strands are effective.

In Figure 5.7c, line OA represents the applied moment that divides bond failure from flexural failure. This line intersects the origin and the point where flexural cracking will occur in the transfer zone of a debonded strand. If the line were moved to the right, or in other words, if the strand's embedment was lengthened, then the beam would fail in flexure; strand anchorage would be undisturbed. If the line were moved to the left, then the concrete would crack in the anchorage zone of the strand and bond failure would be expected. This boundary is defined by the relationship:

$$\frac{M_{cr4}}{L_b} = \frac{M_{ult}}{L_b + L_e}$$

By substituting M_{ult} and M_{cr4} with appropriate values, then the equation relating L_e to L_b is established:

$$L_b = 0.486\ L_e$$

In the bond failure prediction model shown in Figure 5.7a, this relationship is given by line OA. This line is the boundary separating flexural failure from bond failure for beams with concurrent debonding (debonding terminating at the same point for all strands). Combinations of embedment length, L_e and debond length, L_b to the right of the line predict flexural failures. Values for L_e and L_b to the left of the line predict bond failures.

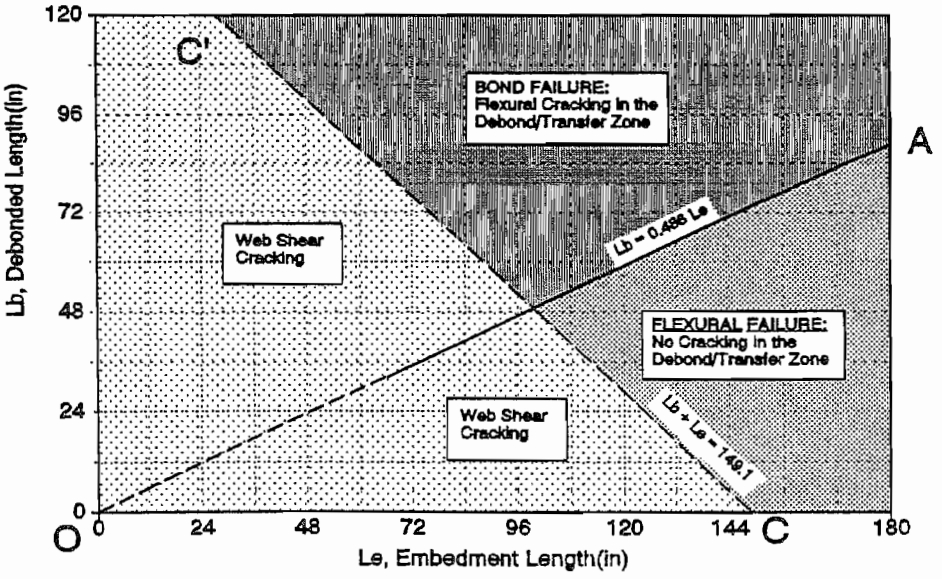

Figure 5.7a Prediction of Cracking and Bond Failure (DB850 Test Series: Beams With Debonded Strands)

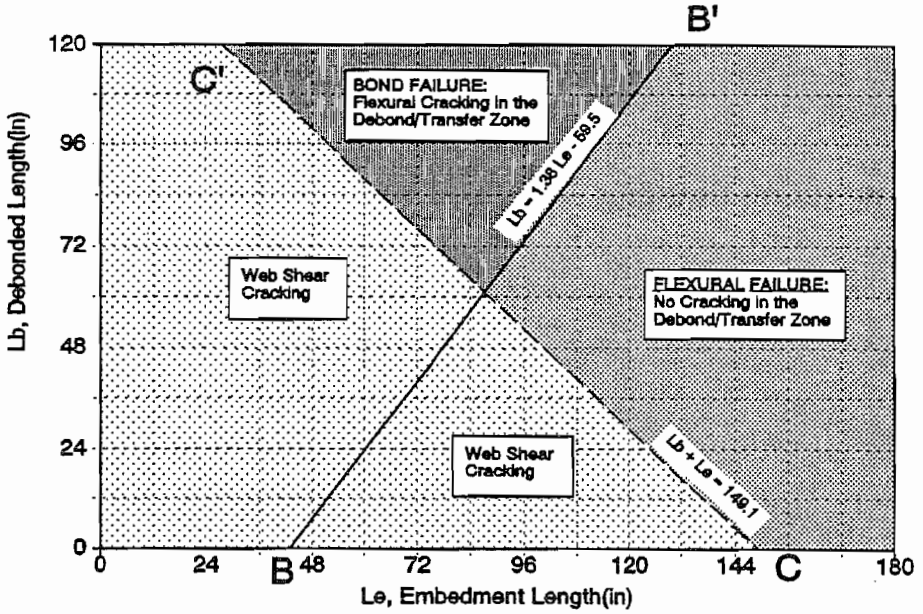

Figure 5.7b Prediction of Cracking and Bond Failure (DB850 Test Series: Beams With Debonded Strands)

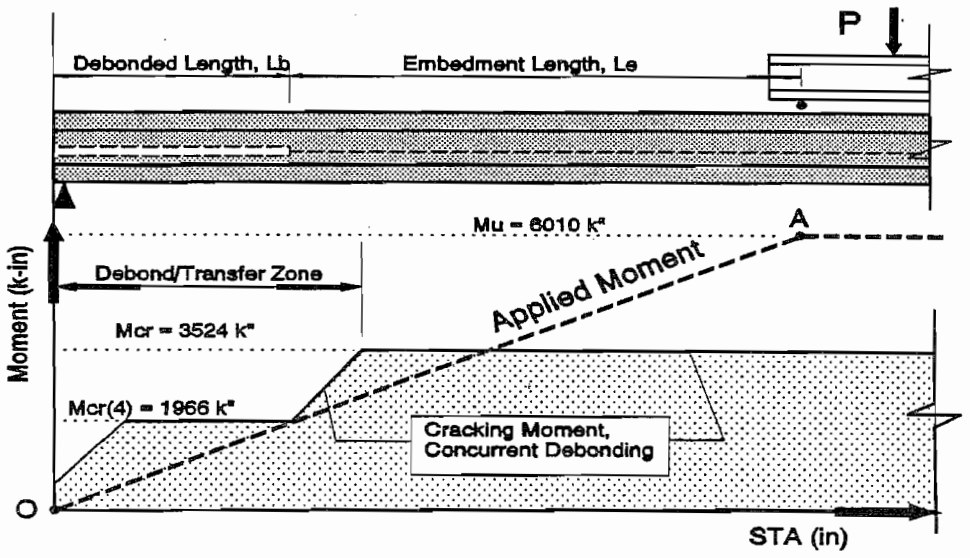

Figure 5.7c Applied Moment vs. Cracking Moment (Beams With Concurrent Debonding)

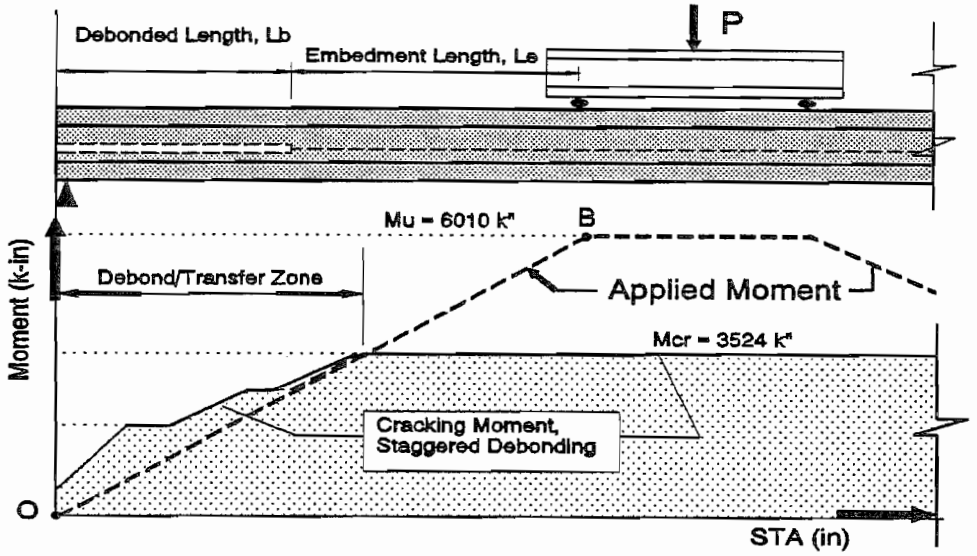

Figure 5.7d Applied Moment vs. Cracking Moment (Beams With Staggered Debonding)

Similarly, a relationship can be established separating bond failure from flexural failure for staggered debonding. In Figure 5.7d, this condition is given by line OB. Line OB is defined by the point where the resistance to flexural cracking attains its maximum at the end of the transfer zone for the debonded strands. From this plot, it should be noted that different combinations of debonded lengths and relative numbers of debonded strands will affect the points where applied moment can exceed the cracking resistance. However, in general, for beams with staggered debonding, the point of first cracking in the transfer zone coincides with the end of the transfer zone for debonded strands. Again, if strand embedment is lengthened, the line representing applied moment will move right and flexural failure will occur. But if the embedment length is shortened and the line of applied moment is moved to the left, then cracking will occur in the transfer zone of the debonded strands and bond failure will result.

The mathematical relationship for line OB is given by similar triangles:

$$\frac{M_{cr}}{L_b+L_t} = \frac{M_{ult}}{L_b+L_e}$$

Substituting in the values for M_{ult} = 6080 k-in, M_{cr} = 3524 k-in and L_t = 25 inches, an equation relating L_b and L_e is given:

$$L_b = 1.38L_e - 59.5$$

This relationship is given by line BB' in Figure 5.7b. Areas to the left of this line, with shorter embedment lengths, should result in bond failures while regions to the right of the

line denote combinations of embedment length and debond length that will result in flexural failure.

Two important facts are illuminated by the plots in Figure 5.7a and 5.7b. First of all, the embedment length required to prevent bond failure is dependent on the length of debonding. Therefore, development length is a function of debonded length, $L_d \rightarrow f(L_b)$. And the corollary, longer debonded lengths require longer embedment lengths for the strands. Also, it is important to note that if strands are concurrently debonded, then the required development length is much greater than if the debonding was staggered.

Lastly, a relationship can be established that predicts the occurrence of web shear cracking. It relates the shear span to the ultimate moment and the web cracking shear:

$$L_b + L_e = \frac{M_{ult}}{V_{cw4}}$$

The value for web shear cracking can be obtained by calculating V_{cw} for the cross section at a distance from the support equal to the height of the beam. Substituting values for M_{ult} and V_{cw4} yields the relationship:

$$L_e + L_b = 149.1''$$

which might be termed the critical shear span. This line is given by the dashed line CC' in the figures.

In the tests performed on the FA550 and FA460 series beams, web shear cracking was soon followed by bond failure of the strand anchorages, although there were examples of strands maintaining anchorage beyond web cracking. In the tests performed by Dane and Bruce[17], web cracking was observed without causing anchorage failures because all of the strands were contained within the bottom flange of the I-shaped beams. Web shear cracks did not propagate through the bottom flange and disturb anchorage. Evidence indicates that the boundary defined by web shear cracking may not always be a borderline between bond failure and ductile failure. For this reason, the line is dashed. However, the boundary line remains significant because bond failure is much less likely to occur if the concrete does not crack.

5.5 Testing Program

Altogether, 10 tests were performed on 6 specimens. As stated before, the beams were designed so that test results would characterize, as much as possible, the full range of behavior for beams with debonded strands. Each beam contained eight 0.5 inch strands, four of which were debonded. Four beams were 40 feet in length with the debonded length equal to 78 inches. The other two beams were 27 feet, 6 inches in length with a debonded length equal to 36 inches. The beams all possessed identical cross sections, illustrated in

Figure 5.8. Cross section properties are given in the figure. Shear reinforcement was spaced at 6 inches for all specimens. No variation was made in shear reinforcement along the length. No special confining steel or anchorage details were provided on the debonded strands.

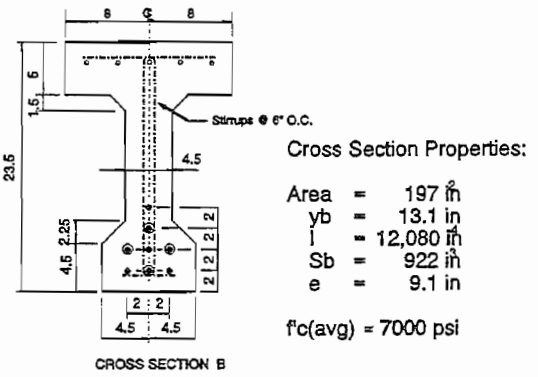

Figure 5.8 Cross Section for DB850 Beams

A total of eight 0.5 inch seven-wire strands were required to fulfill the needs of the testing program. A minimum of four debonded strands were required to perform staggered debonding and, at the same time, to debond in a symmetrical pattern. Fewer debonded strands would not allow symmetrical debonding patterns. Debonding percentages are typically less than 50%. Therefore a total of 8 strands was the minimum number of strands to give adequate breadth to the testing program.

5.5.1 Variables. The variables tested for the debonded beams included:

1. The length of debonding, L_b;
2. Type of debonding cutoff (staggered (S) or concurrent (C)); and,
3. Embedment length, L_e.

Table 5.4 gives the beam length, the debonded length and the type of debonding for each specimen.

TABLE 5.4

VARIABLES BY TEST SPECIMEN FOR DB850 BEAMS

Test	Beam Length, L (in)	Debonded Length, L_b (in)	Embedment Length, L_e (in)	Type of Debonding[1]
DB850-1A	330	36	84	S
DB850-1B[2]	330	36	84	S
DB850-2A[2]	330	36	76	S
DB850-2B[2]	330	36	88	C
DB850-3A	480	78	80	S
DB850-3B	480	78	108	S
DB850-4A	480	78	120	S
DB850-4B	480	78	100	S
DB850-5A	480	78	120	C
DB850-6A	480	78	150	C

1. "S" denotes staggered debonding.
   "C" denotes concurrent debonding.
2. Steel Cladding is attached to the webs of these specimens.

The debonded length, L_b, and the type of cutoff were established before the beam was cast. Debonded lengths were selected in order to test embedment lengths between 1.0 and 2.0 times the basic development length given in AASHTO equation 9-32. Because the current code requires doubling the development lengths for debonded strands (except that under specific

conditions, the basic development length is adequate), the testing of embedment lengths between 1.0 and 2.0 times the basic development length seemed appropriate.

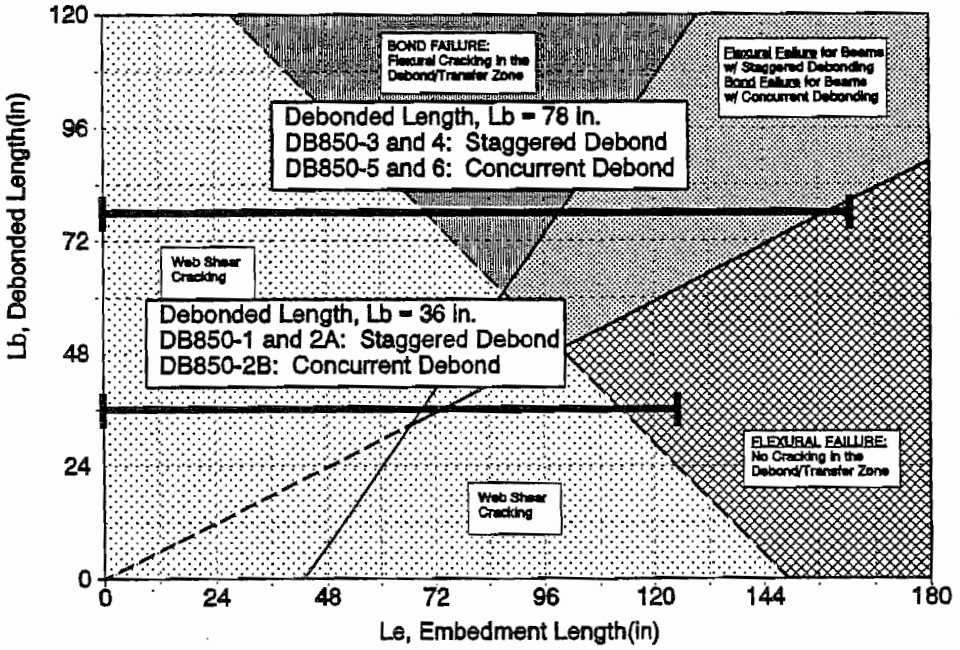

Figure 5.9 Range of Possible Embedment Lengths (DB850 Test Series: Beams With Debonded Strands)

For specimens DB850-3 through 6, the debonded length was selected as 78 inches. Specimens DB850-1 and 2 had debond lengths equal to 36 inches. Figure 5.9 illustrates the possible range of test values for embedment lengths. For debonded lengths of 78 inches, possible embedment lengths range from less than 72 inches to about 160 inches. A length of 72 inches was required to develop fully bonded strands in the FA550 series.

In specimens DB850-3 and DB850-4, debonded strands were staggered. From the prediction model, flexural failure should result if the embedment length was greater than 100 inches. Specimens DB850-5 and DB850-6 contained concurrently debonded strands. These specimens would require an embedment length in excess of 100 inches for the strands to develop tension for the beams to fail in flexure.

In specimens DB850-1 and DB850-2, the debonded lengths were 36 inches. In tests DB850-1A, DB850-1B and DB850-2, the debonding was staggered. In test DB850-2B, the strands were concurrently debonded. The model in Figure 5.9 predicts that for short debonded lengths, no difference would exist between staggered debonding and concurrent debonding. More importantly, the model predicts that web shear cracking will occur before the beam can fail in flexure.

5.5.2 Fabrication of the Test Specimens. Fabrication of the beams followed the same basic procedures that were used to construct the fully bonded test series, outlined in Section 4.5, as follows:

1) Stress strands to 75% f_{pu} (202.5 ksi)
2) Placement of the mild reinforcement
3) Placement of the debonding material
4) Placement of the formwork
5) Casting of the concrete
6) Curing of the concrete in place (two days)
7) Release of pretensioning.

The only variation from fabrication of the fully bonded specimens is the placement of debonding material. The debonding material consisted of white plastic tubing, made from semi-rigid plastic that was deformable because of its thinness. The tubing was split along its length to make it easy to install. The tubing was placed on the strand where debonding was required. The tubing's natural curl snapped it to the strand, providing a reasonably tight fit. The tubing would also fit a variety of strand sizes. Debonding was sealed by taping each end of the debonding tube, but the longitudinal joint fit tightly and was not taped.

The strands are labeled in Figure 5.10 by letters of the alphabet, A through H to simplify record keeping. The debonding schedule is also shown in Figure 5.10. Note that strands B and G are contained within the core of shear reinforcement.

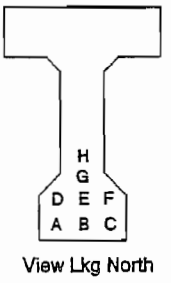

Debonding Schedule

Beam		Strand B	D	F	G
-1	(S)	36	18	18	36
-2	(C)	36	16N 36S	16N 36S	36
-3	(S)	78	39	39	78
-4	(S)	78	39	39	78
-5	(C)	78	78	78	78
-6	(C)	78	78	78	78

Figure 5.10 Strand Pattern and Debonding Schedule for DB850 Beams

The shorter beams, DB850-1 and DB850-2 required some modification during testing. Test A on DB850-1 resulted in total bond failure after the beam's web cracked from the shear load. The web shear cracking caused the debonded strands to slip and subsequent shear failure of the beam. Steel cladding was glued to webs for the three remaining tests to prevent web shear cracks from propagating through the anchorage zone of the strands. A photograph of the steel cladding is shown in Figure 5.11. Cladding extended to a distance approximately 72 inches from the ends of the beams. The steel cladding was made from steel plate, $^1/_4$" x 4", which was glued to the web of the beams as shown with a Sika two part epoxy, brand name Sikadur. Epoxy was applied to the steel. Then the steel was bolted to the web of the beams with concrete expansion anchors to reduce the glue line to its narrowest possible dimension and ensure bond. By gluing the plate to the webs, the steel plate was made composite with the concrete and strains in the concrete would be matched by strains in the steel. On specimen DB850-1B, the steel cladding was discontinuous 42 inches from the end.

5.5.3 Material. The strand surface was "mill condition" as furnished, having never been exposed to weathering. The strand's ultimate strength was specified at 270 ksi. The seven-wire, low relaxation prestressing strand used in these tests is the current industry standard for prestressed applications. The strand's ultimate strength was 283 ksi as given by the manufacturer. Load versus Strain response is shown in Figure A2.

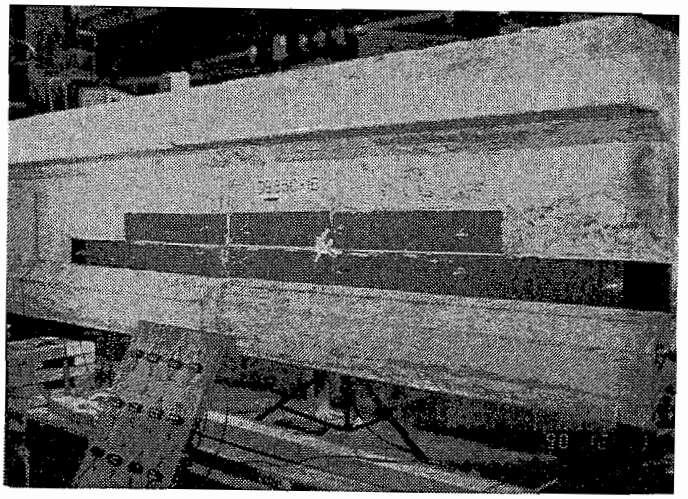

Figure 5.11 Steel Cladding Attached to Web of Beam DB850-1B

The concrete strengths were designed to be 4500 psi at release and 6000 psi for design ultimate. Concrete proportions are given in Table 4.1. Concrete strengths for the DB850 series beams are given in Table 5.5. Concrete strengths over time are also plotted for DB850 series beams in Appendix B, Figures B8 through B12.

5.5.4 Testing Apparatus. The same testing apparatus was used for the debonded beams as for the fully bonded beams. A photograph of the testing equipment and loading frame is shown in Figure 4.4. The apparatus included a loading frame, an hydraulic actuator, a spreader beam to create a constant moment region, and floor beams to provide variable support locations.

TABLE 5.5

CONCRETE STRENGTHS OF BEAMS WITH DEBONDED STRANDS

Beam	Release Strength	Strength at Flexural Test	
		Moist Cure	Field Cure
DB850-1	4640	7000	7410
DB850-2	4640	7000	7410
DB850-3	5080	6610	6830
DB850-4	5060	7370	6860
DB850-5	5580	7460	-
DB860-6	5150	6940	7300

Concrete Strengths vs. Time are plotted in Appendix B.

A typical test setup is shown in Figure 5.12. The dimensions illustrate the setup for Test DB850-3A. In this test, the North end of Beam DB850-3 was tested. The debonded length was 78 inches, L_b = 78 in. As discussed earlier, debonding for this beam was "staggered". In this debonding pattern, debonding covered two strands for a length of 78 inches from the end of the beam while the other two debonded

strands were staggered; and debonding was terminated at 39 inches. The staggered debonding is denoted with an "S" above the representation for debonded strands.

For this test, the embedment length was set at 80 inches, L_e = 80 inches to correspond to the 1.0 times the required development length given by AASHTO equation 9-32. The embedment length, L_e and span were varied for each test. In all of the tests, the area between the load points was a constant moment region. Constant moment is achieved by matching the proportions of the dimensions of the load atop the spreader beam to the proportions for the overall beam support and load application. The spreader beam spanned 24 inches.

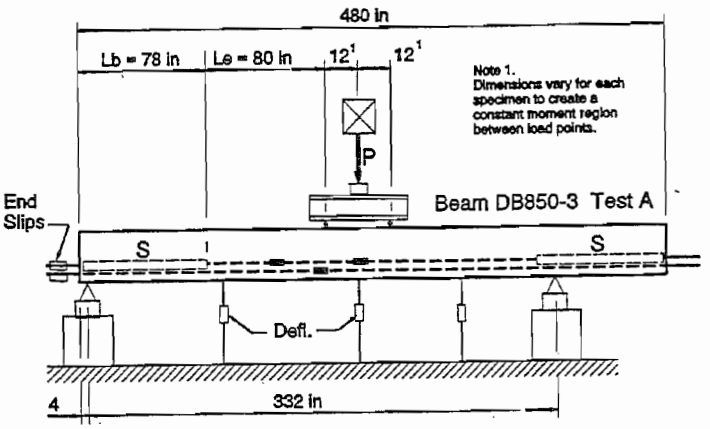

Figure 5.12 Typical Test Setup for Beams With Debonded Strands

5.5.5 Instrumentation. This test series used the same instrumentation as the series of development length tests on fully bonded beams, discussed in Chapter 4. Instrumentation measured the applied load, beam deflections and strand end slips. These data were measured electronically and stored by the data acquisition system used at FSEL. Other data measured electronically included hydraulic pressure and electrical resistance strain gages (ERSG's) applied to strands.

Load was measured from an electronic load cell at the hydraulic actuator. Deflection and end slips were measured by linear potentiometers. All of the electronic instruments were calibrated prior to testing. End slip measurements are accurate to $\pm$0.001 inches, thus, even very small strand slips were detected. Top fiber concrete strains were measured in the constant moment region for each test. Measurements were taken at each load increment with the DEMEC gage system discussed in Chapter 3.

End slips were measured on seven of the eight strands. The four debonded strands, strands B, D, F and G, were always monitored for end slip. Strand E was the only strand not monitored for end slip because the clamping device that held the potentiometer would not fit between the other strands and their end slip clamps.

5.5.6 Test Procedure. Beams were loaded statically until failure. Load was increased at regular increments. Measurements were recorded at every load increment, approximately 2.0 to 5.0 kips until cracking. Cracking loads and crack locations were noted and recorded. After cracking, load was increased in smaller increments. Any special behavior was noted and crack patterns were marked with a broad ink marker on the

specimen. Significant end slips were noted and recorded. Failure was defined by the beam's inability to resist increased load. Flexural failures resulted when the top flange of the beam failed in compression. Anchorage failures resulted in general slip of the strand relative to the concrete and a sudden loss of capacity.

The embedment lengths were varied for each test depending on results from previous tests in the series. By comparing the results from each test to the prediction model, the embedment lengths were chosen for each test so that the results from the complete test series would span the probable failure modes. By varying the embedment lengths for specimens with the same debonded lengths, the principles underlying the overall beam behavior were established by the test results.

Each beam was tested at least twice, once at each end. The first test on a specimen is designated Test "A" while the second test is designated Test "B". This procedure was possible because individual anchorage zones exist at each end of each pretensioned beam. In the cases of beams DB850-5 and DB850-6, the longer development length requirements precluded an effective second test. Beam DB850-5 was tested twice, but the results from the second test are unreliable because of damage caused by the first loading. Beam DB850-6 was tested only once.

5.6 Test Results

Discussion of the test results is presented in three parts. Results from tests on the longer beams with staggered debonding are discussed first. These beams include DB850-3 and DB850-4. Next, results from the beams with concurrent debonding are presented. These beams include DB850-5 and DB850-6. Beams DB850-3 through 6 all had debonded lengths equal to 78 inches, L_b = 78 inches. Those discussions are followed by results from tests on the shorter beams, DB850-1 and DB850-2 with debonded lengths of 36 inches, L_b = 36 inches.

In each of the tests, the mode of failure was of primary importance. Ductile flexural failures where concrete crushes in compression after yielding of the steel are desirable for two reasons. First, flexural failures provide an easily predicted limit state, and secondly, flexural failures provide warning before collapse. This combination makes structures both safe and predictable. On the other hand, anchorage failures oftentimes are accompanied by a sudden and violent collapse of the structure. Such failures are neither safe nor predictable and should be avoided. To understand the results from these tests, the mode of failure becomes the primary source of data.

Test results are shown in Tables 5.6 and 5.7. Table 5.6 summarizes the failure mode for each test and compares it to the embedment length, L_e. The embedment length for these tests is taken as the length from the debond termination point to the point of maximum moment. Table 5.6 also compares the embedment length, L_e to the development

length, L_d for each test. L_d is calculated using AASHTO equation 9-32 (ACI Section 12.9.1) as follows:

$$L_d = (f_{ps} - \frac{2}{3} f_{se}) d_b = 80''$$

Values for the variables are assumed to be f_{ps} = 260 ksi, f_{se} = 150 ksi and d_b = 0.5 inches, which are representative for the specimens in this series.

TABLE 5.6

SUMMARY OF FLEXURAL TESTS ON BEAMS WITH DEBONDED STRANDS

Test	Debonded Length, L_b (IN)[1]	Embedment Length, L_e (IN)	% L_d[3]	Failure Mode
DB850-1A	36(S)	84	1.05	BND/SHEAR
DB850-1B[2]	36(S)	84	1.05	BND/SHEAR
DB850-2A[2]	36(S)	76	0.95	BND/SHEAR
DB850-2B[2]	36(C)	88	1.10	FLEXURE
DB850-3A	78(S)	80	1.00	BOND
DB850-3B	78(S)	108	1.35	FLEXURE
DB850-4A	78(S)	120	1.50	FLEXURE
DB850-4B	78(S)	100	1.25	FLEX w/SLIP
DB850-5A	78(C)	120	1.25	BOND
DB850-6A	78(C)	150	1.875	FLEX/BOND

1. "S" denotes staggered debonding.
   "C" denotes concurrent debonding.
2. Steel Cladding is attached to the webs of these specimens.
3. L_d = 80 inches (f_{ps} = 260 and f_{se} = 150 ksi)

Table 5.7 compares the maximum moment at failure, M_u, with the calculated nominal capacity. In cases of flexural failure, the tested maximum moment nearly equals or exceeds the calculated flexural capacity. If a beam's ultimate capacity at failure does not approach the nominal flexural capacity of the section and significant strand slips have occurred, then anchorage failure of the strands is considered to have occurred. Notice that even in extreme cases of obvious bond failures, the section still achieves a very large percentage of the nominal capacity. This sometimes makes it difficult to distinguish a flexural failure from a bond failure.

5.6.1 Test Results: Debonded Length = 78 inches with Staggered Debonding. Figure 5.13 shows the test dimensions for Test DB850-3A. This test is typical of bond failure in beams with debonded strands. Note that the embedment length, L_e = 80 inches approximates 1.0 times the basic development length given by AASHTO equation 9-32. The debonded length is 78 inches, L_b = 78 in. Figure 5.13 also plots load versus deflection and end slip. The first flexural cracking occurred at a load of 43.8 kips. This corresponds to a flexural cracking moment of 3376 k-in, within 5% of the cracking moment predicted by elastic analysis and a cracking tensile stress of $7.5\sqrt{f'_c}$.

As load increased, the number of cracks also increased and flexural cracking progressed away from the load point towards the beam's support. At a total load of 66.3 kips, flexural cracks formed at stations 88 inches and 96 inches from the beam's end, well within the transfer zone of the debonded strands. Upon formation of these cracks,

TABLE 5.7

APPLIED LOAD AT FAILURE
TESTS ON BEAMS WITH DEBONDED STRANDS

Beam	Le (in)	Ultimate Load			Concrete Strain at Ultimate ($^{in}/_{in} \times 10^{-6}$)	Mode of Failure
		P_u (kips)	$M_{u,test}$ (k-in)	$M_{u,test}/M_n$ [1]		
DB850-3A	78(S)	69.58	5358	0.98	2844	BOND
DB850-3B	78(S)	69.32	5615	1.03	2896	FLEX
DB850-4A	78(S)	70.33	6038	1.00	2808	FLEX
DB850-4B	78(S)	75.39	6029	1.00	2704	FLEX
DB850-5A	78(C)	81.16	5590	0.93	2136	BOND
DB850-6A	78(C)	52.24	5851	0.97	2876	FLEX
DB850-1A	36(S)	88	5104	0.85	1276	BOND
DB850-1B	36(S)	93.6	5738	0.95	2104	BOND
DB850-2A	36(S)	95.97	5622	0.94	2210	BOND
DB850-2B	36(C)	93.29	5778	0.96	2426	FLEX

1. M_n = 6010 k" for DB850-1,2,4,5 and 6; M_n = 5447 k" for DB850-3.

strands B and G slipped through the concrete. The applied moments at these crack locations were 2915 k-in at station 88 and 3181 k-in at station 96. Cracking patterns for Test DB850-3A are illustrated in Figure 5.14 and a photograph of the beam is shown in Figure 5.15. The cracks at 88 inches and 96 inches are visible. Only the debonded strands were affected by the cracking. None of the other strands slipped and the beam continued to resist load. Flexural failure was observed with crushing of the concrete. However, this beam failed at a load significantly less than its nominal flexural capacity. The load at failure was 69.58 kips resulting in a maximum applied moment 5358 k-in, which is only 88% of the calculated nominal capacity (Dead load moment was only 116 k-in at the center of the span and its inclusion does not significantly affect the result).

Test A on beam DB850-4 characterizes a typical flexural failure. Its failure met the two criteria required to classify a failure as flexural, capacity and ductility. In test DB850-4A, first flexural cracking occurred at a load of 41.7 kips and a corresponding applied moment of 3580 k-in, or only 1.5% greater than the calculated cracking load. Loading was continued until flexural failure occurred at 70.3 kips. Flexural failure is evidenced by crushing of the concrete after yielding of the strand. Load is plotted versus deflection and end slips in Figure 5.16. The maximum applied moment from testing was 6035 k-in, or

99.3% of the calculated nominal capacity. Concrete strains exceeded 2800 microstrains (2800 x 10^{-6} $^{in}/_{in}$) at crushing. Total midspan deflection exceeded 4.5 inches.

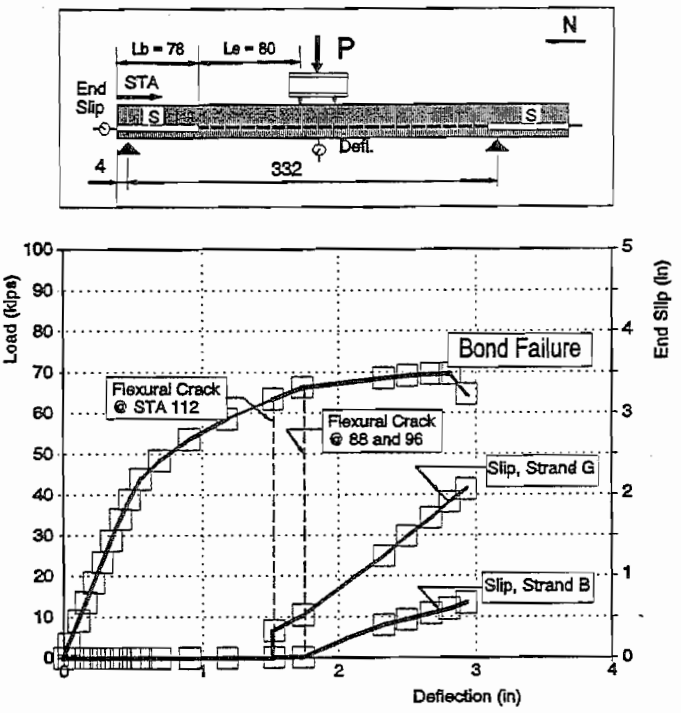

Figure 5.13 Beam DB850-3 Test A

Flexural cracking did not extend into the transfer zone of the debonded strands and no significant end slips were observed. The nearest flexural crack from the support was located at station 118. The photograph in Figure 5.17 illustrates the flexural cracking patterns observed in this and other flexural failures. This crack formed at a load of 68.5 kips under an applied moment of 3577 k-in, only 1.5% greater than the calculated cracking moment.

Tests DB850-3B and DB850-4B also had debonded lengths of 78 inches with staggered debonding. Load versus deflections plots and end slips for Tests DB850-3B and DB850-4B are shown in Figures 5.18 and 5.19. Note that Test DB850-4B has an embedment length of 100 inches that places this test on the borderline between flexural failure and bond failure. Overall this test exhibited flexural behavior because it achieved the ultimate flexural capacity of the section and it maintained load through large deformations. However, strands B and G also experienced significant slipping. At failure, the total slip for strand B was 0.22 inches, and for strand G the total slip was 0.12 inches. Slip was initiated by a crack at 108 inches from the beam end. Another crack formed at 95 inches from the end. However, these cracks formed at loads very near the ultimate load and did not significantly alter the beam's behavior except for the end slip noted.

As an aside, some small movements, less than 0.02 inches, were observed for all of the debonded strands, B, G, D and/or F. However, these slips do not reflect actual bond slippage. Instead they were caused by normal displacements of the unbonded strand relative to the cross section. As the cross section deformed under the influence of applied moment, the end slips measured the elongation of the concrete fibers at the same elevation. An approximation for the corresponding elongation can be obtained by multiplying the change in curvature,which is approximately equal to the curvature at zero moment (ϕ_0) times the debonded length (L_b) times the eccentricity of the end slip device (e_{ps}) and integrating ($^1/_2$) over the length:

$$\frac{1}{2} \bullet \phi_0 \bullet L_b \bullet e_{ps} = 0.013''$$

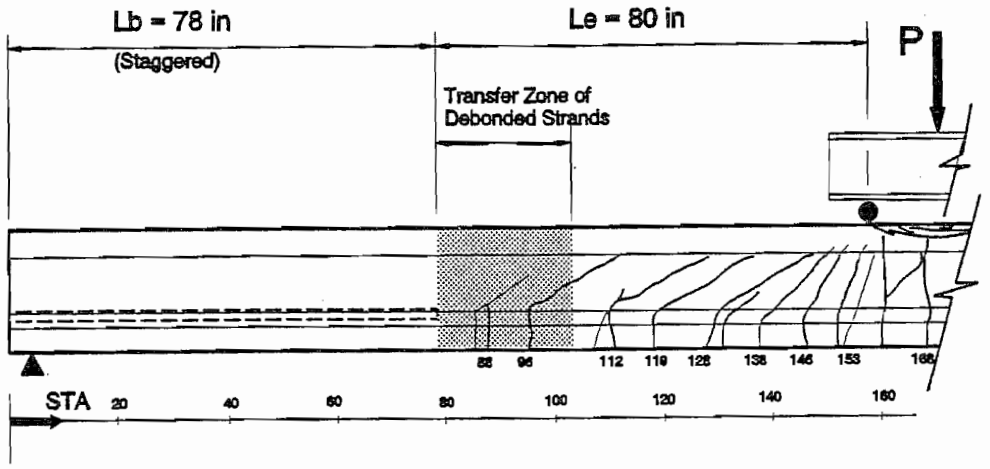

Figure 5.14 Cracking Pattern DB850-3A

5.6.2 Test Results: Debonded Length = 78 inches with Concurrent Debonding. As noted before, only two tests with reliable data were obtained from the two beams DB850-5 and DB850-6. Each of these beams contained four concurrently debonded strands. Debonding was terminated at the same point for all of the strands, 78 inches from the end of the beam. A second test was performed on DB850-5, but cracking from the first test caused this beam to fail prematurely.

Test DB850-5A had an embedment length of 120 inches, L_e = 120 in. In Test DB850-4A, an embedment length of 120 inches proved to be adequate for development of the debonded strands. However, DB850-4 had staggered debonding whereas DB850-5 had concurrent debonding. Test DB850-5A failed when the anchorage of the debonded strands failed. The plot of load versus deflection and end slip is shown in Figure 5.20. Note the large end slips measured on strands B and G. Strand B slipped nearly one inch whereas strand G slipped in excess of 3.5 inches. Strands D and F also experienced slips in excess of 0.5 inches, but are not shown in the figure.

First flexural cracking for DB850-5A occurred at a load of 51.8 kips, which is only 1% larger than the calculated cracking moment. As load increased, cracking extended towards the debond/transfer zone. At a load of 77.8 kips, flexural cracks propagated through the debond transfer zone. The first flexural cracking in the debonded/transfer zone formed at Station 80, which affected the anchorage of the debonded strands. This crack was followed by another crack at Station 92 and again by a crack at Station 106. The cracking pattern can be observed in the photograph in Figure 5.21. This progression of cracking from

the ends toward the middle of the beam is typical for bond failures (it was first observed in the fully bonded FA550 and FA460 series). This behavior suggests that as the strands lose bond, the transfer zone is extended, precompression is diminished and incidence of flexural cracking increases in previously uncracked regions.

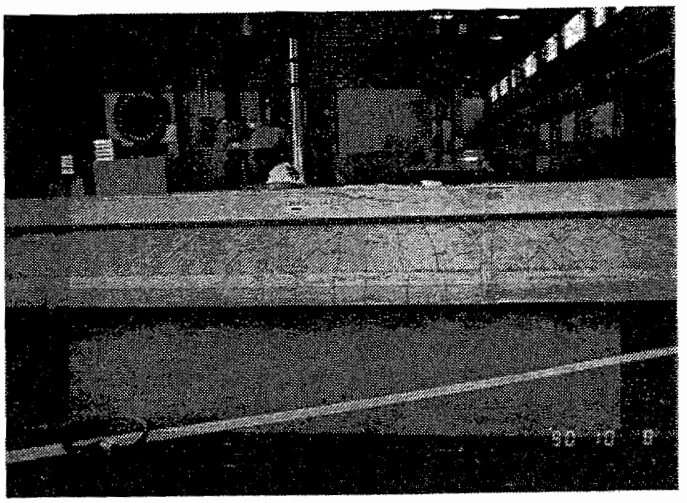

Figure 5.15 Photograph of Test DB850-3A Cracking Patterns

Test DB850-6A failed in much the same manner as DB850-5A, however its embedment length, 150 inches, was long enough to induce a hybrid failure between flexural and bond failure. Load versus deflections and end slips are shown in Figure 5.22. First flexural cracking occurred at 31.33 kips, the predicted cracking load. Load was increased, and the region of cracking expanded. However, the primary region of flexural cracking extended only to about 144 inches from the end. At the load of 51.7 kips, a flexural crack formed at 78 inches from the end, nearly the exact point where debonding is terminated. This also corresponds to the station point where cracking is predicted by the behavioral model. The crack pattern of DB850-6A is shown Figure 5.23. In the photograph, the crack at 78 inches is separated from the region of primary cracking by a wide distance. This cracking pattern exemplifies the reduced M_{cr} resulting from debonded strands. End slips coincided with the formation of the crack at Station 78. These results demonstrate that the behavior of beams with debonded strands can be accurately predicted by the rational behavioral models presented in this chapter.

This beam was loaded a second time. Crushing strain of the concrete was achieved albeit at a lower load. Maximum end slips remained relatively small, about 0.03 inches, indicating that the strands were being anchored and that the specimen could be loaded several times with only minor deterioration of bond.

5.6.3 Test Results: Debonded Length = 36 inches. Two beams were cast with short debonded lengths, DB850-1 and DB850-2. These beams were intended to demonstrate that the strands could be developed at embedment lengths less than 1.0 times the basic development length. From the prediction model, Figure 5.9, if web shear cracks were disregarded, then flexural failure would occurinstead of bond failure for embedment lengths less than 1.0 L_d. However. these tests demonstrated, quite graphically, the relationship

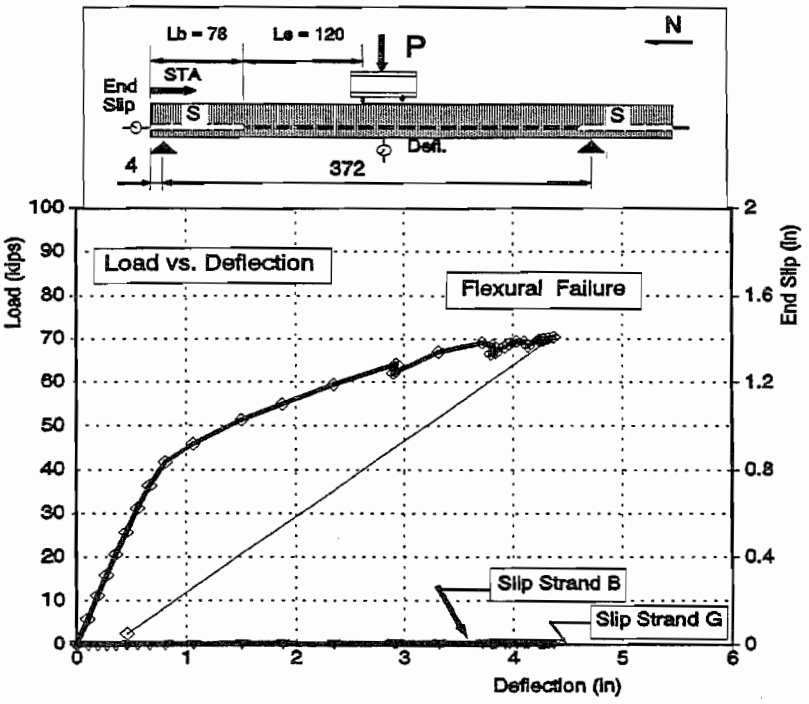

Figure 5.16 Beam DB850-4 Test A

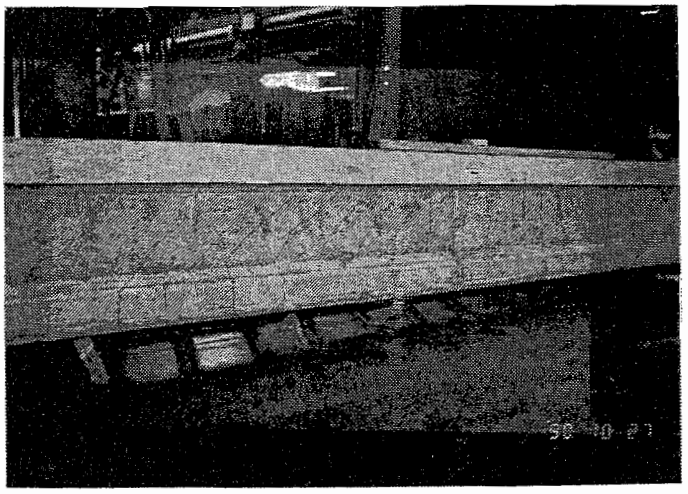

Figure 5.17 Photograph of Cracking Pattern, DB850-4A

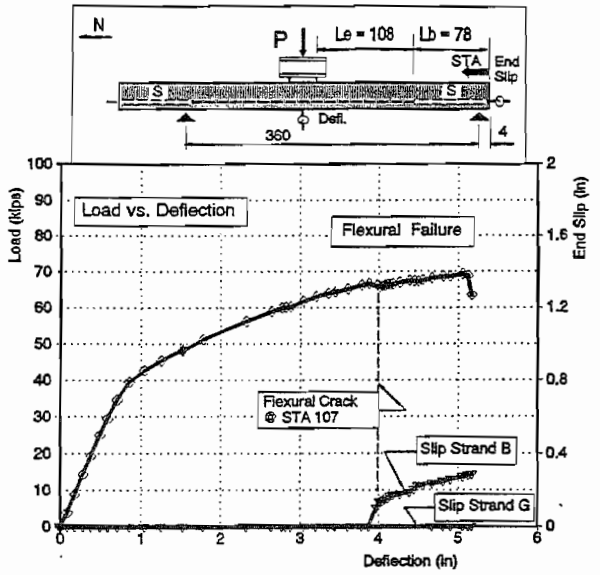

Figure 5.18 Beam DB850-3 Test B

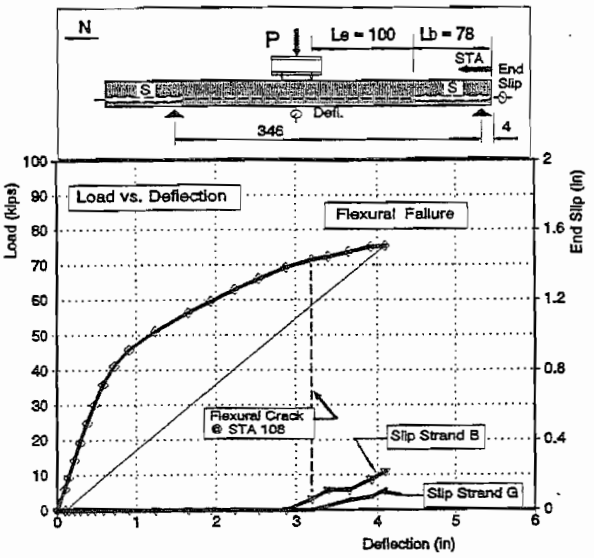

Figure 5.19 Beam DB850-4 Test B

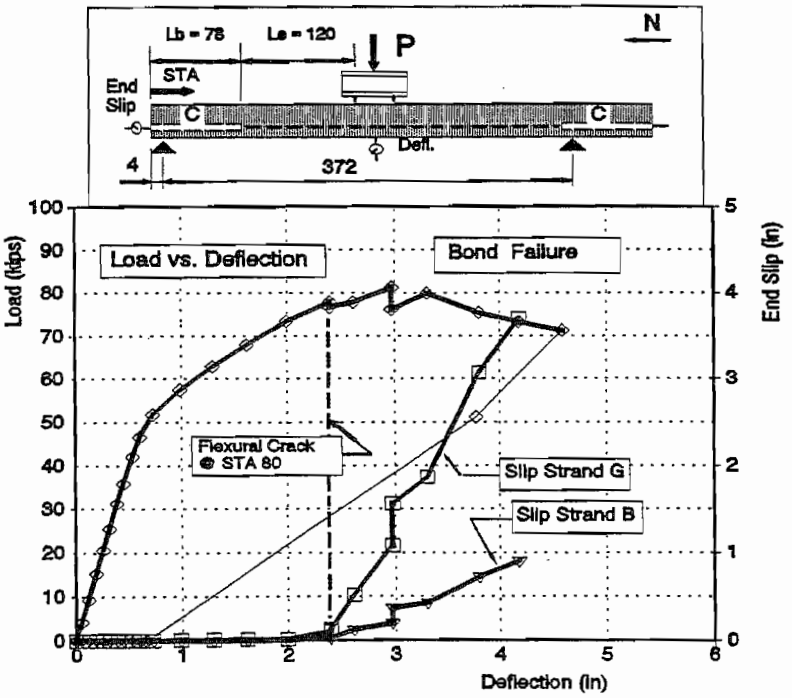

Figure 5.20 Beam DB850-5 Test A

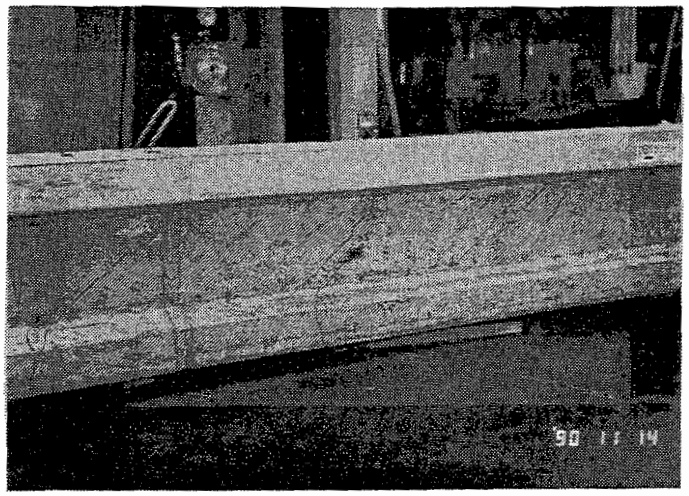

Figure 5.21 Photograph of Cracking Pattern, DB850-5A

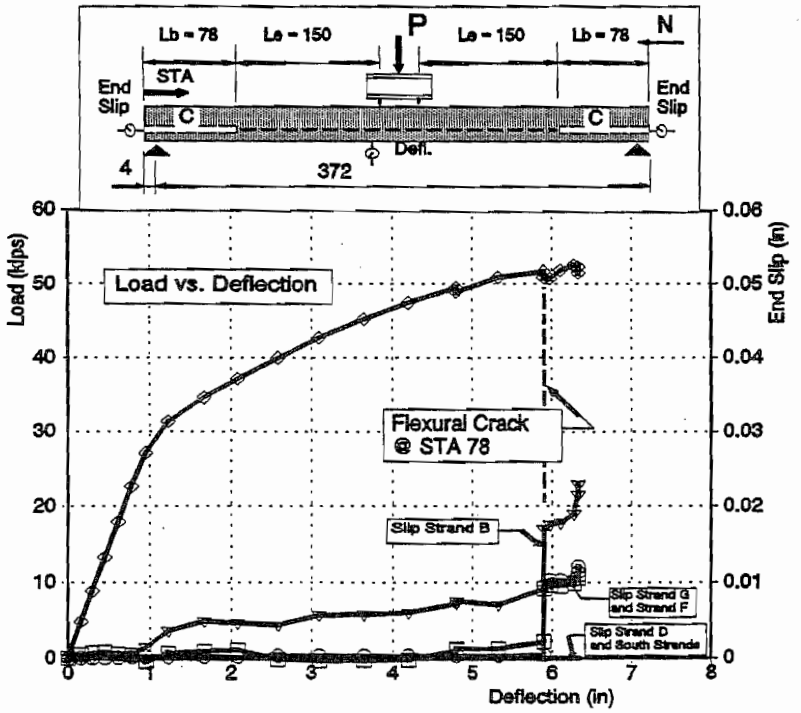

Figure 5.22 Beam DB850-6 Test A

between web shear cracking and subsequent bond failure. All of these tests experienced web shear cracking. The first of these tests, DB850-1A failed in bond immediately upon formation of the web shear cracks. In the three remaining tests, steel cladding was glued to the webs of the beams in an effort to limit web cracking. While web shear cracking was not eliminated, crack propagation was controlled and anchorage failure was delayed. The results clearly demonstrate the relationship between web shear cracking and anchorage failures.

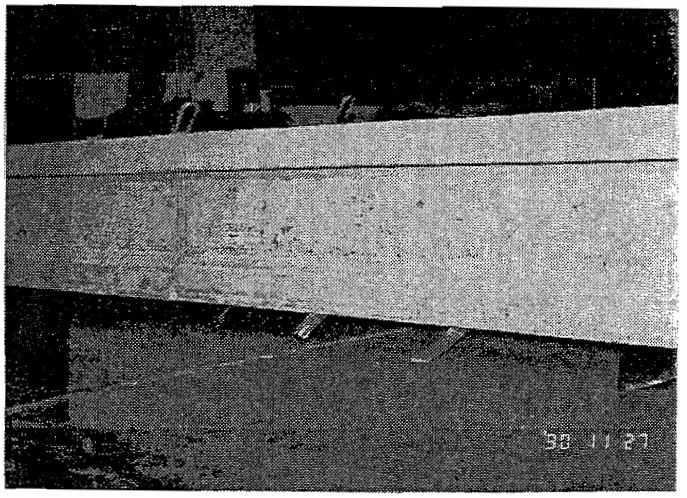

Figure 5.23 Photograph of Cracking Pattern, DB850-6A

Test DB850-1A had staggered debonded strands to a length of 36 inches, L_b = 36 inches. The embedment length was 84 inches, L_e = 84 inches or 1.05 L_d. Cladding was not applied to the web of the beam in this test. The beam failed when web shear cracks formed in the shear span and caused anchorage failure of the strands. The web shear cracks formed at a total load of about 88 kips and an applied shear of about 44 kips. Complete collapse resulted and is shown in the photograph in Figure 5.24. The plot illustrating load versus deflection and end slip is shown in Figure 5.25.

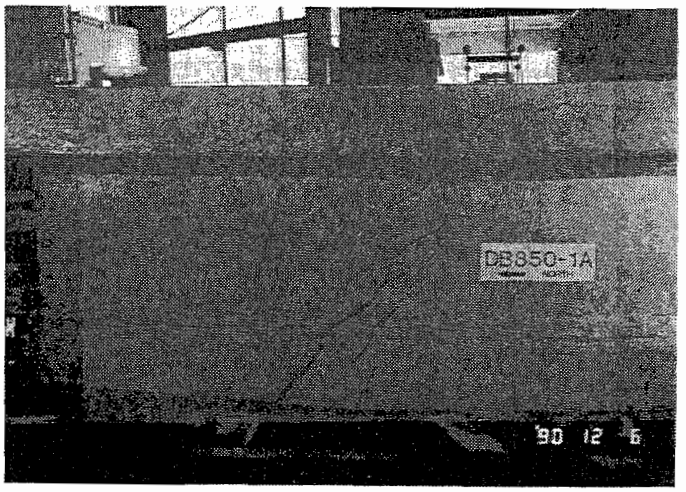

Figure 5.24 Photograph of Web Shear Cracking and Bond Failure, DB850-1A

For Test DB850-1B, the sides of the web were clad with steel plate as described earlier in Section 5.5.2. However, a seam was left in the steel at a distance 42 inches from the end of the beam where the steel cladding was not joined together. As the beam was

loaded, web shear cracks formed in the concrete above the steel cladding, as shown in Figure 5.26. The total load of 80 kips corresponds to an applied shear of 42.4 kips, approximately the same value as for Test DB850-1A.

Increased loading produced another shear crack closer to the middle of the beam. Also note that no web shear cracks were observed except at the end regions and no bottom flexural cracks developed. Web shear capacity is a function of the precompression stresses, so as more of the prestressed force becomes effective by transfer of the debonded strands, the resistance to web shear cracking increases.

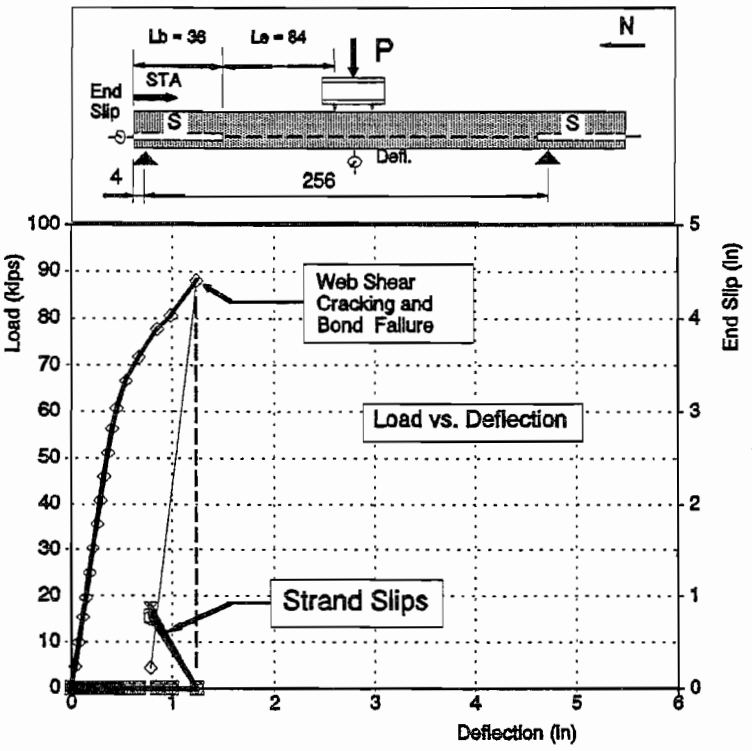

Figure 5.25 Beam DB850-1 Test A

Loading was increased incrementally without further damage until a load of 93.6 kips was applied. At this load, a web shear crack formed through the seam in the steel cladding and extended through the bottom flange. Strand anchorage failed completely and total collapse of the beam resulted. The applied shear at this load was 49.5 kips. The photograph of the beam at failure is shown in Figure 5.27. This test is very significant for the following reasons:

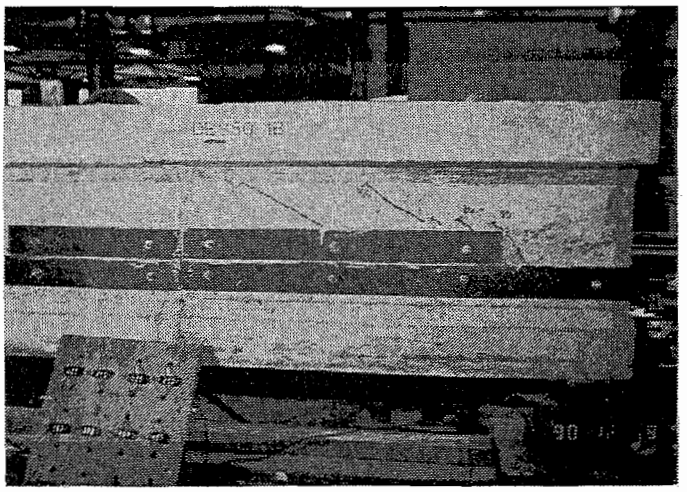

Figure 5.26 Initial Web Shear Cracking, Chack Propogation Delayed by Steel Cladding, DB850-1B

This test demonstrates that bond slippage and subsequent failure is preceded by cracking in the transfer zone of a strand. Both the applied shear and the applied moment in Test DB850-1B exceeded the shear and moment applied in Test DB850-1A. If failure was initiated by bond slippage, by simply pulling out of the strands and relieving prestress force, then these two tests would have been expected to fail at similar loads. Instead, web strengthening in Test B increased the beam's resistance to cracking, and preserved integrity of the bond until the failure shear crack formed. When the crack propagated through the bottom flange, the strands' anchorage was disturbed and bond failure resulted.

Load versus deflection and end slip for test DB850-1B is given in Figure 5.28.

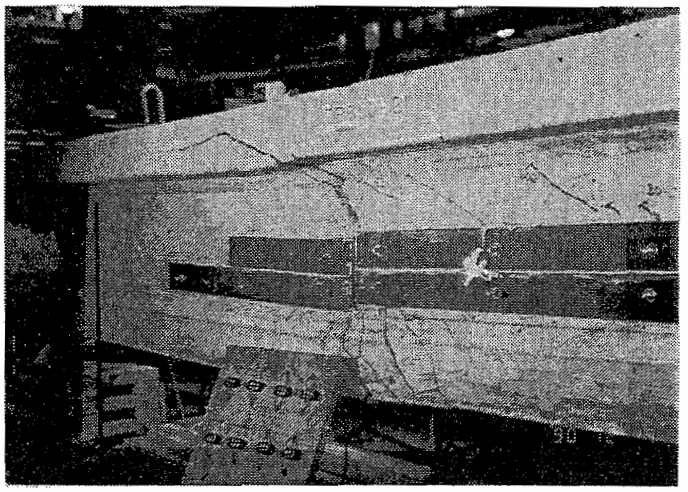

Figure 5.27 Web Shear Cracking and Bond Failure DB850-1B

Tests DB850-2A and DB850-2B also had steel cladding applied to the web, but the steel was made continuous; no seam was left between cladding plates. In both tests, the web cladding delayed the propagation of cracks through the strands' transfer zone. As shown in Figure 5.29, increased loading developed shear cracking at the top of the bottom flange chamfer. These shear cracks also precipitated bond failure of the strands. Figure 5.30 illustrates load versus deflection and end slip for Test A on Beam DB850-2.

For Test B, the embedment was lengthened slightly. At this end of Beam DB850-2, the strands were concurrently debonded. However, the prediction model shows that for short debonded lengths, the required development length would be the same for either type of debond termination. The photograph in Figure 5.31 shows the cracking pattern. The load versus deflection and end slips for Test DB850-2B are shown in Figure 5.32. Cracking was effectively prevented in the transfer zone until the ultimate load was achieved. From Figure 5.31, note that a single horizontal crack formed from the flexural crack at Station 56, and propagated longitudinally through the transfer zone of the debonded strands. The crack extended longitudinally to Station 36, the point where debonding terminates. This crack is a splitting crack caused by the strand as it is being pulled through the concrete while resisting external loads. The crack is marked "2.6," and is located directly above strand F in the specimen. The measured slip in strand F exceeded the slips in the other strands.

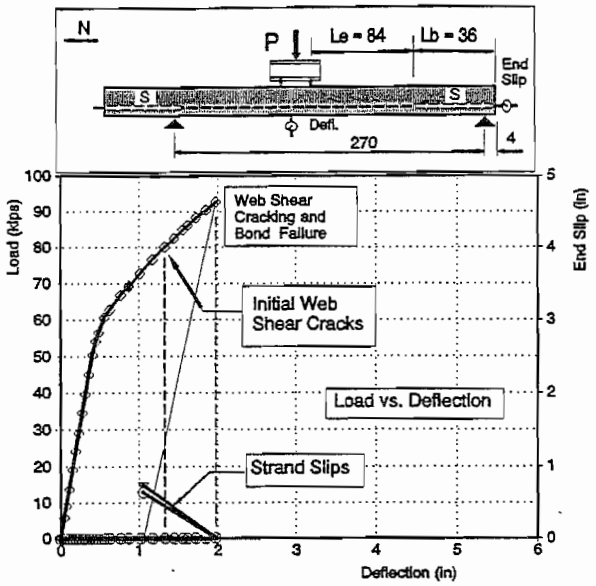

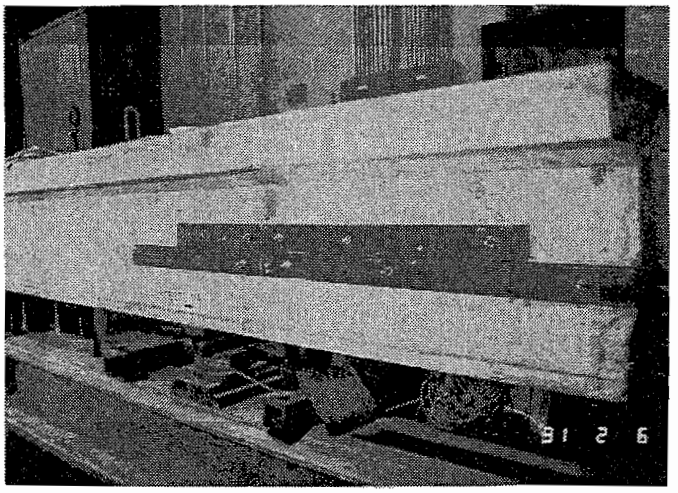

Figure 5.28 Beam DB850-1 Test B

Figure 5.29 Propogation of Web Shear Cracks Through Reinforced Web at High Shear Loads: Cracking in the Transfer Zone and Bond Failure, DB850-2A

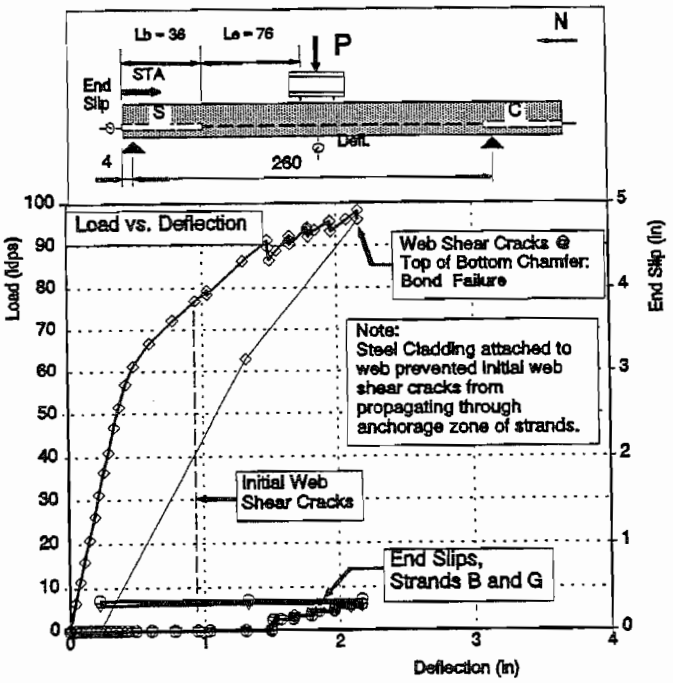

Figure 5.30 Beam DB850-2 Test A

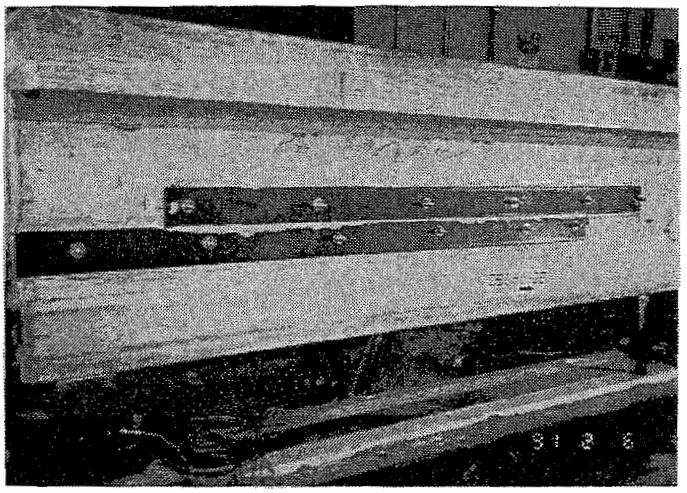

Figure 5.31 Flexural Failure With Splitting Crack in Transfer Zone at Strand F, DB850-2B

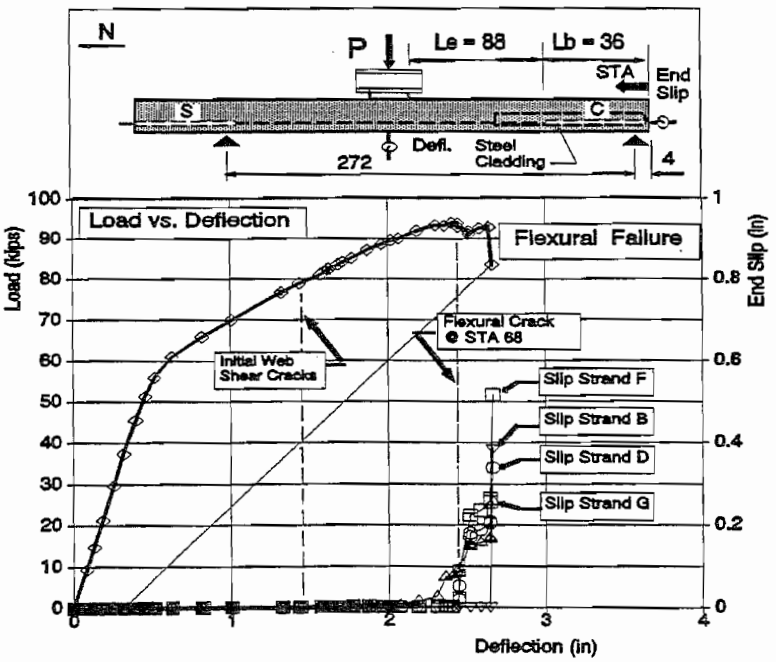

Figure 5.32 Beam DB850-2 Test B

5.7 Discussion of Results

5.7.1 Comparison of Results with Predicted Behavior. Chapter 5 began with the development of a model to predict bond failure of pretensioned beams made with debonded strands. The premise for the model is that bond will fail when cracks propagate across the transfer zone of a strand. By predicting the formation of cracks, bond failure is also predicted.

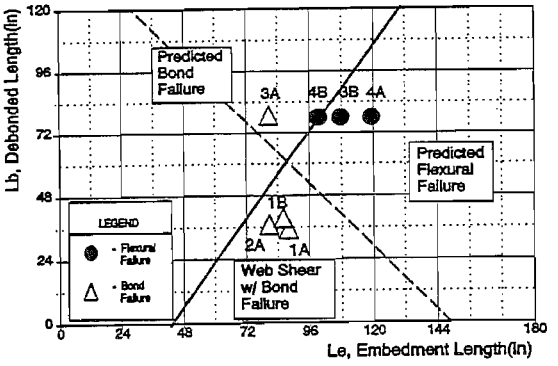

Figure 5.33 Overlay of Test Results (Beams With Staggered Debonding)

Test results are overlaid onto the prediction model in Figures 5.33 and 5.34. Results were presented earlier in Tables 5.6 and 5.7. Figure 5.33 illustrates the results from tests with staggered debonding and Figure 5.34 presents the results from tests with concurrent debonding.

Figure 5.33 illustrates the results from the seven tests on beams with staggered debonding. In Test DB850-3A, the specimen contained gradually debonded strands at a debonded length of 78 inches. The test resulted in a bond failure where the strands slipped and the ultimate moment was not achieved. The embedment length, 80 inches, was equivalent to 1.0 times the basic development length as given by AASHTO equation 9-32. This embedment length was shown to be sufficient for fully bonded beams, however, in this case with debonded strands, bond failed before the ultimate flexural capacity was reached. The bond failure was clearly predicted by the model following flexural cracking in the debond/transfer zone.

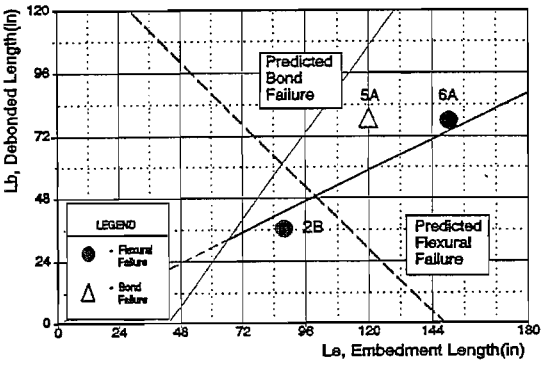

Figure 5.34 Overlay of Test Results (Concurrently Debonded Beams)

In Test DB850-4A, the specimen also contained staggered debonded strands to a debond length of 78 inches. However, for this test, the embedment length was 120 inches. The beam failed in flexure, attaining its ultimate flexural capacity and maintaining its load through large deformations. The model clearly predicts flexural failure for this test as shown in Figure 5.33.

The model also accurately predicted the test results of DB850-3B and DB850-4B. Test DB850-4B is placed on the borderline between flexural failure and bond failure. In this test, the beam was able to achieve its ultimate flexural capacity and also demonstrate some ductility; therefore, it is classified as a flexural failure. However, one crack did form in the transfer zone of the debonded strand. When the crack at Station 78 propagated across the transfer zone of the debonded strand, some strand slip was recorded. In this manner, Test DB850-4B experienced a hybrid behavior between bond failure and flexural failure, as predicted.

In tests on beams with relatively short debonded lengths, L_b = 36 inches, the primary cause of beam failure was failure of strand anchorage. Bond failures were caused by the propagation of web shear cracks across the transfer zone of all the strands, both fully bonded and debonded. Of the specimens with staggered debonding, all three failed in bond caused by web shear cracks. Steel cladding applied to the web effectively delayed crack propagation to much higher loads, however shear cracks eventually found their way through the cross section and caused bond failure.

The most significant test of the short debonded lengths was Test DB850-1B where the steel cladding was not joined at Station 42. This test was identical to Test DB850-1A except that Test A had no steel cladding. Test A failed in bond upon first incidence of web shear cracking. Test B exceeded this load by a large margin. However, Test B did fail in bond, but only after a web shear crack propagated through the seam in the steel cladding. Until the results from these two tests, it could have been argued that bond failure is caused simply by pulling out of the strands because of the tension in the strands, and that cracking is due to the loss of prestress and not the cause of it. Instead these two tests clearly show that cracking is the cause of bond failure, not the reverse. Test B exceeded the load that caused failure in Test A only because cracks were not allowed to disturb the anchorage zone of the strands. When cracks did propagate through the stands' transfer zone, then bond failure occurred and the beam failed.

Figure 5.34 depicts the results from tests on beams with concurrent debonding. Again, strand slip and bond failure are accurately predicted by the incidence of cracking in the strands' anchorage zones. Test DB850-5A had an embedment length of 120 inches and was clearly a bond failure.

DB850-6A achieved flexural failure, but with some end slips. The cracking pattern (Figure 5.23) from test DB850-6A graphically demonstrates two separate cracking regions. The first flexural cracks formed at the region of maximum moment where all of the strands are bonded and active. The second region of cracking occurred in the debond transfer zone and is distinctly separated from the other cracking zone, clearly demonstrating the reduced cracking resistance that results from debonding strands. In this and other cases, cracking in the debond/transfer zone precipitated bond slip.

Test B on DB850-2 also illustrated a flexural failure with some bond slip. In this test, steel cladding prevented the propagation of web shear cracks into the lower portion of the cross section at the strands' anchorage zone. Consequently, the strands were able to develop their full tension required to resist the nominal flexural capacity of the section. Small amounts of strand slip did occur with the formation of a flexural crack at Station 68, however the beam was able to achieve its flexural capacity.

5.7.2 Staggered Debonding versus Concurrent Debonding. In a beam with staggered debonding, the termination points of vary from strand to strand. Conversely, in beams with concurrent debonding, all debonding is terminated at the same point along the length of the beam. These tests show that beams with staggered debonding perform better than beams with concurrent debonding. For example, two tests, DB850-4A and DB850-5A had the exact same debonded length, L_b, and the same embedment length, L_e. However, Beam DB850-4 had staggered debonding whereas DB850-5 had concurrent debonding. At lower loads, these two beams behaved identically. However, as loads increased, DB850-5A suffered cracking in the debond/transfer zone at lower loads because the greater number of debonded strands lowered the beam's resistance to cracking. This cracking led to slip of the debonded strands and subsequent bond failure. As expected, Beam DB850-4A failed in flexure whereas Beam DB850-5A failed in bond.

Moment diagrams for these two specimens are compared in Figure 5.35. Note that Beam DB850-4 has a larger cracking moment in the critical Debond/Transfer Zone DB850-4 than Beam DB850-5. As the load is increased, the applied moment exceeds M_{cr} at the transfer zone of the debonded strands in Test DB850-5A. When these flexural cracks form, the strands slip and lose anchorage. As a result, the beam fails in bond. Conversely, in Test DB850-4A, the applied moment does not exceed M_{cr} in the debond/transfer zone. The beam's ultimate flexural capacity is reached at the region of maximum moment before cracking occurs at the anchorage zone. Consequently the beam fails in flexure.

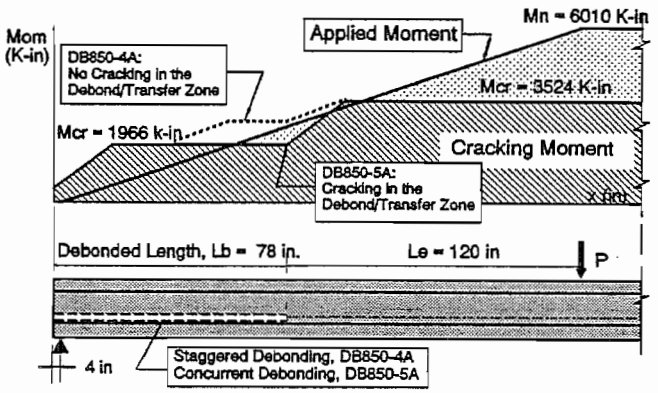

Figure 5.35 Staggered Debonding vs. Concurrent Debonding (Test DB850-4A vs. DB850-5A)

Comparison of these two tests demonstrate that beams with staggered debonding will behave better than strands with concurrent debonding. By staggering debonding, the beam enjoys greater resistance to cracking. This example demonstrates flexural behavior, but the same principles are true for any other type of behavior such as shear behavior.

5.7.3 Prediction of Cracking. Success of the prediction model is dependent upon the ability to predict the formation of cracks, both flexural cracks and web shear cracks. In Table 5.8 the first occurrence of flexural cracking is compared to the calculated value. Altogether there are ten test cases. First cracking occurred at moments ranging from a low of 97% of the calculated value to a high of 107%. The average cracking moment was 101% of the calculated value, demonstrating only one percent error. The cracking moment was calculated based on an effective prestress force of 160 ksi and a concrete strength of 6000 psi. The values for M_{cr} are given in Table 5.8.

TABLE 5.8

FIRST CRACKING LOADS AND MOMENTS TESTS ON BEAMS WITH DEBONDED STRANDS

Beam	First Cracking		
	P_{cr} (kips)	Mom (k-in)	Mom/M_{cr} [1]
DB850-3A	43.84	3376	0.99
DB850-3B	39.53	3297	0.97
DB850-4A	41.71	3580	1.02
DB850-4B	45.81	3664	1.04
DB850-5A	51.80	3567	1.01
DB850-6A	31.33	3509	1.00
DB850-1A	60.78	3525	1.00
DB850-1B	56.47	3461	0.98
DB850-2A	61.26	3588	1.02
DB850-2B	61.02	3779	1.07

1. M_{cr} = 3524 k" for DB850-1,2,4,5 and 6; M_{cr} = 3410 k" for DB850-3; using, f'_c = 6000 psi, $f_r = 7.5\sqrt{f'_c}$, and f_{se} = 160 ksi.

Occurrence of web shear cracking is given in Table 5.9. Figure 5.6 gives values for V_{cw}. For four effective strands, V_{cw} = 40.3 kips, and for eight effective strands, V_{cw} = 51.0 kips. However, the beam pictured in Figure 5.6 has L_b = 78 inches. The beams in this series that cracked in web shear had L_b = 36 inches. From the table, all of the web cracking occurred at shear loads between 40.7 kips and 52.1 kips. First web cracking occurred in the range of 40.7 kips to 42.5 kips. Resistance to web shear cracking, V_{cw}, was calculated by an elastic mechanic solution as outlined in Figure 4.16. Again, as with the prediction of flexural cracking, web shear cracking was accurately predicted.

5.7.4 Effects of Cracking on Bond Slip. Table 5.9 also reports the incidence of initial strand slip. In every case, the initial strand slip corresponded with the propagation of cracking through the transfer zone of the strands. In Beams DB850-3 through DB860-6, flexural cracking occurred in the transfer zone. In Beams DB850-1 and DB850-2, web shear cracking occurred in the transfer zone. These results clearly demonstrate that cracking precipitates bond slip.

5.7.5 Strand Slip without Bond Failure. In several of the tests, it is noted that small strand slips occurred without complete bond failure. This parallels results found in the literature and results from the fully bonded development length tests. Certainly, it must be concluded that strands have the ability to develop the required tension even if some bond slip does occur. Bond slip with flexural failure has been noted for several tests. However,

TABLE 5.9

SUMMARY OF END SLIPS COMPARED TO CRACKING IN THE DEBOND/TRANSFER ZONE

Beam	Le (in)	Cracking in the Debond/Transfer Zone			End Slips		Mode of Failure
		Load at Cracking (kips)	Station[1]	M_{cr} or V_{cw} [2]	Initial Slip	Slip at Failure (in)	
DB850-3A	78 (S)	63.44	112	3426$^{k'}$	Yes	2.02	Bond
		66.27	88	2785$^{k'}$	—		
			96	3048$^{k'}$			
DB850-3B	78 (S)	66.07	107	3119$^{k'}$	Yes	0.28	Flex
DB850-4A	78 (S)	—	—	—	—	0	Flex
DB850-4B	78 (S)	71.40	108	3413$^{k'}$	Yes	0.219	Flex
		75.11	95	3142$^{k'}$	—		
DB850-5A	78 (C)	77.78	80	2259$^{k'}$	Yes	3.70	Bond
			92	2616$^{k'}$	—		
			106	3032$^{k'}$			
DB850-6A	78 (C)	50.93	78	1884$^{k'}$	Yes	0.03	Flex
DB850-1A	36 (S)	88	24	44^{k}	Yes	0.85	Bond
DB850-1B	36 (S)	80.14	20	42.5	No[3]	0.75	Bond
		93.6	42	49.5	Yes		
DB850-2A	36 (S)	76.93	15	41.7^{k}	No[3]	0.36	Bond
		86.5	36	46.9^{k}	No[3]		
		89.67	42	48.6^{k}	Yes		
		95.97	—	52.1^{k}	—		
DB850-2B	36 (C)	78.9	20	40.7^{k}	No[3]	0.52	Flex
		93.29	73	3322$^{k'}$	Yes		

1. Distance from the end of the beam
2. Measured moment, M_{cr}, or measured shear, V_{cw}, at the crack location; calculated by statics
3. Steel cladding attached to the web prevented strand slips

it must be pointed out that many of the tests that combined slip with flexural failure had embedment lengths on or very near the borderline separating expected behaviors. As such, any cracking in the transfer zones occurred at loads very near the nominal capacity. In those cases, the debonded strands may not have developed any additional tension, but rather, transferred their load to the fully bonded counterparts. This would explain why results from Rabbat et al and from Dane and Bruce measured significant strand slips, but were still able to develop the ultimate load. It would also explain similar results in these tests.

5.8 Comparison to Code Provisions

This research indicates that the current code provisions may be too restrictive in some cases. But more importantly, test results demonstrate that current code provisions do not establish an accurate model for behavior of beams with debonded strands. Consequently, current code provisions are, at best, misleading and could potentially lead to unsafe designs.

Two very important facts are illuminated by the plots in Figure 5.7a and 5.7b. First of all, the embedment length required to prevent bond failure is dependent on the length of debonding. Therefore, development length is a function of debonded length, $L_d \rightarrow f(L_b)$. And the corollary, longer debonded lengths require longer embedment lengths for the strands.

Many of these tests had embedment lengths that did not conform to the code requirement for twice the basic development length. Yet these strands demonstrated their ability to maintain bond integrity and strand anchorage. The most extreme example is Test DB850-2B. Strands in this specimen demonstrated the bond strength to develop ultimate flexural capacity, yet the embedment length was only 88 inches, not the 160 inches required by ACI and AASHTO codes.

On the other hand, Test DB850-6A approached conformance with the code provisions. Its embedment length was 150 inches and even though its failure was classified as a flexural failure, some strand slips were measured. Generalizing this behavior to a more extreme case, perhaps with longer spans and longer debonded lengths, many design cases would exist where the requirement to double the development length would still allow cracking in the debond/transfer zone; these designs may be unsafe.

It is also important to note the differences in the bond behavior of strands whose debonding is staggered compared with those strands whose debonding is concurrent. If strands are concurrently debonded, then the required development length is much greater than if the debonding was staggered. The code makes no distinctions or requirements towards staggering debonding. This research indicates that staggered debonding should either be required by code language, or better yet, encouraged by code provisions that are more closely related to behavior.

5.9 Summary

This chapter began with an analytical rationale to predict the anchorage failure of beams with debonded strands. The model presumes that a strand will slip when cracks propagate across the anchorage zone of a strand. Tests were designed and performed using this prediction model. Agreement between results and predicted behavior was very good. Additionally, these tests demonstrated that cracking in concrete could be accurately predicted and that cracks in the transfer zone of a strand, whether due to flexure or shear, do cause that strand to slip.

CHAPTER 6
REPEATED LOAD TESTS

6.1 Introduction

Repeated load tests are necessary to establish structural behavior under duress imitating the service life of a structure. Repeated load tests were necessary in this project to determine the performance of bond through many load cycles. Some small end slips were noted in static tests, and it must be established whether bond will stabilize under repeated load, or if repeated load will eventually cause the bond to fail.

Five beams were tested under repeated loads. Four of the beams contained eight 0.5 inch diameter strands, four of which were debonded, while the fifth beam contained four fully bonded 0.6 inch diameter strands. A total of eight tests were performed. The beams used in these tests were companion beams to the beams used in the static test series. In fact, the two sets of beams are identical in every way, except of course, small variations in concrete strength and/or strand tension.

In each test, load was cycled from 25% of service load to 100% of service load (0.25 P_{sv} to 1.0 P_{sv}) for at least one million cycles or until failure. Static load tests were performed at intermediate stages to test the beams for loss of stiffness or loss of bond. These intermediate static loads were overloads that exceeded the service load by factors of 1.3 to 1.6 to mimic large truck traffic or special loads that a bridge might be required to support in its service life. Each beam was "precracked" prior to the repeated load testing, so all of the repeated loads were applied to a cracked beam.

Results from these tests are remarkably similar to the results from the static tests on companion beams. These tests demonstrate that the same behavioral models that were developed for static tests are accurate for structures subjected to repeated loads. It should be noted that some bond fatigue was observed, where bond slip occurred simply through the repetition of load. However, strand slips appeared to stabilize after a finite number of load cycles. Significant slip from bond fatigue was observed in only one specimen, a specimen that was predicted to fail in bond because of a short embedment length.

6.2 Design and Fabrication

A total of five beams were tested in this series. All of the beams were companion beams to others that were tested statically. Four of the beams contained eight 0.5 inch strands, with four debonded strands, whereas the fifth beam, FA460-F4 contained four fully bonded 0.6 inch strands. The debonded beams are labeled DB850-F1 through F4.

DB850-F1 and DB850-F2 are identical to each other and to two beams from the static test series, DB850-3 and DB850-4. These beams all had debonded strands with

staggered debonding. By definition, the debonded length is taken as the longest length of debonding, in this case, L_b = 78 inches. Likewise, beams DB850-F3 and DB850-F4 are identical to each other and to beams DB850-5 and DB850-6, from the static test series. These beams all had debonded strands, but with concurrent debonding. The debonded length, L_b of these beams is also 78 inches. The cross sections and beam details are given in Figure 6.1. Strand patterns and the debonding schedule are given in Figure 6.2.

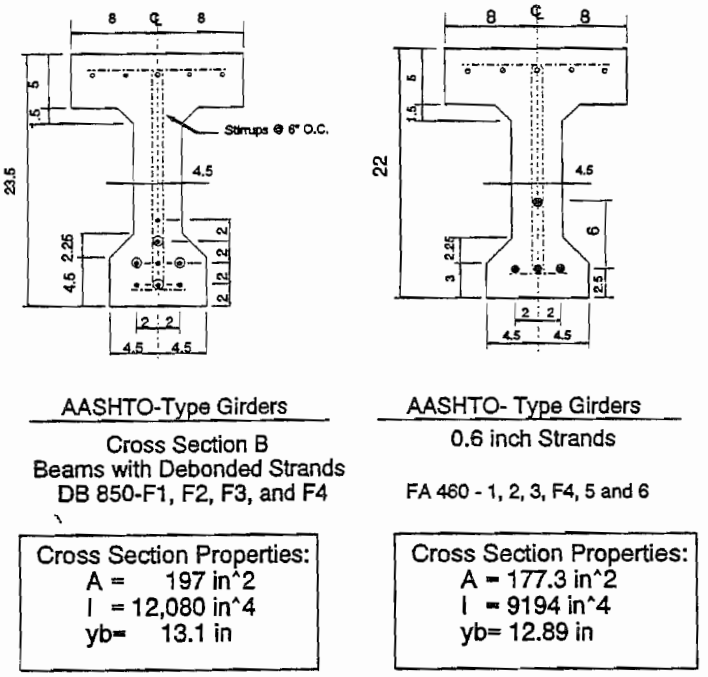

Figure 6.1 Cross Section Details Repeated Load Tests

The shear reinforcement consisted of #3 reinforcement, placed in pairs. The cross section details illustrate the shear reinforcement. Stirrups were placed at 6 inch spacings for all of the beams with the exception of beam FA460-F4. Its shear reinforcement was placed at 6 inch centers within 10 feet from ends of the beam and 8 inch centers in the interior portion of the beam.

The beams were fabricated by the same procedures that were used for the beams in the static test series (Section 5.5.2). Strands were stressed to 75% of f_{pu} for initial tensioning. Initial tension was measured using a pressure indicator showing the hydraulic pressure applied to tension the strand. Strand elongations were also measured to assure correct tensioning. Elongation measurements are given in Table 6.1. These beams were stored for longer periods of time before testing when compared to beams that were tested statically. The effective prestress force was calculated from the elongation measurements taken while tensioning the strands and adding the initial prestress of 10.4 ksi for 0.5 inch strands and 7.3 ksi for 0.6 inch strands, then

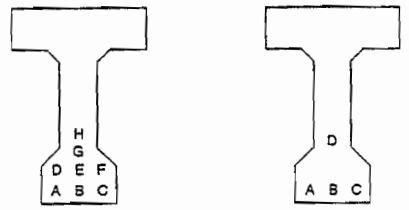

DEBOND SCHEDULE				
Strand	B	D	F	G
FA460-F4	0	0	-	-
DB850-F1	78	39	39	78
DB850-F2	78	39	39	78
DB850-F3	78	78	78	78
DB850-F4	78	78	78	78

Figure 6.2 Strand Patterns and Debonded Schedule Repeated Load Tests

deducting losses calculated by the General Method from the Precast/Prestressed Concrete Institute, given in Appendix D of reference 26. For beam FA460-F4, the effective prestress force was calculated to be 160 ksi. For beams DB850-F1 through F4, the effective prestress force was calculated to be 152 ksi.

TABLE 6.1

STRAND ELONGATIONS
AND
CALCULATION OF EFFECTIVE PRESTRESS

REPEATED LOAD TESTS

BEAM	STRAND ELONGATIONS (in)								
	A	B	C	D	E	F	G	H	AVG.
FA460-F4	5.906	5.563	5.625	-	-	-	-	-	5.698
DB850-F1	5.500	5.516	5.438	5.438	5.469	5.484	5.438	5.500	5.473
DB850-F2	5.500	5.516	5.609	5.531	5.547	5.625	5.844	5.547	5.590
DB850-F3	5.797	5.469	5.516	5.516	5.359	5.516	-	5.500	5.525
DB850-F4	5.453	5.609	5.547	5.594	5.469	5.469	5.328	5.281	5.469

The plots of concrete strengths given in Appendix B also depict the number of days after casting that a beam was tested. Because of this, the beams used for repeated load tests suffered greater time dependent losses than in the beams from the static test series. Consequently, the effective prestress and cracking moments are lower for these beams than their companions that were tested statically.

The age of the concrete also affected concrete strength at the time of testing. Concrete strengths are given in Table 6.2. Concrete strength over time is plotted in Figures B6 and B13 through B16 in Appendix B. The beams were cast with concrete having the same concrete mix proportions as the statically tested beams. Concrete mix proportions are given in Table 4.1. As always, care was taken to properly consolidate the concrete with both external form vibrators and internal vibrators. Strand load versus strain is given in Figure B1.

6.3 Test Setup and Instrumentation

6.3.1 Testing Equipment. The same testing apparatus was used for these tests that was used for all previous flexural tests, but with different hydraulic equipment. The load frame and support beams remained the same. As noted earlier, the support beams allowed the support locations to vary from test to test. Photographs of the testing apparatus are shown in Figures 6.3 and 6.4. For the repeated load tests, a fatigue rated hydraulic actuator was used. Its fatigue capacity was rated at approximately 115 kips. Its static capacity was

200 kips. The repeated load cycles were controlled by a closed loop system. An electronic controller regulated the load cycle by signalling a servo-controller mounted on a four way valve. Load was controlled by controlling the direction and flow of hydraulic fluid. The controller monitored the applied load from the load cell positioned directly under the actuator. The load varied as a sine wave with the peak at 100% of service load moment, M_{sv}, and the valley at approximately 25% M_{sv}.

A static hydraulic system was used for the initial static tests and the subsequent static tests, including tests to failure. Safety precautions require the use of a static hydraulic system in tests to failure because hydraulic pressure is relieved with gross deformations of the beam. If the beam were to fail under load, the resulting displacements would also result in a loss of hydraulic pressure, making the system inherently safe. The static system used a conventional electrical or mechanical pump and different hydraulic lines.

TABLE 6.2

CONCRETE STRENGTHS[1]

REPEATED LOAD TESTS

Beam	Release Strength	Strength at Flexural Test	
		Moist Cure	Field Cure
FA460-F4	4836	6516[2]	-
DB850-1	4642	7408	7004
DB850-2	4043	8349	-
DB850-3	4396	7020	7488
DB850-4	4805	-	7339

1. Concrete Strengths vs. Time are plotted in Appendix B.
2. Concrete Strength at 28 days. Testing was performed approximately 300 days after casting.

6.3.2 Stress Ranges and Load Histories. Each test began with a static test that "precracked" the beam. Flexural cracking increases the stress range in the steel beyond the stress range for an uncracked section. Previous fatigue tests[18,23,35,40] have shown that very little distress will occur before cracks develop. Additionally, bond stresses between concrete and steel are directly related to the change in strand tension. Higher stress ranges also place greater demands on related bond stresses. Prior to cracking, bond stresses remain very small, and precracking the beam is necessary to provide an adequate test for bond fatigue.

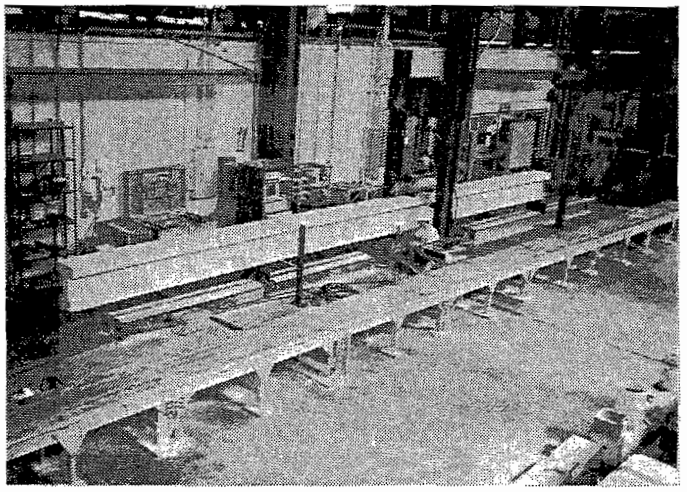

Figure 6.3 Photograph of Test Setup and Beam DB850-F1

After the initial static tests, load was cycled between a minimum load (approximately equal to 25% of the service load) and a maximum load (approximately equal to 100% of service load). The service load is defined as the load that causes a tensile stress equal to $6\sqrt{f'_c}$ on the bottom fiber of the uncracked section.

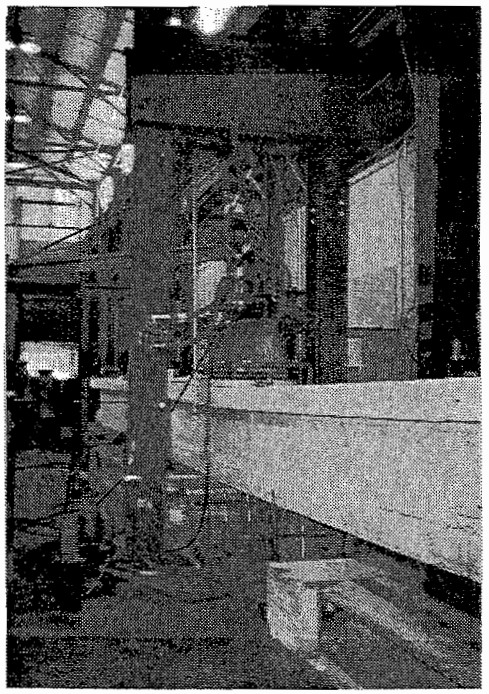

Figure 6.4 Photograph of Testing Apparatus

Strand stress ranges are illustrated in Figures 6.5 and 6.6. Moment is plotted versus strand stress. Moment versus curvature was computed assuming that the beams act in pure flexure and that strains are linear across the cross section. Strand strain is assumed to be the strain at the centroid of the c.g.s. of the prestressing steel. Strand stress is related to strain by the data provided by the manufacturer as shown in Appendix B, Figure B1. Calculations are made by analyzing the cracked section.

Periodically, overloads were applied to each specimen. Overloads were applied to mimic overloads that occur in the life of a bridge structure. Overman, Breen and Frank[35] noted that occasional modest overloads can produce extremely detrimental effects. In this research, the magnitude and frequency of overloads varied from test to test. Overloads varied from 1.3 times the service load to 1.6 times the service load. After the overload cycle, repeated loading was continued as before. Static overloads are described in detail in later discussions of each beam tested in this series.

6.3.3 Instrumentation. The instrumentation for these tests was essentially the same as for the statically tested beams. Instrumentation measured applied load, beam deflection and strand end slip during the static tests. These data were measured electronically and the data was stored by the data acquisition system. Other data measured electronically included hydraulic pressure and electrical resistance strain gages applied to the strands. Figure 4.6 illustrates the instrumentation and locations where measurements were taken.

Load was measured from an electronic load cell at the hydraulic actuator. Deflection and end slips were measured by linear potentiometers. The electronic potentiometers used to measure end slips are pictured in Figure 6.7. All of the electronic instruments were calibrated prior to testing. End slip measurements are accurate to ± 0.001 inches.

Concrete strains were measured in the constant moment region of each test. Measurements were taken at each load increment with the DEMEC gage system discussed in Chapter 3.

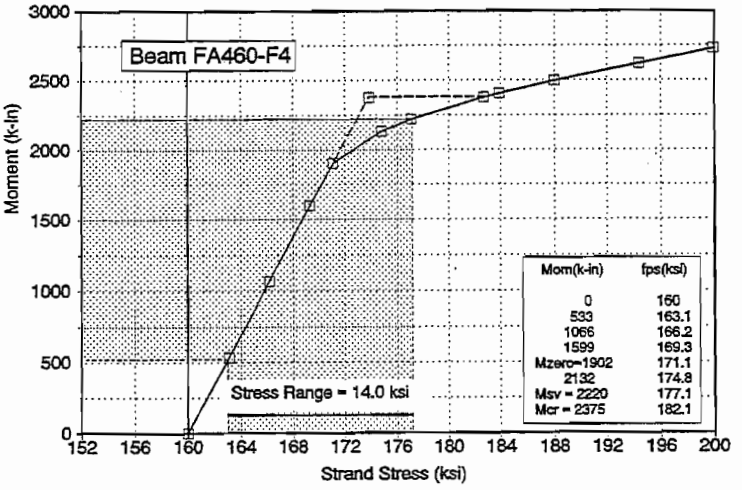

Figure 6.5 Stress Range for Repeated Load Tests

6.4 Repeated Load Tests; Procedures and Results

As noted before, eight repeated load tests were performed on five beams. Three of the beams were tested twice, once on each end. Two of the beams were tested only once. In this section, the test sequence and the loading histories for each test are described along with the major variables. As each test progressed, certain behavioral characteristics were noted that affected the procedure and the outcome for each test. These behaviors are also noted in this section.

6.4.1 Test Variables. The major variables for this test series are the debonded length(L_b), the type of debonding("S" or "C"), the embedment length(L_e), the number of load cycles(N) and the magnitude and frequency of the intermediate overloads. Values for the first three variables are given in Table 6.3. Please note that all of the debonded beams (DB850-F1 through F4) contained eight 0.5 inch strands whereas the fully bonded beam (FA460-F4) contained four 0.6 inch strands. The embedment length is again taken as the distance from where bond begins to the point of maximum moment. For the beams with staggered debonding, the debonded length, L_b, is always taken as the longest extent of debonding.

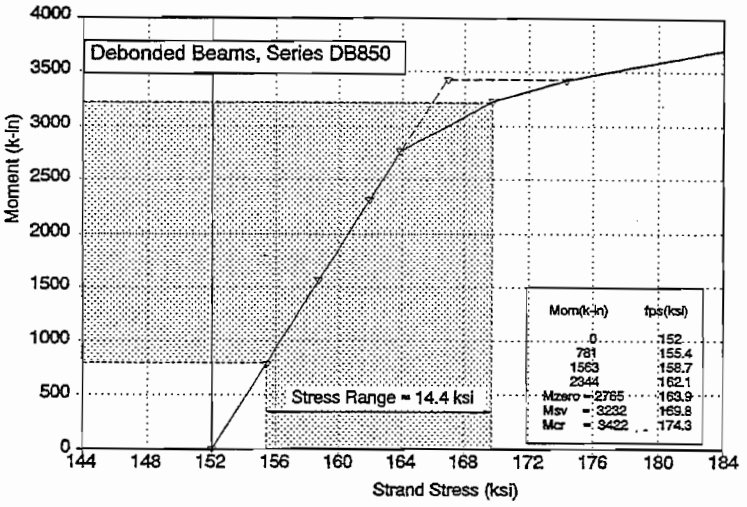

Figure 6.6 Stress Range for Repeated Load Tests

The remaining variables, the number of cycles and the magnitude and frequency of the intermediate loadings changed as each test evolved. All of the test specimens were intended to cycle through a minimum of 1 million loads, however some of the beams failed

before this many load cycles were achieved. The most significant damage occurred during the intermittent static overloads. Therefore, the magnitude of the intermittent static loads was adjusted to match each individual test so that some cracking would occur, but would not preclude further repeated load testing. Even so, two of the tests, DB850-F2A and DB850-F4, failed at relatively small loads during intermediate tests. These two failures resulted from bond failures and inadequate strand embedment.

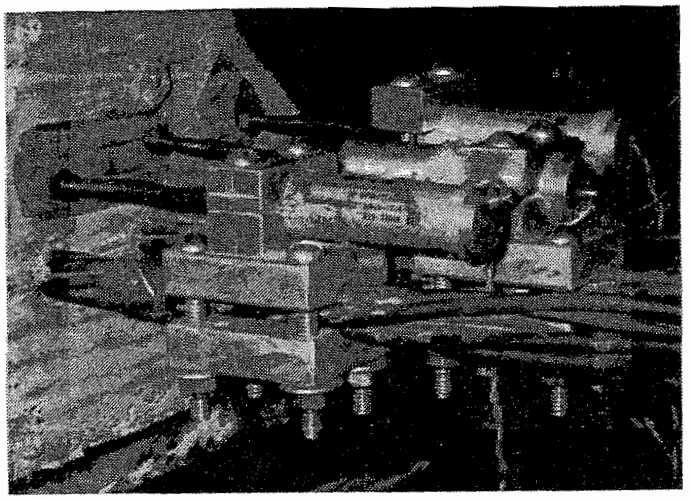

Figure 6.7 Photograph of Electronic Potentiometers to Measure End Slips

In the next eight sections, each test is described briefly. For each test, the load histories are described with information in both tabular and figure form. The figures plot the magnitude of the load versus the number of cycles, N. End slips are also plotted versus number of cycles, N, in these same figures. These figures demonstrate that damage to prestressing bond occurred primarily during the static overloads. The tables also report deflections at the beginning and end of each static test and also the deflection at the service load. Large increases in deflection indicate a loss of stiffness in the beam. Deflections were measured under the load point.

Finally, the final static test to failure is plotted for each test. These figures plot load versus deflection, end slips versus deflection and also illustrate the geometry of each test.

Any significant behavioral results from the intermediate static tests are also reported, such as strand slip that occurred concurrently with cracking. For each test, the final static loading was applied until the beam failed, either in flexure or in bond.

6.4.2 Beam FA460-F4, Test A. This first test specimen, Beam FA460-F4, contained four 0.6 inch strands. Currently, 0.6 inch strands are not allowed in pretensioned applications by the Federal Highway Administration (FHWA), primarily because their bond behavior is unknown. Tests on this beam add to the understanding of these larger diameter 0.6 inch strands and their behavior under service load conditions.

All of the strands contained in this specimen are fully bonded. In the static tests reported in Chapter 4, the development length of 0.6 inch strands was measured to be about 84 inches. For the first test, Test FA460-4A, the embedment length was chosen to be 120 inches, or 1.25 times the development length currently required by the code. Figure 6.8 is

a photograph showing this beam and the test setup. The loading history for this beam is reported in Table 6.4 and Figure 6.9.

TABLE 6.3

VARIABLES BY TEST SPECIMEN FOR REPEATED LOAD TESTS

Test	Beam Length, L (in)	Debonded Length, L_b (in)	Embedment Length, L_e (in)	Type of Debonding[1]
FA460-F4A	480	0	120	-
FA460-F4B	480	0	96	-
DB850-F1A	480	78	100	S
DB850-F1B	480	78	80	S
DB850-F2A	480	78	80	S
DB850-F2B	480	78	110	S
DB850-F3	480	78	120	C
DB850-F4	480	78	100	C

1. "S" denotes staggered debonding.
"C" denotes concurrent debonding.

The beam was cracked in the initial static loading to 1.6 P_{sv}. The nearest crack to the end of the beam formed at Station 88, or 88 inches from the end of the beam. There was no strand slip. In all of the subsequent repeated load cycles and intermediate static tests, no additional cracks formed near the support and no strand slips were reported. The test specimen withstood 1,770,265 load cycles. Figure 6.10 illustrates the load-deflection curve for the final static test to failure. The beam failed at a load of 55.36 kips and a moment of 3905 k-in. The beam clearly failed in flexure at 99% of the calculated nominal capacity with no end slip.

6.4.3 Beam FA460-F4, Test B. As in Test FA460-F4A, all four 0.6 inch strands were fully bonded for Test FA460-F4B. The embedment length was set at 96 inches, or 1.0 times the development length, L_d as given by the current code. This beam was cracked in the initial static loading to 1.6 P_{sv}. The nearest flexural crack to the support formed 75 inches from the end of the beam. Only very small strand slips were measured, less than one thousandth of an inch. The loading sequence on this beam was very severe. Subsequent static overloads of magnitude 1.6 P_{sv} were applied at 10, 129, 1000, 12,226, and 138,321 cycles. No additional cracking occurred and no significant strand slips occurred throughout the repeated load tests or the intermediate static tests. Loading histories are given in Table 6.5 and Figure 6.11.

A total of 1,400,000 cycles were applied to the beam, after which the beam was statically loaded until failure. The results of the final static test are illustrated in Figure 6.12. The beam failed in flexure with very little strand slip. At failure, the maximum moment was 3874 k-in, or 98% of the calculated nominal flexural capacity.

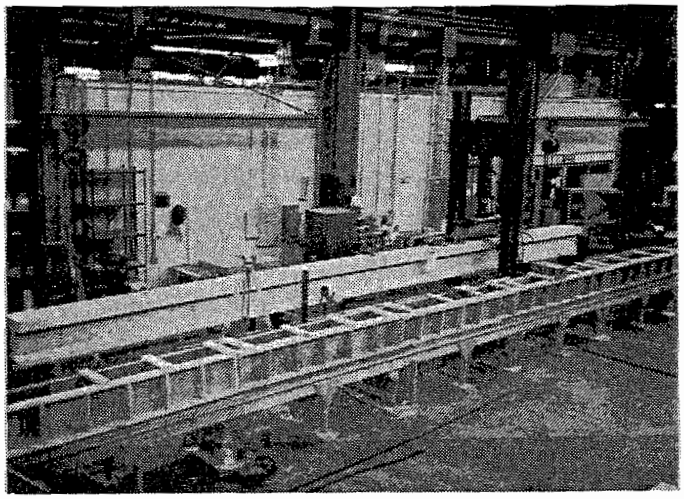

Figure 6.8 Photograph of Test Setup and Beam FA460-F4

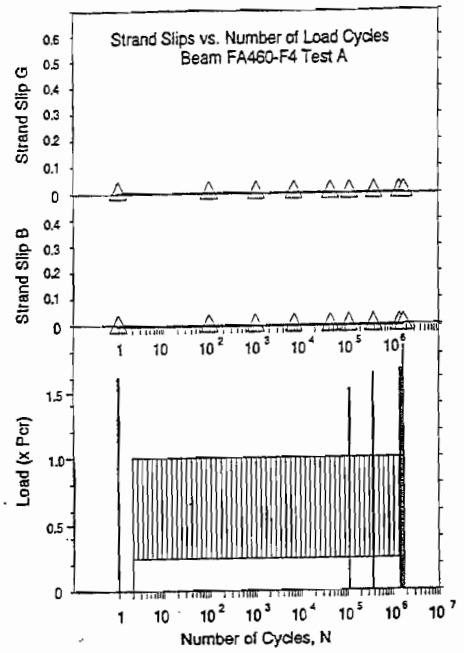

Figure 6.9 Loading History: Beam FA460-F4 Test A

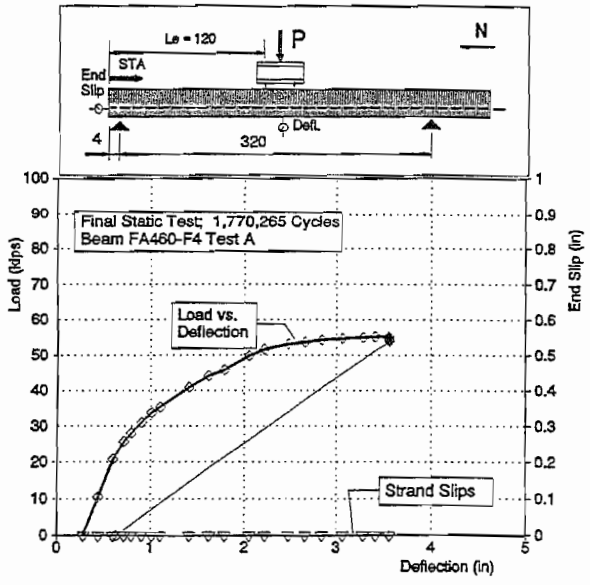

Figure 6.10 Load vs. Deflection and End Slips Beam FA460-F4 Test A

TABLE 6.4

BEAM FA460-F4 TEST A
STATIC LOAD TESTS

L_e = 120 in ; P_{sv} = 30.2 k" ; P_u = 54.0 k"

Load Cycle N	Max. Load (kips)	% P_{sv}	Deflections			Slip B		Slip G	
			Beg	End	@ P_{sv}	Beg	End	Beg	End
1	48.62	1.6	0	0.113	0.426	0	0	0	0
2	30.2	1.0	0.06	0.06	0.63	0	0	0	0
100	30.2	1.0	0.06	0.06	0.63	0	0	0	0
1000	30.2	1.0	0.06	0.06	0.64	0	0	0	0
7000	30.2	1.0	0.09	0.09	0.72	0	0	0	0
42,815	30.2	1.0	0.09	0.09	0.69	0	0	0	0
113,020	45.0	1.5	0.09	0.10	0.69	0	0	0	0
391,971	49.0	1.63	0.125	0.156	0.71	0	0	0	0
1.52 mil	50.0	1.66	0.156	0.156	0.75	0	0	0	0
1.77 mil	55.36	1.83	0.281	0.506	0.87	0	0	0	0

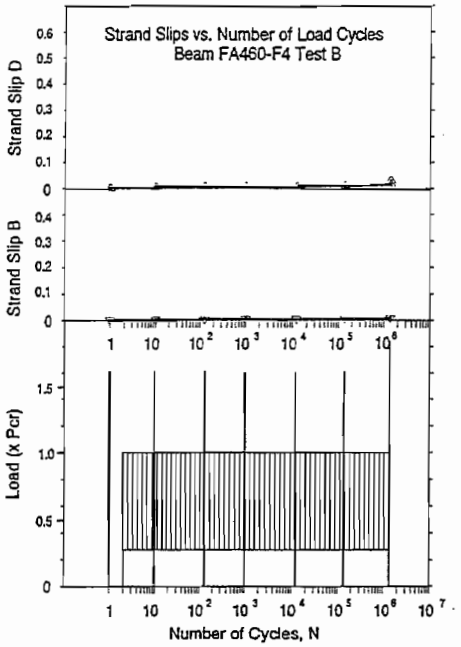

Figure 6.11 Loading History: Beam FA460-F4 Test B

TABLE 6.5

BEAM FA460-F4 TEST B
STATIC LOAD TESTS

L_e = 96 in ; P_{sv} = 38.4 k" ; P_u = 68.1 k"

Load Cycle N	Max. Load (kips)	% P_{sv}	Deflections			Slip B		Slip G	
			Beg	End	@ P_{sv}	Beg	End	Beg	End
1	58.69	1.6	0	0.057	0.36	0	.0003	0	0.0026
10	58.6	1.6	0.052	0.072	0.45	0.0018	0.0028	0.0037	0.0047
129	58.4	1.6	0.064	0.061	-	0.0033	0.0044	0.0064	0.0061
1,000	58.4	1.6	0.069	0.073	0.49	0.0048	0.0054	0.0069	0.0072
12,226	58.5	1.6	0.075	0.079	0.51	0.0053	0.0058	0.0067	0.0084
138,321	58.6	1.6	0.076	0.081	0.50	0.0062	0.0062	0.0114	0.0111
1400,000	66.95	1.83	0.093	-	0.51	0.0082	0.0090	0.0158	0.0298

6.4.4 Beam DB850-F1, Test A. The dimensions for this test exactly matched the static test performed on DB850-4B. The debonding patterns and the debonded lengths are identical for the two beams, L_b = 78 inches with staggered debonding. The embedment length for both tests was set at 100 inches. The span for the two tests was also identical, 346 inches.

Test DB850-4B failed in flexure at a load of 75.4 kips. Its load versus deflection curve is illustrated in Figure 5.19. Note also that strand B slipped approximately 0.2 inches and strand G slipped approximately 0.1 inches.

Testing on specimen DB850-F1A began with application of an initial static load of 1.6 times the service load. During the initial loading, at a load of 62.3 kips, a crack formed 105 inches from the end of the beam. This crack formed very near the transfer zone.

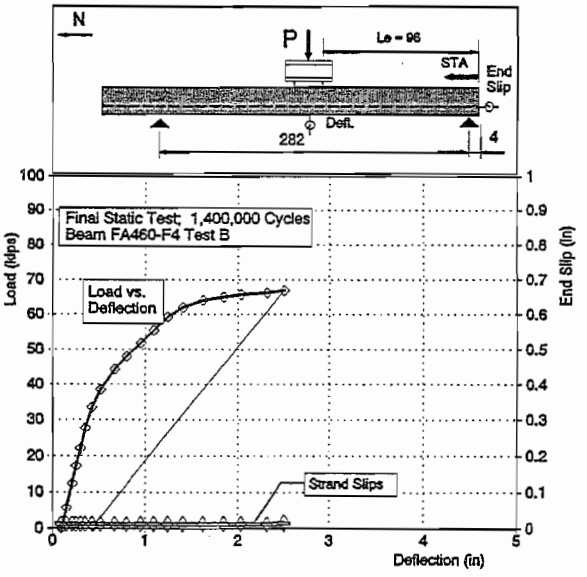

Figure 6.12 Load vs. Deflection and End Slips Beam FA460-F4 Test B

Note that if the transfer length of the debonded strand was 25 inches, then the transfer zone would extend to 103 inches. When the crack formed at Station 105, strand slips on strands B and G were measured to be about 0.02 inches. In the static test on Specimen DB850-4B, a similar crack formed at Station 108, but at a load of 71.4 kips. The greater resistance to cracking may reflect a larger effective prestressing force in Beam DB850-4, which was tested at a younger age and had lower prestressing losses.

After the initial static test was completed, repeated load testing commenced. The load history and strand slips are plotted in Figure 6.13. These data are also reported in Table 6.6. Load was varied between a maximum load equal to the service load, P_{sv} and a minimum load approximately equal to 25% of P_{sv}. End slips increased slightly through the early repeated load cycles, from 0.02 inches to about 0.03 inches through the first 1000 cycles. At load cycle 1023, another static overload test to 1.6 P_{sv} was conducted and end slips increased from 0.03 inches to 0.09 inches for strand B and to approximately 0.05 inches for strand G. Additional repeated load testing increased strand slips only very slightly.

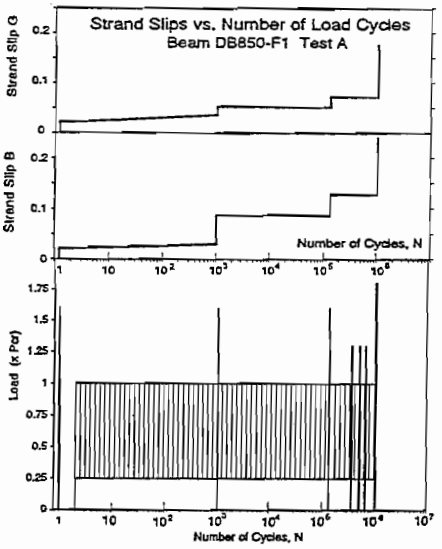

Figure 6.13 Loading History: Beam DB850-F1 Test A

At load cycle 381,864, another static overload equal to 1.6 P_{sv} was placed on the beam. Again strand slips increased in response to the overload. Additional repeated loads failed to produce any additional strand slips.

After 1,040,000 cycles, the beam was loaded statically until failure. The beam failed at a load of 70.05 kips with end slips of 0.24 inches on strand B and 0.18 inches on strand G. Load versus deflection is illustrated in Figure 6.14. The beam failed at a load of 70.05 kips and at a moment of 5602 k-in. Failure

TABLE 6.6

BEAM DB850-F1 TEST A
STATIC LOAD TESTS

L_e = 100 in ; P_{sv} = 40.4 k" ; P_u = 75.1 k"

Load Cycle N	Max. Load (kips)	% P_{sv}	Deflections			Slip B		Slip G	
			Beg	End	@ P_{sv}	Beg	End	Beg	End
1	62.26	1.6	0	0.129	0.63	0	.0209	0	0.0217
1023	62.4	1.6	0.127	0.154	0.97	0.0296	0.0867	0.035	0.0522
134,912	62.4	1.6	0.197	0.215	1.08	0.087	0.128	0.052	0.071
381,864	50.0	1.3	0.23	0.24	1.14	0.128	0.128	0.072	0.071
524,053	50.0	1.3	0.29	0.29	1.18	0.128	0.128	0.071	0.071
703,174	50.0	1.3	0.29	0.29	1.17	0.128	0.128	0.072	0.072
1,040,050	70.05	1.8	0.29	0.35	1.17	0.128	0.240	0.072	0.176

was a classical flexural failure with crushing of the concrete in the top compression fibers. However, the failure load was only 93% of the ultimate capacity of its companion, specimen DB850-4B, and only about 93% of the calculated ultimate capacity. Concrete crushed at a strain of about 0.0025 in/in. This strain is somewhat lower than expected for crushing strain and may have contributed to the earlier than expected failure.

Beam DB850-4B of the static load test series failed in flexure. The embedment length of 100 inches placed this test on the borderline between flexural failure and bond failure as predicted by bond failure model, Figure 5.33. The repeated load test DB850-1A is also on the border between flexural failure and bond failure. Interestingly, the failure exhibited a hybrid type of behavior failing in flexure, but with some strand slip.

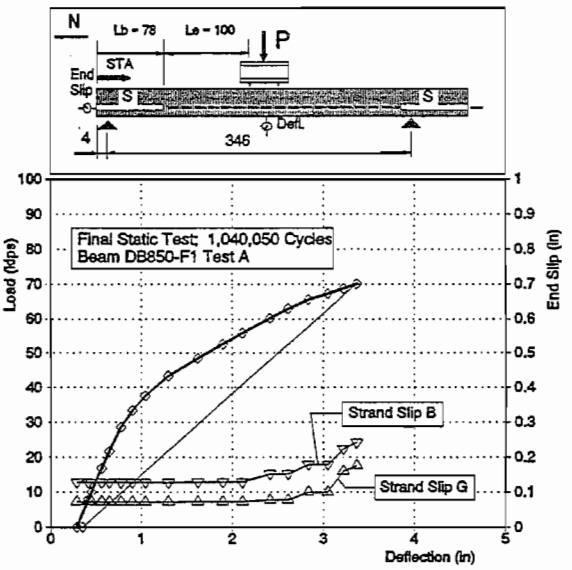

Figure 6.14 Load vs. Deflection and End Slips Beam DB850-F1 Test A

6.4.5 Beam DB850-F1 Test B. This test had an embedment length 80 inches with staggered debonding on four of the eight 0.5 inch strands. The loading history and end slips are shown in Figure 6.15. Values of end slips and beam deflections are given in Table 6.7.

The initial static test and subsequent intermediate static tests loaded the beams to a maximum load of only 1.3 P_{sv} which is a significantly smaller overload than in previous intermediate tests. At these lower loads, flexural cracking extended to only 130 inches from the end of the beam, and did not affect the anchorage of the strands significantly. Accordingly, there was no appreciable strand slip from these early repeated loads. After 386,878 load cycles, the beam was loaded to 1.6 P_{sv}. At this loading, flexural cracks extended through the transfer zone of the debonded strands at Station 88. Strands slips were measured to be about 0.13 inches on Strand B and 0.086 inches on Strand G. Through the remaining repeated loads, strand slips increased only slightly to about 0.16 inches on Strand B and 0.093 inches on Strand G.

The final static test was performed after 1,027,083 cycles. Load versus deflection and end slips are illustrated in Figure 6.16. After the decompression load was reached, strand slips increased as load increased until failure. The beam failed at a load of 82.6 kips and a moment of 8672 k-in. Failure occurred through crushing of the concrete in a flexural failure. However, bond slips at failure were relatively large and overall failure must be considered a bond failure. In spite of the strand slips, beam behavior was surprisingly similar to flexural failure, indicating that large bond stresses can exist between concrete and strand even though fairly large slips, 0.093 inches to 0.16 inches, have occurred.

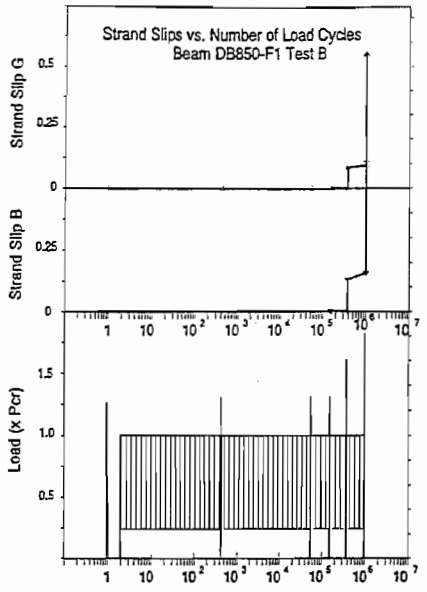

Figure 6.15 Loading History: Beam DB850-F1 Test B

TABLE 6.7

BEAM DB850-F1 TEST B
STATIC LOAD TESTS

L_e = 80 in ; P_{sv} = 47.1 k" ; P_u = 95.0 k"

Load Cycle N	Max. Load (kips)	% P_{sv}	Deflections			Slip B		Slip G	
			Beg	End	@ P_{sv}	Beg	End	Beg	End
1	58.5	1.25	0	0.06	0.56	0	.0002	0	0.0003
432	58.9	1.3	0.029	0.039	0.73	0.0005	0.0006	0.0008	0.0004
54,534	58.9	1.3	0.075	0.081	0.70	0.0009	0.0009	0.0003	0.0002
158,000	58.9	1.3	0.094	0.094	0.73	0.0011	0.0017	0.0002	0.0008
386,878	72.5	1.6	0.094	0.159	0.74	0.0010	0.1292	0.0004	0.0862
1,027,083	82.6	1.75	0.188	0.311	0.77	0.159	0.605	0.093	0.552

6.4.6 Beam DB850-F2, Test A. Like Test B on DB850-F1, this test also featured an embedment length of 80 inches. However, results from this test were quite different because strand slips occurred under repeated applications of service load. In the initial static test, flexural cracking extended to Station 106 at a load of 1.3 P_{sv}. Initial strand slips coincided with the formation of this crack. After the initial static test, strand slips increased under the influence of the early repeated loads. This test is unique because large strand slips occurred from the application of repeated loads to service load levels. This is the only test where significant strand slips occurred during the repeated loads at service load. Strand slips increased from 0.03 inches to nearly 0.4 inches simply from the action of the repeated load tests.

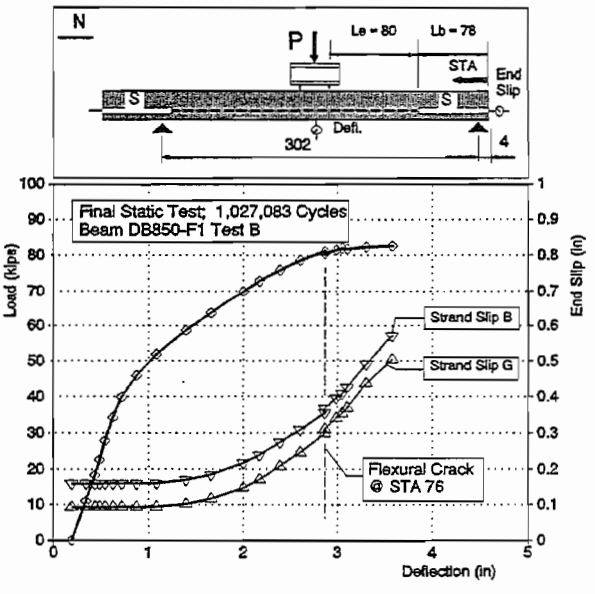

Figure 6.16 Load vs. Deflection and End Slips Beam DB850-F1 Test B

TABLE 6.8

BEAM DB850-F2 TEST A
STATIC LOAD TESTS

L_e = 80 in ; P_{sv} = 41.97 k" ; P_u = 78.1 k"

Load Cycle N	Max. Load (kips)	% P_{sv}	Deflections			Slip B		Slip G	
			Beg	End	@ P_{sv}	Beg	End	Beg	End
1	55.0	1.3	0	0.086	0.61	0	.087	0	0.081
7000	42.5	1.05	0.091	0.096	1.06	0.292	0.293	0.355	0.356
26,310	42.5	1.05	0.116	0.122	1.12	0.325	0.326	0.396	0.395
121,308	55.0	1.3	0.141	0.159	1.20	0.327	0.358	0.396	0.417
192,945	63.78	1.5	0[1]	0.543[1]	1.18[1]	0.383	0.602	0.472	0.676

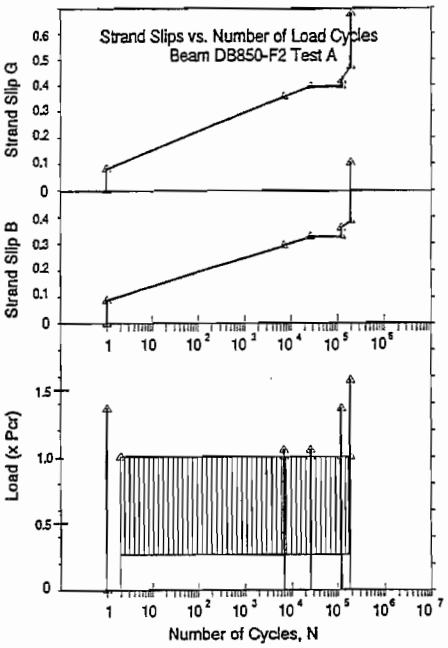

Figure 6.17 Loading History: Beam DB850-F2 Test A

Results of strand slips and deflections through the different load cycles are reported in Table 6.8. Figure 6.17 illustrates the load history and strand slips graphically. The figure depicts the dramatic increase in strand slips as the load cycles increased through the first 121,000 cycles. More importantly, even though strand slips did occur at service load levels, they stabilized after a finite number of repetitions.

In the final static test, the beam clearly failed from the failure of the strand anchorage. Load versus deflection and end slip for the final test are shown in Figure 6.18. Note that end slips were quite large at the beginning of the test and that strand slips increased until failure of the beam. Failure occurred at 63.78 kips and a moment of 4911 k-in., only 82% of the calculated ultimate load.

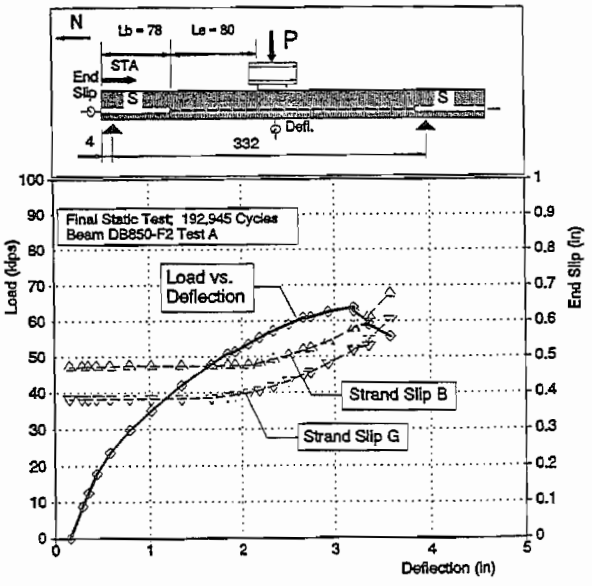

Figure 6.18 Load vs. Deflection and End Slips Beam DB850-F2 Test A

6.4.7 Beam DB850-F2, Test B. The embedment length for this test was set at 110 inches. This embedment length was shown to adequately develop the nominal flexural capacity of the beam in the earlier static test series (Figure 5.33). The load history, strand slips, and deflections through the cyclic loads are reported in Table 6.9 and Figure 6.19. The initial static test loaded the beam to 1.3 P_{sv}, a relatively low initial cracking load. The region

of flexural cracking remained well away from the anchorage zone. The nearest flexural crack formed at Station 142. The strands did not slip in the initial static test.

The beam was then subjected to repeated loads at service load for 1,110,222 cycles. One intermediate static test increased the load to 1.4 P_{sv}, however, no strand slip occurred through any of these loadings. The beam was loaded to failure in the final static test, as shown in Figure 6.20. The beam failed at a load of 81.37 kips by crushing of the concrete at the top compression fiber. Strand slip did occur, coinciding with flexural cracking in the strand's transfer zone. At a load of 76.1 kips, a flexural crack formed at Station 106 causing the initial strand slips. At 80.9 kips, another flexural crack formed at 94 inches from the beam's end, causing the strands to slip even more. The beam continued to resist increasing loads until failure at 81.37 kips. Concrete strain at crushing failure was 2416 x 10^{-6} $^{in}/_{in}$.

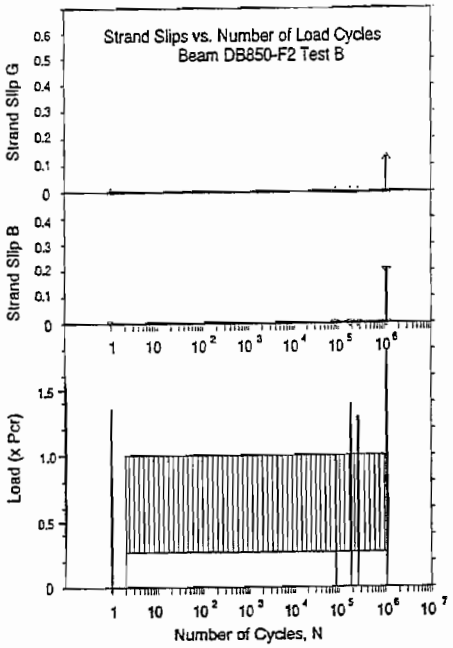

Figure 6.19 Loading History: Beam DB850-F2 Test B

6.4.8 Beam DB850-F3. This beam had the same debonded length of 78 inches as did DB850-F1 and DB850-F2, however, debonding was concurrent. All debonded strands were terminated 78 inches from the end of the beam. The embedment length was chosen to be 120 inches. In the series of statically tested debonded beams, an embedment length of 120 inches with concurrent debonding caused bond failure in specimen DB850-5 (Figure 5.33). The loading history for this beam is illustrated in Figure 6.21 along with strand slips. The same data plus deflection data is contained in Table 6.10.

The initial static load of 1.3 P_{sv} caused little or no damage to the anchorage zone of the debonded strands. The closest flexural crack was 161 inches away from the end of the beam. The beam was loaded with 152,000 cycles without any significant strand slips. At

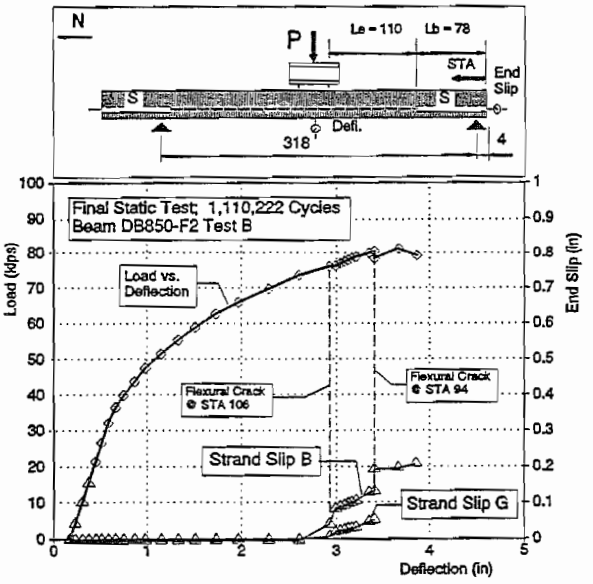

Figure 6.20 Load vs. Deflection and End Slips Beam DB850-F2 Test B

152,538 cycles, a static loading was performed on the specimen to 1.5 P_{sv}. This load represented an increase in load over the previous overloads, consequently new flexural cracks formed at Stations 150 and 140. Strand slips from this loading were very small.

In the remainder of the tests, no other overloads exceeded 1.3 P_{sv} and strand slips stabilized. Through the remaining load repetitions at service load, Strand G slipped to a total of about 0.05 inches.

TABLE 6.9

BEAM DB850-F2 TEST B
STATIC LOAD TESTS

L_e = 110 in ; P_{sv} = 46.95 k" ; P_u = 87.3 k"

Load Cycle N	Max. Load (kips)	% P_{sv}	Deflections			Slip B		Slip G	
			Beg	End	@ P_{sv}	Beg	End	Beg	End
1	61.62	1.3	0	0.086	0.60	0	0	0	0
87,000	47.0	1.0	0.114	-	0.78	0	0	0	0
184,410	65.0	1.4	0.141	0.164	0.80	0	0	0	0
271,194	60.0	1.3	0.175	0.181	0.91	0	0	0	0
1,110,222	81.37	1.8	0.175	-	0.97	0	0.20	0	0.125

After 1,085,569 cycles, the beam was tested statically until failure. The beam failed at a load of 74.23 kips, approximately 92% of the calculated flexural capacity. In the final loading stages, new flexural cracks formed in the transfer zone of the debonded strands. The nearest crack to the end of the beam formed at Station 87 at a load of 67.8 kips. After this crack formed, strand slips increased steadily with increased loading. At beam failure, strand slips had reached 0.46 inches on Strand B and 0.42 inches on Strand G. The load versus deflection and end slips for the final static test are given in Figure 6.22.

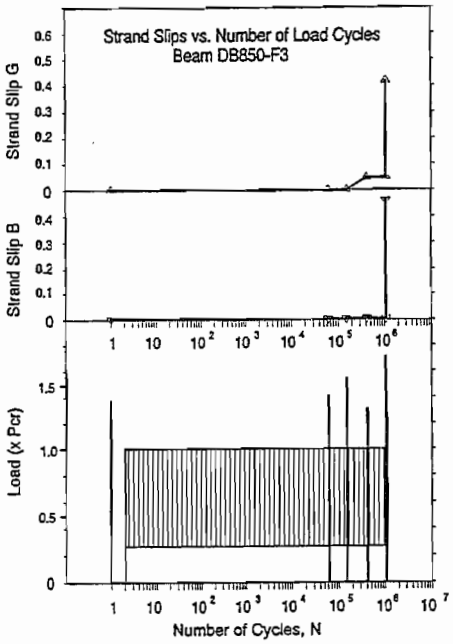

Figure 6.21 Loading History: Beam DB850-F3

6.4.9 Beam DB850-F4. Only one test was possible on this beam because the length of debonding and the concurrent debonding precludes two effective tests. The embedment length was set at 100 inches. The initial static loads and the intermediate static loads were relatively small at 1.3 P_{sv}. The load history and end slips are plotted in Figure 6.23 and Table 6.11. As the figure indicates, there were no strand slips before the static load to failure.

The static test at 266,147 cycles was intended to be an intermediate load to 1.6 P_{sv}, however, the beam failed before this load was achieved. The load versus deflection and end slips are illustrated in Figure 6.24. The beam failed in bond when flexural cracking propagated through the transfer zone of the debonded strand at Stations 88, 90, 102, 103 and 111. These cracks all

formed at a load of 65.0 kips. Strand slips occurred upon formation of these cracks. It is also observed that Strand D and Strand F, which were also debonded for a length of 78 inches, had strand slips in similar magnitude to Strands B and G. Strand slips for Strands D and F are not reported in the table or the figure, but closely resemble the slips from Strands B and G.

TABLE 6.10

BEAM DB850-F3
STATIC LOAD TESTS

L_e = 120 in ; P_{sv} = 43.59 k" ; P_u = 81.1 k"

Load Cycle N	Max. Load (kips)	% P_{sv}	Deflections			Slip B		Slip G	
			Beg	End	@ P_{sv}	Beg	End	Beg	End
1	57.65	1.3	0	0.086	0.60	0	0.0018	0	0
62,418	58.0	1.3	-	-	-	0.0016	0.0025	0	0.0002
152,538	65.0	1.5	0.174	0.203	0.847	0.0017	0.0022	0.0002	0.0002
414,844	55.0	1.3	0.203	0.215	0.920	0.0031	0.0033	0.0455	0.0475
1,085,569	74.23	1.7	0.234	0.481	0.947	0.0025	0.459	0.0479	0.418

The beam failed at a load of 69.34 kips, or 87% of the calculated ultimate capacity. Note the steady increase in strand slips after the initial cracks occurred (See Figure 6.24) in the transfer zone of the debonded strands. The beam failed in flexure due to a loss of anchorage of the debonded strands.

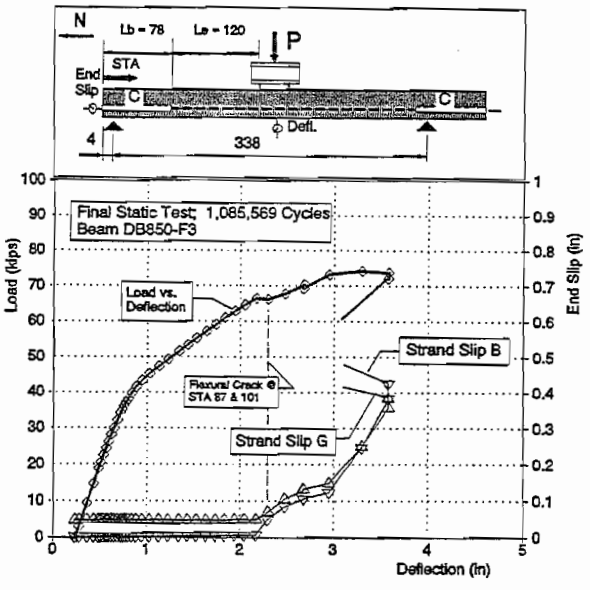

Figure 6.22 Load vs. Deflection and End Slips Beam DB850-F3

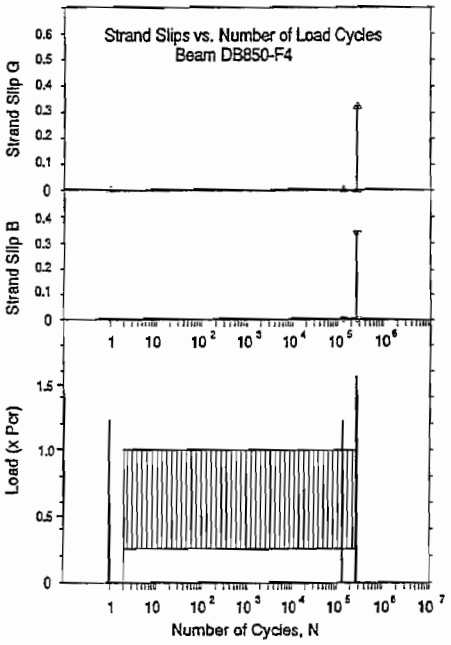

Figure 6.23 Loading History: Beam DB850-F4

TABLE 6.11

BEAM DB850-F4
STATIC LOAD TESTS

L_e = 100 in ; P_{sv} = 46.12 k" ; P_u = 85.8 k"

Load Cycle N	Max. Load (kips)	% P_{sv}	Deflections			Slip B		Slip G	
			Beg	End	@ P_{sv}	Beg	End	Beg	End
1	55.92	1.2	0	0.05	0.54	0	0	0	0
135,652	55.0	1.2	-	-	0.71	0.003	0.003	0.003	0
266,147	69.34	1.5	-	-	-	0.003	0.336	0	0.323

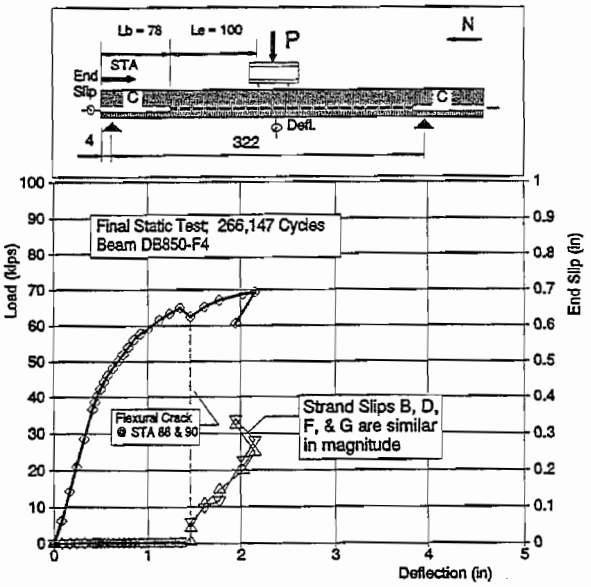

Figure 6.24 Load vs. Deflection and End Slips Beam DB850-F4

6.5 Discussion of Test Results

6.5.1 Hybrid Failures: Flexural Failures with Strand Slip. In these tests, as in the previous test series, the primary interest is whether or not the strands were able to develop the tension required to resist the nominal flexural capacity of the section. Bond slip is indicates that anchorage of the strand may be inadequate to develop the strand's tension. Strand slips indicate that the strand's bond may have failed. On the other hand, the static test series provided many examples of strands that slipped and yet the test specimen still achieved its ultimate flexural capacity. Examples of this behavior include DB850-2B, 3B, 4B, and 6A. Furthermore, the repeated load tests on beams with debonded strands provide even more examples of strands that have slipped and yet the beams still achieved flexural capacity. For instance, Test DB850-F1A suffered strand slips up to 0.24 inches. Yet the beam was able to achieve a ductile flexural failure at a very high percentage of the nominal flexural capacity. It is apparent that slipping of the strands does not preclude bond stresses from acting to restrain the strand and resist additional strand tension.

Flexural failures occurring with the presence of significant strand slips can best be described as hybrid failures. Many of these failures result from tests whose variables, the embedment length, L_e, and the debonded length, L_b, fall near the boundary line between flexural failure and bond failure. Two examples of this behavior are DB850-F1A and DB850-F2B.

In Figures 6.25 and 6.26, the failure modes are overlaid upon the prediction model for cracking and bond failure. Tests were performed on Specimens DB850-F1A and DB850-F2B, with embedment lengths of 100 inches and 110 inches, respectively. These embedment lengths place these two specimens at or near the boundary line between flexural failure and bond failure. Not surprisingly, both of these specimens failed in flexure with strand slips in

excess of 0.2 inches. It must also be noted that these two specimens failed at only 93% of their calculated ultimate capacity (and that the calculated flexural capacity was corroborated from the static tests on debonded beams).

6.5.2 Effects of Repeated Loads on Strand Slips. In reviewing the data of strand slips versus the loading history of each beam, it is obvious that large strand slips resulted directly from the applied intermediate overloads. Conversely, the repeated load cycles to service load affected the overall bond performance very little. This result indicates that very little deterioration of bond in prestressed strands occurs due to repeated loads at service loads. Furthermore, strand slips and subsequent bond failures result from significant overloads and not from distress caused by repeated loads. To summarize, these results would indicate that bond fatigue is not very important to the overall performance of the pretensioned prestressed concrete beam.

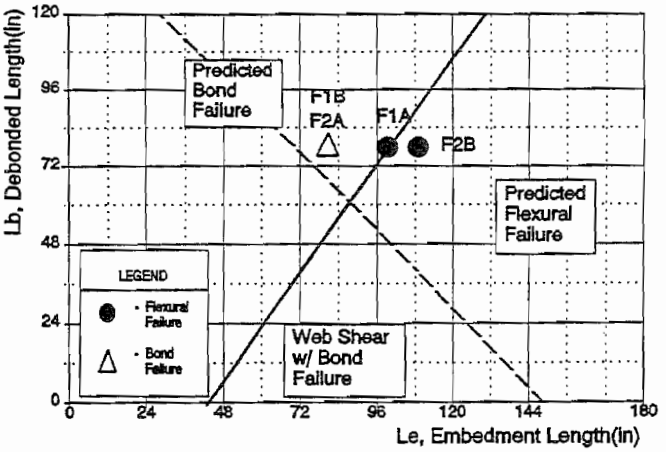

Figure 6.25 Comparison of Test Results With Prediction (Repeated Load Tests on Beams With Staggered Debonding)

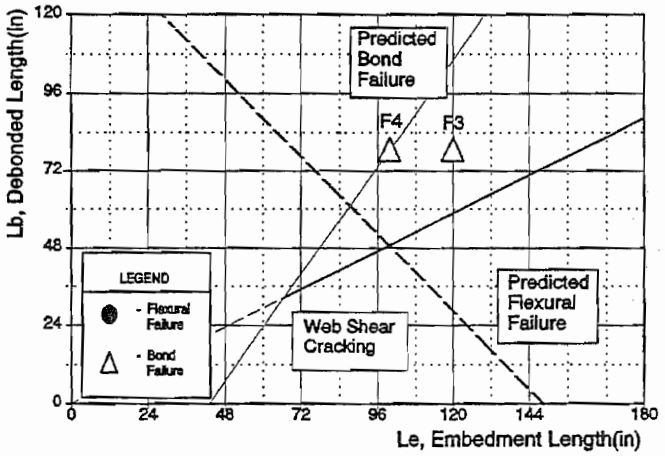

Figure 6.26 Comparison of Test Results to Prediction (Repeated Load Tests on Concurrently Debonded Beams)

On the other hand, there are examples of strands slipping from the action of repeated loads without the action of intermediate overloads. In fact, in almost every test, strand slips increased from solely from repeated loads. Most of these increases in strand slips were very small, of magnitude approximately 0.001 inches as reported in Tables 6.4 through 6.11. One example, however, demonstrates large strand slips through the action of repeated loads, Specimen DB850-F2A. In this test, the initial static overload caused a flexural crack to form at Station 106. This crack occurred just at the maximum applied load of 55.0 kips for this static test. The initial strand slips were small, only about 0.09 inches. However, as repeated loads were applied to the beam, strand slips increased. Figure 6.17 illustrates that strand slips increased from 0.09 inches to nearly 0.4 inches simply from repeated service loads in the first 26,000 load cycles. This demonstrates that bond stresses are susceptible to fatigue distress from repeated loading. However, the conditions where slips from repeated loads can occur are very specific.

In this case, two circumstances conspired to form the conditions whereby strand slips increased so dramatically with repeated loads, the magnitude of the initial load and the location of the crack. Strand slips were initiated by the flexural crack that formed 106 inches from the end of the beam at a load of 55.0 kips. This crack was located at or very near the end of the transfer zone for the debonded strands B and G. For the beam, the debonded length is 78 inches. If the transfer length is 25 inches, then the transfer zone would extend to 103 inches from the end of the beam. Because the crack occurred near the end of the transfer zone, the strands' anchorage remained fairly well intact, at least initially, but was susceptible to distress from repeated loads. If the crack had formed well within the transfer zone, then the initial strand slip would have been much larger, and total strand slip from new loadings would have been stabilized.

In other tests, the initial crack through the transfer zone occurred much closer to where the debonding was terminated and initial end slips were much larger. Along the same lines, if the initial static load had been increased beyond 55.0 kips, after the crack at Station 106 had formed, then the strands would have suffered more slip in the initial static test. Greater slips in the initial static loading would have stabilized the strands and slips would not have increased as much during the repeated loads.

Figure 6.17 also illustrates that strand slips stabilized after 26,000 cycles and remained constant until the final static test. This result is very important because it demonstrates that strand slips will stabilize, even in extreme cases. Interestingly, strain gages attached to these same two strands, B and G, indicate that as the strands slipped, their effective prestress was reduced approximately 94 ksi (Note: The strain gages were attached to the strands in the region of maximum moment). If these two strands were losing tension, but yet the beam was resisting the same load, then tensile forces must be redistributed to the other six strands. As tension was redistributed, the strand slips stabilized because the strands were not required to carry as much tension as before.

In Figure 6.27, strand stress is plotted versus the number of load cycles, N. These same data are reported in Table 6.12. The zero line in the figure represents the effective prestress of 152 ksi. The plot demonstrates a large decrease in strand stress between the first cycle and 26,000 cycles. The total loss of prestress is approximately 95 ksi, shich represents over 60% of the strands' effective prestress. However, also note that strand stresses do increase under static load. The spikes in the plot illustrate the change in steel stress during the intermediate static loadings. These spikes indicate increases in strand tension under load, which also indicate that bond stresses are active in restraining the strands, even though they had slipped significantly.

The loss of tension in the debonded strands must be offset by increases in tension from the other strands. The beam is adversely affected by a significant loss of stiffness coupled with large increases in strand stress range. The strands that do not slip are required to resist significantly larger tensile stresses than before, and suffer from significantly larger stress ranges. If six strands instead of eight strands were resisting the same applied loads,

the stress range would exceed 72 ksi. However, Figure 6.27 also demonstrates that the debonded strands, even with large strand slips, are restrained enough to increase their tension under load and help resist applied moments. The actual stress range is represented more accurately by the stress range of about 30 ksi, illustrated in the Figure 6.27. A stress range of about 30 ksi is represented by the spikes at 7000 and 26000 cycles.

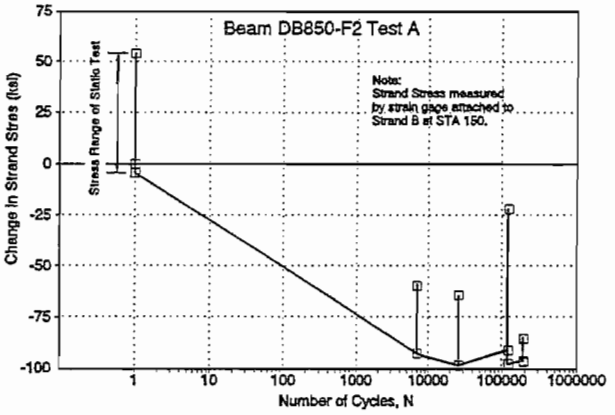

Figure 6.27 Changes in Strand Stress From Repeated Loads

The loss of bond creates a potential failure under service loads, even if only a few strands are affected. From the example of DB850-F2A, stress range in the strands is increased from 14 ksi to over 30 ksi. Fatigue tests that have been done on pretensioned girders indicate that the fatigue life is dramatically reduced for similar changes in magnitude. Overman[35] indicates the following formula for service life as a function of stress range:

$$\log N = 11 - 3.5\log(S_r)$$

where S_r is the stress range and N is the number of cycles to failure. Using this formula, if the stress range is 14 ksi, then the strands would fail at 10 million cycles. However, if the stress range increased to 30 ksi, the strands would fail at only 700,000 cycles.

In the other repeated load tests, strand slips also stabilized during repeated loading, but at far less slip than in Test DB850-F2A. For example, Table 6.6 reports strand slips for Test DB850-F1A. After the initial loading, strands B and G had slipped 0.0209 inches and 0.0217 inches respectively. Through the first 1023 repeated load cycles, strand slips increased to 0.0296 inches for Strand B and 0.035 inches for Strand G. The intermediate static overload applied at N = 1023 caused

TABLE 6.12

CHANGE IN STRAND STRESS DB850-F2 TEST A

LOAD CYCLE	STRAND STRESS (ksi)		
	BEGINNING	MAXIMUM	END
1	0	+54.1	-4.3
7000	-92.5	-59.5	-92.5
26,310	-98.6	-64.1	-98.3
121,308	-91.2	-22.0	-97.6
192,945	-96.1	-85.4	-96.8

1. Stress measured by strain gage attached at Station 150.
2. Stress = 0 at the effective prestress of 152 ksi.

additional slips; however, there were no increases in slip beyond this load cycle until the next static overload was applied. Strand slips became stable and the strand was able to develop the tension required to resist external loads. More importantly, strand slips stabilized after very small total slips and without large losses in strand tension. Because slips were small in these cases, the beam did not suffer much loss in serviceability due to the strand slips.

To summarize this section, some strand slips did occur as the direct result of repeated service loads. These strand slips demonstrate that bond can deteriorate as a direct result from repeated loadings. However, increases in strand slip were very small, for the most part, and did not affect the overall performance of the beams. In every case, strand slips stabilized after a finite number of loads, and bond failure caused only by repetitions at service load did not appear probable.

TABLE 6.13

FIRST CRACKING LOADS AND MOMENTS INITIAL STATIC TESTS ON REPEATED LOAD TESTS

Beam	First Cracking		
	P_{cr} (kips)	Mom (k-in)	Mom/M_{cr} [1]
FA460-F4A	33.76	2381	1.00
FA460-F4B	40.93	2369	1.00
DB850-F1A	41.02	3281	0.96
DB850-F1B	48.58	3337	0.98
DB850-F2A	42.50	3273	0.96
DB850-F2B	46.93	3231	0.94
DB850-F3	45.77	3393	0.99
DB850-F4	47.30	3359	0.98

1. M_{cr} = 3422 k" for DB850-F1, F2, F3, and F4; for f'_c = 7733, $f_r = 7.5\sqrt{f'_c}$, and f_{se} = 152 ksi.
   M_{cr} = 2875 k" for FA460-F4; for f'_c = 6500 psi, $f_r = 7.5\sqrt{f'_c}$, and f_{se} = 160 ksi.

On the other hand, large strand slips were caused by static overloads that were applied to the beams at intermediate cycles. These slips were initiated by flexural cracking at or near the transfer zone of the debonded strands. In cases where the beam failed due to bond, large end slips resulted from the large overloads that exceeded service load by a large margin.

6.5.3 First Cracking Loads and Moments. The ability to predict bond slips and subsequent bond failure is dependent on the ability to predict cracking in concrete. In the previous test series, initial cracking was compared favorably to the predicted cracking load. In this test series, too, first cracking is compared to the predicted cracking load. That comparison is tabulated in Table 6.13. The results demonstrate remarkable accuracy in predicting cracking loads. Specimen DB850-F2B cracked at only 94% of the predicted load, however this was the largest disagreement between actual and predicted cracking loads. It should be noted that all of the predicted cracking moments were calculated using the actual tested cylinder strength of the concrete which exceeded the design strength of 6000 psi in

every case. Also, the effective prestress force was calculated and the values are contained in the footnotes of the table.

6.5.4 Strand Slips and Cracking in the Debond/Transfer Zone. Table 6.14 reports the first incidence of cracking in the transfer zone of debonded strands for every test. From these data, initial strand slip can be compared to the formation of cracks at or near the transfer zone of debonded strands. In the table, the distance from the end of the beam to the nearest flexural crack is also reported. In some cases, cracking did not extend to the debond/transfer zone. For the debonded beams, the length of debonding equals 78 inches. If the transfer length is 25 inches, then the debond/transfer zone extends 103 inches from the end of the beam. In the fully bonded beam with 0.6 inch strands, the transfer zone is approximately 30 inches.

TABLE 6.14

SUMMARY OF END SLIPS COMPARISON TO CRACKING IN THE DEBOND/TRANSFER ZONE

INTERMEDIATE STATIC TESTS

Beam	Load Cycle, N	Extreme Crack; Debond/Transfer Zone		End Slips		Mode of Failure
		Max Load at Test (kips)	Station[1]	Initial Slip	Slip at Failure (in.)	
FA460-F4A	1	48.62	—	—	—	Flex
	1,770,265	55.36	—	—	—	
FA460-F4B	1	58.69	75	—	—	Flex
	1,400,000	66.95	—	—	0.0298	
DB850-F1B	1	62.26	106	Yes	—	Flex
	1,040,050	70.05	—	—	0.240	
DB850-F1B	1	58.5	130	—	—	Bond
	386,878	72.5	88	Yes	—	
	1,027,083	82.6	76	—	0.605	
DB850-F2A	1	55.0	106	Yes	—	Bond
	192,945	63.78	—	—	0.676	
DB850-F2B	1	61.62	142	—	—	Flex
	1,110,222	81.37	94	Yes	0.20	
DB850-F3	1	57.65	161	—	—	Bond
	152,538	65.0	140	—	—	
	1,110,222	74.23	87	Yes	0.459	
DB850-F4	1	55.92	159	—	—	Bond
	266,147	69.34	88	Yes	0.336	

1. Distance from the end of the beam

In every case, end slips were initiated by flexural cracking through or near the transfer zone of the debonded strands. This demonstrates the important role played by cracking in the disruption of strand anchorage. For example, in Specimen DB850-F2, Test B, flexural cracking extended to Station 106, as shown in the photograph of Figure 6.28. As indicated in the photograph, the crack formed at an applied load of 76 kips. When this crack formed, strand slips were initiated, see Figure 6.20. As load was increased, another flexural crack formed at Station 94 from an applied load of 81 kips. This crack is shown in the photograph in Figure 6.29. Strand slips increased suddenly, initiated by the new crack propagating through the strands' anchorage zone at Station 94. The plot in Figure 6.20 illustrates the

relationship between cracking and increases in strand slip. End slips on Strand B increased suddenly when the concrete cracked at Station 94. The evidence from these two photographs demonstrate very clearly that cracking disrupts the anchorage zone of the strand, and that these cracks initiate strand slips.

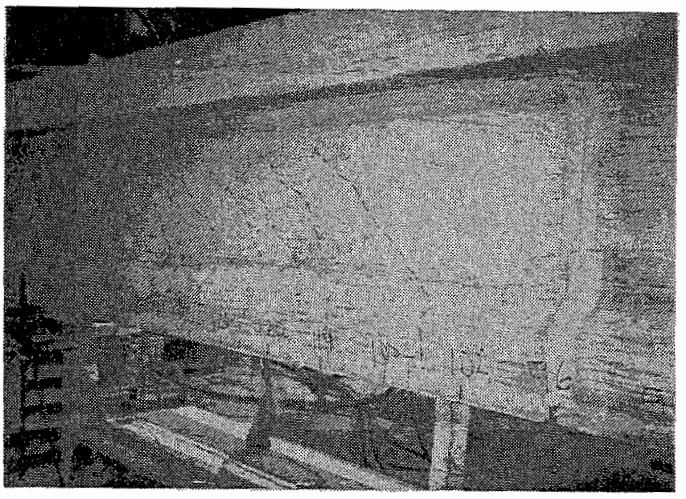

Figure 6.28 Test DB850-F2B at Load = 76 kips

Another example of the influence of cracking on bond slip is clearly demonstrated in the photograph in Figure 6.30. This figure depicts the cracking patterns of Beam DB850-F3 well within the transfer zone of the debonded strand. These cracks initiated bond slip. Consequently, this beam failed in bond. Interestingly, the photograph shows two splitting cracks that formed directly above Strand F. The splitting cracks extend between flexural cracks, the first between Stations 108 and 125 and the other between Stations 88 and 102. These cracks graphically demonstrate that bond stresses are large enough to generate bursting stresses, even in cracked regions of the beam. Some questions exist as to the strand mechanics at bond failure. Does the strand twist freely through the concrete, or if enough twist restraint is provided, are some bond stresses developed? The splitting cracks suggest that some bond stresses are developed, and that they are large enough to develop splitting cracks.

Splitting cracks notwithstanding, the important point of this section is that cracking in the transfer zone of a prestressing strand causes the strand to slip. Furthermore, if cracking is prevented in the transfer zone, then these tests show that the strands will be able to develop the section's nominal capacity. If cracking is avoided, strand anchorages are sufficient to develop adequate strand tension to resist external loads. On the other hand, if cracks propagate through or near the transfer zone of pretensioned strands, then some strand slip will occur and strand anchorage will be weakened. However, these initial bond slips do not necessarily lead to complete anchorage failures, as tests DB850-F1A and DB850-F2B demonstrate. Modest bond stresses can develop even in cracked regions of the beam.

6.5.5 Determination of Failure Mode. In each phase of this project, the primary test result has been the mode of failure. Beams have failed either in flexure or in bond. If strands were sufficiently anchored, a beam would fail in flexure. Conversely, if the strand anchorages were insufficient, then the strands failed in bond. In previous tests, it has been

relatively simple to differentiate between the two modes of failure. Flexural failures are characterized by two criteria, capacity and ductility. If a beam reached its nominal flexural capacity and was able to sustain that load through significant deformations, then the failure was a flexural failure. Conversely, anchorage failures were characterized by gross displacements of the strands relative to the concrete (end slips) and either a lessened capacity or an inability to sustain load.

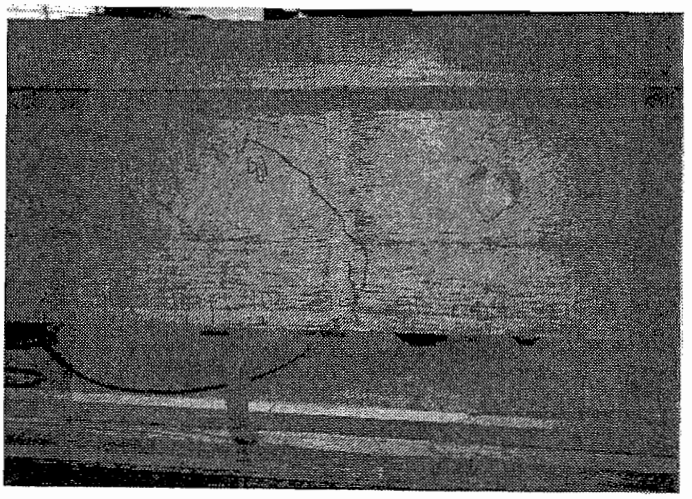

Figure 6.29 Test DB850-F2B at Load = 81 kips

In the development length tests on beams with fully bonded strands, the failure modes were easily categorized. Bond failures were more easily distinguished from flexural failures because bond failures were more sudden and abrupt. In the static test series on debonded beams, the differences became more difficult to distinguish because hybrid failures occurred where the beams failed in flexure but the strands exhibited some slip. These hybrid failures are caused, in part, by the combination of fully bonded and debonded strands. In several of the tests, strands B and G (debonded the full debonded length) would slip because of cracking through their transfer zone. On the other hand, the remaining six strands enjoyed a relatively undisturbed anchorage, and slips were not observed in these strands. This leads to a condition where loads from strands B and G are redistributed to the other strands. Even in an extreme case where strands B and G would completely lose anchorage, the beam would still fail in flexure. The only difference might be a somewhat lower failure load along with greater deflections. In effect,

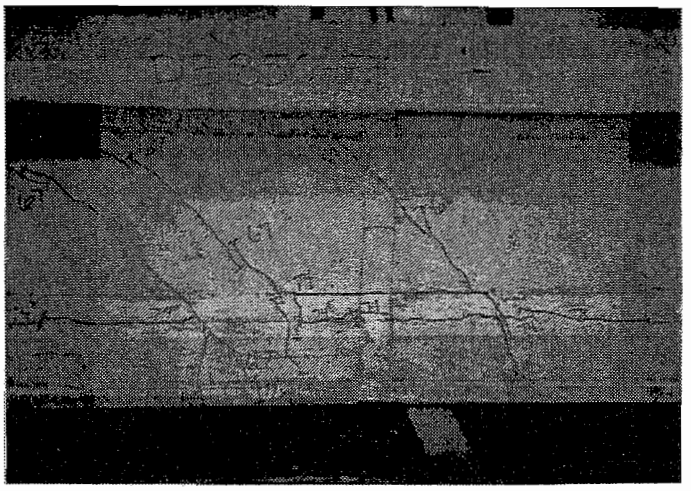

Figure 6.30 Cracking in the Debond/Transfer Zone of DB850-F3

it becomes very difficult to distinguish flexural failures from bond failures. In these cases, flexural failures must still be characterized by capacity and ductility.

In these repeated load tests on debonded beams, it is even more difficult to distinguish between flexural failures and anchorage failures. In every test, significant strand slips occurred. However, in some cases, the beams appeared to achieve their flexural capacity. The difficulty lies in that the apparent flexural failures of Tests DB850-F1A and DB850-F2B occurred at loads that were only about 93% of the calculated capacity. In these cases, the concrete crushed in compression at lower strains than the crushing strains for the static test series.

This difference is demonstrated in Figure 6.31 comparing the static test performed on DB850-4B and the final static test performed on repeated load specimen DB850-F1A. These two beams had identical loading and beam geometry. Both tests had spans of 346 inches and embedment lengths of 100 inches. In the static test, Test DB850-4B, concrete crushed at a strain of 0.002704 in/in. (It should be noted that concrete strains were measured at the top compression fibers on top of the beams, in between the load points. However, crushing often occurred just under the load point, so the strain at the actual point of crushing may vary from the measured value.) Deflection of the beam, measured at the load point, was 4.10 inches.

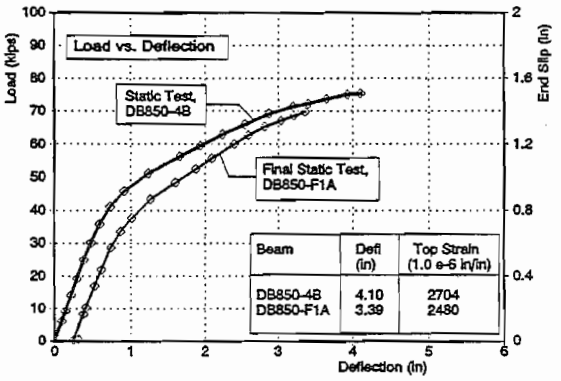

Figure 6.31 Comparison of Final Static Test on Repeated Load Test Specimen, DB850-F1A to Companion Static Test Specimen, DB850-4B

The final static test on DB850-F1A was performed after 1 million cycles. As shown in the figure, the beam had 0.29 inches of permanent deflection. DB850-F1A failed when the concrete crushed at a compressive strain of only 0.002480 in/in. The concrete strain represents the total amount of strain from the combined effects of the repeated loads plus the static loads. Initial concrete strain readings were measured before the initial static load was applied, so stated concrete strains include the effects from the total load history of the beam. Note the similarity between the two curves. From the stiffness of Specimen DB850-F1A, all of the strands must be active in resisting tension and strand anchorage has not failed. Furthermore, if the concrete in test DB850-F1A had demonstrated a higher strain capacity, then failure would have occurred at a higher load similar to the static test on DB850-4B. From these data, it is concluded that Specimen DB850-F1A failed in flexure,

even though failure was only 93% of the calculated nominal capacity. A similar argument can be made for Specimen DB850-F2B.

Table 6.15 summarizes the modes of failure for each test for the repeated load tests. From the tests on debonded beams with 0.5 inch diameter strands, specimens DB850-F1A and DB850-F2B failed in flexure. In both tests, the flexural capacity was only 93% of the calculated value. The embedment length for these two tests were 100 inches and 110 inches, respectively. The statically tested companion beams to these specimens also failed in flexure. The other four tests on debonded beams failed in bond with large amounts of bond slips. The applied moments in these tests varied from 82% to 94% of the calculated flexural capacity. Table 6.14 lists the amount of bond slip at failure for each beam. Bond slips are quite large, on the order of 0.5 inches, for each of the specimens that failed in bond.

TABLE 6.15

SUMMARY OF FAILURE MODE AND APPLIED LOAD AT FAILURE

REPEATED LOAD TESTS

Beam	L_b (in)	Le (in)	Ultimate Load			Mode of Failure
			P_u (kips)	$M_{u,test}$ (k-in)	$M_{u,test}/M_n$ [1]	
FA460-F4A	0	120	55.36	3905	0.99	FLEX
FA460-F4B	0	96	66.95	3874	0.98	FLEX
DB850-F1A	78(S)	100	70.05	5602	0.93	FLEX w/ SLIP
DB850-F1B	78(S)	80	82.57	5672	0.94	BOND
DB850-F2A	78(S)	80	63.78	4911	0.82	BOND
DB850-F2B	78(S)	110	81.37	5602	0.93	FLEX
DB850-F3	78(C)	120	74.23	5503	0.92	BOND
DB850-F4	78(C)	100	69.34	5249	0.87	BOND

1. M_n = 3940 K" for FA460-F4.
   M_n = 6010 k" for DB850-F1, F2, F3 and F4.

Note that the two tests on Beam FA460-F4 both failed in flexure. The embedment length for Test FA460-F4B was 96 inches, or 1.0 times the development length required by AASHTO and ACI. Even though strand slips of about 0.03 inches were measured, this beam clearly failed in flexure. The required development length for the 0.6 inch strands was 84 inches, based on test results from the static test series on FA460 beams. These two tests conform to the static test results in spite of 1.7 million cycles on Test A and 1.4 million cycles on Test B.

6.5.6 Comparison with Prediction of Cracking and Bond Failure. Figures 6.25 and 6.26 overlay the test results onto the prediction model discussed in Chapter 5. Although the data points are somewhat limited, the results remain consistent with earlier static tests. In Figure 6.25, results from tests on beams with staggered debonded strands are shown. Note that the results conform to the prediction. Similarly, Figure 6.26 shows the results

from tests on beams with concurrent debonding. Again, the results conform to the prediction model.

6.6 Summary

Eight repeated load tests were performed. Six tests were performed on beams with eight 0.5 inch strands and two tests were performed on one beam that contained four 0.6 inch diameter strands.

The tests with 0.6 inch diameter strands confirm the conclusions from the tests performed earlier under static loading. In these two tests, embedment lengths were provided that exceeded the measured development length from the static tests, and the beam failed in flexure in both repeated load tests. The beam tested under repeated load, FA460-F4, was identical to beams from the static test series. The beams had the same cross sections and the same strand pattern with four 0.6 inch strands, fully bonded from the end of the beam. In the repeated load tests, embedment lengths were 120 inches for FA460-F4A and 96 inches for FA460-F4B. The AASHTO code requires a development length of 96 inches, using the current code expression. In the tests on statically loaded beams, an embedment length of 84 inches was sufficient to develop the strand. The test results demonstrate that the repeated load tests match the results of statically tested beams.

Conclusions from the debonded beams are best expressed in Figures 6.25 and 6.26 where repeated load test results are displayed upon the prediction model. These results demonstrate that the repeated load tests conform to the same principles as the statically tested beams.

There is some evidence of bond distress caused by repeated loading. In nearly every case, strands continued to slip as repeated loads were applied to the beams. However, in most cases, these slips were quite small and represented very little loss of tension. In every case, strand slip stabilized at a finite number of load cycles. In the test FA850-F2A, strand slips grew quite large under repeated load, which pointed out a potential problem with increasing stress ranges in the strands.

CHAPTER 7
TESTS ON FULL-SIZED COMPOSITE GIRDERS

7.1 Introduction

Heretofore, all of the tests have been performed on scale model test specimens. These tests have been instrumental in understanding the underlying behavioral principles that govern the transfer and development of pretensioned strands. Specifically, it has been noted that bond failure can be prevented if cracking, either flexural cracking or shear cracking, is prevented from propagating through the transfer zone of pretensioned strands. However, tests on full-sized specimens were needed to confirm earlier observations and provide credibility to the conclusions. Therefore, repeated load tests were performed on three full-sized composite girders to determine if the behavior noted in the smaller specimens can be expected to govern the design of larger specimens. This chapter discusses the tests performed on three full-sized girder tests, results obtained from these tests, and the impact the results have on the design and fabrication of pretensioned girders.

7.2 Testing Program and Specimen Design

Design of the test specimens was generated from a hypothetical design case, and design details conformed to requirements of the Texas Department of Transportation (TxDOT). Design parameters included bridge loads, span length, girder spacing, slab thickness and the number of strands. Values for these parameters were selected to fulfill the objectives of the testing program. The specimens were required to test the behavior and reliability of debonded strands in full-sized girders, and as corollary, the tests were also required to further examine the behavioral principles established in previous tests.

In the State of Texas, most pretensioned girder bridges are built from one of two standard I-shaped sections, AASHTO Type IV girders (56%) and Texas Type C girders (33%). AASHTO Type IV girders are 54 inches deep and are used for longer spans, from 70 to 125 feet[61]. Texas Type C girders are 40 inches deep and are used for spans under 90 feet.

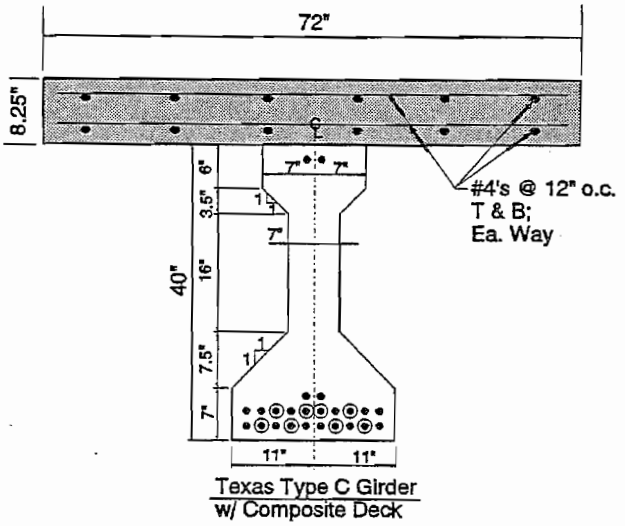

Section Properties					
Type C Girder			w/ Deck Slab*		
A	= 495	in^2	A	= 970	in^2
yb	= 17.09	in	yb	= 30.33	in
I	= 82,602	in^4	I	= 262,460	in^4
Sb	= 4833	in^3	Sb	= 8654	in^3

* E(slab) = 0.8 E(beam)

Figure 7.1 Cross Section Details of Composite Girder

Three Texas Type C girders were fabricated at a prestressing plant in central Texas. The girders were shipped to Ferguson Structural Engineering Laboratory (FSEL) at the University of Texas at Austin where an unshored, composite deck slab was cast on each girder. Testing was also conducted at FSEL. Cross section details and section properties for the composite sections are given in Figure 7.1. The cross section properties are calculated using transformed areas and $E_{slab} \approx 0.8\ E_{beam}$. This is typical for the concrete strengths of the beam, $f'_c \approx 6000$ psi, and of the slab, $f'_c \approx 4000$ psi.

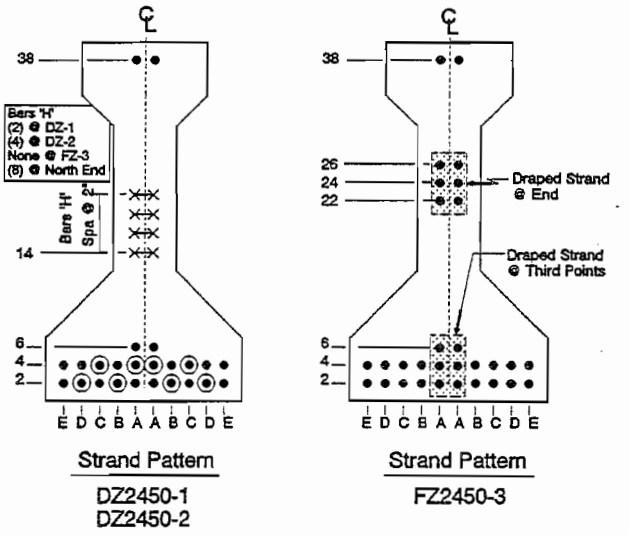

Debonding Schedule		
Strand	Debond Length	
	North	South
A4	0"	72"
B2	36"	36"
C4	36"	96"
D2	72"	72"

Figure 7.2 Strand Patterns and Debonding Schedule; DZ2450-1, DZ2450-2 and FZ2450-3

Each girder contained 24 low relaxation 0.5 inch diameter strands. Two of the girders, DZ2450-1 and DZ2450-2 contained debonded strands. In these two girders, eight of the 24 strands were debonded. The third girder, FZ2450-3, contained some strands that were draped, but all of the strands were fully bonded. All three girders were designed for the same strength and serviceability requirements. Design details were nearly identical so that the beams would have similar elastic properties, cracking resistance and strength properties. Strand patterns and debonding patterns are shown in Figure 7.2.

Slab thickness was determined from TxDOT requirements for slab thickness based on the clear span between girders. In this design case, the girder spacing was 82 inches and the clear span was about 68 inches. This spacing required a deck slab thickness of 7.25 inches. The deck slab for the test specimens has slightly different dimensions, a thickness of 8.25 inches and a width of 72 inches, but the slab has the same area of concrete, so the behavior of the composite test girder should be nearly identical with that of the design case.

The cross section was designed for HS20-44 lane loadings established by Appendix A from the *AASHTO Standard Specifications for Highway Bridges*[48]. The cross section was designed based on the flexural requirements for a 70 foot span with girders at 6.8 foot girder spacing. The allowable tensile stress at the bottom fiber gives the requirement for the number of pretensioned strands:

$$f_b = -F_{se}\left(\frac{1}{A}+\frac{e}{S_b}\right)+\frac{M_{DL}}{S_b}+\frac{M_{LL}}{S'_b} \le 6\sqrt{f'_c}$$

where A is the area of the girder, e is the eccentricity of the prestressing force, S_b is the bottom fiber section modulus for the girder alone and S'_b is the bottom fiber section modulus for the composite girder.

The section properties used in these calculations are given in Figure 7.1. Dead load moment, M_{DL}, and live load moment, M_{LL}, are given by the following expressions:

$$DL = 1.134klf \Rightarrow M_{DL} = \frac{1.134\times 70^2}{8} = 798k'$$

and

$$M_{LL}=1075.1\frac{k'}{lane} \times \frac{6.8}{11}\times 1.25 = 830.8\ k'$$

where 6.8/11 is the load distribution factor based on girder spacing and 1.25 is the impact load factor. Assuming that f'_c = 6000 psi, then the required effective prestress force is computed from the formula for bottom fiber tension, and the number of strands, N, is determined. For this cross section, 24 strands were required. Top fiber compression is given by the expression:

$$f_t = -F_{se}\left(\frac{1}{A}-\frac{e}{S_t}\right)-\frac{M_{DL}}{S_t}-\frac{M_{LL}}{S'_t} \ge -0.4f'_c$$

Figure 7.3 illustrates the girders' stress condition at midspan. The bottom fiber tension at midspan is not equal to $6\sqrt{f'_c}$ because N, the number of strands, are selected in discrete pairs. Oftentimes, in real designs, this selection process diminishes the bottom fiber tension at service loads compared to the design case.

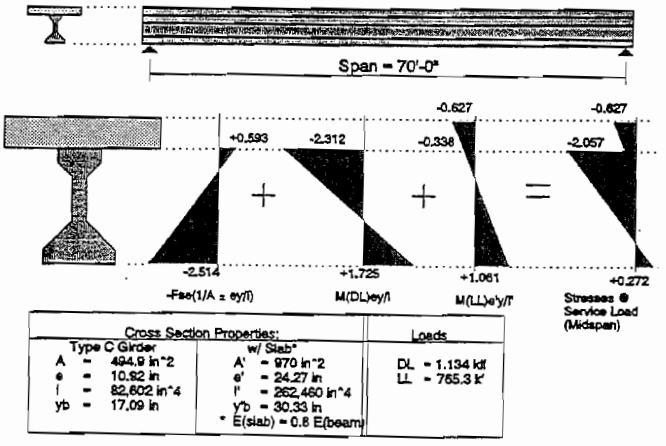

Figure 7.3 Design Stresses for Composite Section

7.2.1 Modifications of Span Length for Testing. As stated above, the cross section for the test specimens was designed based on a 70 foot span length.

Unfortunately, this span length would cause considerable difficulties in the laboratory. The specimens would be quite heavy and would exceed the safe capacity of the lifting equipment. Also, the cost of the testing program would increase somewhat proportionally with the size of the girders.

Initially, consideration was given to testing in the laboratory with a span of 60 feet with the loading shown in Figure 7.4a. The overall girder length of 49 feet (and a test span of 48 feet) was developed to satisfy the testing requirements while decreasing the handling problems in the laboratory. The shorter span was tested without impact on the overall results when the loading was revised as shown in Figure 7.4b.

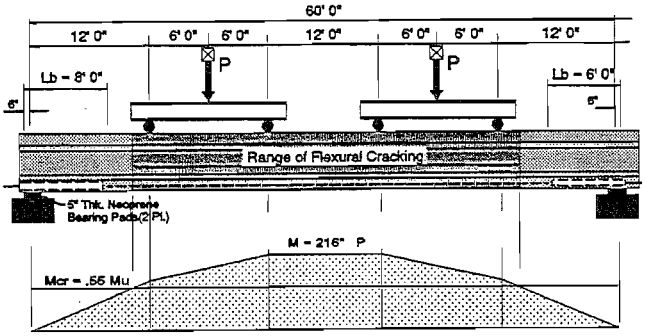

Figure 7.4a Symmetrical Loading Arrangement with 60' Span

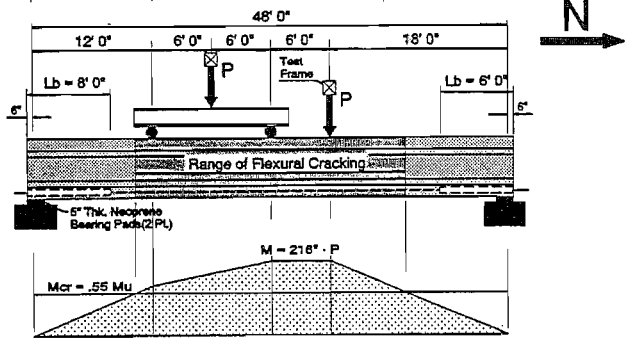

Figure 7.4b Test Setup and Dimensions for Full Sized Girder Tests, DZ2450-1 and 2 and FZ2450-3

Figure 7.4 Comparison of Loading Arrangement and Moment Diagrams: 60'-0" Idealized Span to 48'-0" Test Span

The loading arrangement shown in Figure 7.4b is asymmetrical. By using this loading arrangement, two separate objectives were accomplished. First, the resulting moment distribution is somewhat irregular, but approaches a parabolic shape in the South end of the beam. In earlier tests, the applied moment varied linearly along the beams, creating a special case that could potentially skew the test findings. In these tests, the loading arrangement represents a more generalized load case with varying moment distribution.

Secondly, by using this loading arrangement, the size of the specimen is reduced while maintaining moments and shears on the shorter test spans. In the symmetric 60 foot span, the maximum moment is given by the load, P, times 216 inches, and the maximum shear is equal to the load applied by one ram, P. Likewise, in the 48 foot test span, the maximum moment is also P times 216 inches with a maximum shear equal to P. When comparing the actual test span with the 70 foot design span, some additional differences existed, particularly the shear applied to the test span must be larger than the shear that would be present in a 70 foot span. However, by using this loading arrangement, a 25% reduction in span was achieved with only a 17% increase in the applied shear.

Applied loads were controlled by the bottom fiber tensile stress. Even though the test span was considerably shorter than the design span, the cross section experienced the

same service load moment and cracking load moment that were the basis for design. In this manner, a 48 foot span was tested that was comparable to a 70 foot design.

7.2.2 Debonding Requirements. Stresses near the end of the girder were given by the following relationships:

$$f_b = -F_{si}\left(\frac{1}{A}+\frac{e}{S_b}\right)$$

and where F_{si} was the prestress force immediately after transfer and before creep and

$$f_t = -F_{si}\left(\frac{1}{A}-\frac{e}{S_t}\right)$$

shrinkage losses further reduced the effective prestress force. If f_{si} = 180 ksi, then f_{top} = +0.667 ksi exceeded the allowable tensile stress. Therefore, either debonding or draping was required. In specimens DZ2450-1 and DZ2450-2, eight out of the 24 strands were debonded to control end stresses. For this particular design case, only six debonded strands were actually required, however, more strands were debonded to help demonstrate the behavior of beams with debonded strands.

In Figure 7.5, cracking moment and applied moment are plotted along the length of the girder. The applied ultimate moment was generated by applying the load to the beam that causes a moment equal to the beam's nominal flexural capacity. The cracking moment is based on a bottom fiber tension equal to $7.5\sqrt{f'_c}$. Cracking moment is dependent on the amount of precompression in the beam, so the cracking moment varies along the length of the beam. Also, note the increase in the cracking moment from the end of the beam over the initial transfer zone as the fully bonded strands transfer their prestressing force into the concrete. The next more gradual increase in cracking resistance is developed from the debonded strands as they transfer additional prestress to the concrete.

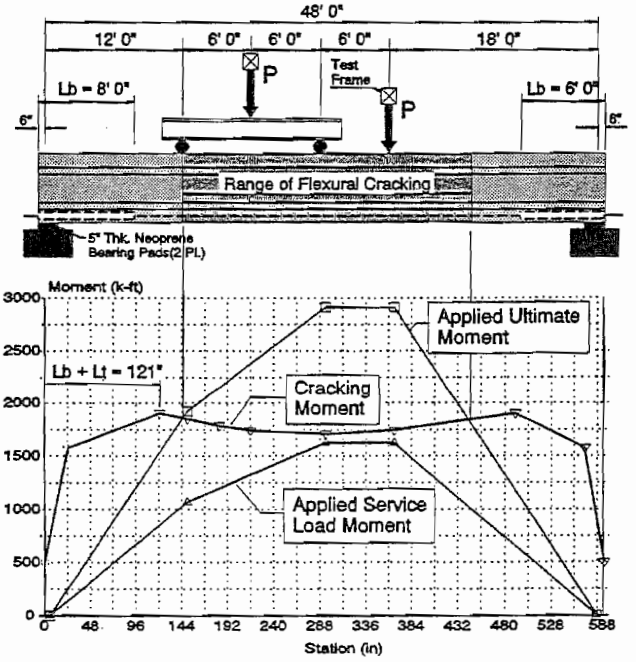

Figure 7.5 Applied Moment vs. Cracking Moment, Full-Sized Composite Girders

Figure 7.5 shows that the transfer zone of the debonded strands extended 121 inches from the end of the beam. This region in the beam, the debonded length plus the transfer

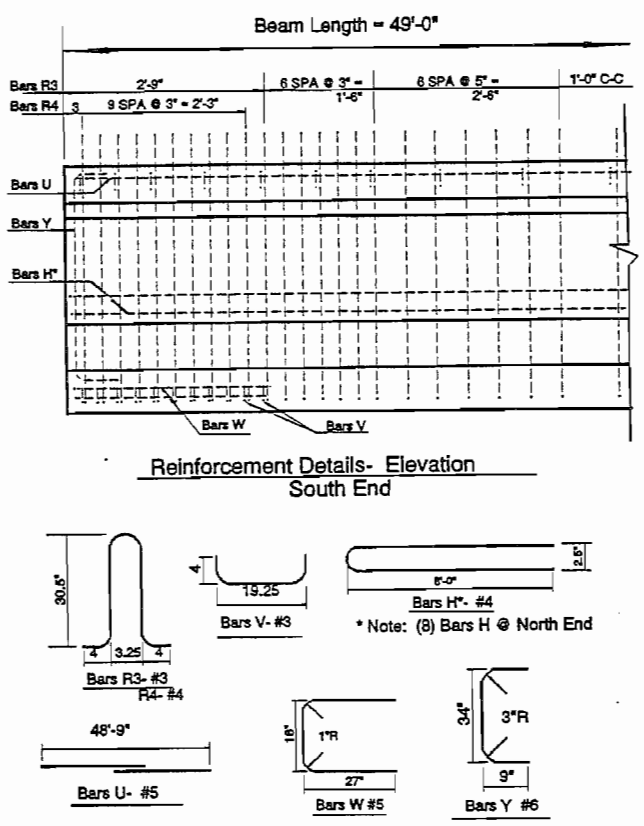

Figure 7.6 Reinforcement Details, DZ2450-1

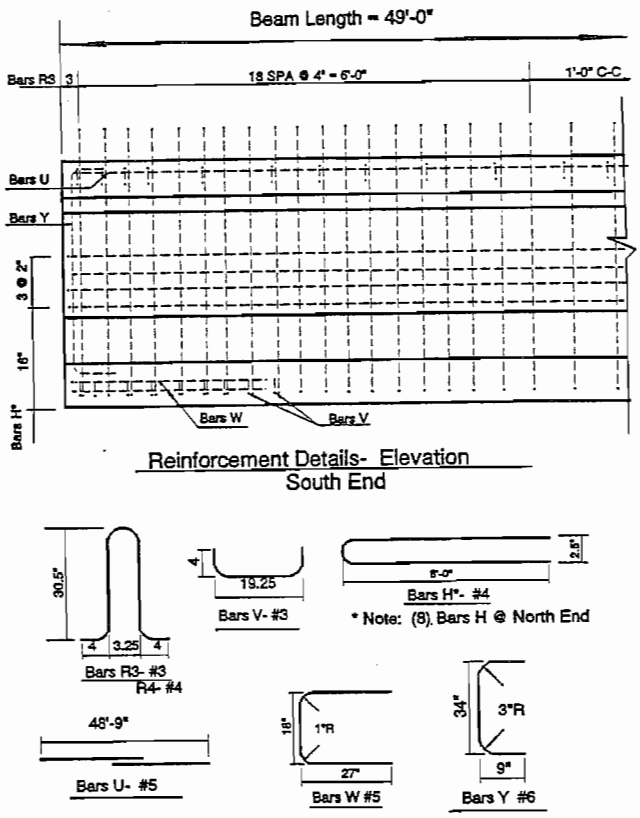

Figure 7.7 Reinforcement Details, DZ2450-2

Figure 7.5 shows that the transfer zone of the debonded strands extended 121 inches from the end of the beam. This region in the beam, the debonded length plus the transfer length, is referred to as the *debond/transfer zone*. The debond length was designed so that flexural cracking would not occur in the debond/transfer zone. The region of flexural cracking, shown in the figure, corresponds to the region where the applied moments at ultimate exceed the cracking moment of the beam. Results from earlier tests had indicated that cracking in the transfer zone of debonded strands caused bond failure, so the debonded length was designed so that the debond/transfer zone would not be affected by flexural cracking.

7.2.3 Draping Requirements. The strand arrangement at midspan was controlled by the service load requirements. Twenty four strands were placed with an eccentricity of 10.92 inches. As stated previously, excessive concrete stresses at the ends of the beam required the strands to be either draped or debonded. Girder FZ2450-3 had draped strands as shown in the cross section details (Figure 7.2). By draping the strands as shown in the figure, the prestressing eccentricity is reduced from 10.92 inches to 5.92 inches. In turn, reducing the eccentricity reduces concrete stresses to within allowable limits. Draping hold downs were located at third points within the beam, 16 feet and 4 inches from either end of the girder.

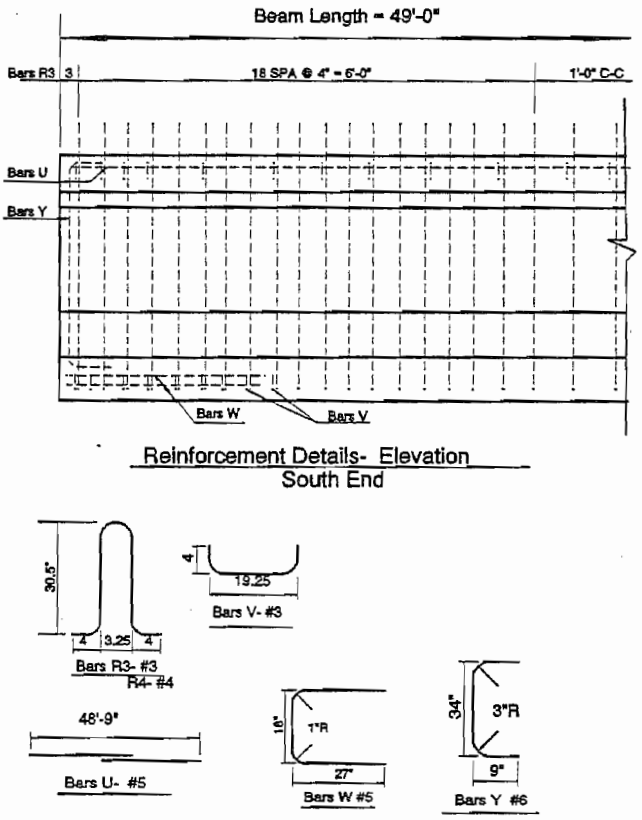

Figure 7.8 Reinforcement Details, FZ2450-3

7.2.4 Shear Reinforcement. Shear reinforcement is shown in Figures 7.6, 7.7 and 7.8. These beams were designed with some significant variations from the standard Texas details shown in standard TxDOT drawings. In earlier tests (discussed in chapter 4), web shear cracking caused bond failure of pretensioned strands. These tests demonstrated that pretensioned strands were ineffective in developing any plastic shear mechanisms because the pretensioned strands could not maintain the bottom chord tension in the truss analogy as cracking developed in their transfer zone.

In the full-sized girder specimens, longitudinal mild reinforcement was placed in the web to complement the vertical shear reinforcement that is normally contained within the web. The longitudinal steel is accurately described as shear reinforcement because its

purpose was to develop the bottom chord tension required by shear loads. The vertical stirrups provided in the end regions exceeded the amount required by AASHTO.

Girders DZ2450-1 and DZ2450-2 contained both longitudinal and vertical shear reinforcement. DZ2450-1 contained two longitudinal 'H' bars whereas DZ2450-2 had four longitudinal 'H' bars (See Figures 7.6 and 7.7). Vertical and horizontal shear reinforcement was designed using a truss analogy with a crack angle of 30°. The capacity of four 'H' bars is sufficient to resist 30% of the applied shear at the ultimate load. No contribution from the concrete was included in design of the mild reinforcement. FZ2450-3 did not contain horizontal reinforcement because of interference with the draped strands. Both horizontal and vertical shear reinforcement was continued throughout the debonded length.

7.3 Fabrication of the Test Specimens

Girders were fabricated at a prestressing plant in central Texas. An elevation showing the approximate location of the girders in the casting bay is shown in Figure 7.9. Girders were fabricated using TxDOT standard practices. Fabrication of the girders followed the same general procedures that were used to fabricate the earlier specimens at FSEL. The outline of procedures is as follows:

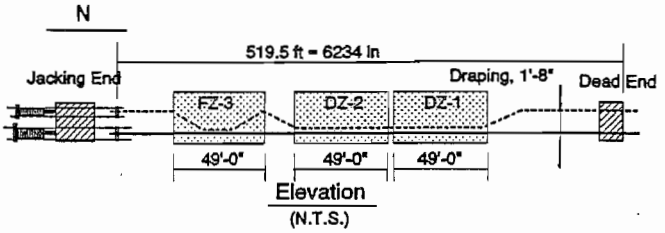

Figure 7.9 Schematic Evaluation of Pretensioning Bed

1. Pretensioning the strands.
2. Deflecting the draped strands.
3. Placement of debonding material over the strands.
4. Placement of mild reinforcement.
5. Placement of the formwork.
6. Casting of the concrete.
7. Removal of the forms and detensioning.
8. Shipment of the specimens to FSEL.

Deck slabs were cast at FSEL.

7.3.1 Strand Tensioning and Draping. The total length of the prestressing bed was 519.5 feet, or 6234 inches. Prestressing steel was stressed to approximately 75% of f_{pu}, corresponding to 31.0 kips per strand, or 202.5 ksi. Each strand was initially tensioned with a 2000 pound dead weight. Subsequent tension was applied with an hydraulic ram. For strands to reach the proper pretensioned stress, an additional elongation of 41.625 inches was required, assuming an elastic modulus of 28,000 ksi.

Strands were tensioned in three groups. First, the sixteen straight bottom strands were tensioned until an elongation of 41.625 inches was reached, corresponding to 75% f_{pu}. At full elongation, the hydraulic pressure was 2.14% less than the calculated required pressure. TxDOT specifies a ±5% tolerance. The six draped strands were tensioned next. These strands were tensioned straight to an initial elongation of 37.25 inches, before draping. Draping the strands elongated the strands an additional 4.375 inches, thereby tensioning the strands to the prescribed stress equal to 75% f_{pu}. Proper tension in these strands was checked by measuring the strands' deflection caused by a known weight suspended from the strand supported over a known distance. The top two strands were tensioned last. These strands were also tensioned to 41.625 inches of elongation.

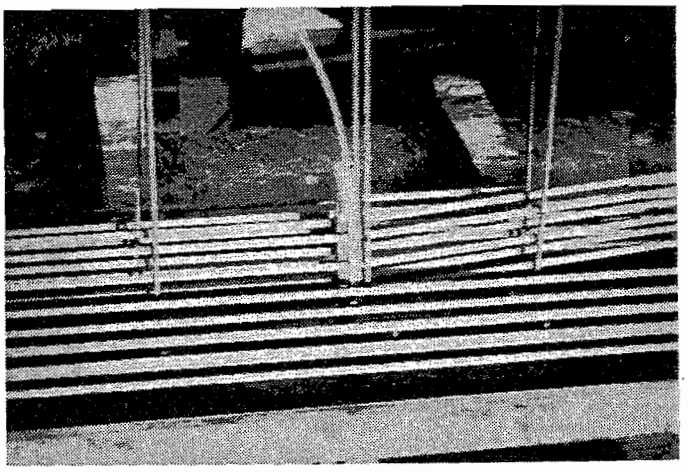

Figure 7.10 Draping Hold-Down

The draped strands were deflected with a double-headed hydraulic ram. The ram pushed against standard hold down devices which in turn pushed against and deflected the strands. The strands were deflected until the proper elevation was achieved. The ram was held in place by reacting against a single vertical tendon that was anchored to the bottom of the sofit form. A draping hold-down is pictured in the photograph in Figure 7.10.

7.3.2 Placement of Mild Reinforcement and Debonding. Mild reinforcement was placed after the strands were fully tensioned. Mild reinforcement was generally quite rusty. Stirrups and other standard bent shapes are stockpiled at the prestressing plant and used as needed, so the steel is subjected to extreme weathering.

The debonding material consisted of split white plastic tubing. The tubing was placed around the prestressing strands where required, effectively preventing the concrete paste from bonding to the strand over a desired length. This type of tubing is split along its length so that it can be snapped onto the strand. This procedure is relatively easy to perform and is not labor intensive provided there is not too much debonding material to apply. Duct tape was placed over the longitudinal seam to prevent leakage.

7.3.3 Placement of the Formwork. Formwork was installed quickly and easily. The side forms were clamped together and to the bottom sofit form by passing tension rods underneath the sofit. This procedure was quite rapid, however, there was a noticeable tendency to pull the tops of the forms wider than they were required. This problem was partly overcome by installing steel pins that fit into the tops of both side forms and prevented the side forms form pulling apart at the top.

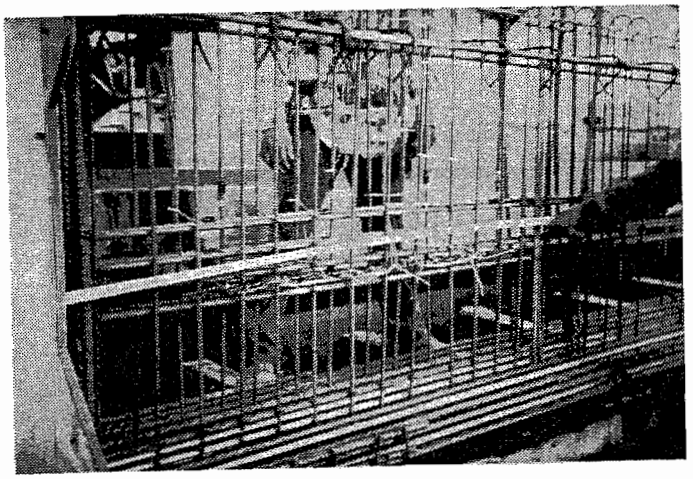

Figure 7.11 Photograph of Shear Reinforcement

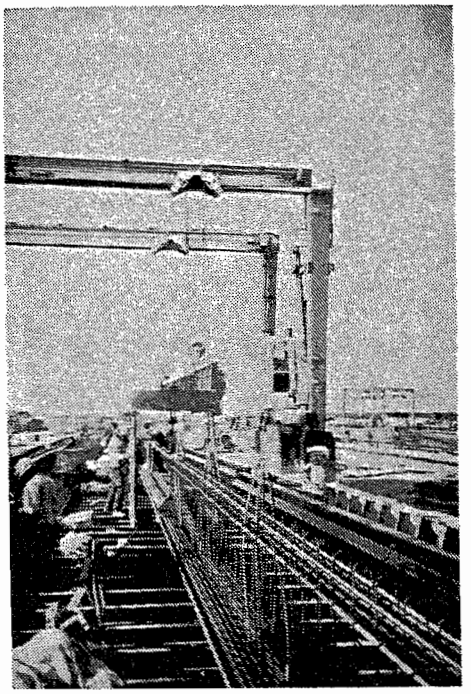

Figure 7.12 Erection of Formwork

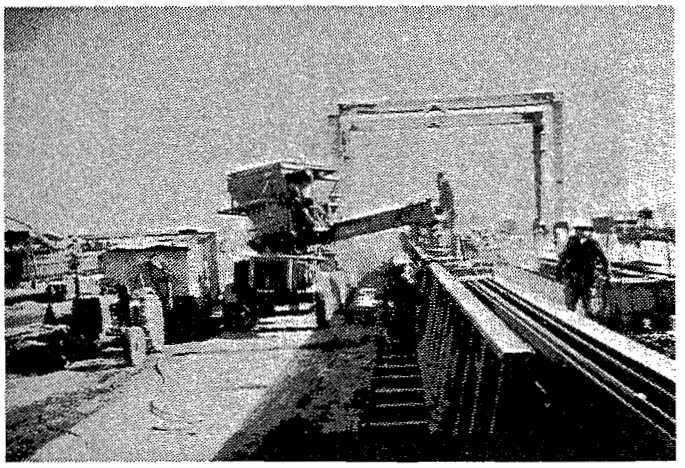

Figure 7.13 Placement of Concrete

7.3.4 Placement of the Concrete. Concrete was mixed at a batch plant located onsite. The concrete mix design for the girders is given in Table 7.1. Concrete strength was specified at 6000 psi for 28 day cylinder strength. However, the prestressing plant uses the same mix design for all highway girders regardless of specified design strength. Even though this concrete mix consistently delivers concrete strengths exceeding design requirements, the prestressing plant continues to use this mix in order to obtain adequate release strengths at 18 hours. Concrete strengths were measured from 4 x 8 cylinders taken at the time of casting. Concrete strength of the girders proved to be about 10,000 psi at the time flexural testing was initiated. Cylinder strengths are shown in Figures 7.14 through 7.16.

Figures 7.11, 7.12 and 7.13 are photographs of girder fabrication.

TABLE 7.1
CONCRETE MIX PROPORTIONS
TEXAS TYPE C GIRDERS

MATERIALS	WEIGHT PER CUBIC YARD
Type III Cement	658 LBS.
Water	257 LBS.
Coarse Aggregate (3/4 inch Crushed Rock)	1798 LBS.
Fine Aggregate(Sand)	1366 LBS.
High Range Water Reducer[1] (WRDA-19)	6 to 20 fluid oz/CWT

7.3.5 Release of the Pretensioning Steel. The girders were cast at about 11:00 AM on November 20, 1991. The following day, at 6:00 AM, cylinder strength was 6300 psi which exceeded the specified release strength of 4500 psi. Detensioning was performed by flame cutting the strands. It should be noted that standard procedure at this particular prestressing plant is to gradually detension the strands by the slow release of hydraulic pressure at the jacking end of the prestressing bed. However, flame cutting was performed because past research has suggested that bond is weakened by flame cutting[7,8,18,39].

TABLE 7.2
CONCRETE MIX PROPORTIONS

Bridge Deck Slabs
on
Full Sized Composite Girders

MATERIALS	WEIGHT PER CUBIC YARD
Type I Cement	658 LBS.
Water	292 LBS.
Coarse Aggregate (3/4 inch Crushed Rock)	1712 LBS.
Fine Aggregate(Sand)	1280 LBS.
Water Reducer[1] (M.B. 761-N)	20 fluid oz/CWT

7.3.6 Casting of the Composite Deck Slab. Deck slabs were cast onto each beam at FSEL. Formwork was supported entirely from the beam, so that slab construction was completely unshored. Figure 7.17 shows a photograph of the deck slab formwork. Concrete mix proportions for the deck slab concrete

are shown in Table 7.2. Concrete strengths of the deck slabs are also given in Figures 7.14 through 7.16. Deck concrete was cast surrounding two layers of #4 bars on 12 inch centers, each way, as shown in Figure 7.1. After casting the bridge deck, the slab was covered with plastic and allowed to cure two to three days before the formwork was removed.

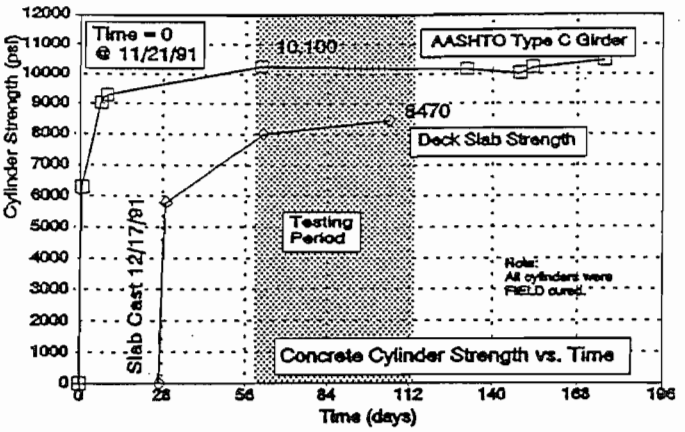

Figure 7.14 Concrete Cylinder Strengths: Girder FZ2450-3 and Bridge Deck

7.4 Test Setup and Test Procedures

7.4.1 Testing Apparatus. Test Specimen FZ2450-3 and the testing apparatus are shown in the photograph of Figure 7.18. In Figure 7.19, an elevation of the test setup is illustrated. Load was applied through two hydraulic actuators. The static capacity of each actuator was slightly greater than 200 kips and the fatigue capacity of each actuator was about 120 kips. The girders were supported at each end by two large neoprene bearing pads, 5 inches thick, 24 inches wide and 12 inches long. The 48 foot span is measured from the center of the bearing pads. The shape of the moment curve from the loading shown approximates a parabola. Note that a constant moment region exists between the North load point and the spreader beam.

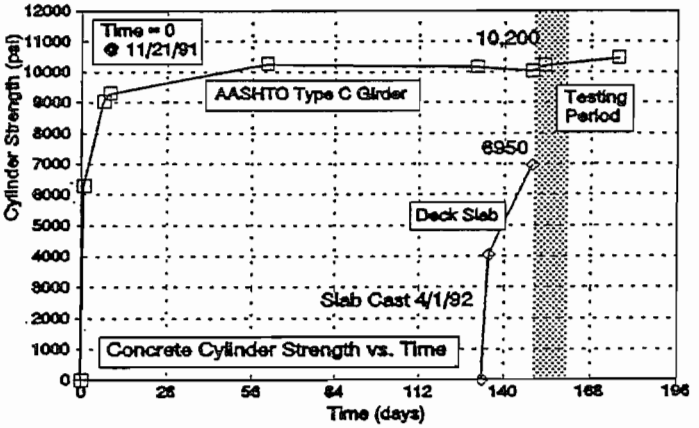

Figure 7.15 Concrete Cylinder Strengths: Girder DZ2450-2 and Bridge Deck

The depth of the composite section is 48.25 inches, so the aspect ratio of the South shear span is about 3:1. In previous tests, embedment length and span were varied from test to test. However, for these three tests the geometry of the load arrangement remained constant.

Two separate hydraulic systems were used for the testing. Static loading was applied through a static hydraulic test system. Safety precautions required the use of a static hydraulic system because hydraulic pressure is relieved with gross deformation of the test specimens. Hydraulic oil pressure was supplied by a conventional pump, driven by air.

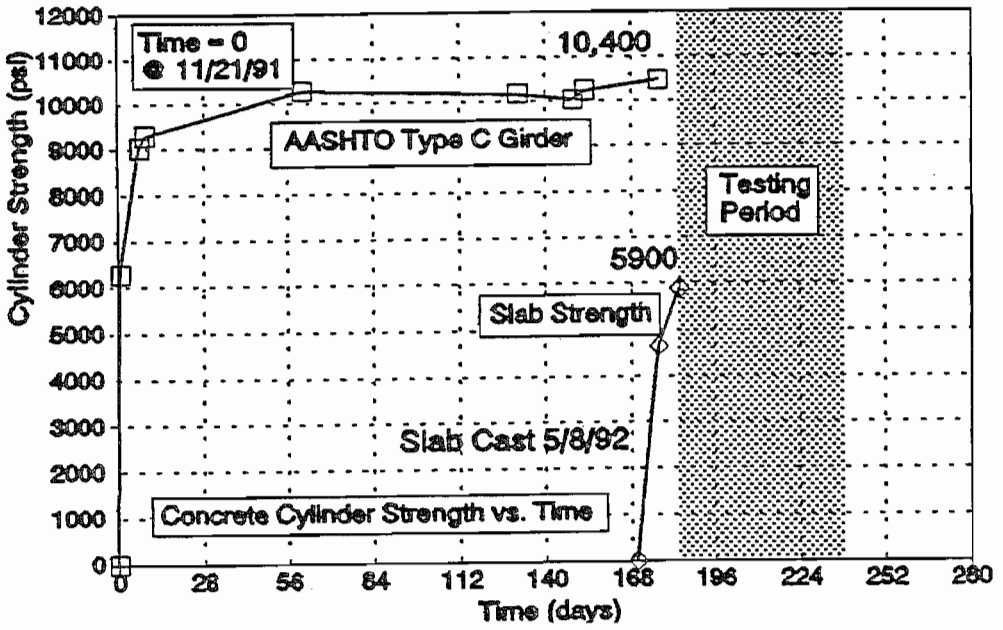

Figure 7.16 Concrete Cylinder Strengths: Girder DZ2450-1 and Bridge Deck

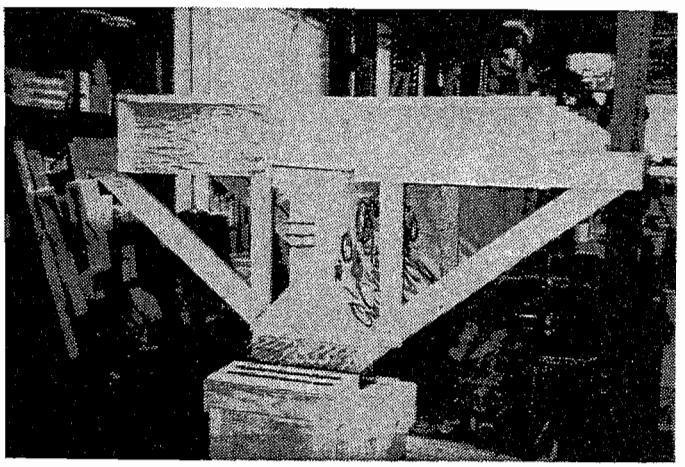

Figure 7.17 Formwork for Deck Slab

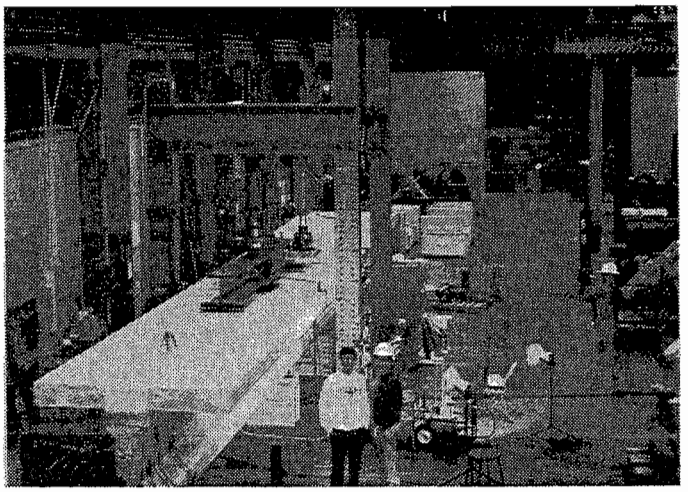

Figure 7.18 Girder FZ2450-3 and Test Setup

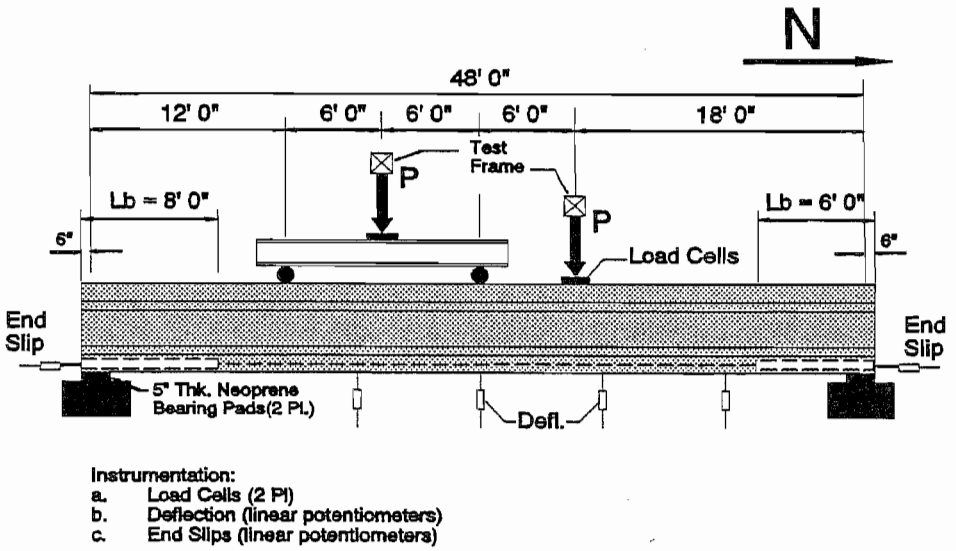

Figure 7.19 Test Setup and Dimensions for Full-Sized Girder Tests, DZ2450-1 and 2 and FZ2450-3

Repeated loads were applied through a closed-loop system consisting of the two hydraulic actuators, two servo-controlled four-way valves, and a digital controller that simultaneously controlled both servo-valves. Input to the controller came from the load cells. Output from the controller went to the servo-controlled valves which in turn controlled oil flow to each of the actuators. Hydraulic oil was supplied to the system by a 35 gpm oil pump. The oil was pumped through a combination of hard piping and portable hydraulic lines to the testing apparatus.

7.4.2 Instrumentation. Instrumentation measured the applied load, beam deflections and end slips. These data were measured electronically and the data was stored by the data acquisition system. Strain gages were applied to longitudinal and vertical shear reinforcement and also to the concrete in critical locations. However, these strain gage data are not analyzed within the scope of this report. Mechanical strain readings were taken at specific locations.

Load was measured from an electronic load cell at each hydraulic actuator. Beam deflections and end slips were measured by linear potentiometers. All of the electronic instruments were calibrated prior to testing. End slip measurements are accurate to ± 0.001 inches. End slips were measured on all debonded strands, the two strands at location A6 (see Figure 7.2), and other fully bonded strands that are at critical points throughout the cross section.

In addition to the linear potentiometers, deflections were also measured with a piano wire system. The system consisted of a piano wire, a high precision steel rule, a mirror, two posts to support the piano wire, and a weight to maintain constant tension on the piano wire. The piano wire was strung between the two posts, which were attached to each end of the beam, directly above the supports. On one end, the piano wire's support post contained a roller that allowed the piano wire to change lengths without changing tension in the wire. The weight held the piano wire in constant tension. The high precision steel rule and the mirror were glued to the beam at midspan. The ruler was positioned to read vertical deflections and the mirror was adjacent to the ruler. Deflections were measured by reading the high precision steel rule

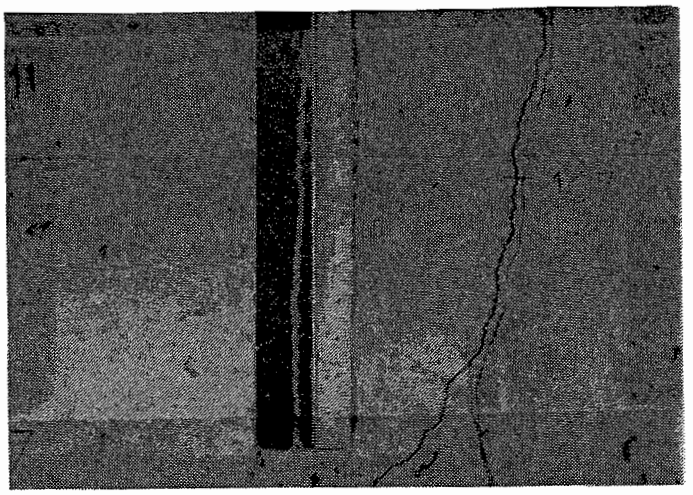

Figure 7.20 Piano Wire, Precision Rule and Mirror to Measure Girder Deflections

at the elevation where the piano wire traversed the steel rule. The mirror was required to ensure that the deflection readings were always taken from a perpendicular perspective. By visually aligning the piano wire with its reflection, deflection readings are always taken exactly perpendicular to the mirror. The photograph in Figure 7.20 shows the piano wire, the steel rule and the mirror. This system was an extremely effective method for measuring deflections throughout the testing life of the girders. Whereas linear potentiometers must be either depressed or removed during repeated loading, the piano wire system remains in place constantly.

7.4.3 Test Procedure. Testing on each girder began with a static test that "precracked" the specimen. As discussed in the chapter 6, the beams were cracked to increase the stress range beyond the stress range for an uncracked section. Similarly, bond stresses also increase as the stress range in the steel increases.

After the initial static tests, load was cycled between a minimum load of approximately 50% of service load and a maximum of approximately 100% of service load. The service load is defined as the applied load that produces a bottom fiber tension equal to $6\sqrt{f'_c}$ on the uncracked section. Service load for these tests, P_{sv}, equaled 98.1 kips.

Periodically, overloads on the order of 1.3 P_{sv} to 1.6 P_{sv} were applied to each specimen to approximate their detrimental effects that occur in the life of a bridge structure. Overloads are depicted in the load history diagrams as occasional sharp spikes. Each beam was subjected to a different loading sequence. Load histories are given in Tables 7.3 through 7.5 and in Figures 7.21 through 7.23.

Web shear cracking was induced in the South shear spans of Girders DZ2450-2 and FZ2450-3. This loading was performed as the third load cycle in specimen FZ2450-3 and after 80,000 cycles in DZ2450-2.

None of the girders failed during the repeated loading. Upon completion of the repeated loading cycles, each girder was statically tested to failure. Failure was considered to have occurred when a beam experienced large deformations without increases in load.

7.4.4 Strand Stress Range. The computed strand stress range is shown in Figure 7.24. The applied load, P, is plotted versus strand stress. The stress range was computed using the cross section shown in Figure 7.1. The stress range was calculated at the midspan of the girder where all of the strands are bonded and in their fully deflected positions. The computed stress range was about 14.0 ksi for these tests. The moment-curvature relationships were computed assuming that strains vary linearly across the cross section. Strand strain and stress was computed at the centroid of the steel, 6.06 inches from the bottom of the girder.

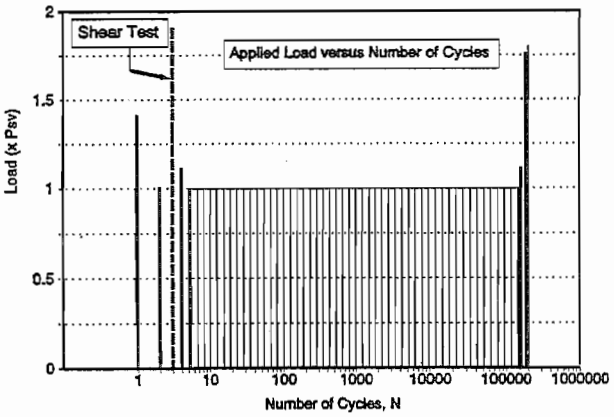

Figure 7.21 Loading History, Girder FZ2450-3

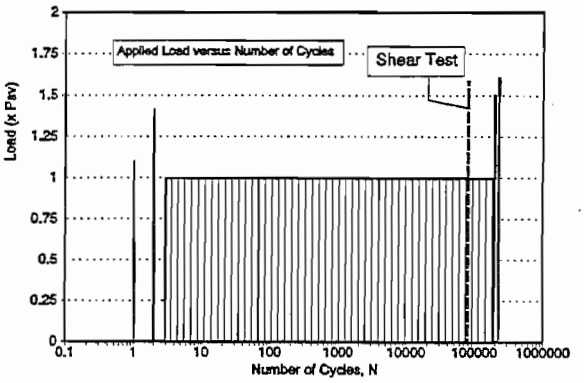

Figure 7.22 Loading History, Girder DZ2450-2

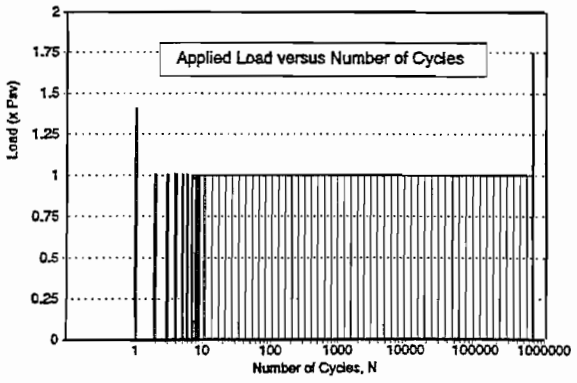

Figure 7.23 Loading History, Girder DZ2450-1

TABLE 7.3

GIRDER FZ2450-3
LOADING HISTORY

Load Cycle N	Max. Load (kips)	% P_{sv}	Deflections			Slip 22AE, South[3]		Slip 22AW, South[3]	
			Beg	End	@ P_{sv}	Beg	End	Beg	End
1[1]	135.62	1.4	0	0.08	0.49	0	0	0	0
2	99.54	1.0	0.07	0.08	0.69	0	0	0	0
3[2]	V=185	-	0.21	0.28	0.69	0	0.008	0	0.008
4	105	1.1	0.26	0.26	1.15	0.008	0.008	0.008	0.008
157,330	110	1.1	0.26	0.26	1.26	0.048	0.049	0.035	0.035
225,000	173.2	1.75	0.24	1.31	1.21	0.049	0.049	0.035	0.035
225,001[4]	177.4	1.8	1.37	1.84	3.24	0.049	0.049	0.035	0.035

1. @ Initial Static Test, flexural cracking to Station 222.
2. Beam was loaded asymmetrically until web shear cracking occurred in the South shear span. Web shear cracking occurred at V=185.5 kips. Flexural cracking to Station 146.
3. Strands 22AE and 22AW were draped strands. These strands showed the largest slip. Very little slip was detected in other strands. Slips were measured at the South end.
4. Test to Failure. Beam failed in flexure.

TABLE 7.4

GIRDER DZ2450-2
LOADING HISTORY

Load Cycle N	Max. Load (kips)	% P_{sv}	Deflections			Slip 4D-W, South[4]		Slip 2E-W, South[4]	
			Beg	End	@ P_{sv}	Beg	End	Beg	End
1[1]	112.7	1.1	0	0.05	0.48	0	0	0	0
2	138.37	1.4	0.05	0.13	0.54	0	0	0	0
80,000[2]	V=154	-	0.14	0.18	0.73	0	0.042[4]	0	0.050[4]
193,970	149.6	1.5	0.21	0.25	0.85	0.054	0.058	0.071	0.076
228,500[5]	157.1	1.6	0.24	-	0.91	0.062	0.939	0.080	0.914

1. @ Initial Static Test, flexural cracking to Station 299.
2. Beam was loaded asymmetrically until web shear cracking occurred in the South shear span. Web shear cracking occurred at V=154.6 kips. Flexural cracking to Station 220.
3. Strands 4D-W and 2E-W were fully bonded strands. These strands showed the largest slip. Similar slips were detected in other fully bonded strands strands, however, no slip was recorded in debonded strands until failure. Slips were measured at the South end.
4. Strand slips initiated by bursting cracks at South support. Debonded strands showed similar end slips, however, those slips do not represent bond slips.
5. Test to Failure. Beam failed from horizontal shear failure.

Strand stresses shown in Figure 7.24 include the effects from slab shrinkage. When the slab shrinks after casting, it imposes downward deflection and curvature on the simply supported girder. This reduces the precompression at the bottom of the cross section. Likewise, the cracking moment is reduced, the decompression moment is reduced and the strand stress range is increased. Figure 7.25 shows the strand stress if slab shrinkage is not considered, which is the procedure for most design cases. In a later section of this chapter, deflections from slab shrinkage are reported along with a short discussion of the effects of slab shrinkage on pretensioned girder behavior.

TABLE 7.5

GIRDER DZ2450-1

LOADING HISTORY

Load Cycle N	Max. Load (kips)	% P_{sv}	Deflections			Strand Slips[3]	
			Beg	End	@ P_{sv}	Beg	End
1[1]	137.13	1.4	0	0.10	0.48	-	-
696,158[3]	170.27	1.74	0.23	-	0.94	-	0.013

1. @ Initial Static Test, flexural cracking to Station 216.
2. No significant strand slips were detected throughout the tests. During the loading to failure, bursting cracks formed above the support. These cracks caused small amounts of slip, however, slips were well controlled as the cracks did not appear to grow much larger than their initial width. The maximum slip measured was 0.013 inches on strand 4E-East, North end.
3. Test to Failure. Beam failed in flexure. Flexural cracking to Station 136.

7.5 Presentation of Test Results

The girders were tested in reverse numerical order. FZ2450-3 was tested first, DZ2450-2 was tested second and DZ2450-1 was tested last. Because test results from earlier tests influenced some of the procedures employed in subsequent tests, the test procedure and results will be reported in chronological order, not in the numerical sequence of the test series.

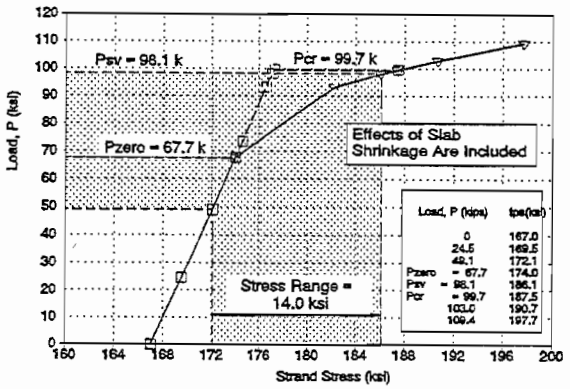

Figure 7.24 Stress Range for Repeated Load Tests (Slab Shrinkage Effects Included)

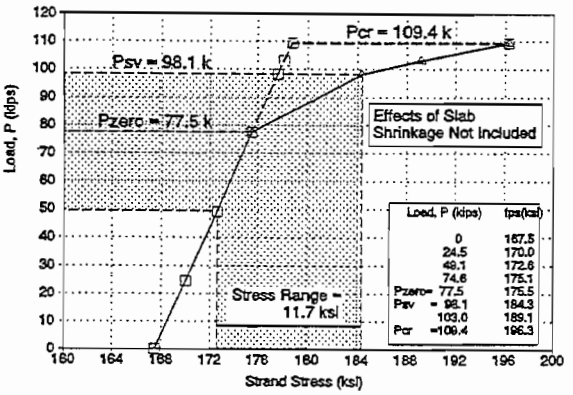

Figure 7.25 Stress Range for Repeated Load Tests (Slab Shrinkage Effects are not Included)

In the next three sections, each test is described briefly. For each test, load versus deflection curves are presented for the initial static tests, for the static shear loadings, and for the final static tests. The load histories are reported in both tabular and graphical form. End slips are reported in the tables that present the load histories. End slips that are reported are taken from the strands where the largest slips occurred. Midspan deflections are also reported in these tables. Deflections at the beginning and at the end of each static loading are reported along with the total deflection of the beam at the service load, P_{sv} = 98.1 k.

All of the girders were cast on November 20, 1991. However, the slabs were cast on three different dates. The age of the slab at the time of testing varied widely and may have influenced the cracking loads and other beam behavior. For example, the slab was cast for FZ2450-3 on December 17, 1991, while the beam was relatively young. However, the initial static test was not performed until January 17, 1992, one full month after casting the slab. In the other specimens, the initial static test was performed approximately two weeks after casting the slab. As a result, slab strengths for DZ2450-1 and 2 were considerably lower than the slab strength in FZ2450-3. Consequently, the disparity in cracking loads from the test results may have resulted from varying ages and strengths of the slabs.

7.5.1 Presentation of Results, FZ2450-3. The initial static test was performed January 17, 1992. The age of the girder was 57 days and the age of the slab was 31 days. Concrete strengths are reported in Figure 7.14. The final static test to failure was performed on March 12, 1992 after 225,000 cycles of load.

The girder was loaded initially to crack the beam and to provide a basis for load-deflection relationships. The girder was loaded in approximately 5 kip increments. First cracking occurred at Station 325, or 325 inches from the beam's South end, at a load of 106.0 kips. The initial load deflection curve is shown in Figure 7.26.

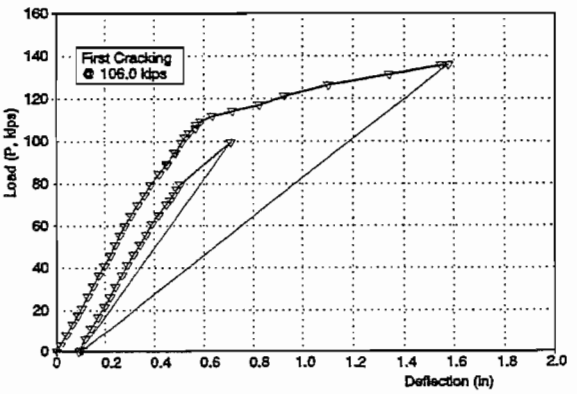

Figure 7.26 Initial Static Test, Beam FZ2450-3

In the third static loading, the girder was loaded asymmetrically to induce web shear cracking in the South shear span. Web shear cracking occurred at a shear of 185.5 kips, with P_{south} = 237.0 kips and P_{north} = 99.8 kips. Shear versus midspan deflection is plotted in Figure 7.27. The noncontinuous curve is caused by alternating loading on the two hydraulic rams. As one ram is loaded, load on the other is relieved, even though the total load is increasing.

The most significant result from the web shear cracking is that the draped strands slipped approximately 0.01 inches upon formation of the web shear cracks. Draped strands are positioned within the web where they are vulnerable to web shear cracking. However, in these tests, the depth of the girder ensured that the first intersection between the draped strands and the web shear cracks occurred outside of the strands' anchorage zone. If an assumed shear crack forms in the web on an angle of approximately 30° to the horizontal, the crack would not intersect the web until 30 inches from the beam end if projected from the center of bearing at the support. Furthermore, the crack would not intersect the draped strands until a distance even further from the beam's end. At that location, the draped strands would have fully transferred their prestressing force, and the loss of anchorage for the draped strands does not pose a serious threat.

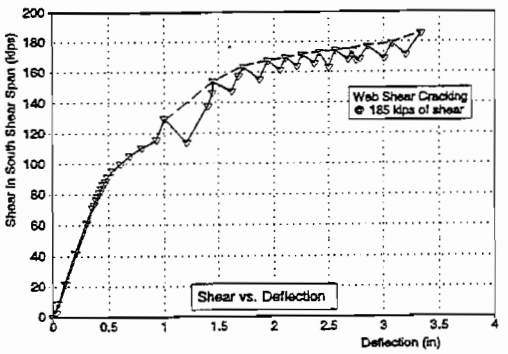

Figure 7.27 Static Test to Web Shear Cracking, Beam FZ2450-3

The loading history for FZ2450-3 is given in Table 7.3 and Figure 7.21. The end slips reported in Table 7.3 are end slips from draped strands on the South end of the beam. Note that small increases in end slip occurred from the static shear loading until the static test was performed at 157,330 cycles. Increases were small, similar to end slip increases noted in the repeated load tests from the previous chapter. No other strands suffered significant end slips.

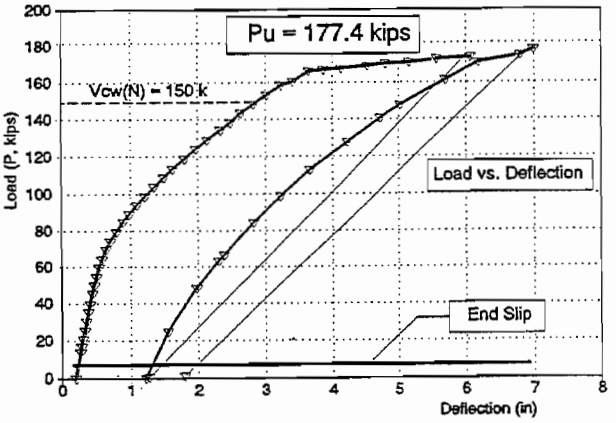

Figure 7.28 Final Static Test, Girder FZ2450-3

The final static tests were performed on March 12 and 13, 1991. A total of 225,000 cycles were placed on the girder, at which time the girder was loaded statically to failure. The load deflection curves for the final static tests are shown in Figure 7.28. Nearly 7 inches of deflection was reached at a load of 177.4 kips. The test was terminated because load was not increasing significantly with large increases in deflection. Failure was a pure flexural failure with yielding of the strands and large plastic rotations. Cracking extended into the deck slab.

7.5.2 Presentation of Results, DZ2450-2. The initial static test was performed April 16, 1992. The age of the girder was 148 days and the age of the slab was 15 days. Concrete strengths are reported in Figure 7.15. The beam was tested statically until failure on April 27, 1992 after 228,452 cycles of load.

The initial static test was performed to precrack the beam and to develop the load-deflection relationship. The girder was loaded in approximately 5 kip increments. The first flexural crack formed at Station 331 at a load of 101.2 kips. The load-deflection curve from the initial test is shown in Figure 7.29.

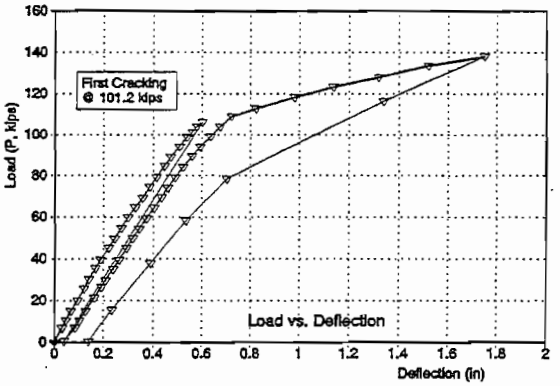

Figure 7.29 Initial Static Test, Beam DZ2450-2

Table 7.4 reports the loading history for DZ2450-2. The same data is illustrated graphically in Figure 7.22. A static test to induce web shear cracking was also performed on this girder. Shear at the South end of the beam is plotted versus girder deflection in Figure 7.30. Web shear cracking occurred at approximately 155 kips of shear. V_{cw} was smaller for DZ2450-2 than for FZ2450-3 because eight of 24 strands were debonded (V_{cw}(FZ3) = 185 kips > V_{cw}(DZ2) = 155 kips). As discussed earlier, debonding strands reduces the precompression which in turn weakens the girder's resistance to web shear cracking.

During the static shear loading, a vertical crack formed directly above the South bearing pad. Strand slips coincided with formation of this crack. The crack formed immediately above the centerline of the neoprene bearing pad and propagated vertically until the crack reached the web where it bent towards the load. This crack is shown in the photograph in Figure 7.31. The end slips reported in Table 7.4 were taken from fully bonded strands at the South end of the beam and represent the maximum strand slips measured on any strand. End slips were also measured on the debonded strands. However, these end slips measured the width of the vertical crack and do not necessarily represent slip of the debonded strand in relation to the concrete.

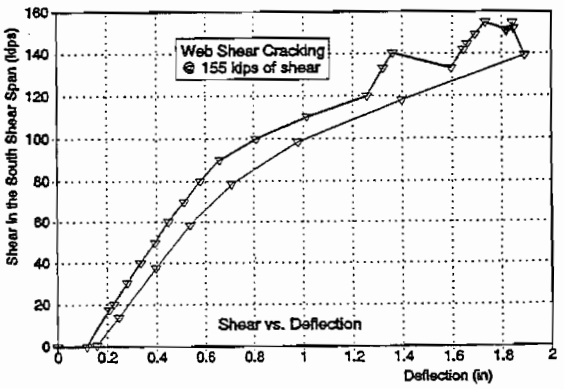

Figure 7.30 Static Test to Web Shear Cracking, Beam DZ2450-2

The final static test was performed on April 29, 1992 after approximately 228,000 load cycles. The load deflection curve from the final static test is given in Figure 7.32. As load increased, deflections also increased. The North shear span developed web shear

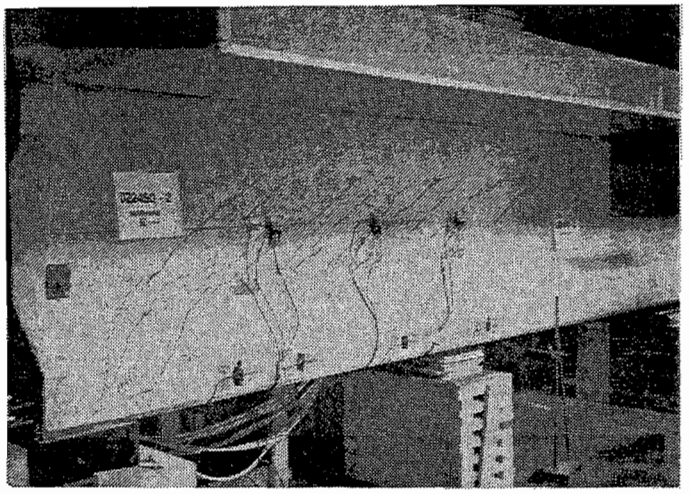

Figure 7.31 Web Shear Cracking Pattern, South Shear Span of DZ2450-2

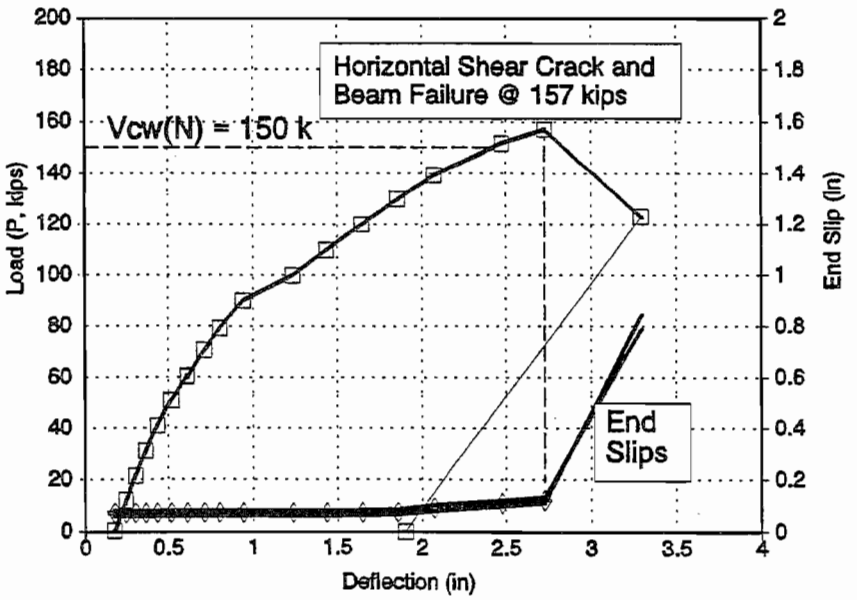

Figure 7.32 Final Static Test, Girder DZ2450-2

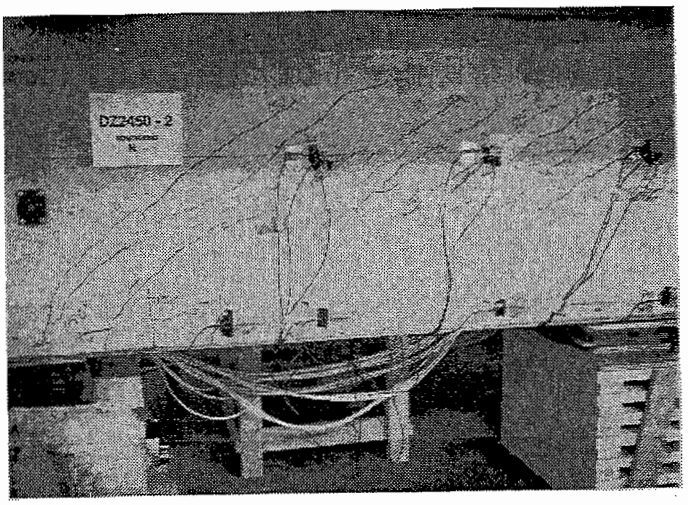

Figure 7.33 Cracking Pattern at P = 140 kips, DZ2450-2

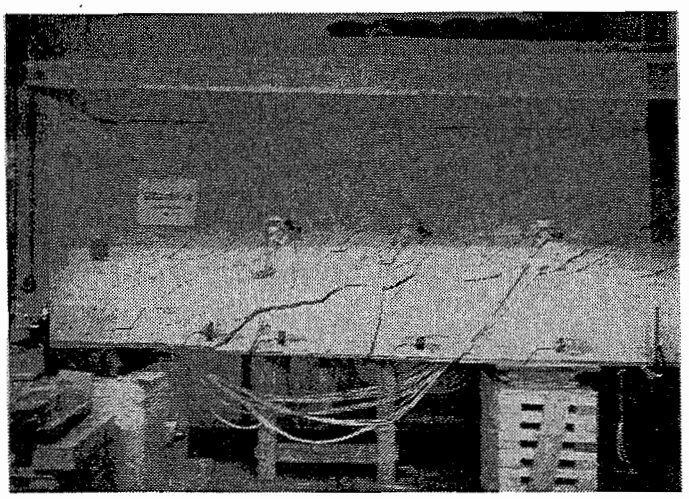

Figure 7.34 Cracking Pattern at Horizontal Shear Failure, DZ2450-2

cracking at about 150 kips, however, these cracks did not influence the behavior of the girder. As load increased beyond 150 kips, additional shear cracks began to form in the South shear span. Cracks that were previously formed began to grow. Several web shear cracks extended from the web downward into the bottom flange. The three photographs pictured in Figures 7.31, Figure 7.33, and Figure 7.34 illustrate the progression of cracking in the end regions as load was increased. In Figure 7.33, note the appearance of new cracks at Stations 26 and 28 and the splitting crack between Stations 20 and 26. The photograph in Figure 7.34 shows the girder at failure.

At an applied load of about 157 kips, several of these smaller shear cracks joined together as a large horizontal shear crack formed, located approximately at the intersection between the web and the bottom flange. Formation of this crack was followed by complete girder failure as this horizontal shear crack propagated through the bottom flange and the web, effectively separating the bottom flange from the web and the remainder of the beam. This failure is illustrated by the photograph in Figure 7.34.

The horizontal shear crack intersected the bottom of the beam 28 inches from the end. It continued on an average angle of 10° to 15° as it progressed up through the bottom flange. The crack intersected the bottom of the web at Station 90 and the top of the web at Station 116 to 120. This crack appeared to have jumped from one web shear crack to another as it formed along the bottom flange. Longitudinal shear reinforcement that extended 96 inches from the end of the beam may have influenced this crack to propagate lengthwise instead of upward and through the web. Once the crack was clear of the horizontal reinforcement, it proceeded through the web at an angle of approximately 30°, an angle parallel to other web shear cracks.

This failure occurred through a combination of effects including the effects of repeated loading, the impact of debonding strands, and reinforcement details. Web shear cracking had been induced in the span at 80,000 cycles. Subsequent loading added nearly 150,000 cycles of loading to the beam. Although the crack widths did not increase dramatically over that loading, additional loading did cause some further damage to the beam, especially in the end regions where the shear cracks had formed.

Debonding strands also contributed to this failure because precompression of the bottom flange was lessened. By employing debonded strands, the effective prestress force is reduced in the end regions. Because of the lower precompression, cracks can propagate through the bottom flange more easily. In this test, web shear cracks extended into the bottom flange. Under extremely high loads, these cracks grew wider and the bond characteristics of the fully bonded strands was affected. However, it is doubtful that the debonded strands contributed to this failure by any other means than reducing the effective prestress force. In fact, it is likely that the debonded strands were able to maintain their bond up until collapse of the beam occurred.

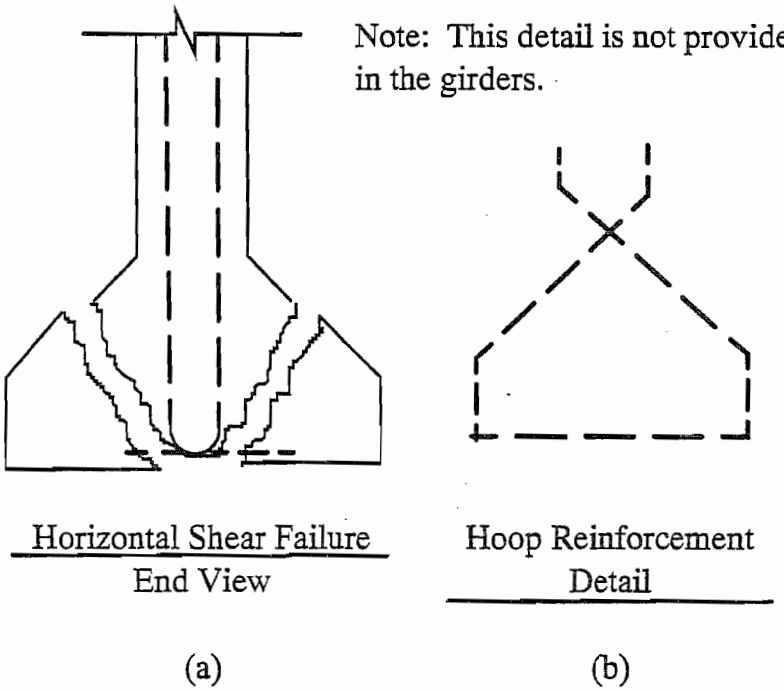

Figure 7.35 Horizontal Shear Failure, Girder DZ2450-2

One final factor contributing to this failure was the reinforcement detailing in this region. Figure 7.35a shows an end view of the failure mechanism. As the figure shows, the bottom flange was ripped away from the rest of the beam by large horizontal shear stresses. In the figure, the web portion of the beam remains intact, even through the bottom flange to the bottom of the beam. This section of concrete was held together by the stirrups. Note in the reinforcement details that stirrups had only a short 90° hook on the bottom. Reinforcement details were not provided to arrest a horizontal shear crack and keep it from growing. Figure 7.35b shows the standard detail of hoop reinforcement that can be provided around the bottom flange. This reinforcement detail would have probably prevented this failure. However, this reinforcement is usually only provided in the extreme end regions of the beam, directly above the support.

7.5.3 Presentation of Results, DZ2450-1. The initial static test was performed May 19, 1992. The age of the girder was 181 days and the age of the slab was 11 days. Concrete strengths are reported in Figure 7.16. The final static test was performed on July 22, 1992 after 696,158 cycles.

In the initial static test, the girder was loaded in approximately 5 kip increments. First cracking occurred at Station 325 at a load of 101.1 kips. The initial load deflection curve is shown in Figure 7.36. The load history for this girder is given in Table 7.5 and illustrated in Figure 7.23. For this beam, no intermediate overloads were applied, only repeated loadings to service loads. On the other hand, the number of cycles applied to this girder exceeded the other tests by a factor of three.

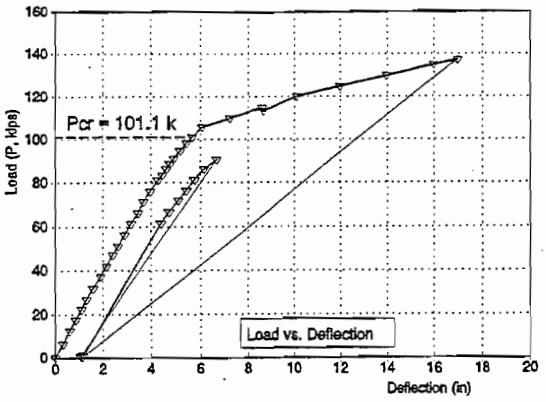

Figure 7.36 Initial Static Test, Girder DZ2450-1

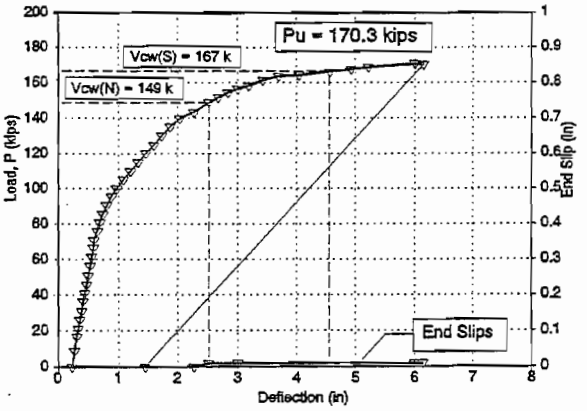

Figure 7.37 Final Static Test, Girder DZ2450-1

The final static test was performed after 696,158 cycles. The load-deflection curve is shown in Figure 7.37. Loading was relatively uneventful as deflections continued to increase with load. At a load of 149 kips, the North shear span developed web shear cracks. Web shear cracks appeared in the South shear span at a load of 167 kips. Cracking in the North and South shear spans is shown in the photographs in Figures 7.38 and 7.39. The test was terminated when load reached 170.3 kips at 6.15 inches of deflection. Flexural failure of the beam was imminent. This test is classified as a flexural failure.

TABLE 7.6

FIRST FLEXURAL CRACKING LOADS
FULL-SIZED COMPOSITE GIRDERS

GIRDER	$P_{cr(test)}$	No Slab Shrinkage		w/ Slab Shrinkage	
		$P_{cr(calc)}$	test/calc	$P_{cr(calc)}$	test/calc
FZ2450-3	106.0	109.4	0.97	99.7	0.94
DZ2450-2	101.2	109.4	0.93	99.7	1.02
DZ2450-1	101.1	109.4	0.92	99.7	1.01

1. Concrete strengths of deck slabs varied:
   f'_c(slab) = 8000 psi for FZ2450-3
   f'_c(slab) = 6950 psi for DZ2450-2
   f'_c(slab) = 5900 psi for DZ2450-1

Figure 7.40 illustrates the cracking pattern resulting from the final static test to ultimate. This cracking pattern is typical for flexural failures. The other two girders, FZ2450-3 and DZ2450-2 demonstrated very similar cracking patterns.

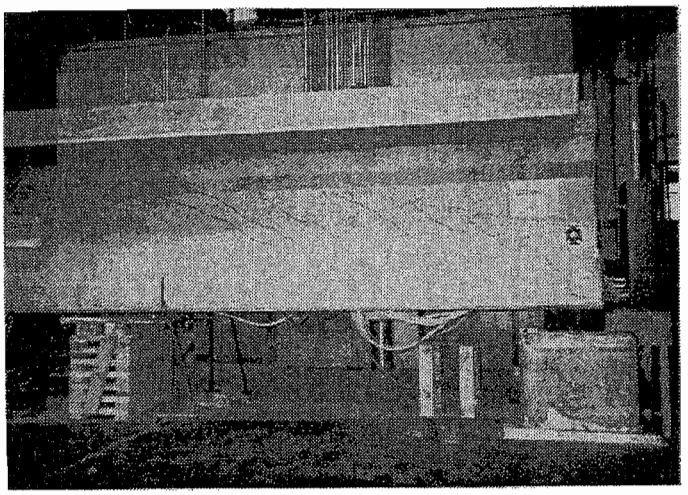

Figure 7.38 Web Shear Cracking Pattern North Span of DZ2450-1

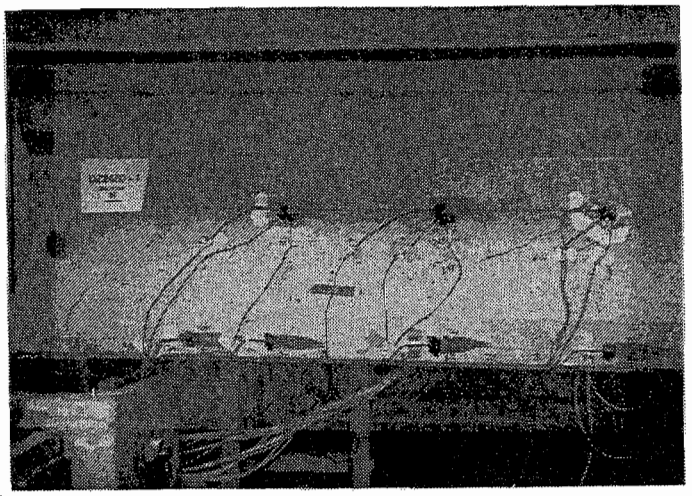

Figure 7.39 Web Shear Cracking Pattern South Span of DZ2450-1

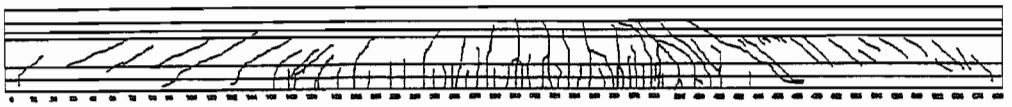

Figure 7.40 Cracking Pattern for DZ2450-1, Final Static Test to Ultimate

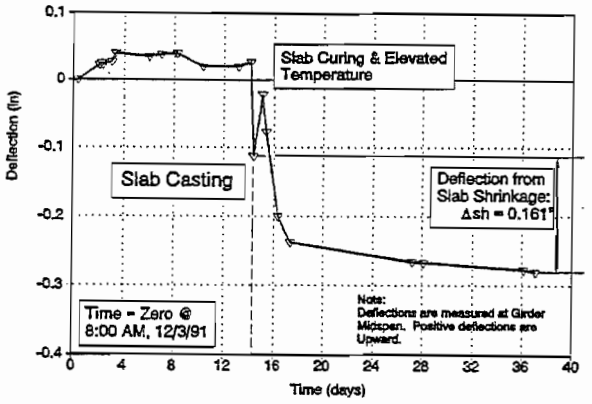

Figure 7.41 Time Dependent Deflections: FZ2450-3

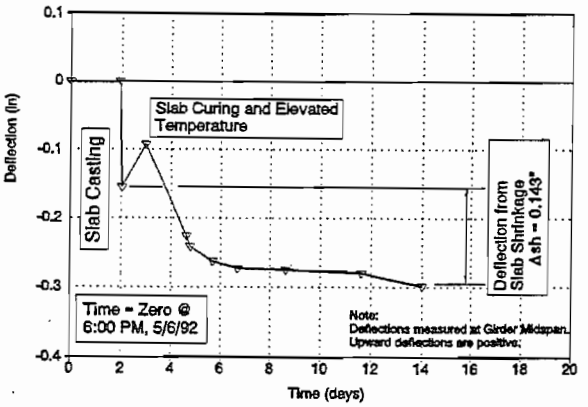

Figure 7.42 Time Dependent Deflections: DZ2450-1

7.6 Discussion of the Results

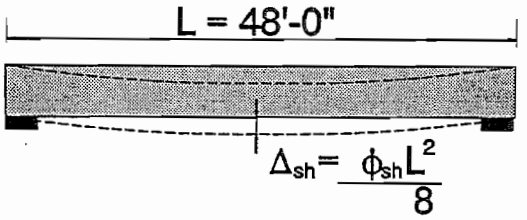

Figure 7.43 Deflection From Shrinkage

7.6.1 Measurement and Effects of Slab Shrinkage. Slab shrinkage was measured indirectly by measuring the deflections of the composite girders after the slab was cast. Deflection measurements are plotted over time for Girders FZ2450-3 and DZ2450-1, and illustrated in Figures 7.41 and 7.42. From these deflection measurements, the curvature from shrinkage can also be calculated as shown in Figure 7.43. As the slab shrinks, the slab imposes net compressive strains and stresses into the cross section, whereas the girder restrains the slab. Because the shrinkage forces are eccentric to the composite section, curvature is induced into the cross section. The combined affects are illustrated in Figure 7.44. Because slab shrinkage is restrained by the girder, the slab experiences tensile stresses.

For the case of FZ2450-3, total girder deflection in the time immediately following casting of the slab was 0.161 inches. This leads to a shrinkage curvature, ϕ_{sh} = 3.88 x 10^{-6} $^{rad}/_{in}$. The relationship between ϕ_{sh} and F_{sh} is given by:

$$\phi_{sh} = \frac{F_{sh} e_{sl}}{EI}$$

and F_{sh} = 336.1 kips. Also,

$$\epsilon_{sh} = \frac{F_{sh}}{AE}$$

and ϵ_{sh} = 161.7 x 10^{-6} $^{in}/_{in}$, where e_{sl} is the eccentricity of the slab, and F_{sh} is the total shrinkage force. From these calculations, the stress and strain distributions that result from

slab shrinkage can be computed. The results are shown in Figure 7.45 as the residual stresses and strains resulting from slab shrinkage.

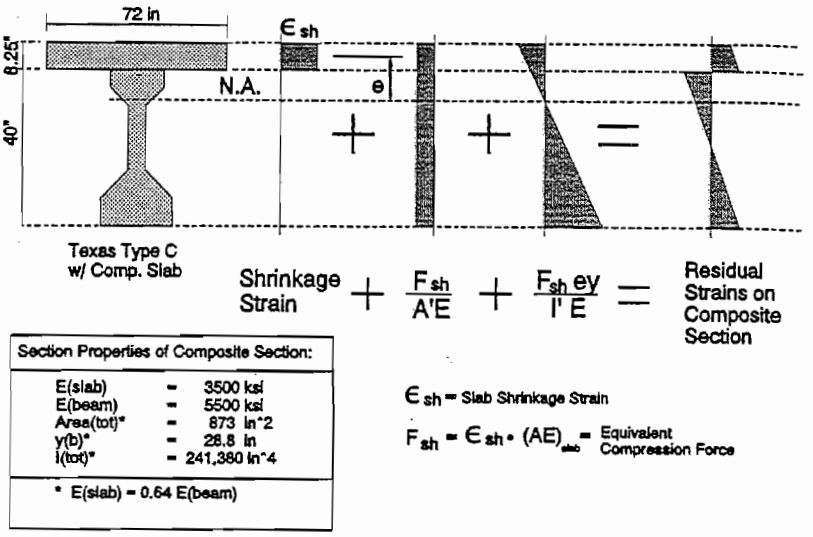

Figure 7.44 Residual Strains From Slab Shrinkage

From the figure, precompression in the bottom fiber is reduced 229 psi. Likewise, the cracking load and the decompression load are also reduced. From Figures 7.24 and 7.25, the calculated cracking load is reduced from 109.4 kips to 99.7 kips. Decompression load is reduced from 77.5 kips to 67.7 kips, if slab shrinkage is considered. Similarly, the stress range is increased. Increases in stress range have been shown to decrease the life of a bridge structure, so the influence of slab shrinkage is important. Note also from Figure 7.45, that the precompression in the top of the girder is increased. Increases in precompression increase the girders' resistance to web shear cracking, particularly as precompression is increased in the top of the cross section. In composite highway girders, elastic analysis will usually show that the critical point for inclined tensile cracking is located at the top of the web. In girder FZ2450-3, precompression increased 422 psi in the top of the web. In this manner, slab shrinkage has a large and positive effect on the ability of a composite girder to resist web shear cracking.

As a side note, these time deformations are almost certainly caused primarily by shrinkage. However, other time dependent factors, such as creep or relaxation, may also influence beam deformations. Fortunately, it is not important to determine what other factors are involved nor is it important to know how much influence other factors may exert. It is only important that the cross section is deforming, over time, because some internal mechanism(s) cause(s) curvature across the cross section.

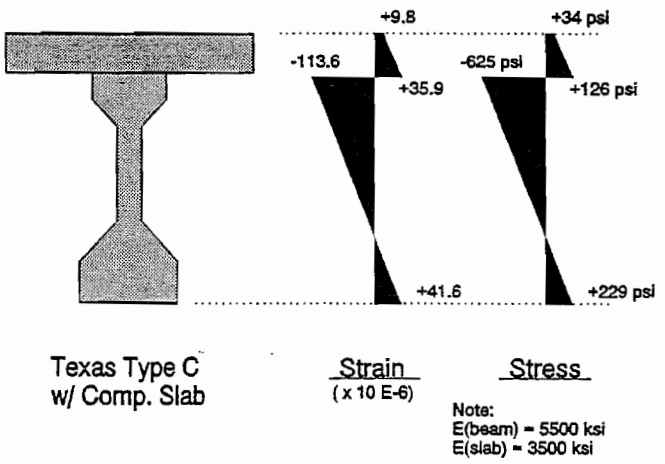

Figure 7.45 Residual Stresses and Strains From Slab Shrinkage, FZ2450-3

Regardless of the origin, these known curvatures produce residual stresses in the cross section that affect the behavior and performance of composite girders.

7.6.2 Prediction of First Flexural Crack. The loads at which the first flexural crack occurred are shown in Table 7.6. The cracking loads are compared to two different calculated cracking loads. The first, 109.4 kips, was calculated without considering the effects of slab shrinkage. In the second, the predicted cracking load is equal to 99.7 kips. This load was calculated by superimposing the residual stresses from slab shrinkage. Cracking load was calculated as the applied load necessary to impose a bottom fiber stress equal to $f_r = 7.5\sqrt{f'_c}$.

TABLE 7.7

WEB SHEAR CRACKING LOADS FULL-SIZED COMPOSITE GIRDERS

GIRDER	N or S	Number of Cycles	$V_{cw(test)}$	No Slab Shrinkage		w/ Slab Shrinkage	
				$V_{cw(calc)}$	test/calc	$V_{cw(calc)}$	test/cal
FZ2450-3	S	3	185	133	1.39	175	1.03
FZ2450-3	N	225,000	150	133	1.13	175	0.86
DZ2450-2	S	80,000	156	108	1.43	153	1.02
DZ2450-2	N	238,500	150	108	1.43	153	0.98
DZ2450-1	S	696,158	167	109	1.53	153	1.09
DZ2450-1	N	696,158	149	109	1.37	153	0.97

The measured cracking loads were 106.0 kips for FZ2450-3, 101.2 kips for DZ2450-2 and 101.1 kips for DZ2450-1. Each of these cracking loads were compared to the calculated cracking loads. The measured values show very good correlation to the calculated cracking load of 99.7 kips, considering the effects of slab shrinkage.

7.6.3 Effects of Web Shear Cracking. Earlier test series had demonstrated that web shear cracking could cause sudden and violent failures. As the web shear cracks propagated across the transfer zone of pretensioned strands, strand anchorage was disturbed. Many times strand anchorage was destroyed. As pretensioned strands lost their anchorage, they were unable to develop the tension required to support shear loads. Failures were often explosive as the strands pulled through the concrete and the concrete hinged at the compression fiber, and the beam collapsed. Web shear cracking is particularly important to the development of pretensioned reinforcement because the web shear crack will develop more readily in the end regions of the beam.

In light of these failures, it becomes important to understand and predict web shear cracking. In these full-sized girder tests, all of the strands were contained within the bottom flange. Propagation of web cracks through the anchorage becomes more difficult as the bottom flange becomes thicker. However, it remains important to predict and measure the occurrence of web shear cracking.

The web cracking shears, $V_{cw(test)}$, are given in Table 7.7. The measured values are compared to the calculated values. The calculated values are based on an elastic stress equal to $4\sqrt{f'_c}$. Note the large difference between the two calculated cracking shears, $V_{cw(calc)}$. By considering the effects of slab shrinkage, the value for $V_{cw(calc)}$ is increased 30% to 40%. This increase in V_{cw} is directly related to the increase in precompression at the top of web. Slab shrinkage created additional precompression in the top of the girder. At the top of the web, precompression increases 422 psi, and V_{cw} increases accordingly.

From the table, the measured values of $V_{cw(test)}$ demonstrate some scatter. Variations in web thickness, concrete mix proportions, or simply local variations in the hardened concrete can affect this result. However, when compared to $V_{cw(calc)}$ considering residual stresses from slab shrinkage, the measured values are definitely varied around the calculated values. Ratios varied from a low of 0.86 to a high of 1.09.

7.6.4 Incidence of End Slips. End slips occurred in all three specimens. However, with the exception of the horizontal shear failure in DZ2450-2, end slips remained small. The largest measured slip was 0.080 inches in DZ2450-2 before the final test was begun.

In girder FZ2450-3, the largest slips were measured on draped strands. This is due in part to the cracking at the end of the girder caused by separation of the two anchorage zones (See the photograph in Figure 7.38). Slips were first detected after the occurrence of web shear cracking in the South shear span. However, these web cracks did not seriously affect anchorage of the draped strands because the nearest web shear crack was located at least 54 inches from the beam's end, well outside of the transfer zone.

In DZ2450-2, initial end slips occurred on fully bonded strands when bursting cracks developed above the support at the South end. The debonded strands did not slip. All slips were localized at the bursting crack which formed approximately at Station 8. The anchorages of the debonded strands began at Station 36 so they were not affected by the bursting crack. In the final static test on this girder, extensive cracking developed in the anchorage zones of the fully bonded strand, partly as a result of the propagation of web cracks into the bottom flange, and partly because the bursting crack had weakened the anchorage of all fully bonded strands. As the bottom flange lost its precompression, the end region of the girder became more susceptible to cracking. The horizontal shear failure is related directly to the loss of bond on the fully bonded strands and the corresponding loss of the precompression in the concrete. This failure probably would not have occurred except for the shortened test span that caused applied loads to be 17% larger to develop the same moments in the cross section. These increased loads caused bursting cracks at the supports that otherwise would not have developed.

This failure is related to debonded strands only in that their presence decreases the precompression force if similar design cases are compared to a girder with draped strands. Reduced precompression in the end region caused the beam to be somewhat more susceptible to the bursting crack. In evaluating this test result, it should also be noted that

the applied shear is approximately 17% greater in the test beam than for the design case. In actual application, bursting cracks may not have formed.

Girder DZ2450-1 demonstrated very little end slip throughout its testing. Even though this girder was subjected to three times the number of load cycles, no intermediate overloads were placed on the beam. In the final static test to failure, flexural cracking extended to Station 136. However, this crack is outside the debond/transfer zone and no additional end slips occurred because of this crack. The end slips that did occur, again resulted from bursting cracks that formed over the supports. At a load of 149 kips, a bursting crack formed at the North support, coinciding with initial end slips in fully bonded strands at the North end of the beam. There was no evidence that debonded strands suffered any slip.

7.6.5 Comparison to Ultimate and Failure Modes. Table 7.8 compares the failure loads to the calculated ultimate load and also reports the mode of failure for each test. The nominal flexural capacity was calculated using ACI equation 18-3. Failures of FZ2450-3 and DZ2450-1 were both flexural failures. However, in both of these specimens, the loading was halted before actual compression failure of the top flange because of safety considerations. The failure load, $P_{u(test)}$, listed in the table is actually the load at which the test was terminated. In both of these specimens, the top fiber concrete strains were in excess of 0.002 in/in, and the specimens were experiencing large deformations with very little increase in load. Had the tests been continued to failure, the failure loads would have been slightly greater.

TABLE 7.8

ULTIMATE LOADS AND FAILURE MODES FULL-SIZED COMPOSITE GIRDERS

BEAM	$P_{u(test)}$	$P_{n(calc)}$	test/calc	Failure Mode
FZ2450-3	177.4	177.1	1.00	Flexural
DZ2450-2	157.1	177.1	0.89	Horizontal Shear
DZ2450-1	170.3	177.1	0.96	Flexural

7.7 Summary

Three full sized girders were fabricated and tested to determine if the behavior of beams with debonded strands could be predicted; and to determine if their performance was safe and reliable. Two of the girders, DZ2450-1 and DZ2450-2 contained debonded strands. The third girder, FZ2450-3 contained draped strands to serve as a control and companion specimen to the debonded girders. All of the girders were designed for the same loads and spans, and so their cross sections and capacities were nearly identical.

The cross section was designed to support HS24 highway bridge loads across a span of 75 feet, assuming a girder spacing of 6.8 feet. The cross section is shown in Figure 7.1. The specimens were made from Texas Type C girders with a composite bridge deck. For these design parameters, either debonding or draping was required to relieve excessive end

stresses. The actual test span was 48 feet long and the girders themselves were 49 feet long (Figure 7.19).

The debonded girders contained a total of eight debonded strands. Debonding extended a distance of eight feet from the South ends or six feet from the North ends. Debonded strands were staggered, as shown in the debonding schedule (Figure 7.2). Debonded lengths were chosen in this example so that the debonded length plus the transfer length would not extend into regions of flexural cracking.

Earlier tests had demonstrated that strand anchorages would be maintained if cracking was prevented from extending through the transfer zone of the pretensioned strands. Therefore, for these tests, the transfer zone for the debonded strands was not allowed to extend into the region of flexural cracking. Figure 7.5 illustrates that the debond length was designed so that flexural cracking would not occur in the debond/transfer zone. Stated another way, the cracking moment in the debond/transfer zone is greater than the applied moment in the debond/transfer zone, $M_{cr} > M_{applied}$.

Each of the composite girders was "precracked" in an initial static test. Repeated loads were then applied to each girder. The repeated loads were cycled between 50% of service load to 100% of service load. Periodic overloads were applied to FZ2450-3 and DZ2450-2 to simulate actual load conditions in the life of a highway girder. FZ2450-3 and DZ2450-2 were also loaded asymmetrically to produce web shear cracks in the South shear span. After 225,000 to 240,000 cycles, respectively, these beams were loaded statically until failure.

No overloads were applied to Girder DZ2450-1 except for the initial static test to precrack the beam and the final test to failure. However, this girder was subjected to nearly 700,000 load cycles.

Girders FZ2450-3 and DZ2450-1 failed in flexure. Girder DZ2450-2 failed in horizontal shear that was developed partly from damage caused by precracking the beam in web shear cracks. In all of the tests, strand end slips were relatively small. No anchorage failures occurred in the debonded strands.

In conclusion, two girders were designed with debonded strands to test their safety, reliability and strength. Their performance and behavior was compared to a companion girder with identical section properties, but containing draped strands instead of debonded strands. The debonded strands were designed so that their transfer zones would remain unaffected by flexural cracking. No failures or even significant bond slips were noted in the repeated load portion of the testing. In the final flexural tests to failure, the beams with debonded strands did not suffer anchorage failures. The beams made with the debonded strands, DZ2450-1 and DZ2450-2, had similar behavior and equal capacity compared to the beam with draped strands, FZ2450-3. Therefore, these tests demonstrate two things:

1. That girders made with debonded strands can possess the same behavior and strength when compared to beams made with draped strands. Their behavior is both safe and predictable.

2. The debonded strands were designed with the principle that their transfer zone should remain clear of regions of flexural cracking. This procedure ensures that anchorage for the debonded strands will remain intact and that the debonded strands will be able to develop their full nominal strength.

CHAPTER 8
SUMMARY OF STRUCTURAL BEHAVIOR AND DESIGN RECOMMENDATIONS

8.1 Summary

In this chapter, results from the research are reviewed and discussed. Emphasis is placed on observed behaviors that impact design and design philosophy. Test results and observations are used to develop rational models that predict structural behavior. In turn, these behavioral models are used to develop guidelines for design.

Specific bond mechanisms were identified from fundamental research performed in the 1950's.[1,5] These mechanisms proved adequate and essential for explaining the behavior observed in this research. By understanding bond mechanisms, the impact of pretensioned bond on overall structural behavior can be assessed and design recommendations can be made for reliable and safe pretensioned structures.

8.1.1 Cracking and Strand Anchorage Failure. Flexural tests were performed on a wide variety of test specimens. In all cases, cracking through a strand's transfer zone caused bond slip on pretensioned strands. Shear cracks and flexural cracks were found to be equally important. Web shear cracking caused the failure of strand anchorage in I-shaped beams (Chapter 4). Similarly, flexural cracking caused bond failure in rectangular beams when the cracks formed in the transfer zone (Chapter 4). Cracking also caused bond failure of debonded strands (Chapter 5). Flexural cracks propagating through the transfer zone of debonded strands caused those strands to slip, reducing the capacity of the beams. Conversely, when cracking did not occur in the transfer zones of pretensioned strands, the strands were able to develop and maintain their prestressing force.

Furthermore, these tests demonstrate that the failure of pretensioned anchorage can be predicted by predicting the formation of cracks. From a design standpoint, if cracking does not occur in the transfer zone of a pretensioned strand, then that strand can be expected to develop its full tension. The behavior of pretensioned anchorage can be summed up as follows:

> Cracking through the transfer zone of a pretensioned strand will cause its bond to fail locally. Continued loading will precipitate complete bond failure. Conversely, if cracks do not occur within its transfer zone, a pretensioned strand will develop its prestressing force plus any additional tensioned required by external loads .

The transfer length of a pretensioned strand becomes important given the interrelationship between the transfer zone and potential development failures. Transfer

lengths were measured on a wide variety of specimens in varieties of conditions. Results are discussed in this chapter and are used to develop a design recommendation.

8.1.2 Current Code Practice. Current ACI and AASHTO code expressions for anchorage are based on average bond stresses and do not reflect the behavior of pretensioned bond. The current code and the average bond stress values are based upon empirical evidence from earlier research. However, in their current structure, code expressions can result in the unexpected failure of pretensioned structures due to bond failure. Therefore, restructuring of current Code provisions is required to ensure safe and reliable pretensioned structures.

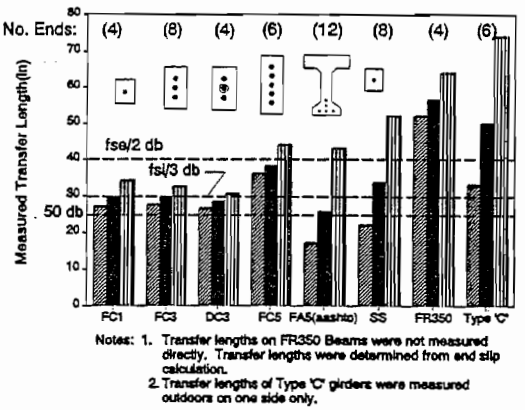

Figure 8.1 Transfer Lengths of 0.5 Inch Strand (Summary by Specimen Series)

8.2 Transfer Length

Figures 8.1 and 8.2 summarize the transfer lengths measured on test series from this research project. All of the transfer lengths represented in the two figures are for fully bonded strands. The current code requirement of 50 d_b is shown on the figures. Alternately, Shahawy's[59] recommendation of $^{fsi}/_{3}\ d_b$ is also shown. From the data on rectangular specimens, Shahawy's recommendation appears to merit consideration as a design guideline. However, for other specimens, the FR350 beams and the Type 'C' girders, $^{fsi}/_{3}\ d_b$ does not accurately predict the transfer lengths. The equation, $L_t = {}^{fse}/_{2}\ d_b$, is shown in the figure and recommended for use in design.

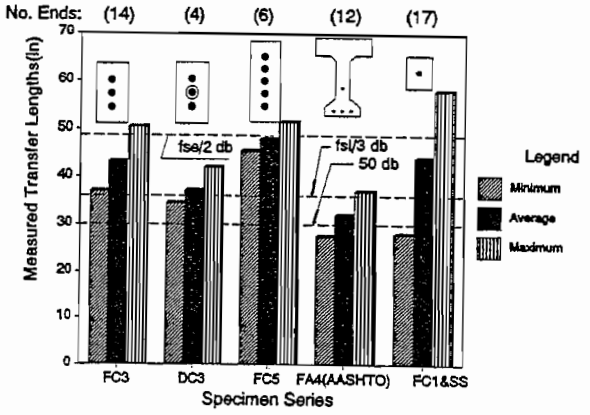

Figure 8.2 Transfer Lengths of 0.6 Inch Strand (Summary by Specimen Series)

Concurrent research is summarized in Figures 8.3 and 8.4. Transfer length tests from North Carolina State University (NCSU) were first reported in 1986[39]. Based on these results, the Federal Highway Administration (FHWA) placed restrictions on pretensioned strands. Tests performed at the Florida Department of Transportation[59] (FDOT) and at the University of Tennessee at Knoxville[51] (UTK) are also summarized in Figures 8.3 and 8.4. [Note: Figures 8.3 and 8.4 summarize results as reported. Different analysis

techniques were used (Chapter 3) that may influence the reported results. FDOT used a plateau intercept method and UTK used a bilinear intersection method. Both are subject to arbitrary interpretation.]

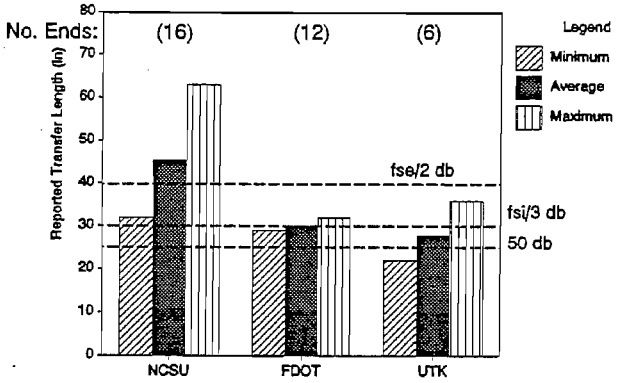

Figure 8.3 Transfer Lengths of 0.5 Inch Strands (Summary of Concurrent Research)

The FDOT and UTK tests are particularly related to this research because their data were measured on AASHTO girders. UTK measured transfer lengths on AASHTO TYPE I girders whereas FDOT measured transfer lengths on AASHTO TYPE II girders in a prestressing plant. The tests performed at FDOT are particularly important because they were performed under similar conditions as were the transfer length tests performed on the TEXAS TYPE C girders in this research project. The FDOT girders demonstrated significantly shorter transfer lengths, about 30 inches for 0.5 inch strands and about 35 inches for 0.6 inch strands.

Results from other researchers must by tempered, however, because of the analysis techniques used. Each researcher used different analysis techniques which can skew the results and prejudice the findings (Chapter 3). FDOT used a plateau intercept method and UTK used a bilinear intersection method. The analysis technique employed at NCSU are not known. In the plateau intercept method, it is very difficult to determine an exact value for transfer length because the parabolic strain curve is becoming asymptotic with the strain plateau. Both of these methods are somewhat arbitrary and should be discounted. Taken collectively, and including data from NCSU, the data represented in Figures 8.3 and 8.4 resemble the data found in tests performed at UT Austin, with wide degree of scatter between various test series.

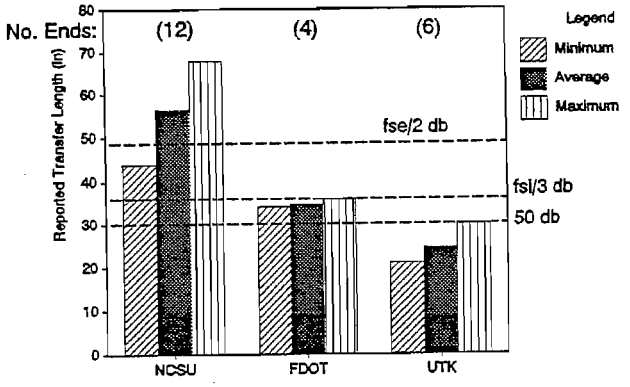

Figure 8.4 Transfer Lengths of 0.6 Inch Strands (Summary of Concurrent Research)

8.2.1 Development of Design Guidelines for Transfer Length. In review of the transfer length data collected in this and other research projects, the data is most

remarkable for its degree of scatter. The data does not converge to a single value nor does it appear to distribute evenly around any particular value. No clear trends appear from which an empirical formula can be developed.

Figures 8.5 and 8.6 present the data in histograms based upon the measured transfer lengths from this research project. The histograms are helpful in that they illustrate the distribution of measured transfer lengths by plotting the number of specimen ends versus their measured transfer lengths. The transfer lengths are grouped in ranges of three inches. For example, Figure 8.5 shows the occurrence of transfer lengths for 0.5 inch specimens. This figure also shows that the number of specimen ends with a transfer length of 30 inches $\pm$1 inch is eleven.

In Figure 8.5, each end of each Texas Type "C" beam is denoted with the letter C. Likewise, each end of each FR350 beam is denoted with the letter R. For example, at a transfer length of 54 $\pm$ 1 inches, two specimens were measured with this transfer length, both of which were measured from an FR350 beam.

Shahawy has suggested setting the transfer length equal to $f_{si}/3$ times d_b. This expression yields transfer lengths of 30 inches for 0.5 inch strand and 36 inches for 0.6 inch strands. However, Shahawy's expression predicts a shorter transfer length than many of the measured transfer lengths. When compared to the 0.5 inch data in Figure 8.5, 29 specimen ends had transfer lengths that were longer than 30 inches. Similarly, comparing the same expression to the data on 0.6 inch strands in Figure 8.6, 34 specimen ends had transfer lengths longer than 36 inches. Well over 50% of the data exceeded the transfer length given

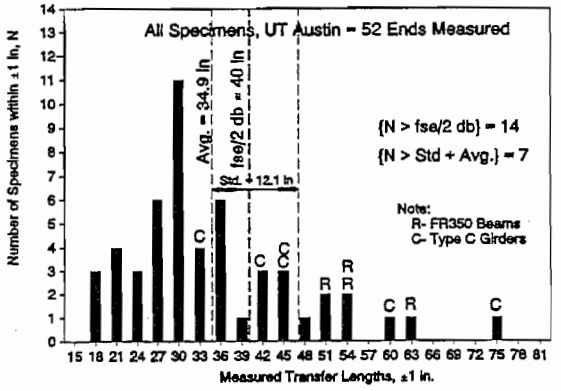

Figure 8.5 Histogram of Transfer Lengths, 0.5 Inch Strands

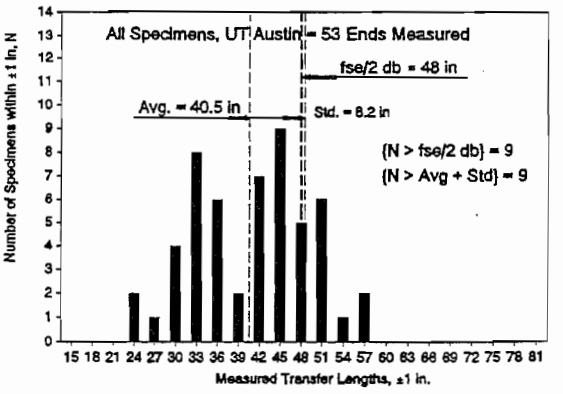

Figure 8.6 Histogram of Transfer Lengths, 0.6 Inch Strands

by Shahawy's expression. These data do not support Shahawy's recommendation.

It would seem more appropriate to select a value or an expression that bounded a greater percentage of the test results. Because transfer length is directly related to the development of strand anchorage, it must be conservatively chosen. A longer value for transfer lengths could be used confidently in a variety of applications. From the data, the following expression is suggested from the figures, and it is recommended for use in design applications:

$$L_t = \frac{f_{se}}{2} d_b$$

The values for transfer length given by this expression, and assuming an effective prestress of 160 ksi, are:

$$L_t(0.5'' \; strand) = 40'' \qquad ; \qquad L_t(0.6'' \; strand) = 48''$$

There are two advantages in using this expression. First, it relates transfer length to strand diameter and to the prestressing force, using the same variables currently used in the ACI Commentary. This allows for evolution to new strand sizes and higher strand strengths. Secondly, this expression exceeds the measured transfer length from most of the data. The value for the transfer length expression is shown on each of the histograms, Figures 8.5 and 8.6. For 0.5 inch strands, 14 specimen ends, or 27% of the data, exceed the recommended value. Special circumstances for these data points are discussed below. For 0.6 inch strands, only 9 specimen ends, or 17% of the data exceed the recommended value.

Data from the 0.5 inch strands is skewed by the data from the FR350 beams and the Texas Type C girders. Each of these data points are represented in Figure 8.5. Each end of the FR350 beams is denoted by 'R' and each end of the Type C girders are denoted by 'C'. As discussed in Chapters 3 and 4, it is suspected that longer transfer lengths resulted from lubricants contaminating strand surfaces.

Other factors are important to consider while analyzing the transfer length data from the FR350 beams and the Type C girders. Transfer lengths from the FR350 beams were not directly measured. Instead, they were calculated from the measured end slips. While end slips are directly related to transfer length, the calculations can never be precise. However, the average transfer length of the FR350 beams was 55 inches, which represents a significantly longer value than other transfer lengths measured at FSEL.

Long transfer lengths measured on the Type C girders are balanced by shorter transfer lengths measured by Shahawy on AASHTO Type II girders in a prestressing plant. Also, transfer lengths on the Type C girders were measured with the difficulty of taking transfer length readings outdoors at the prestressing plant. Also, transfer length measurements were taken on only one side of the girders. On all of the other transfer

length specimens, measurements were taken from both sides. Ambient temperature increased from 50 degrees at the time of initial measurements to about 70 degrees at the final measurement. However, there is no reason to suspect that these temperature changes could have significantly influenced measured transfer lengths.

The transfer lengths measured on the Type C girders and the transfer lengths measured by FDOT both represent measurements taken on full-sized girders in prestressing fabrication yards. While transfer lengths from the Type C girders are relatively long, transfer lengths from the FDOT tests are contained within the recommended transfer length (FDOT transfer lengths averaged 30 inches on 0.5 inch strand). Therefore, the recommended transfer lengths are given by the expression above, $L_t = {}^{fse}/_{2} * d_b$.

8.3 Development Length

8.3.1 Summary of Behavior. In the strength based philosophy of the ACI and AASHTO codes, it is imperative that a structural system achieve a well defined and predictable limit state. In the case of pretensioned prestressing strands used in flexural members, the strands must develop the tensile strength required at the nominal flexural capacity. To develop the required tension, the strand must fulfill two requirements. First, it must possess the tensile strength required to resist external loads, and second, the anchorage must be sufficient to resist the tension in the strand.

In Chapter 2, the bond mechanics in a cracked beam were discussed. Those mechanics are idealized in Figure 2.4. In the immediate vicinity of the cracks, steel stresses increase dramatically to develop the tension required to resist external moments. Increases in steel stresses must be restrained by bond stresses between concrete and steel. These high local bond stresses are developed by mechanical interlocking. As shown in Figures 2.9 and 2.10, distribution of cracking can be directly related to the value of interlocking bond stresses.

Development of mechanical interlocking bond stresses requires that the strand be restrained from twisting. As shown in the figure, twist restraint is provided by anchorage at the transfer zone. If the strand does not slip in the transfer zone, no twist can occur, and bond stresses from mechanical interlocking remain active. Conversely, bond failure may occur when cracks propagate through the transfer zone of the pretensioned strand. Tension in the strand would increase immediately adjacent to the crack, leading to a reduction in diameter of the pretensioned strand. In turn, the strand would lose its anchorage derived from the wedge action of Hoyer's Effect, small slips and twisting would occur. In this manner, cracking in the transfer zone may cause general bond slip and anchorage failure of the pretensioned strand.

Figures 4.7 and 4.8 show the results from development length tests on AASHTO-type beams, 0.5 inch diameter strand and 0.6 inch diameter strands, respectively. The behavior of the AASHTO-type beams was controlled by web shear cracking. The strands slipped

when web shear cracks formed, and eventually led to bond failures. The influence of web shear cracking on anchorage failure is explained in greater detail in Section 4.6.2. These tests indicated that the required development length for 0.5 inch strands was 72 inches. For 0.6 inch strands, the required development length was 84 inches.

Beams with rectangular cross sections were tested to study strand development without influence of web shear cracking. For 0.6 inch strands, the rectangular beams required shorter development lengths than the I-shaped beams (Figure 4.28). On the other hand, rectangular specimens with 0.5 inch strands demonstrated longer development lengths than the I-shaped beams. Ultimately, the tests demonstrated the behavioral relationship between transfer length and development length.

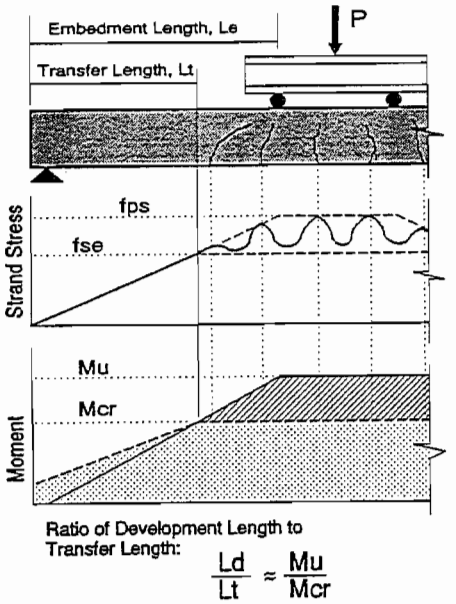

Figure 8.7 Interaction of Transfer Length and Development Length

The interaction between transfer length and development length is illustrated in Figure 8.7. The development length of fully bonded strands is approximately proportional to the transfer length for the strands. Therefore, to prevent bond failure the cracking moment must exceed the applied moment throughout the transfer zone. The result of this condition is that the L_d, the development length becomes a function of the transfer length.

The relationship between transfer length and development length explains the behavior of the rectangular beam specimens containing 0.5 inch strands. The transfer lengths derived from end slips were found to be approximately 55 inches long. Using 55 inches for the transfer length and a ratio of M_u to M_{cr} of 1639 k-in to 940 k-in, the required development length for the specimens FR350-1 and FR350-2 is given by:

$$L_d = \frac{M_u}{M_{cr}} L_t = \frac{1630\ k''}{940\ k''} \times 55'' = 95.4''$$

which is equal to the measured development length of 96 inches (Figure 4.29).

Similarly, if the same calculation is performed for the rectangular beams containing 0.6 inch strands, assuming the transfer length is 30 inches, then:

$$L_d = \frac{M_u}{M_{cr}} L_t = \frac{2200\ k''}{1350\ k''} \times 30'' = 48.9''$$

which is consistent with the development length tests conducted on specimens FR360-1 and FR360-2.

This relationship can become a powerful design tool to predict the development of pretensioned strands, however, its use is limited to simply supported beams where moment distribution is approximately linear (point loads) and in cases where web shear cracking will not control. However, these limitations may not be too severe given that moment distributions are approximately linear in most simple spans, especially near the support of a beam. A requirement could by written so that the cracking moment, M_{cr} could not be exceeded within the transfer zone:

$$M_{cr} > L_t V_u$$

This equation has the advantage of removing the confusion over the location of the *critical section*. Using this expression defines the critical section as the point nearest the support where flexural cracking will occur. Consider a simply supported beam. Near the end regions, shear is approximately constant and the critical section, or the distance from the support where flexural cracking will occur is given by the relation: $^{Mcr}/_{Vu}$. In order for the strand anchorage to be developed, this distance must be greater than the transfer length, L_t. Rearranging terms gives the equation in the form above.

8.3.2 Development of Design Guidelines Fully Bonded Strands. To ensure development of pretensioned strand, cracking must be prevented in the transfer zone of the strands. Two types of cracking are prominent in causing pretensioned anchorage failure, web shear cracking and flexural cracking. This section is divided into two parts, the first to develop design guidelines if web shear cracking will not occur; and the second to develop design guidelines given the possibility that web shear cracking will occur.

8.3.2.1 Development Length Requirements for $V_{cw} > V_u$. To begin the discussion, the design cases where V_{cw} would exceed V_u are numerous. This might be a rectangular beam, or an I-shaped beam with a moderately long span. Recommended design guidelines for this case are described in the section above where development length is related to M_{cr}, the applied shear, V_u and the transfer length, L_t. The following expression would serve to prevent flexural cracking in the transfer zone of fully bonded pretensioned strands and is recommended for design:

$$M_{cr} > L_t V_u$$

Using this expression, strand development would be inadequate if the applied shear were large enough to cause flexural cracks to form in the transfer zone. Some safety is built

into the expression in that the expression assumes that the transfer zone begins at the support. However, in real beams, the end of the pretensioned beam may extend beyond the support for some distance.

8.3.2.2 Development Length Requirements for $V_{cw} < V_u$. This case represents most designs cases where development of the strands should be a real concern. From the testing program, many bond failures occurred as a result of web shear cracking. Failures were both sudden and violent, providing very little warning before collapse.

To prevent bond failures due to web cracking, one alternative would be to require that V_{cw} be greater than V_u. If this were a requirement, anchorage failures due to web shear cracking would be eliminated. Interestingly, this requirement suggests the reintroduction of end blocks. While end blocks may be considered an option by the engineer, other options are available. Another suggestion is to place additional shear reinforcement to control cracking in the webs of pretensioned beams. In that case, horizontal shear reinforcement is required in addition to vertical reinforcement to resist the applied shear. Also, shear reinforcement would be required to extend through the transfer zones of pretensioned strands.

In several cases, the occurrence of web shear cracking did not immediately form failure mechanisms. Failures occurred after increased loading. In these cases, the anchorage of pretensioned strands were generally protected by the widening of the bottom flange or by mild reinforcement placed in the web. The bottom flanges and mild shear reinforcement provided a limited amount of protection to the pretensioned strand that allowed the pretensioned strand to develop anchorage to resist load. However, under increased loading crack widths grew and pretensioned bond failure resulted.

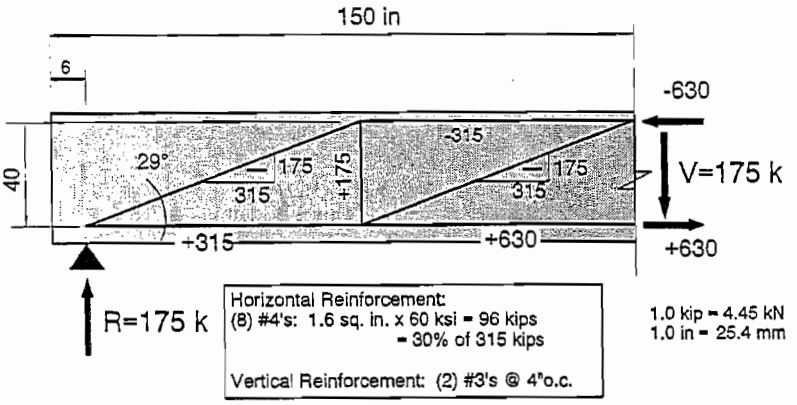

Figure 8.7a Truss Model of Shear Load at Flexural Ultimate Full-Sized Girder Tests

In the full sized Type C girders, mild shear reinforcement was placed both longitudinally and vertically. The mild steel was designed to carry large percentages of the ultimate shear load. In Girder DZ2450-1, horizontal shear reinforcement was designed to resist 15% of V_u (Figure 7.6). In Girder DZ2450-2, horizontal shear was designed to carry 30% of V_u (Figure 7.7). Shear loads for design of the reinforcement were obtained by considering a truss mechanism at an angle of 30°. Figure 8.7a compares the ultimate shear forces given by a truss model with the capacity of shear steel provided.

In both girders, DZ2450-1 and 2, the shear strength of the vertical shear reinforcement, V_s exceeded the ultimate shear load, V_u. During repeated loading, web shear crack widths did not increase. Additionally, only small increases in crack width were measured at ultimate loading. Web shear cracks were present at failure in each specimen, however, the shear reinforcement controlled crack widths and prevented the cracks from propagating into the bottom flange. In addition, all of the strands were placed within the bottom or top flanges of the beam. No strands were located in the web where their anchorages would be susceptible to web shear cracking. In this manner, web shear cracking occurred without detrimental effects on strand anchorage. Therefore, the following design recommendations are made to ensure strand development in the presence of web shear cracks ($V_{cw} < V_u$):

1. Strands should not be located in the webs of pretensioned girders, where practical.

2. Longitudinal and vertical mild shear reinforcement should be provided to ensure shear capacity. The truss analogy is recommended for design of the shear reinforcement, considering an angle of 30° to the horizontal. The shear reinforcement should extend through the entire transfer zone plus a length equal to the depth of the cross section. In these tests, horizontal shear reinforcement equal to 30% of the horizontal shear force was adequate to develop bottom chord tension.

3. The development length provision from the rectangular cross sections must be satisfied:

$$M_{cr} > L_t V_u$$

8.4 Beams with Debonded Strands

8.4.1 Summary of Behavior. Extensive testing was performed on beams with debonded strands. Static tests on I-shaped beams, discussed in Chapter 5, demonstrated that flexural cracking in the transfer zone of debonded strands cause bond failure of those strands. Similarly, web shear cracking also precipitated bond failure. In Chapter 5, an analytical rationale was developed to predict bond failure in beams with debonded strands. Again, bond failure is predicted by the formation of cracks in the transfer zone of pretensioned strands.

Repeated load tests were performed on companion specimens to the statically loaded beams. These tests are discussed in Chapter 6. Repeated loads were found to have no significant effects on strand development or the behavior of beams with debonded strands. Overall, repeated loads did not affect the behavior of pretensioned beams, although some small variations in behavior were observed.

Full-sized composite bridge girders were built and tested in the final phase of the project. Of the three beams, two were made with debonded strands while the third was constructed with draped strands. These beams and the tests are described in Chapter 7.

These specimens were also subjected to repeated loads. Debonded strand patterns were designed so that the debond/transfer zones would not be affected by flexural cracking (Figure 7.5). This simply means that debonding was confined to the end regions of the beam. The beams were designed so that they would crack from the influence of web shear, but web shear cracks were controlled with horizontal and vertical shear reinforcement to prevent crack propagation into the bottom flanges of the girders. The behavior of girders with debonded strands matched closely the behavior of the girder with draped strands and confirmed that rational design guidelines could be developed for the use of debonded strands. These design recommendations are presented in the next section.

8.4.2 Development of Design Guidelines. Just as in the case of fully bonded strands, debonded strands failed in bond when cracks propagated through or very near their transfer zones. Therefore, to prevent bond failure, debonded strand patterns should be designed so that the debond/transfer zones would not be affected by flexural cracking. Figure 7.5 shows that the debond/transfer zone (L_b+L_t = 121 inches) is contained within regions of the beam where the cracking moment, M_{cr} exceeds the applied moment.

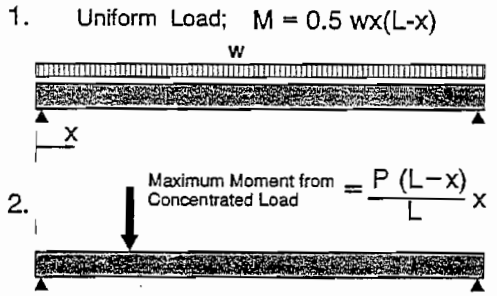

Figure 8.8 Loadings for Parabolic Moment Distributions

In general, the design recommendation is to design the beam so that cracking should not occur in the transfer zone of any pretensioned strand, either debonded or fully bonded. Application of these ideas into design guidelines is complicated by potential variations in the distribution of applied moment from one design case to another. If one considers a uniform distribution of applied load over the length of a simply supported beam, the resulting moment distribution is parabolic. Likewise, if one considers a point load that is allowed to move freely over the length of a simply supported beam, the plot of the maximum moment generated by that point load would also be parabolic. These load cases are depicted in Figure 8.8. From an assumed shape of

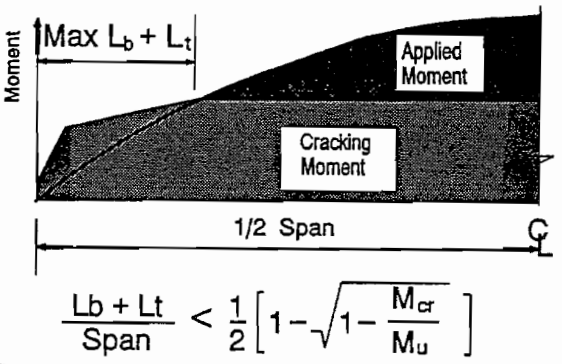

Figure 8.9 Maximum Debond Length (Applied Moment [Uniform Load] vs. Cracking Moment)

parabolic moment distribution over the length of a simply supported beam, an expression for the furthest extent of debonding in pretensioned girders can be derived. This is shown in Figure 8.9.

Figure 8.9 plots "Applied Moment" and "Cracking Moment" from the end of the beam to the beam's centerline. At ends of the beam, cracking moment exceed applied moment. The cracking moment increases rapidly as the fully bonded strands transfer their prestress force into the concrete. A second, more gradual transfer zone depicts the transfer of prestressing force from debonded strands. The debond/transfer zone is the distance from the end of the beam to the point where all of the debonded strands have transferred their effective prestress force into the concrete. This point is given by the debonded length plus one transfer length, $L_b + L_t$.

The parabolic shape of the moment is described mathematically, as a function of the beam length, x, by the relation:

$$M(x) = 4M_u \left(\frac{x(L-x)}{L^2} \right)$$

Combining this equation with the requirement that the cracking moment must be greater than the applied moment at $L_b + L_t$ yields an expression for the limit of the debond/transfer zone:

$$\frac{L_b + L_t}{Span} < \frac{1}{2} \left[1 - \sqrt{1 - \frac{M_{cr}}{M_u}} \right]$$

This expression would control the overall length of debonded strands in simply supported pretensioned girders. For the general case, where girders may not be simply supported and/or where pretensioned members become a structural component of a larger structural system, the designer may be required to check several different loading combinations or geometric arrangements and provide a design where cracking does not occur in the transfer zones of pretensioned strands.

Recommendations for design of beams with debonded strands can be summarized as follows:

1. For simply supported beams:

$$\frac{L_b + L_t}{Span} < \frac{1}{2} \left[1 - \sqrt{1 - \frac{M_{cr}}{M_u}} \right]$$

This expression would apply to simply supported highway bridge girders or multi-span continuous bridge girders.

2. For generalized geometry and loading conditions, bond failure can be prevented if cracking is not allowed to propagate through the transfer zone of pretensioned strands.

3. If $V_u > V_{cw}$, then horizontal and vertical shear reinforcement should be provided to prevent propagation of crack into the transfer zone of pretensioned strands (Section 8.3.3.2).

8.4.3 Discussion of Design Procedures Inclusion of Top Strands. In developing the designs for the test specimens, several comparisons were made with debonding patterns recommended by computer output from PRESTRESS 14, a prestressed concrete design and analysis program developed by and for the Bridge Division of the Texas Department of Transportation (TxDOT). When some of the arbitrary constraints were disabled, such as maximum debonded length and maximum debonded percentages, the computer program suggested designs for debonded strands with extraordinarily high percentages of debonded strands and with debonded lengths stretching far into the mid-regions of the pretensioned girders.

In subsequent hand calculations, the number and length of debonded strands was reduced by locating a small percentage of prestressing strands in the top flanges of pretensioned beams. This simple procedure provided debonded patterns with far less requirements for number of debonded strands and also dramatically reduced the required length of debonding.

The effects of two top strands are illustrated in Figure 8.10. In this figure, the eccentricity of the prestress force is reduced as the strands are debonded. This effect works concurrently with a reduction in prestress force to reduce end stresses to within allowable limits. Consequently, the overall debonding requirements are reduced when top strands are added to the strand pattern. If top strands are not included in the strand pattern, eccentricity does not change appreciably and a greater percentage of strands must be debonded.

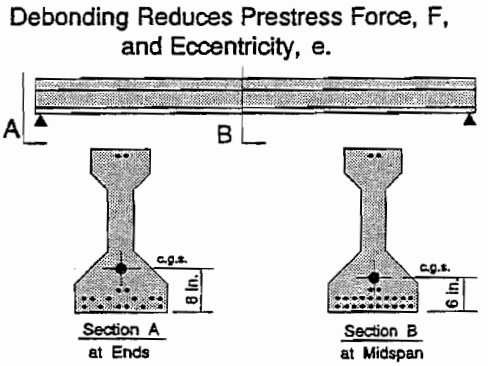

Figure 8.10 Change in Eccentricity From Two Top Strands Used With Debonded Strands

Two top strands improve the design of pretensioned girders by:

1. Significantly reducing the number of debonded strands required to control end stresses. In fact, in many standard span lengths, neither debonding nor draping was required.

2. Significantly reducing the length of debonding. Reducing the length of debonding has a positive effect on overall beam performance in addition to ensuring that debonded strands will remain anchored in the end regions and effective in resisting externally applied load.

3. Eliminates strands in the web and allows placement of mild reinforcement in the web. This provides the required margin of safety if web shear cracks develop in the transfer zone of pretensioned strands.

TABLE 8.1

Cross Section Properties
Type C Girder with Composite Slab

	Type C Girder	w/ Composite Deck Slab
Area (in^2)	495	970
y_b (in)	17.09	30.33
I (in^4)	82,620	262,460
S_b (in^3)	4833	8654
S_t (in^3)	3605	-
w (kips per foot)	0.5155	1.135
$E_{slab} = 0.8\ E_{beam}$		

8.4.3.1 Design Example No. 1A; 60' Span with Two Top Strands. This design is based upon a 60'-0" span, with girders spaced 6.8 feet apart. Half inch diameter strands were spaced at 2 inch centers. Cross section properties are given in Table 8.1.

The number of strands required is given by satisfying the allowable stress requirement for the bottom fiber tension at midspan. The prestress force required is given by the equation:

$$f_b = -F_{se}\left[\frac{1}{A} + \frac{e}{S_b}\right] + \frac{M_{DL}}{S_b} + \frac{M_{LL}}{S'_b} \le 6\sqrt{f'_c}$$

where F_{se} is the effective prestress force after losses, A is the area of a Type C girder, S_b is the bottom fiber section modulus for a Type C girder, S'_b is the bottom fiber section modulus for the composite girder and f'_c is the concrete cylinder strength.

Dead load moment, M_{DL} and live load moment, M_{LL} are given by the following expressions:

$$M_{DL} = \frac{1.135 \times 60^2}{8} = 510.3k\text{-}ft$$

and

$$M_{LL} = 806.5k\text{-}ft \times 1.28 \times \frac{6.8}{11} = 638.2k\text{-}ft$$

The live load moment of 806.5 k-ft is taken from Appendix A of the AASHTO specifications, $^{6.8}/_{11}$ is the distribution factor based on girder spacing and 1.28 is the impact load factor.

Solving the equation above, assuming that eccentricity, e = 11.0 inches, f'_c = 6000 psi and f_{se} is 160 ksi (24.48 kips per 0.5 inch diameter strand), the effective prestress force required for this design is 392.6 kips. Dividing the required prestress force by the force per strand gives the number of strands required:

$$N = \frac{392.6\ k}{24.48\ k/strand} = 16.04\ strands \rightarrow use\ 18\ strands$$

The strand pattern and the midspan stresses are given in Figure 8.11.

Next the allowable stresses at transfer must be checked. For this design, checks made at the ends of the beam are sufficient. Just after release of the tendons, the effective prestress force is assumed to be 180 ksi or 27.54 kips per strand. The effective prestress force is represented by F_{si}. The stresses at the top of the cross section are given by:

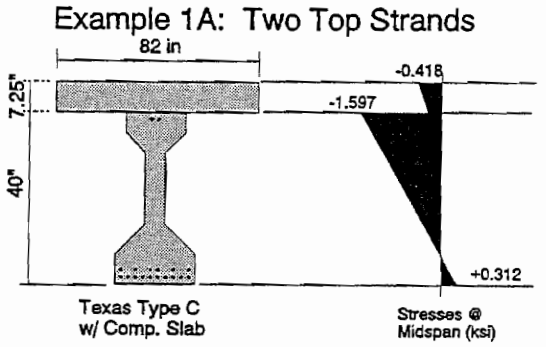

Figure 8.11 Service Load Stresses at Midspan, 60'-0 Span

$$f_t = -F_{si}\left[\frac{1}{A} - \frac{e}{S_t}\right] = +0.431\ ksi \le 0.503\ ksi = 7.5\sqrt{f'_{ci}}$$

The allowable tension is given by AASHTO as $7.5\sqrt{f'_{ci}}$. Concrete strength at release is assumed to be 4500 psi. The stresses at the bottom of the cross section are given by:

$$f_b = -F_{si}\left[\frac{1}{A} + \frac{e}{S_b}\right] = -2.070\ ksi \ge -2.700\ ksi = 0.6\ f'_{ci}$$

The top and bottom stresses at the ends of the pretensioned beam are given in Figure 8.12. Both the top stress and the bottom stress at the ends of the pretensioned girder are within the allowable stresses. Therefore, no debonding is required for this specimen.

8.4.3.2 Design Example 1B: 60'-0" Span with No Top Strands. In this design example, all of the parameters are held constant from the previous example. The span remains 60 foot, the girder is a Texas Type C with girders spaced at 6.8 feet. Cross

sectional properties are assumed to be identical. The only difference is that this girder is designed without any top strands.

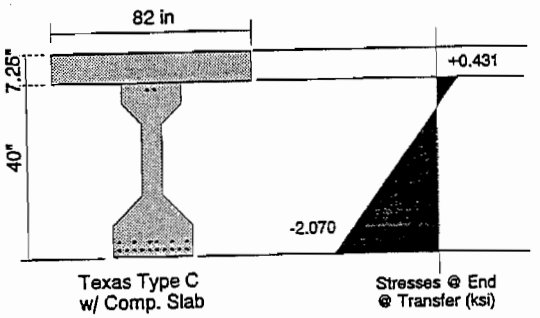

Figure 8.12 Concrete Stresses at Release at End of Girder

The number of strands is determined by satisfying the allowable stress requirement at the bottom fiber, midspan of the girder. Dead load moment and live load moments are the same. In this case, the number of strands required is 16 and the stresses at midspan are given in Figure 8.13. As can be seen, this strand pattern without top strands also satisfies the stress requirements at midspan. However, concrete stresses at the ends of the pretensioned girder are shown in Figure 8.14. The top stress at the end of the girder is +0.862 ksi which exceeds the allowable stress of +0.503 ksi. In this case, either debonding or draping is required.

The number of debonded strands required for this design is given by:

$$N_b = \left(1 - \frac{0.503}{0.862}\right)16 = 6.66 \rightarrow Use\ N_b = 8$$

This design case requires that one half of the strands, or eight out of sixteen strands, must be debonded. The strands must remain debonded until the flexural moment from the self weight of the beam, M_g as a function of x, is large enough to overcome some of the pretensioned stresses at release. This is expressed in equation form:

$$f_t = -F_{si}\left[\frac{1}{A} - \frac{e}{S_t}\right] - \frac{M_g(x)}{S_t} \leq 0.503 ksi$$

Solution of this equation yields the required debonded length, L_b = 8.06 feet, or nearly 100 inches.

Comparison of these two examples clearly demonstrate the advantages of placing a small percentage of the pretensioned force in the top of the cross section. This is especially true considering the weakening effects that reduced prestress can have on resistance to shear cracking and to flexural cracking (Sections 5.4.3 and 5.4.4). In the case of Example 1A where two strands were placed in the top of the cross section, no debonding was required. Yet when these two top strands were omitted, 50% of the strands required debonding and the debonded length extended 8.06 feet into the span, or nearly 14% of the span length.

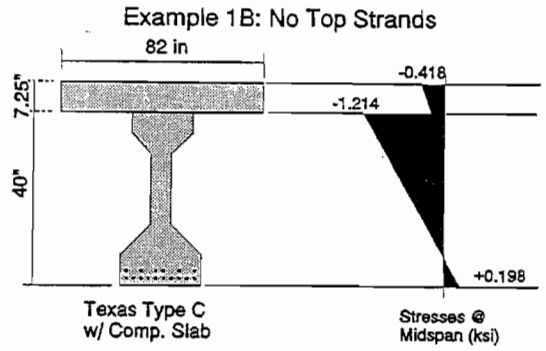

Figure 8.13 Service Load Stresses at Midspan, 60'-0 Span

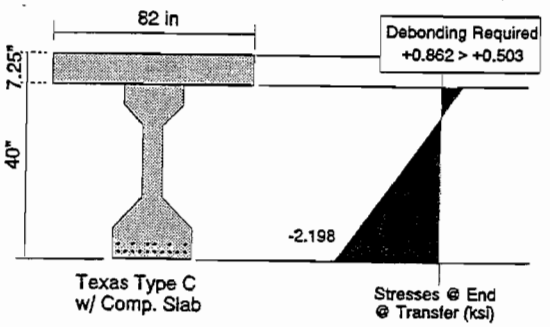

Figure 8.14 Concrete Stresses at Release at End of Girder

8.4.3.3 Example 2A; 80'-0" Span with Two Top Strands. A similar design example was carried out for a span of 80 feet using the same cross section as used before. The cross section properties are given in Table 8.1. For this example, however, the concrete strengths were assumed to be 8000 psi at 28 days and 6000 psi at release. Table 8.2 gives the number of debonded strands required and the debonded lengths required.

In comparing the two designs for 80' spans, the design where two top strands were included require only eight debonded strands whereas the girder without top strands required that 18 out of 28 strands be debonded. Likewise, if two top strands are included in the strand pattern, the debonded length is significantly reduced, from 13.47 feet to 5.33 feet.

TABLE 8.2

Comparison of Debonding Requirements; With and Without Top Strands

Design Case	Number of Strands, N	Number of Debonded Strands, N_b	Debonded Length (ft)
60' Span w/o Top Strands	16	8	8.06
60' Span with Two Top Strands	18	-	-
80' Span w/o Top Strands	28	18	13.47
80' Span with Two Top Strands	30	8	5.33

1. Concrete strength @ 28 days, f'_c = 6000 psi for 60' Spans; f'_c = 8000 psi for 80' Spans. Release strengths are 75% of 28 day strengths.

In summary, the purpose of debonding strands is to allow for straight strand patterns and to eliminate draping. By incorporating two top strands into the design of pretensioned girders, the number and the length of debonded strands can be significantly reduced. These actions strengthen the beam's resistance to web shear cracking and to flexural cracking when compared to debonding as an alternative. Also, by including two top strands in the design, a greater percentage of designs will not require

debonding nor draping. For those beams that do require debonding, their performance will be significantly improved.

8.4.4 Development of Design Criteria for Beams with Debonded Strands. Design criteria should have one goal: to prevent cracking in the *debond/transfer zone* of **all** pretensioned strands. In beams with debonded strands, spans will normally be long enough where flexural cracking should control the design in a majority of cases. In those cases, debonding should be limited to the end regions of simply supported beams where flexural cracking will not occur. The expression given above and repeated here defines a limit for debonding:

$$\frac{L_b+L_t}{Span} \leq \frac{1}{2}\left[1-\sqrt{1-\frac{M_{cr}}{M_u}}\right]$$

M_{cr} and M_u are already calculated to fulfill other requirements for AASHTO and ACI code provisions.

Generally, for highway bridge girders, the ratio of M_{cr} to M_u falls between 0.55 and 0.6. Substituting this ratio into the equation above yields a general rule of thumb for the length of debonding:

$$\mathbf{L_b + L_t < \approx 0.16 \cdot Span}$$

This expression provides a rough guideline for the maximum debonded length of strands in simply supported beams, representing the majority of pretensioned girder bridges.

One important behavioral characteristic makes this rule practical. In some cases, flexural cracking did extend into the transfer zone of debonded strands, the ultimate failure mode was still flexural failure. These cases were, in general, tests where flexural cracking was present only at the extreme region of the transfer zone. In these cases, some slippage of debonded strands did occur. However, small losses in tension in the debonded strands, if they represented only a small percentage of the total number of strands, was supported by increases in tension. Tension was developed in fully bonded strands that were unaffected by the cracking. In these cases, bond failures did not result in violent and sudden failures. Therefore, it is acceptable to allow the debonded lengths to extend to the point where flexural cracking will occur.

Given the presence of debonding, web shear cracking also requires checking. Similar rules from the fully bonded design case should be applied to beams with debonded strands.

8.5 Design Recommendations for Development of Pretensioned Strands in Simply Supported Girders:

For beams with **all strands fully bonded to the ends of the member**, the following recommendations should be followed:

1. $M_{cr} > L_t V_u$.

2. If $V_u > V_{cw}$, then:
   Vertical and **longitudinal** mild steel shear reinforcement should be provided so that web shear cracks are prevented from disturbing the transfer zone of pretensioned strands.

3. Transfer length shall be taken as:
$$L_t = {}^{f_{se}}/_{2} * d_b$$

For beams where **all strands are *not* fully bonded to the ends of the member (debonded strands)**, the following requirements should be met:

1.
$$\frac{L_b + L_t}{Span} \leq \frac{1}{2}\left[1 - \sqrt{1 - \frac{M_{cr}}{M_u}}\right]$$

Note: For I-shaped composite girders, this requirement suggests that:
$$L_b + L_t <= 0.16 \cdot Span$$

2. If $V_u > V_{cw}$, then shear reinforcement should be provided as described in Section 8.3.2.2 and recommendation #2 above.

3. Debond terminations should be staggered. Termination points should be evenly distributed throughout the debond/transfer zone. Debonding should be terminated as gravity moments reduce stresses from pretensioning to within the allowable stresses.

Additionally, to these requirements should be added the strong recommendations that:

4. No more than 33% of the strands should be debonded.

5. At least 6% of the total prestressing force should be included in the top flange of the pretensioned beam.e concrete strengths were assumed to be 8000 psi at 28 days and 6000 psi at release. Table 8.2 gives the number of debonded strands required and the debonded lengths required.

CHAPTER 9
CONCLUSIONS

9.1 Recommendation for 0.6 inch Diameter Strands

The 0.6 inch diameter strands are recommended for use in pretensioned members, without restriction, and subject to the same design provisions of other strand sizes. Flexural behavior of concrete beams pretensioned with 0.6 inch diameter strands closely resembled the behavior of beams containing 0.5 inch diameter strands. The measured transfer lengths and the concrete strain profiles on specimens containing 0.6 inch strands were similar to transfer lengths and strain profiles of specimens containing 0.5 inch strands. Transfer length tests and development tests demonstrated the ability of the 0.6 inch strand to anchor its pretensioned force in the concrete without significant changes in design or fabrication. Furthermore, 0.6 inch strands can be used on 2.0 inch spacings.

9.2 General Conclusion from Development Length Testing

These tests have demonstrated that anchorage failure of pretensioned strands is prevented if cracking does not occur in the transfer zone of pretensioned strands. Therefore, to prevent anchorage failures, beams should be designed so that no concrete cracks will propagate through the transfer zone of a pretensioned strand. This observation is comprehensive for all sizes of pretensioned strand, for all pretensioned applications, and for both fully bonded strands and debonded strands.

9.3 Recommended Design Guidelines

Design recommendations are given in Section 8.5.

9.4 General Conclusions for Transfer Length

1. The design recommendation for transfer length is $f_{se}/2*d_b$, which is approximately 40 inches for 0.5 inch strands. The average measured transfer length for 0.5 inch fully bonded strands was 34.9 inches with a standard deviation of 12.1 inches.

2. The design recommendation is approximately 48 inches for 0.6 inch strands. The average measured transfer length for 0.6 inch strands was 39.0 inches with a standard deviation of 8.2 inches.

3. The data demonstrated characteristic scatter. Measured transfer lengths were considerably longer in specimens where lubricants contaminated strand surfaces.

4. Larger AASHTO-type specimens demonstrated significantly shorter transfer lengths than the smaller "transfer length prisms." This is significant because much of the past and concurrent research was conducted on small rectangular prisms.

5. Higher concrete strengths at release resulted in shorter transfer lengths. However, from these data, it is not possible to develop any quantitative assessment of the relationship between concrete strength and transfer length.

6. Transverse, or confining reinforcement had little or no effect on transfer length in these tests. However, transverse reinforcement must still be required in order to ensure safety for those specimens that do crack upon release.

7. In specimens where 0.6 inch strands were placed on 2 inch spacing, no splitting cracks were observed nor was transfer length adversely affected. The 2.25 inch spacing of 0.6 inch strands had no effect on transfer length.

9.5 General Conclusions for Development Length (Fully Bonded Beams)

1. Current code provisions (AASHTO 9-32) do not reflect actual beam behavior. In many design cases, the pretensioned strand can be developed in shorter distances than required by the code. On the other hand, many designs using current requirements may be unsafe.

2. Sudden and violent bond failures occurred when web shear cracking propagated through the web of I-shaped beams and into the bottom flanges where pretensioned strands were anchored. Web shear cracking was followed by strand slips and subsequent shear/bond failures. These failures were sudden and quite explosive. For this reason, bond failures initiated by web shear cracking should be prevented by providing both horizontal and vertical shear reinforcement.

3. Flexural cracking and web cracking influence the development length; thus the loading pattern and cross sectional shape influence the required development length for a given beam. The design recommendation in Section 8.5 reflects these considerations.

9.6 Behavior of Beams with Debonded Strands; Static Tests

1. The formation of flexural cracking in the transfer zone of debonded strands caused slip of the debonded strands and bond failure.

2. Bond did not fail in beams that did not crack in the debond/transfer zone.

3. Pretensioned strands displayed the capacity to develop additional bond stresses even after initial strand slips had occurred. In many cases, the bond stresses developed

after initial strand slips were sufficient to develop strand anchorage and preserve the flexural resistance of the beam.

4. Web shear cracking in the transfer zone of debonded strands caused strand slips and bond failure. Web shear cracking resulted in sudden and violent collapse of the pretensioned member because all of the strands were affected. Unlike cases of flexural cracking, the beam did not demonstrate additional bond capacity after shear cracks formed in the anchorage zones.

5. All debonding should be staggered. Staggering the debond terminations allows for greater precompression in the debond/transfer zones, preventing adverse behavior due to reduced shear capacity or reduced cracking moment. Staggered debond lengths should be determined by the minimum debonding required.

6. The occurrence of strand slips do not constitute bond failures by themselves; instead, bond failures are accompanied by a reduction in capacity and/or a reduction in ductility.

7. Bond failures were accurately predicted by the formation of cracking in the debond/transfer zone of debonded strands. Bond failures can be accurately predicted by developing rational predictions of cracking in pretensioned girders.

9.7 Conclusions from Repeated Load Tests on Beams with Debonded Strands

1. Overall structural behavior and beam performance were unaffected by repeated loading.

2. Some bond deterioration was caused by repeated loadings at service load. Bond deterioration was evidenced by small increases in strand end slips.

3. Strand slips, if present, stabilized over time for all repeated load tests.

4. Strands that experienced significant slips were able to develop anchorage stresses to resist large intermediate static overloads.

5. Overall beam performance and behavior of the repeated load tests matched very closely the beam behaviors and failure modes of companion tests in the static test series.

9.8 Conclusions from Full-Sized Girder Tests

1. Girder tests demonstrated that the behavioral principles predicting cracking and subsequent bond failure can be used to design full-sized bridge girders. From these tests, design guidelines were developed for full sized bridge girders.

2. Strand slips occurred only when cracks propagated across the transfer zone of a pretensioned strand.

3. The behavior of girders with debonded strands was similar to that of the companion girder containing draped strands as discussed in Section 7.5.

APPENDIX A
STRAIN PROFILES AND TRANSFER LENGTH MEASUREMENTS

This appendix contains the strain profiles of each transfer length specimen. Also shown for each specimen is its measured transfer length, using the method of analysis dscribed in the text.

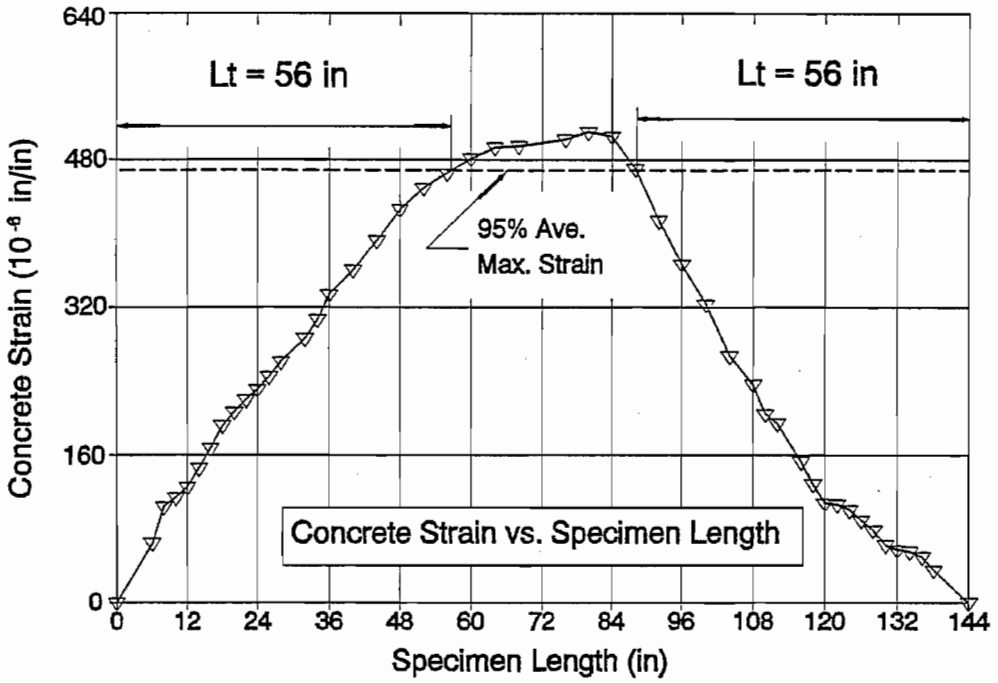

Figure A1. SS150 - 1 , Transfer Length

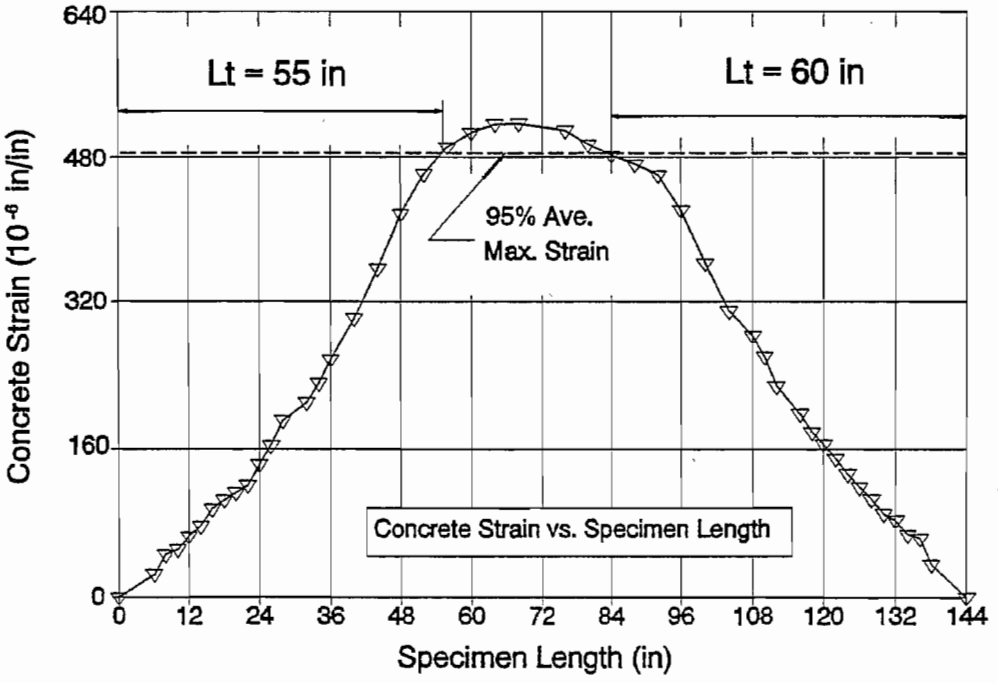

Figure A2. SS150 - 2 , Transfer Length

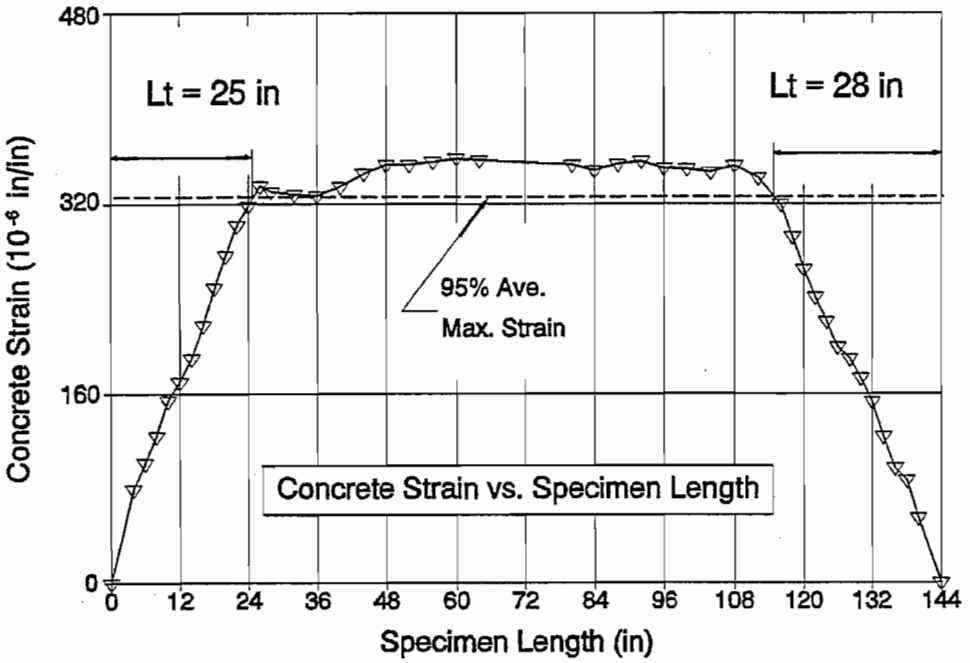

Figure A3. SS150 - 3 Transfer Length

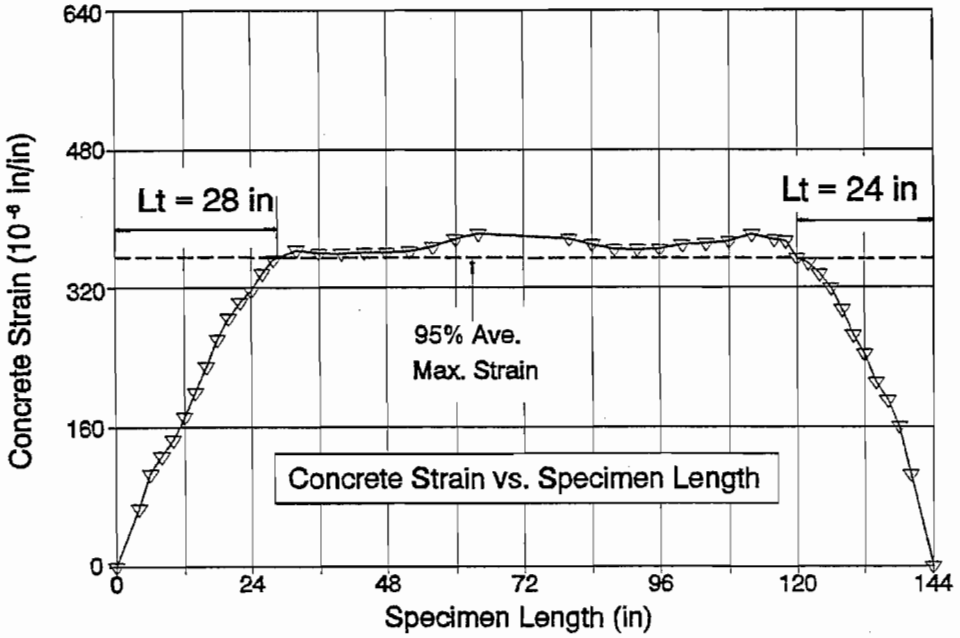

Figure A4. SS150 - 4 , Transfer Length

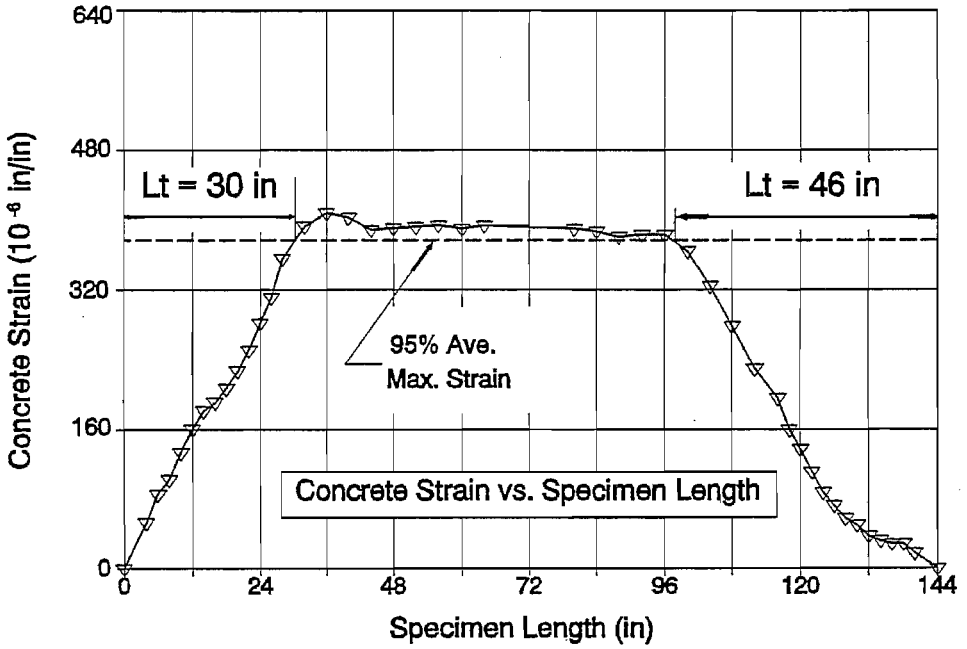

Figure A5. SS150 - 5 , Transfer Length

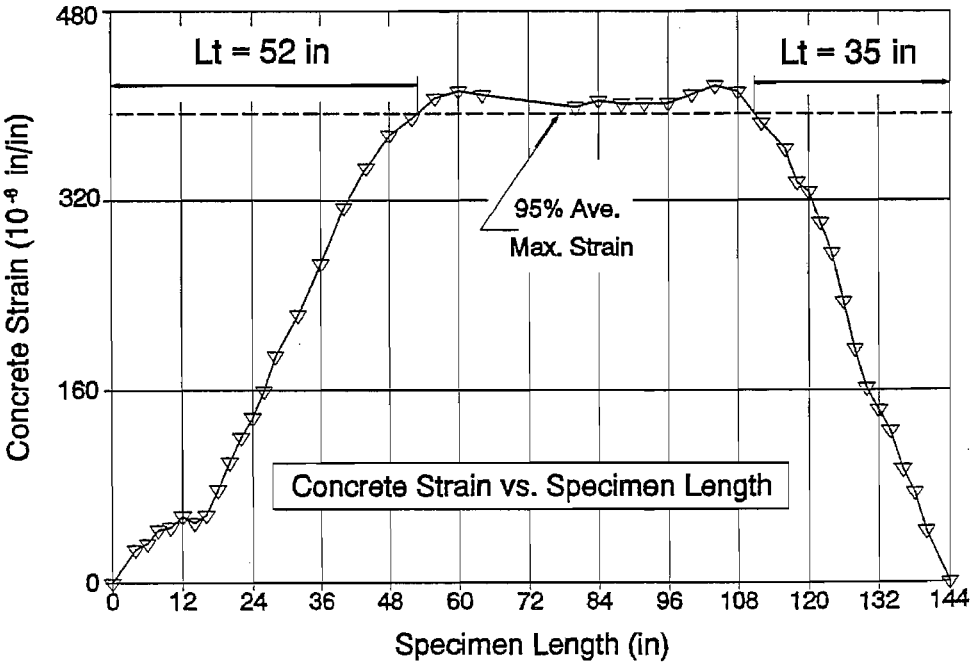

Figure A6. SS150 - 6 , Transfer Length

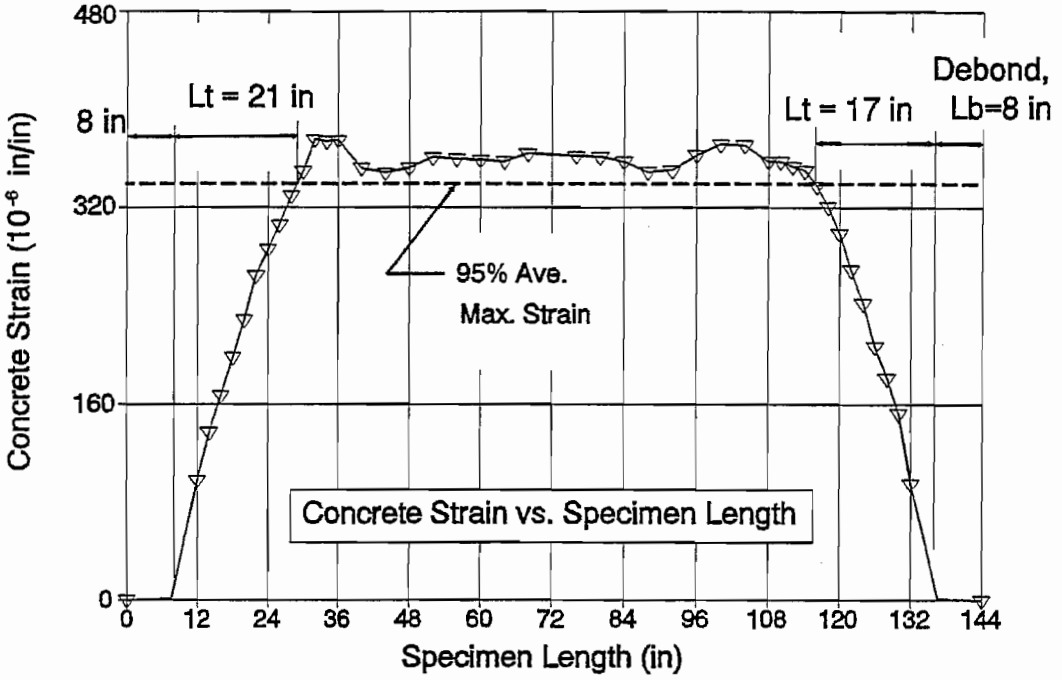

Figure A7. DC150 - 1 , Transfer Length

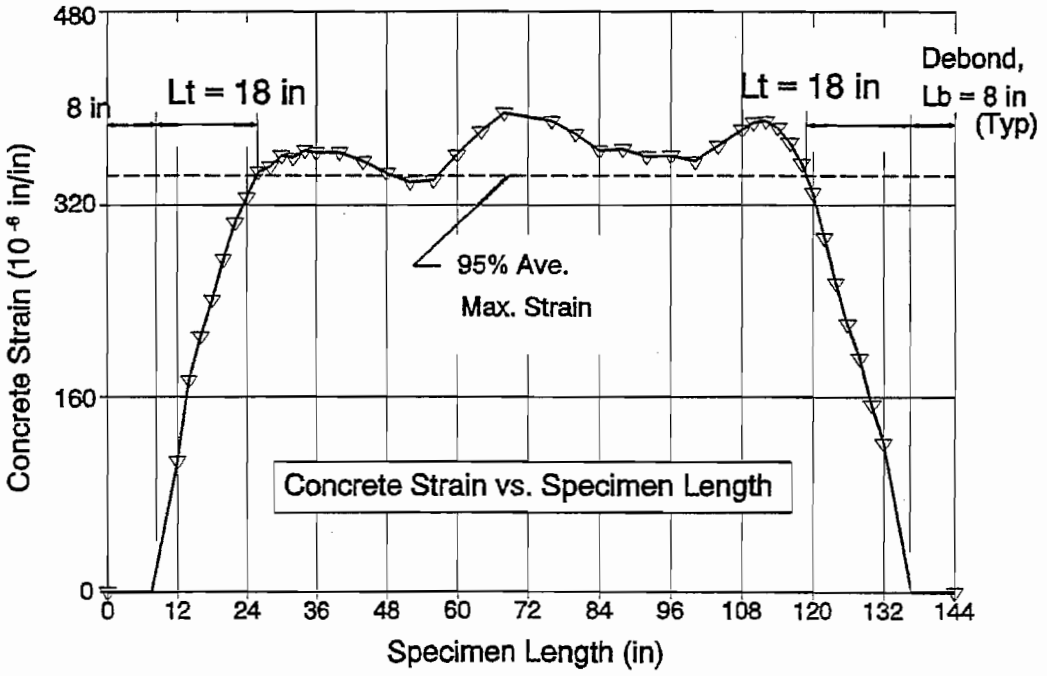

Figure A8. DC150 - 2 , Transfer Length

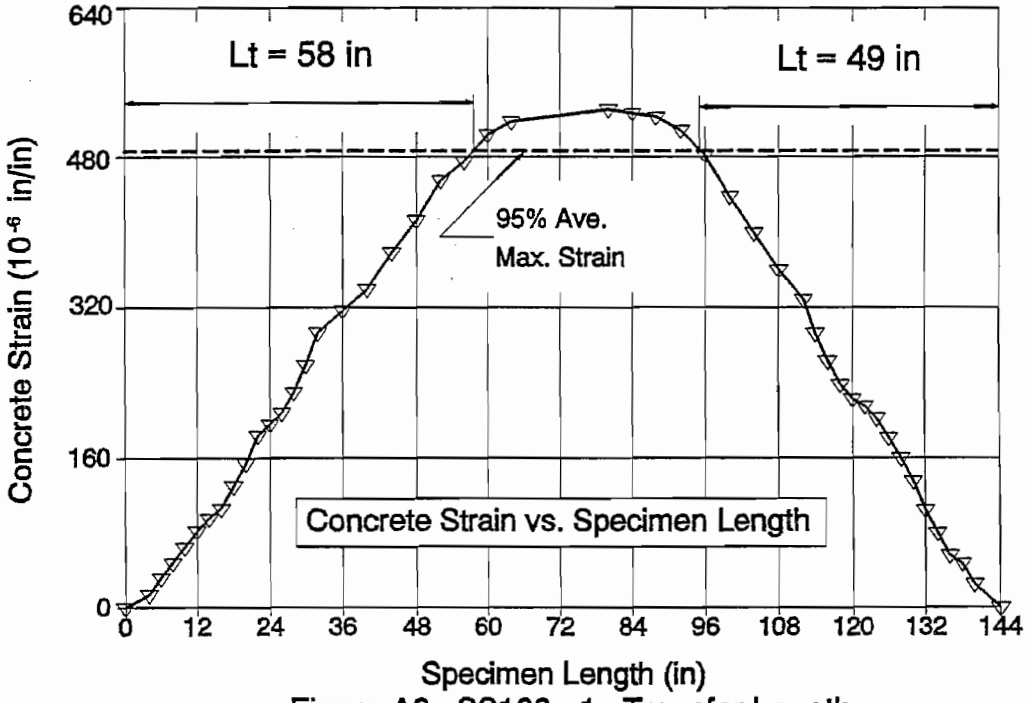

Figure A9. SS160 - 1 , Transfer Length

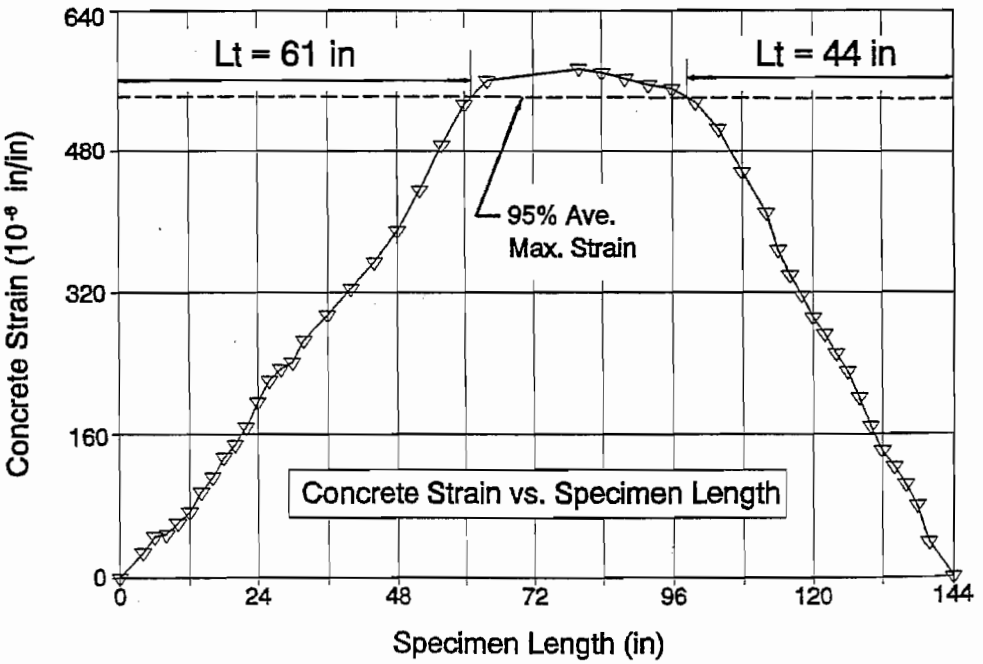

Figure A10. SS160 - 2 , Transfer Length

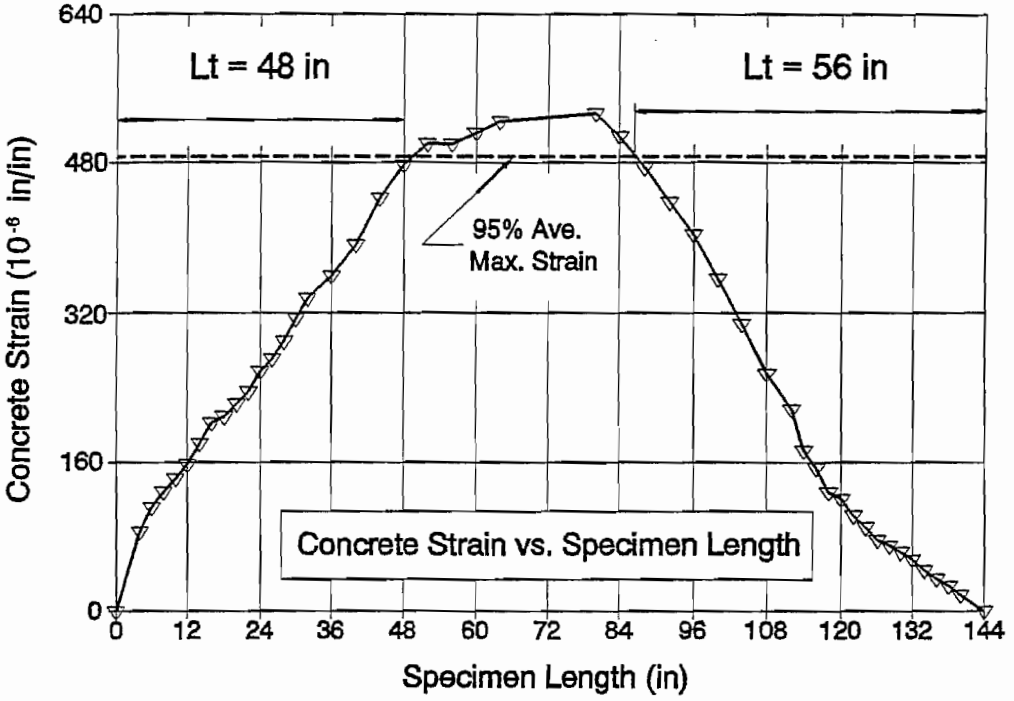

Figure A11. SS160 - 3 , Transfer Length

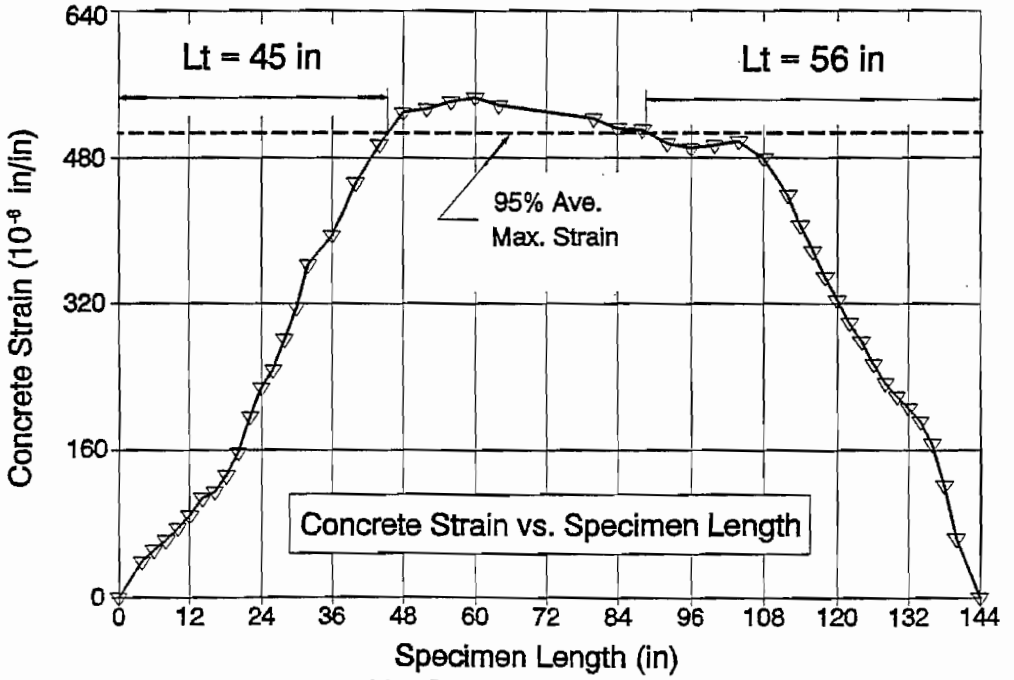

Figure A12. SS160 - 4 , Transfer Length

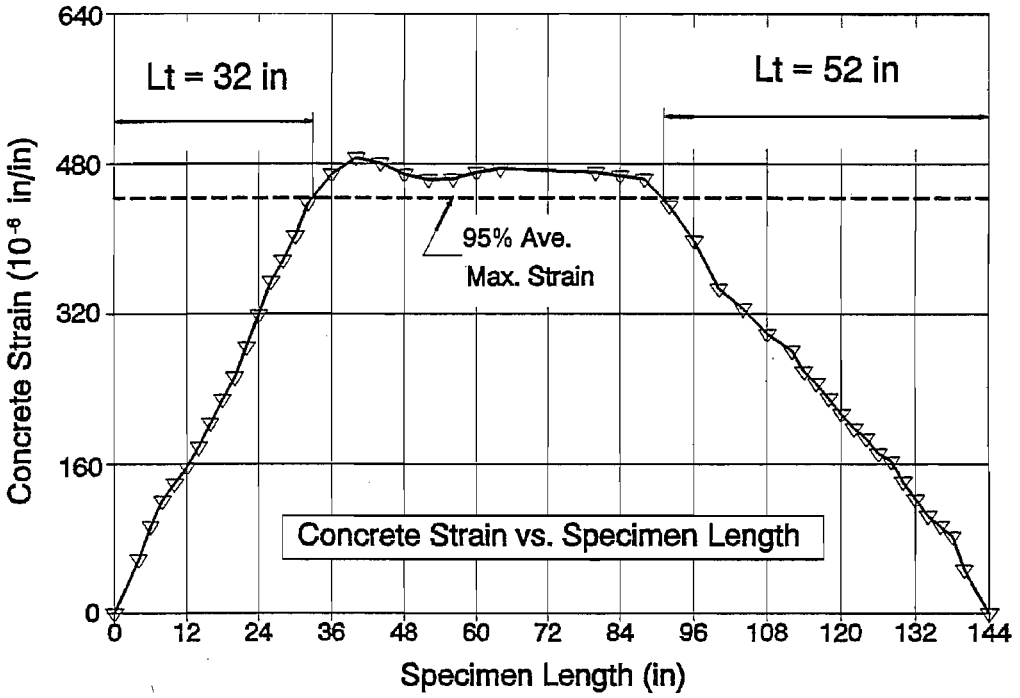

Figure A13. SS160 - 5 , Transfer Length

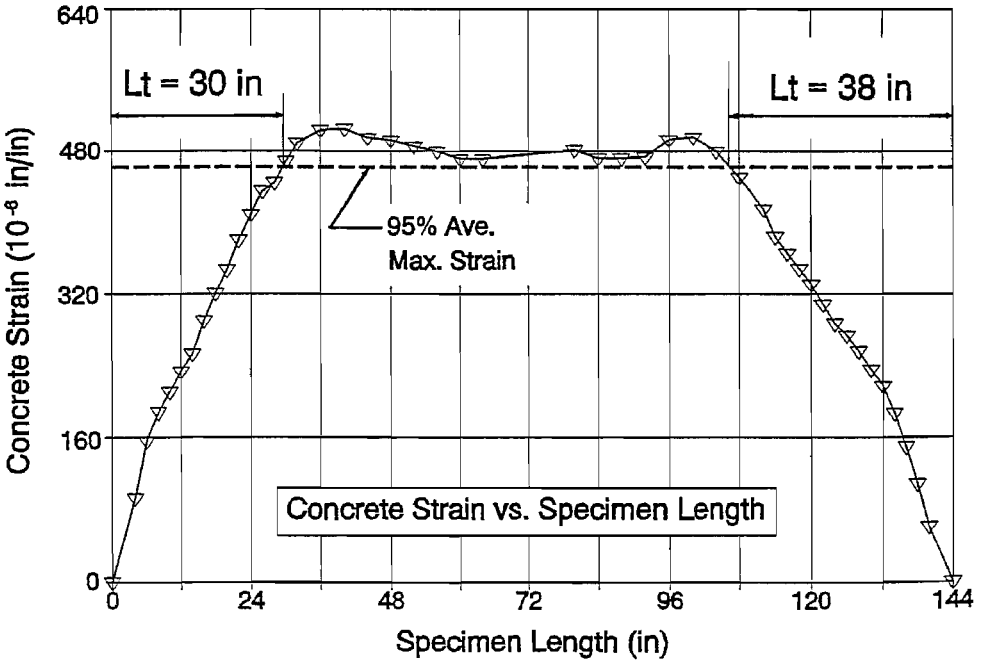

Figure A14. SS160 - 6 , Transfer Length

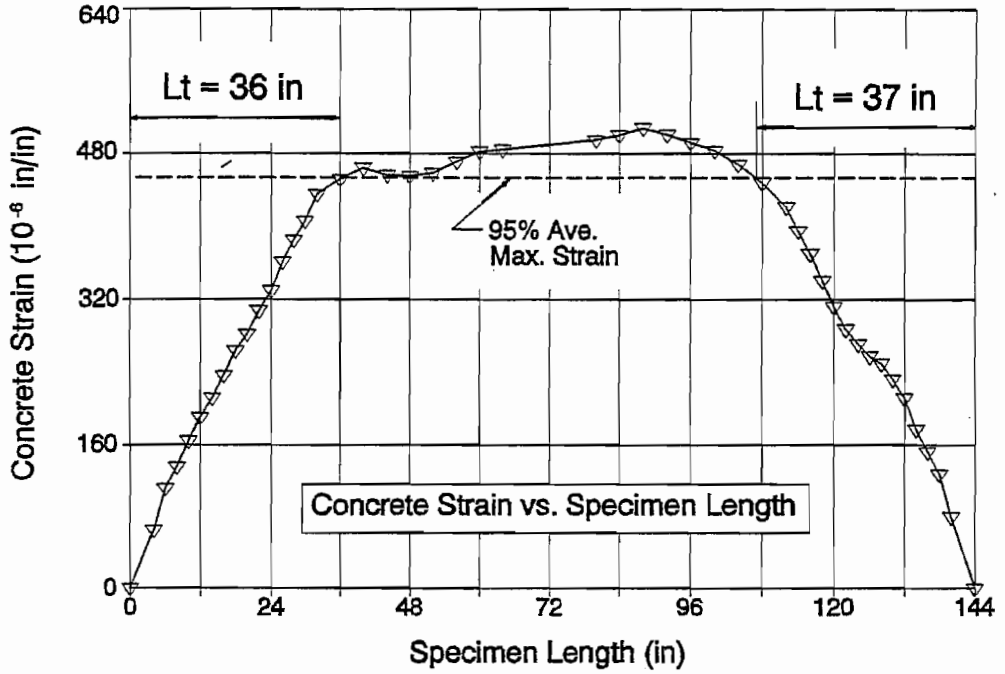

Figure A15. SS160 - 7 , Transfer Length

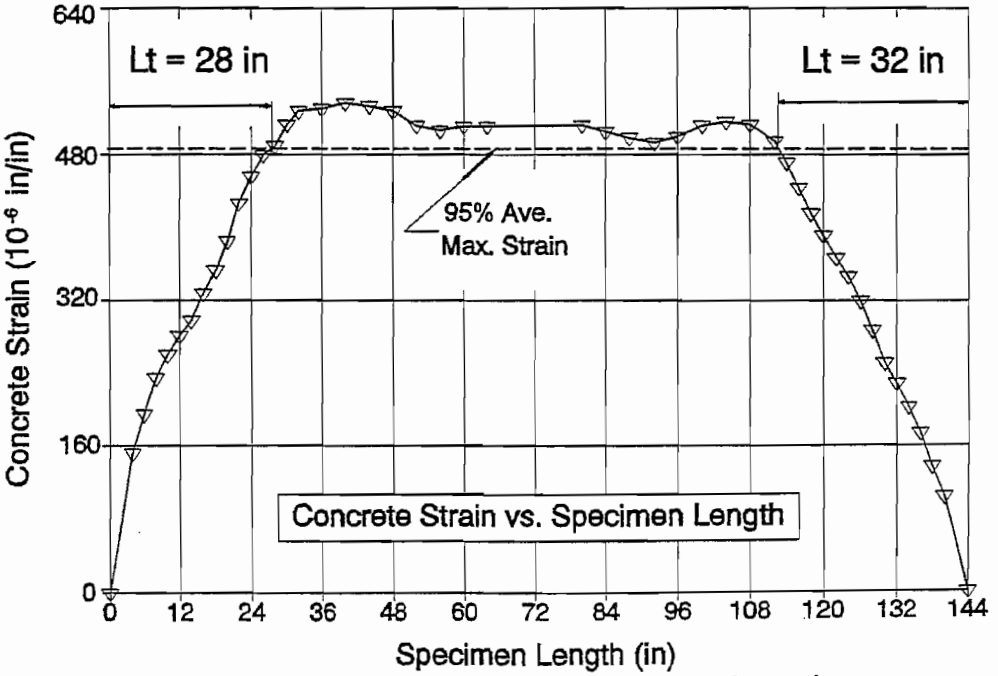

Figure A16. SS160 - 8 , Transfer Length

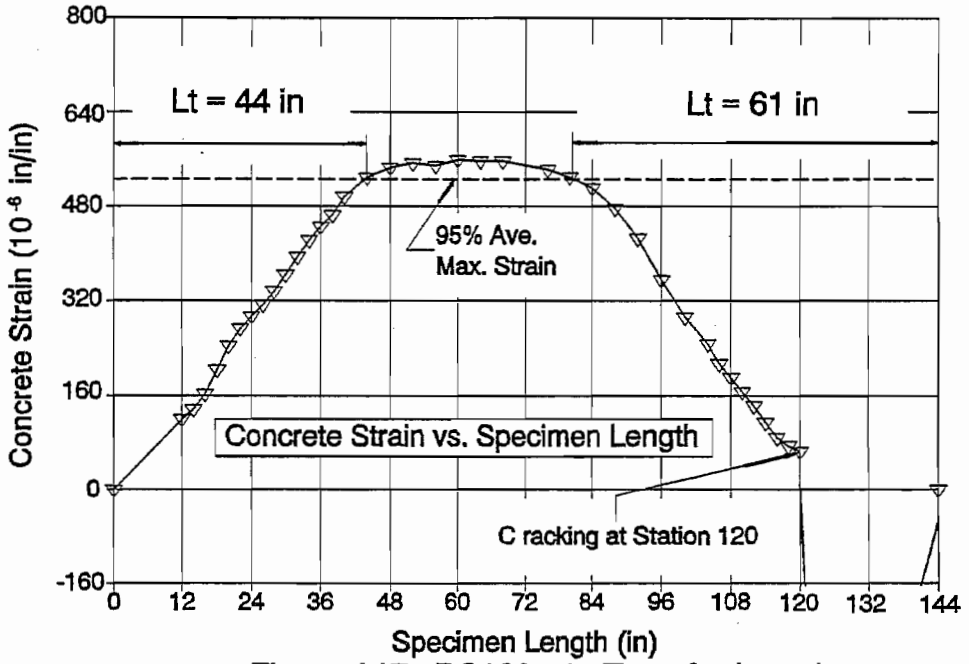

Figure A17. DC160 - 1 , Transfer Length

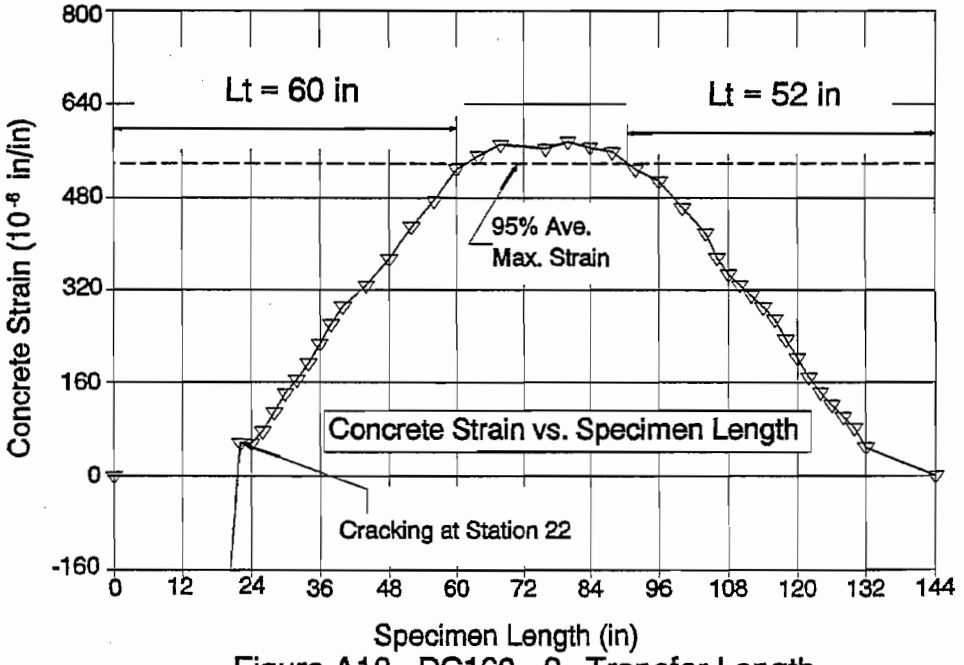

Figure A18. DC160 - 2 , Transfer Length

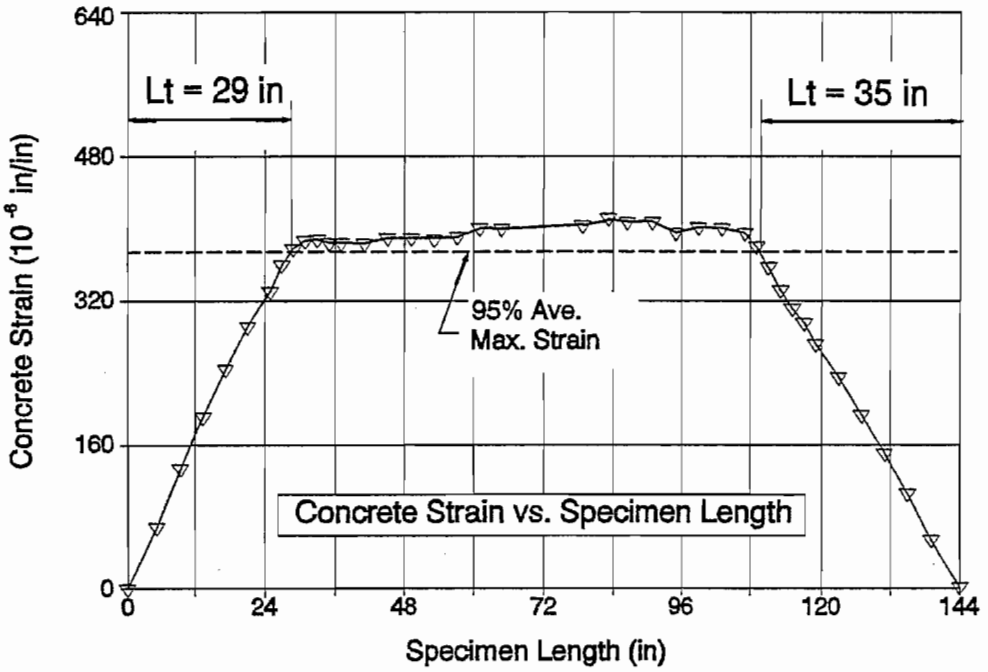

Figure A19. FC150 -11 , Transfer Length

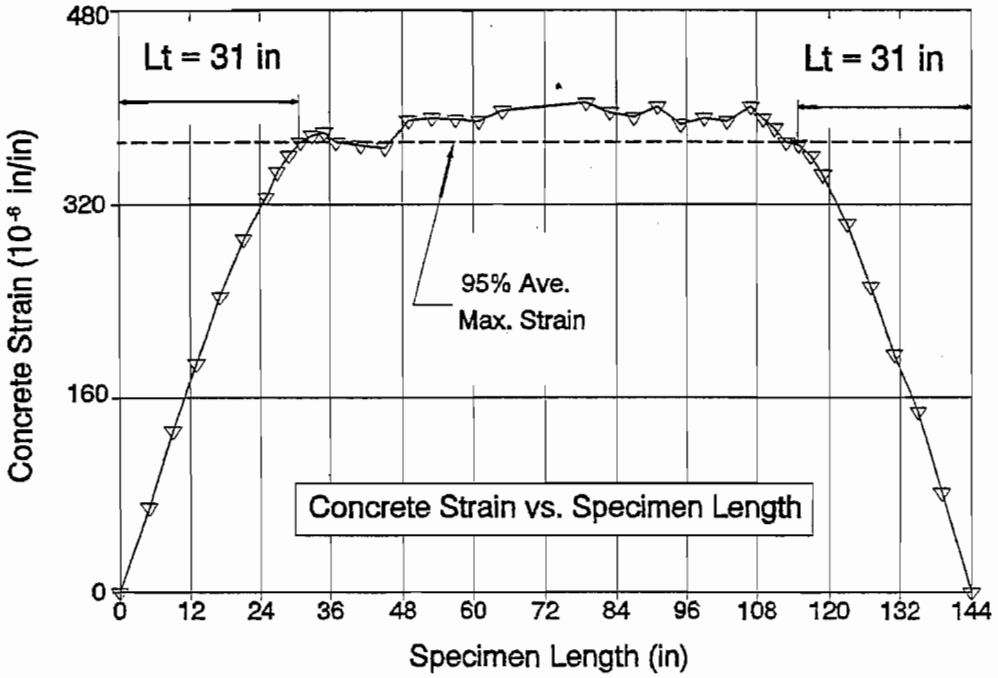

Figure A20. FC150 - 12 , Transfer Length

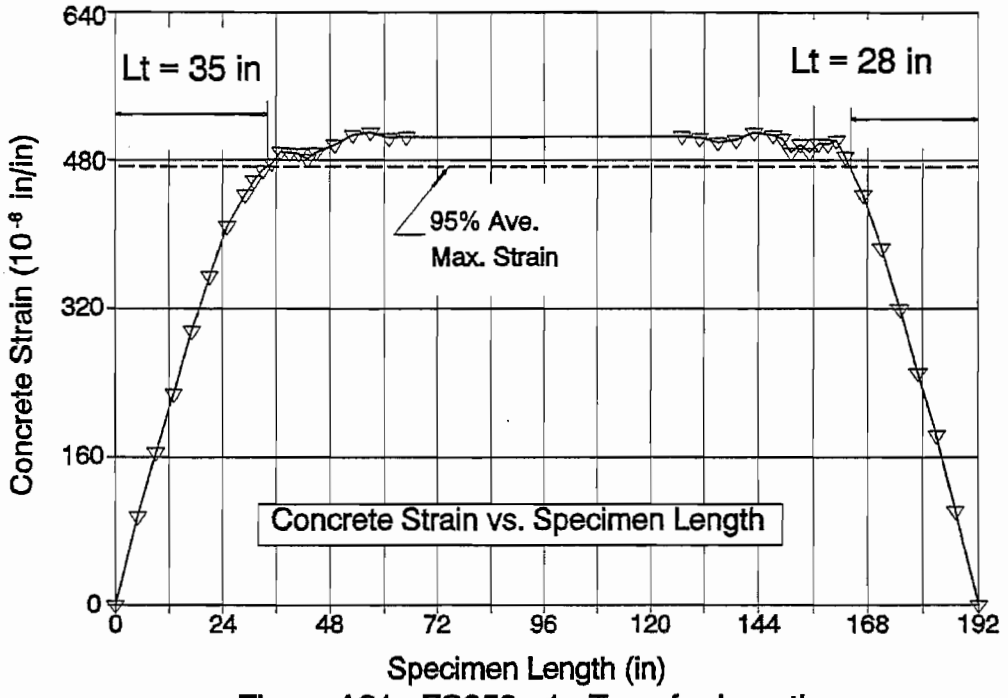

Figure A21. FC350 - 1 , Transfer Length

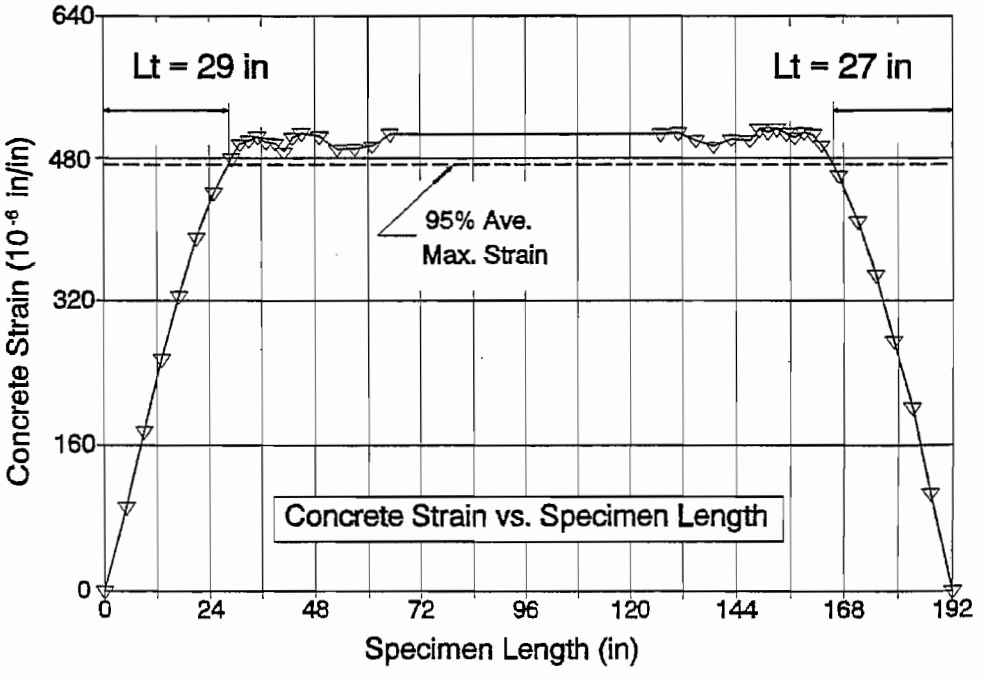

Figure A22. FC350 - 2 , Transfer Length

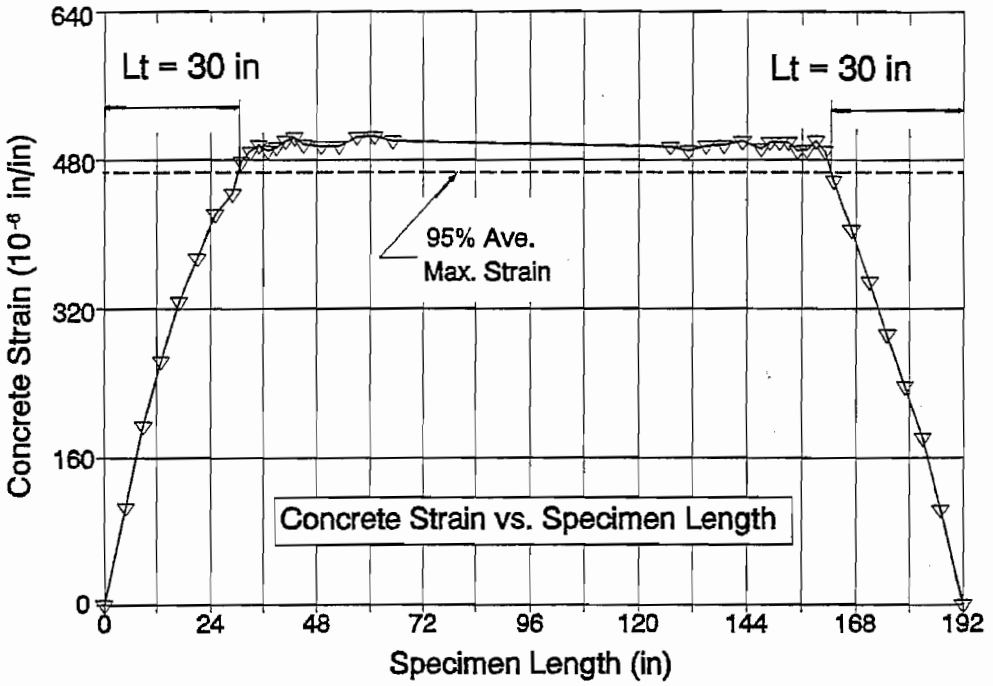

Figure A23. FCT350 - 3 , Transfer Length

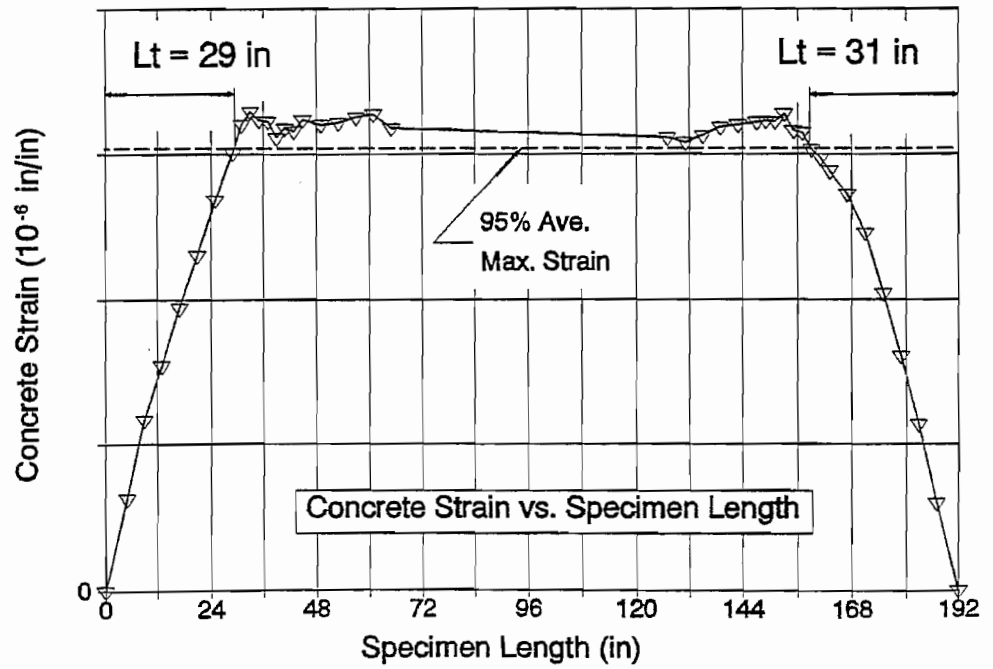

Figure A24. FCT350 - 4 , Transfer Length

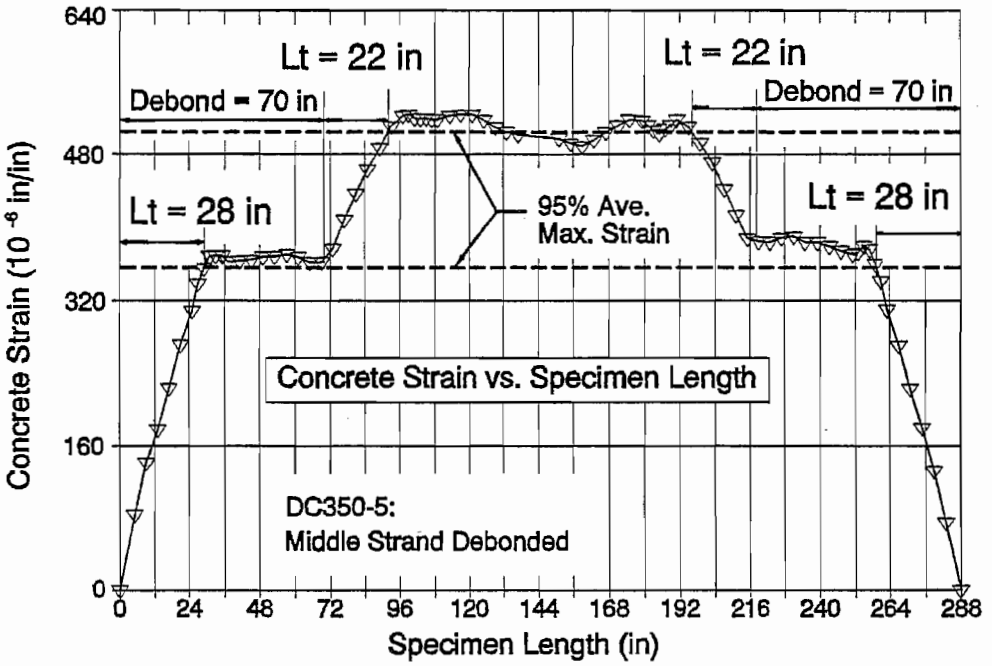

Figure A25. DC350 - 5 , Transfer Length

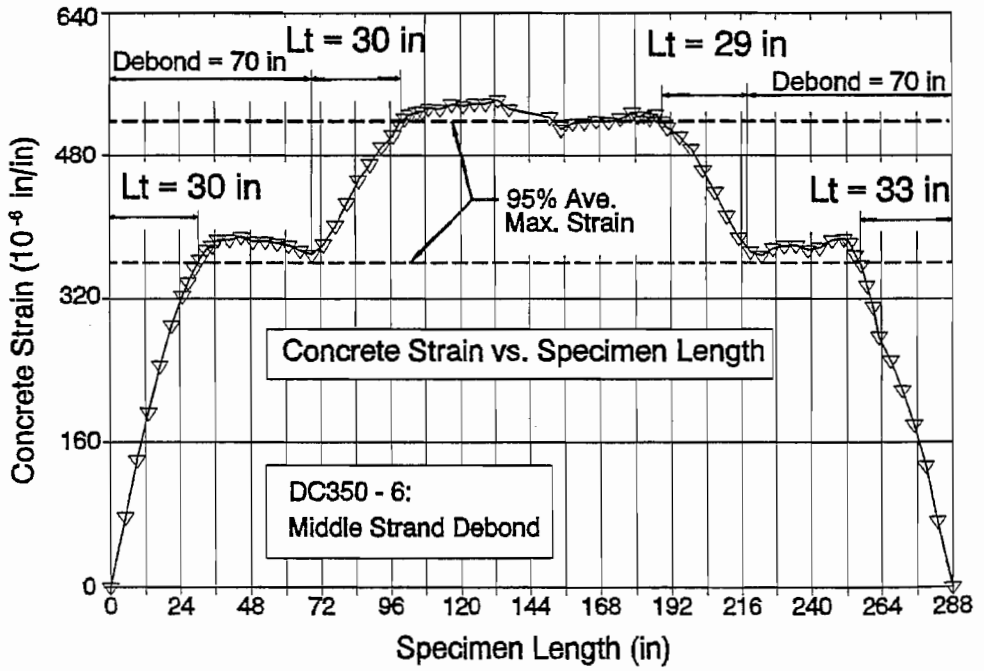

Figure A26. DC350 - 6 , Transfer Length

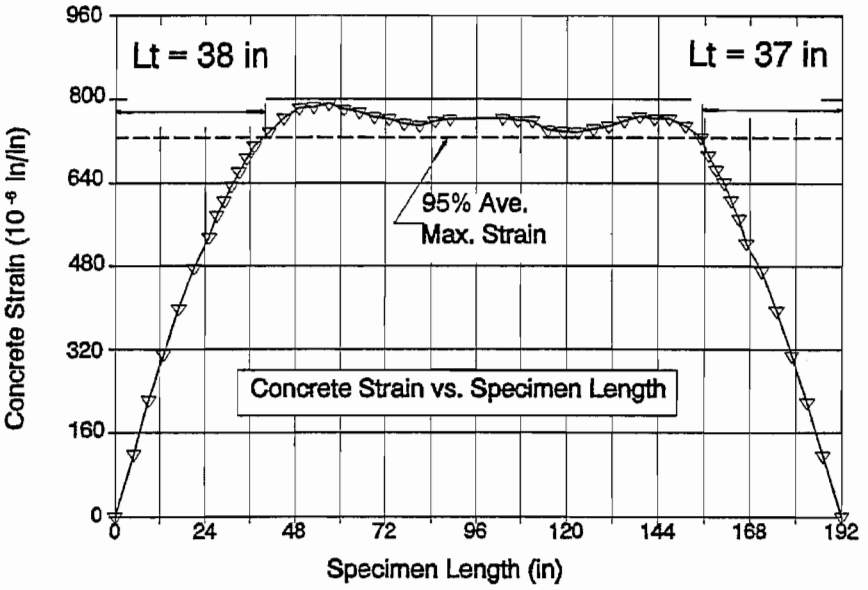

Figure A27. FC550 - 1 , Transfer Length

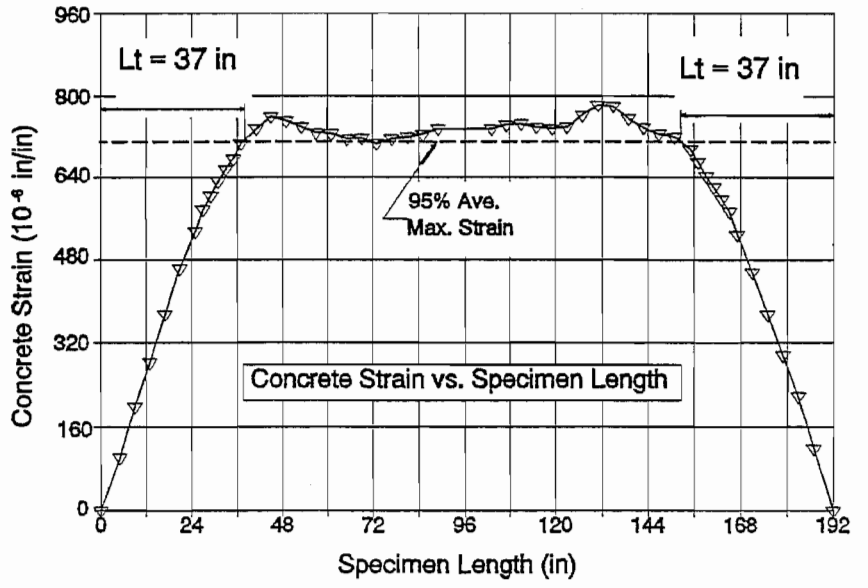

Figure A28. FCT550 - 2 , Transfer Length

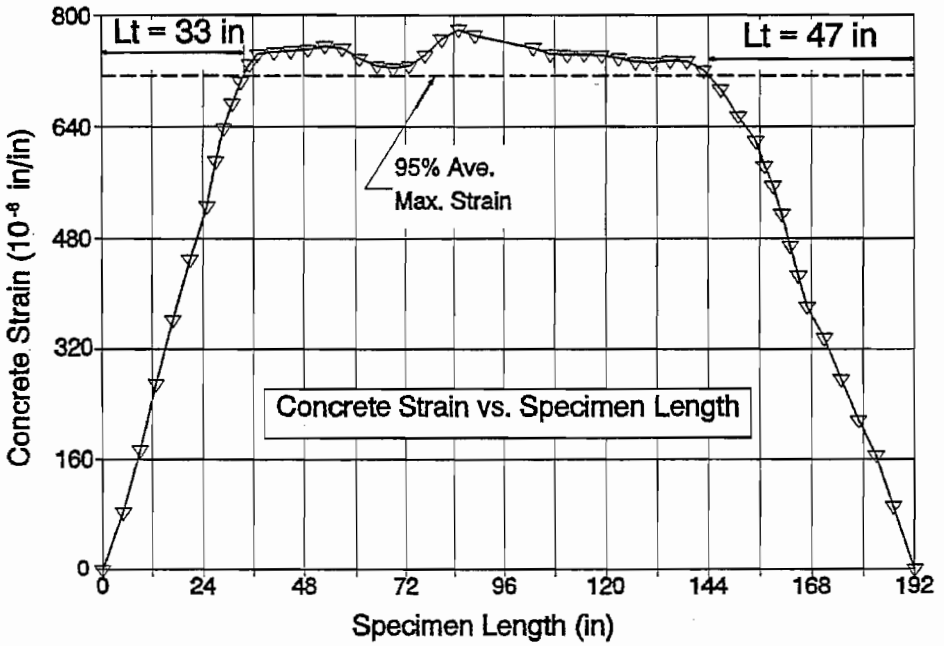

Figure A29. FC550 - 3 , Transfer Length

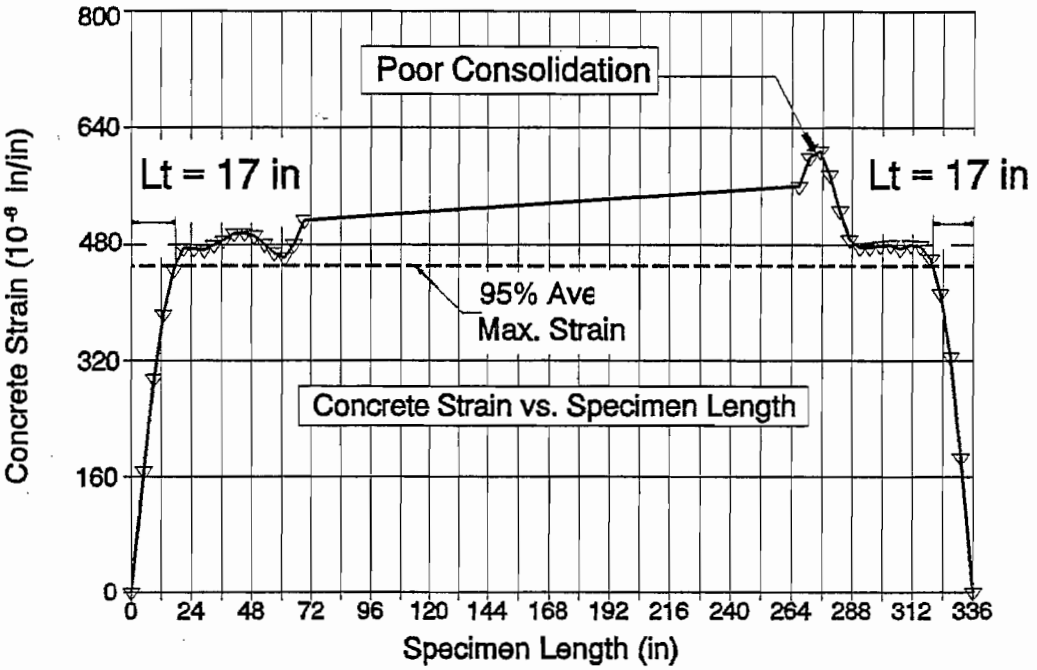

Figure A30. FA550 - 1 , Transfer Length

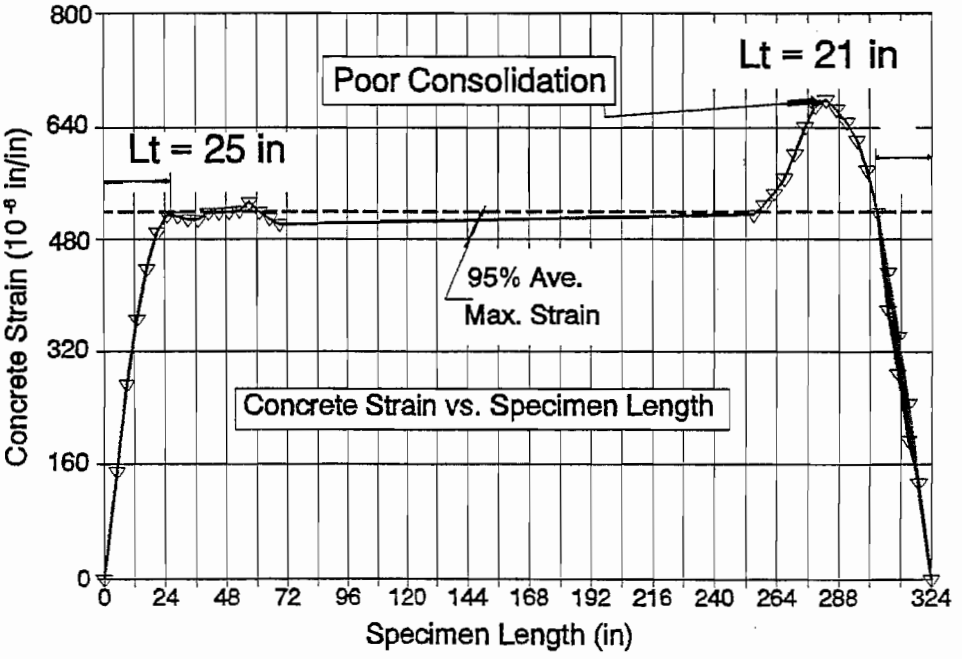

Figure A31. FA550 - 2 , Transfer Length

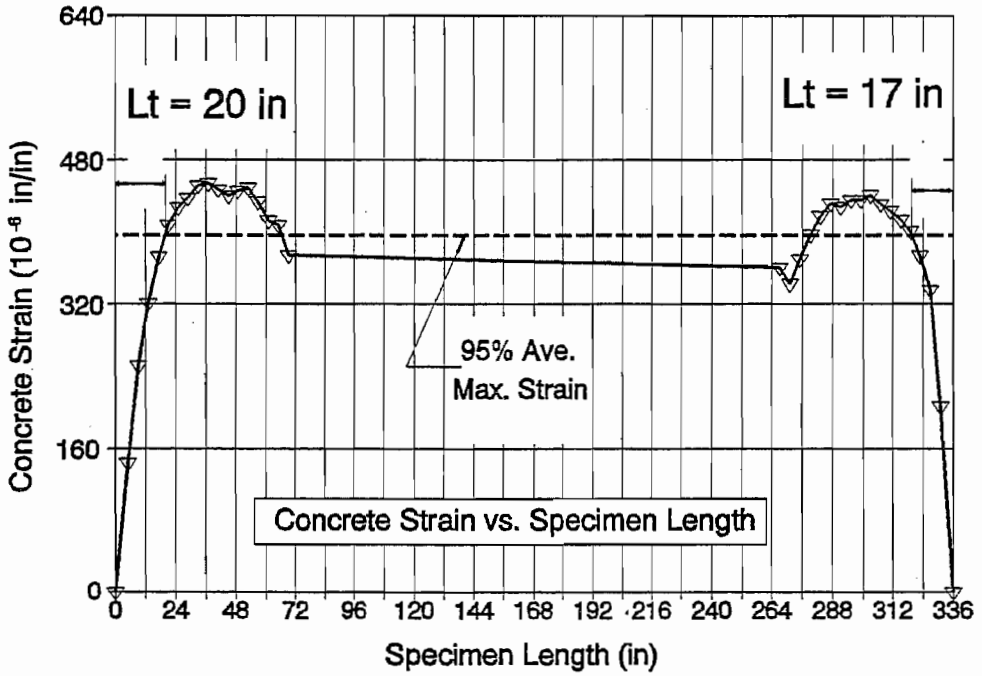

Figure A32. FA550 - 3 , Transfer Length

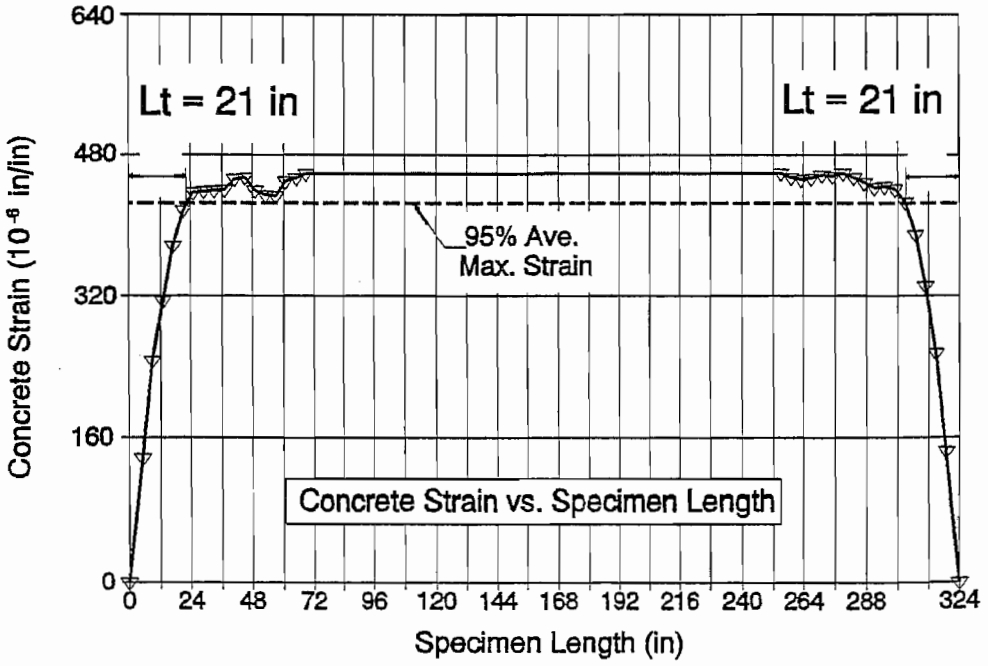

Figure A33. FA550 - 4 , Transfer Length

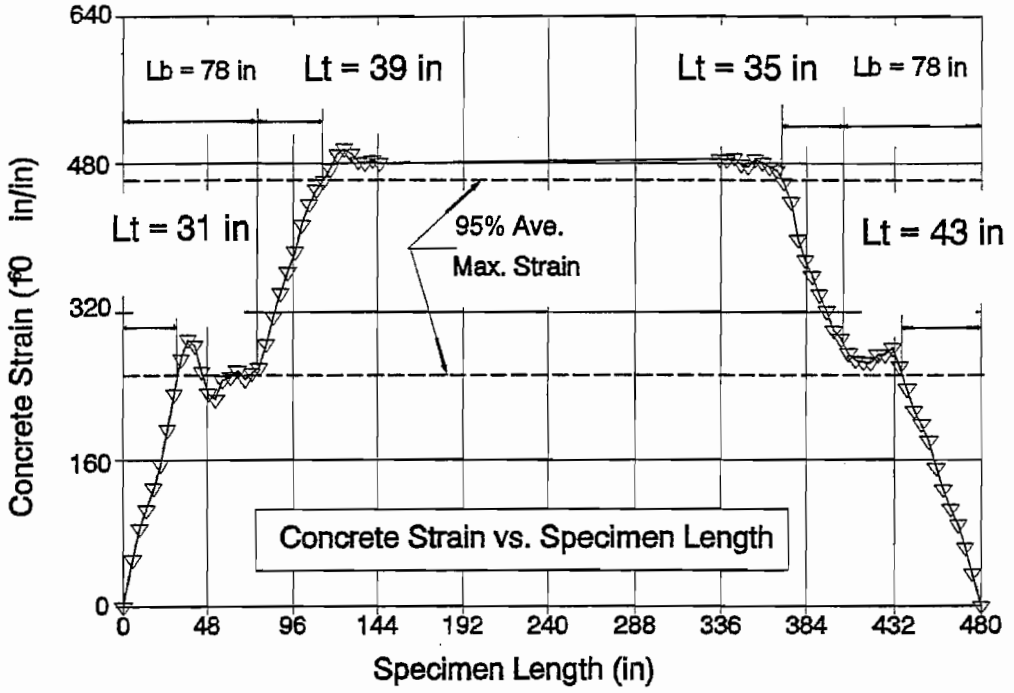

Figure A34. DB850 - 5 , Transfer Length

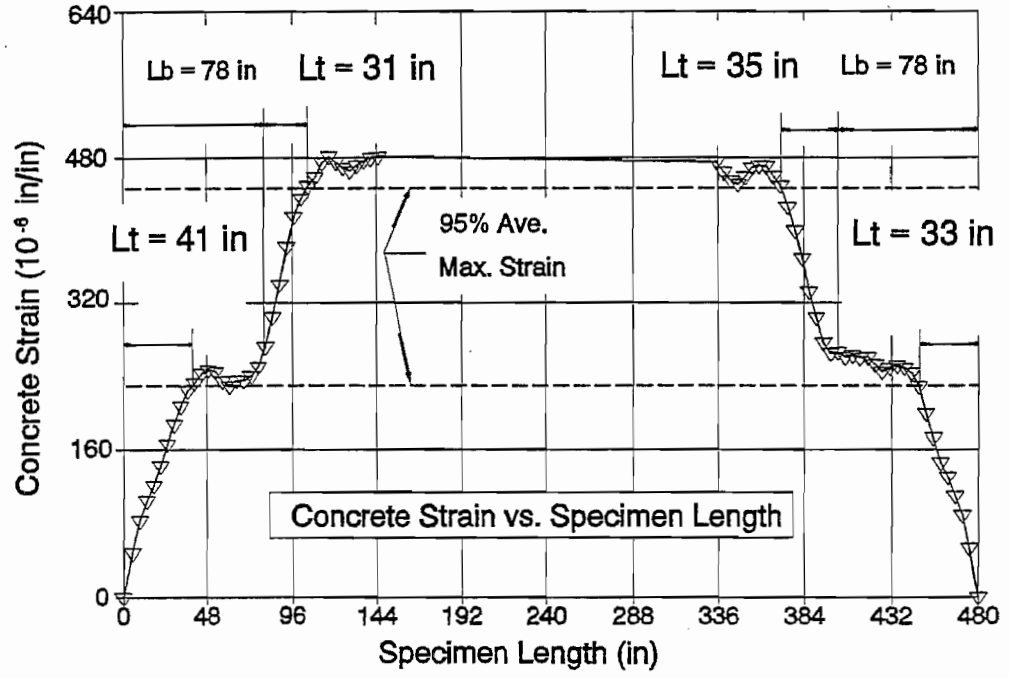

Figure A35. DB850 - 6 , Transfer Length

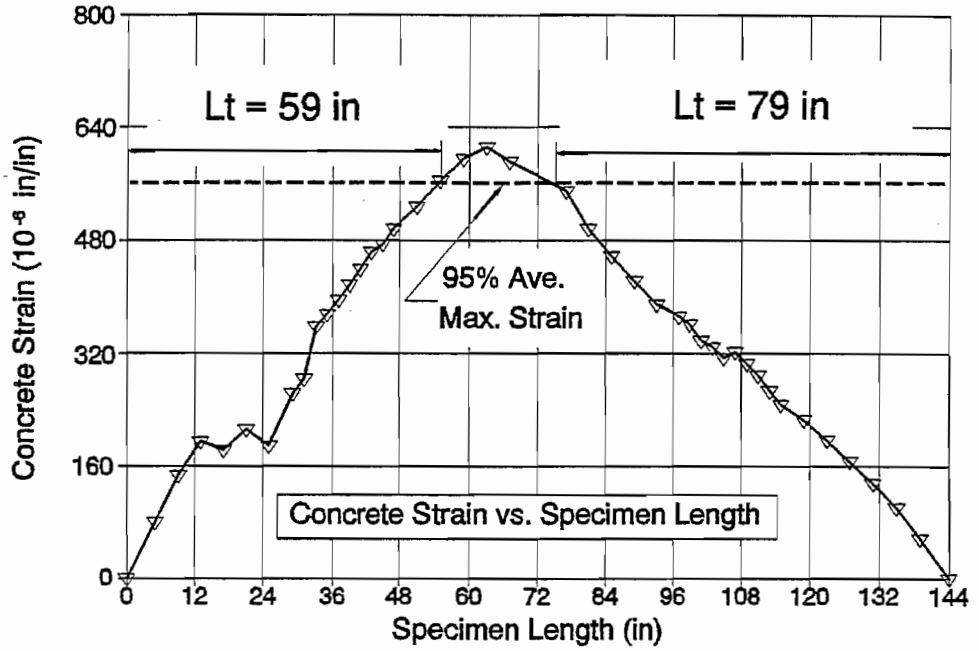

Figure A36. FC160 - 11 , Transfer Length

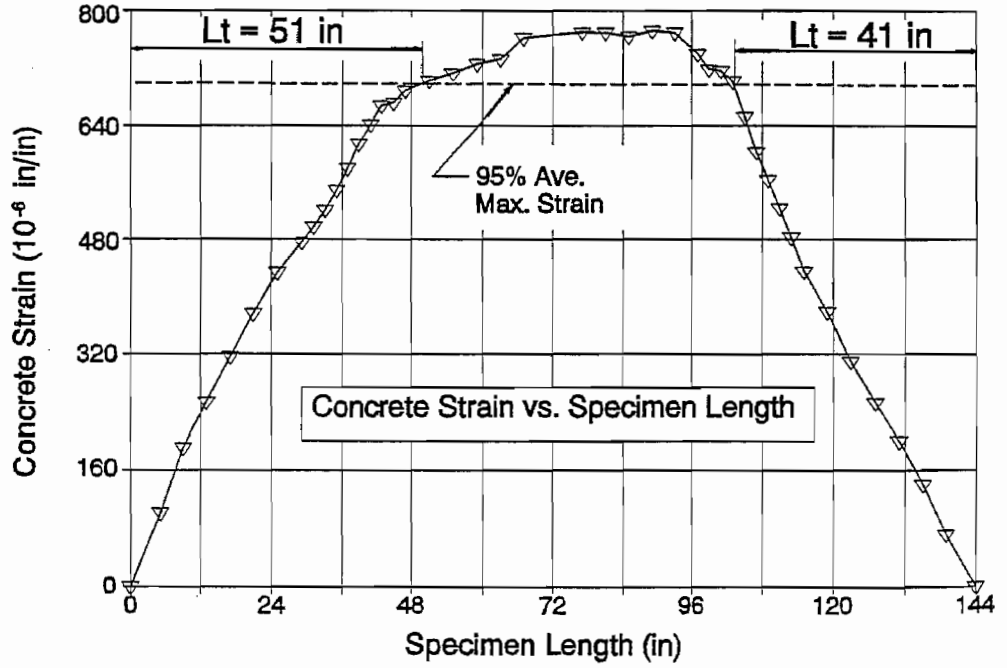

Figure A37. FC160 - 12 , Transfer Length

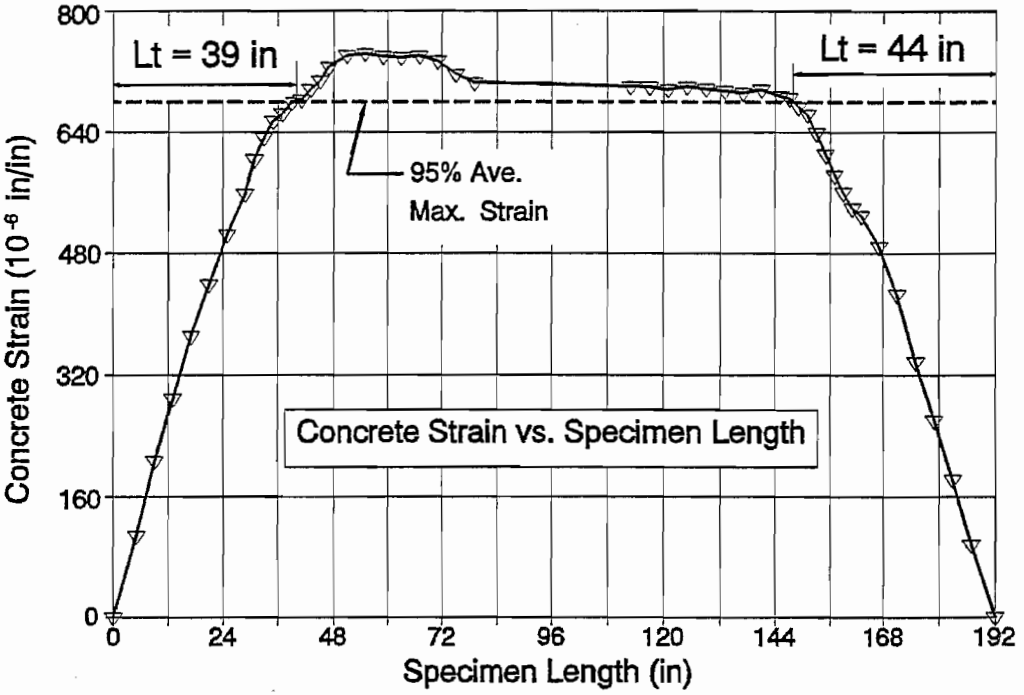

Figure A38. FC360 - 1 , Transfer Length

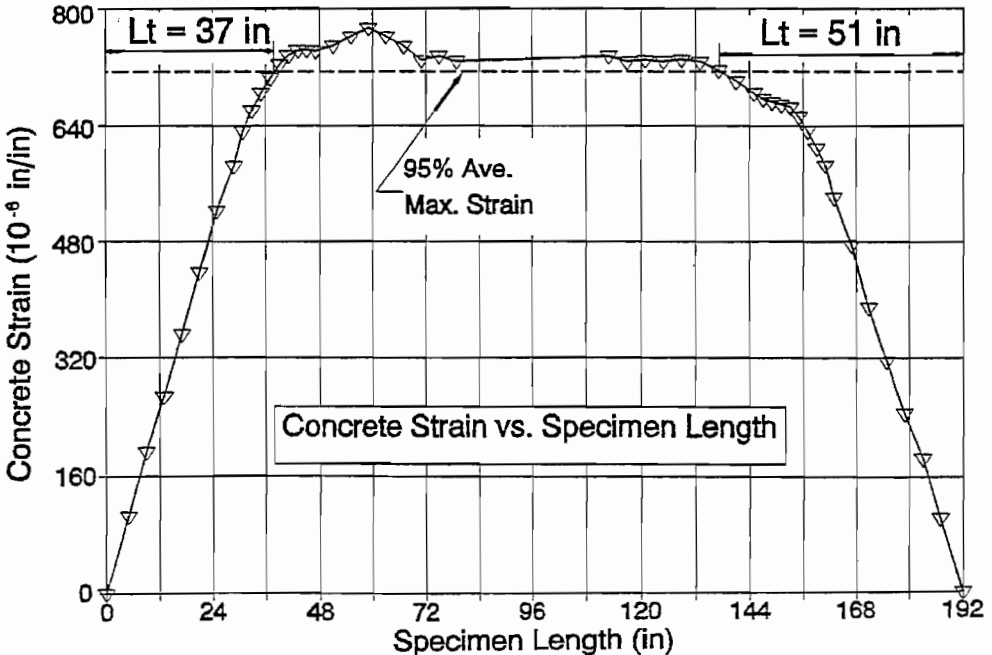

Figure A39. FC360 - 2 , Transfer Length

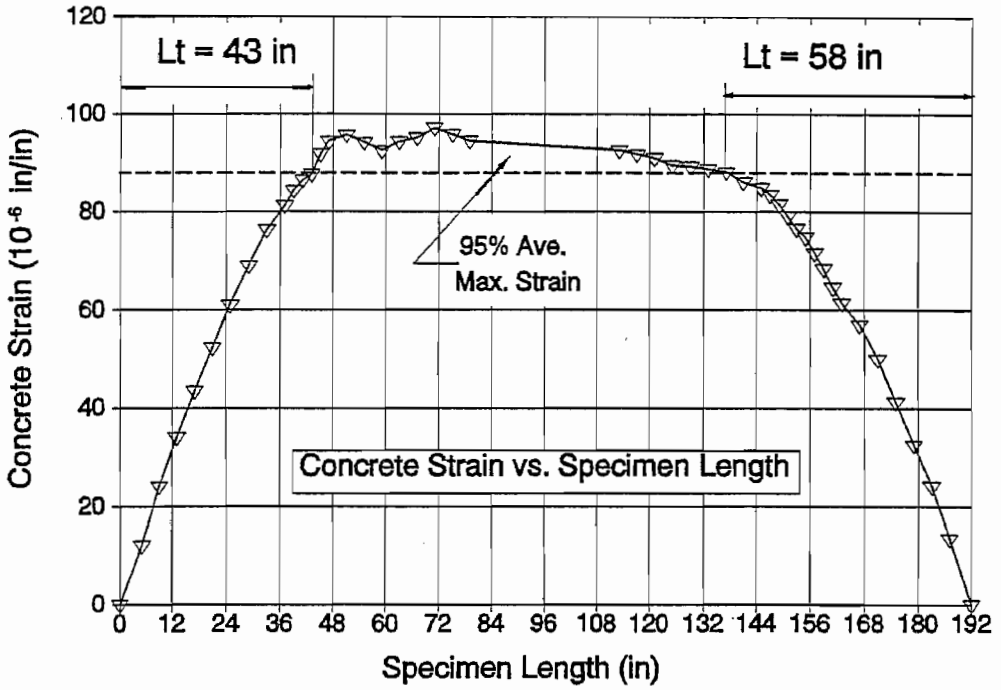

Figure A40. FCT360 - 3 , Transfer Length

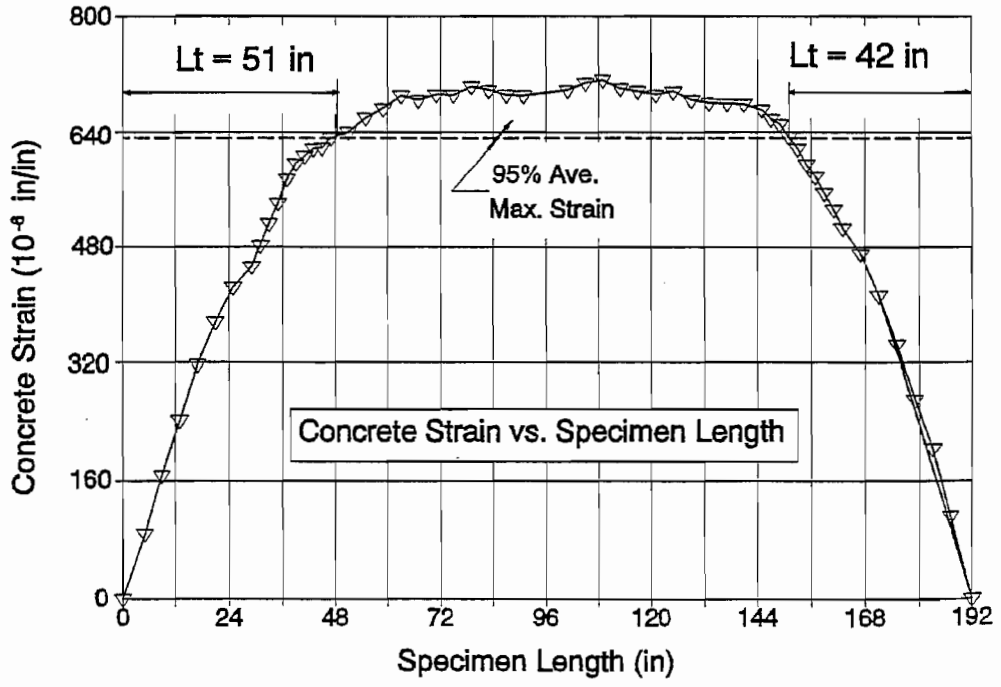

Figure A41. FCT360 - 4 , Transfer Length

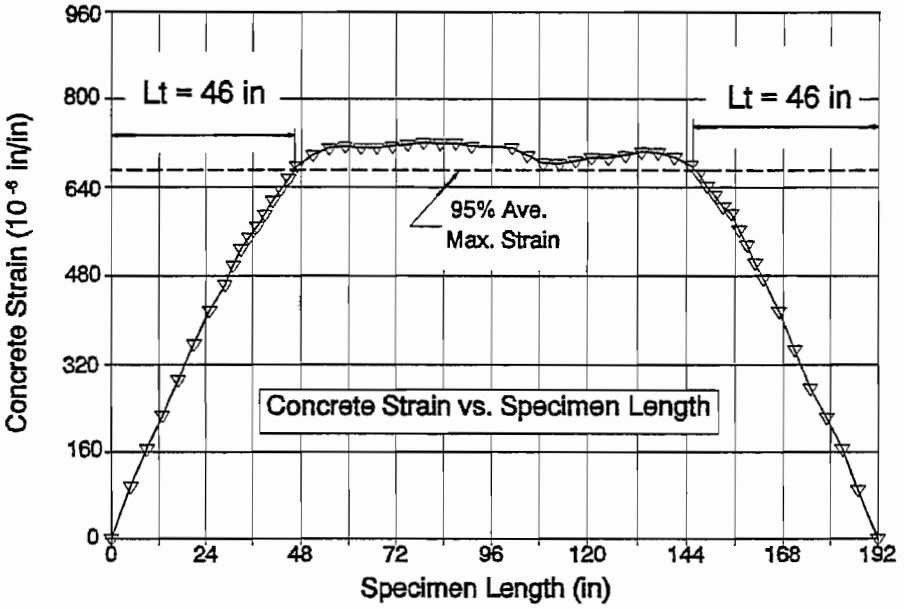

Figure A42. FC362 - 11 , Transfer Length

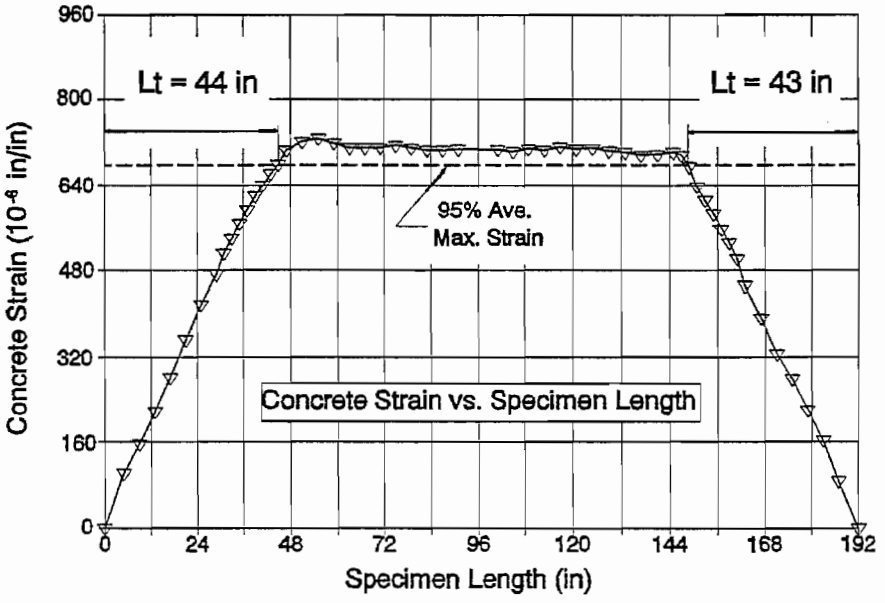

Figure A43. FCT362 - 12 , Transfer Length

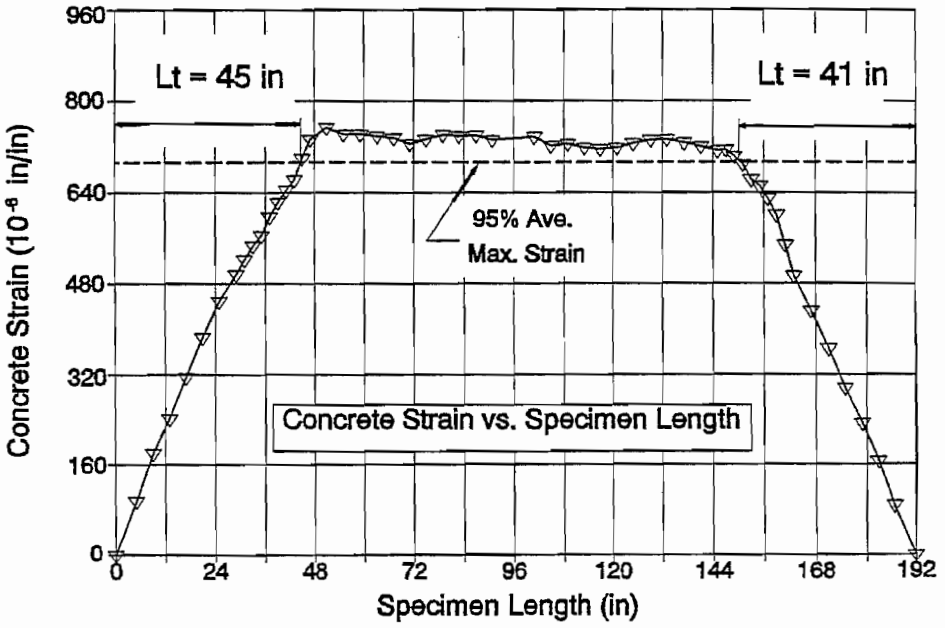

Figure A44. FC362 - 13 , Transfer Length

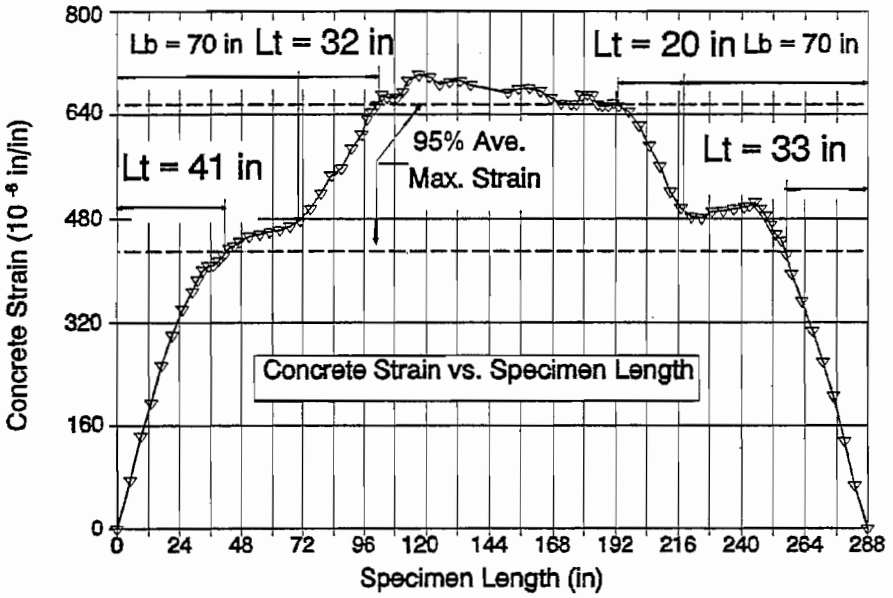

Figure A45. DC360 - 5 , Transfer Length

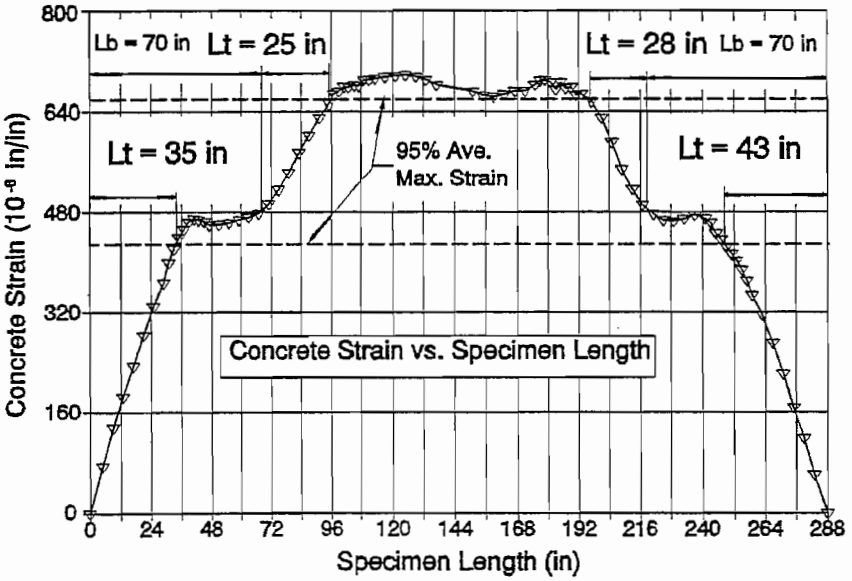

Figure A46. DC360 - 6 , Transfer Length

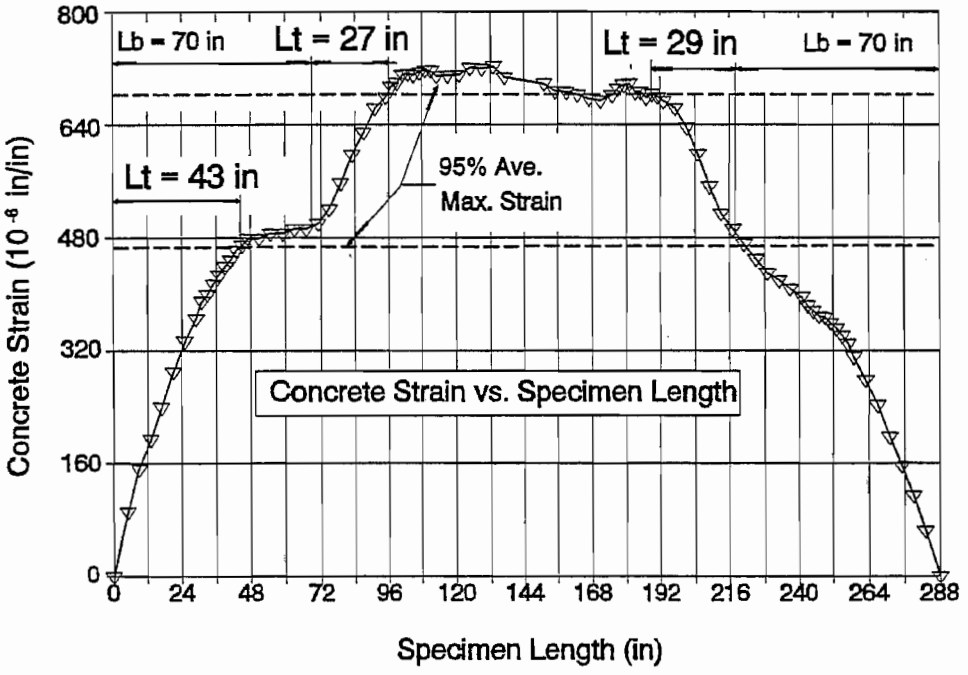

Figure A47. DCT360 - 7 , Transfer Length

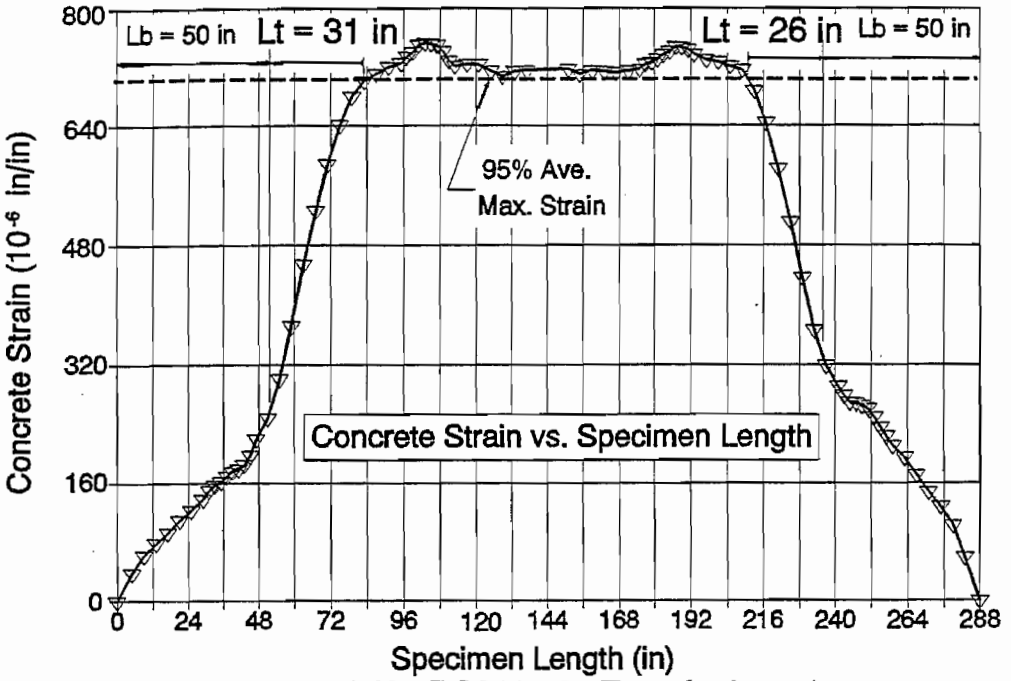

Figure A48. DC360 - 9 , Transfer Length

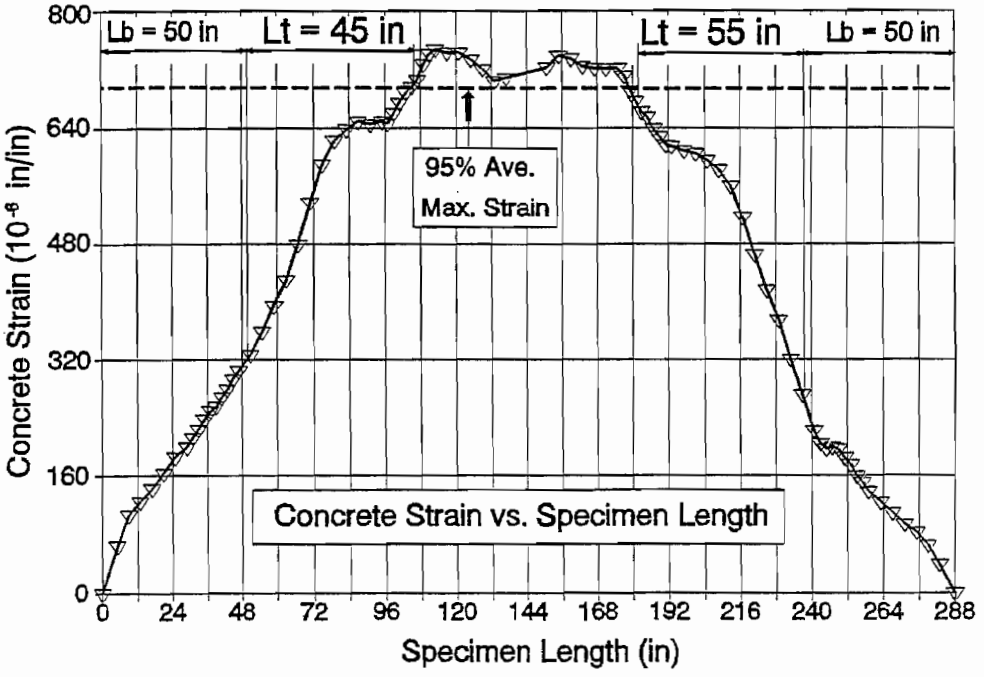

Figure A49. DCT360 - 10 , Transfer Length

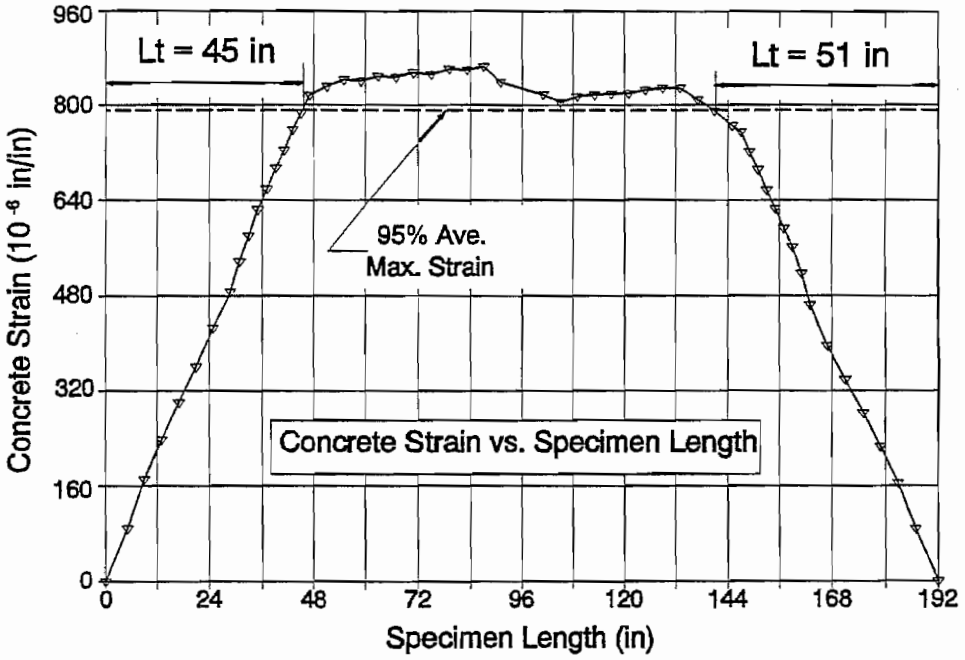

Figure A50. FC560 - 1 , Transfer Length

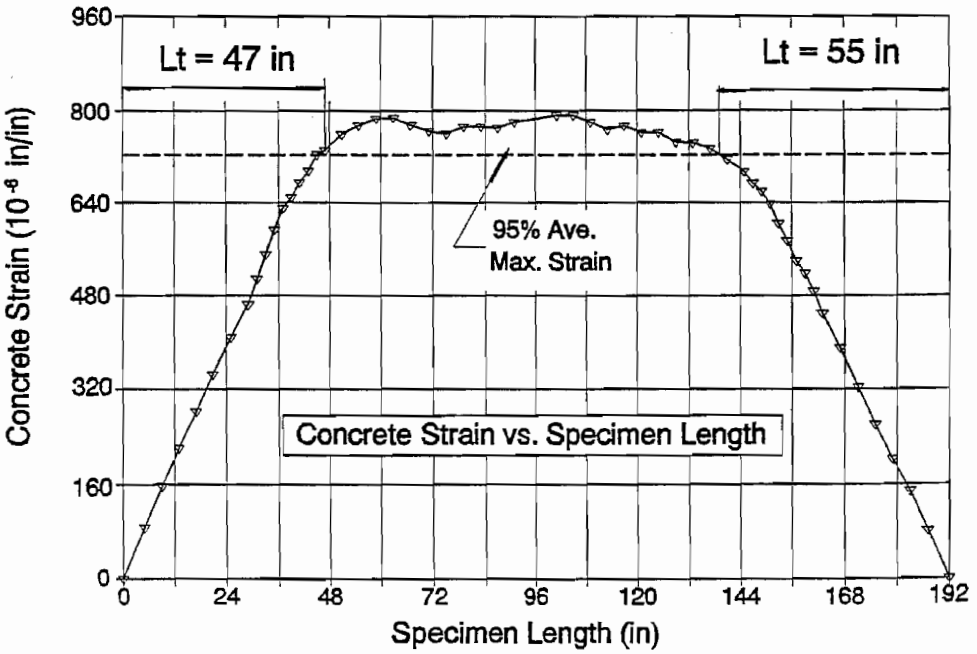

Figure A51. FCT560 - 2 , Transfer Length

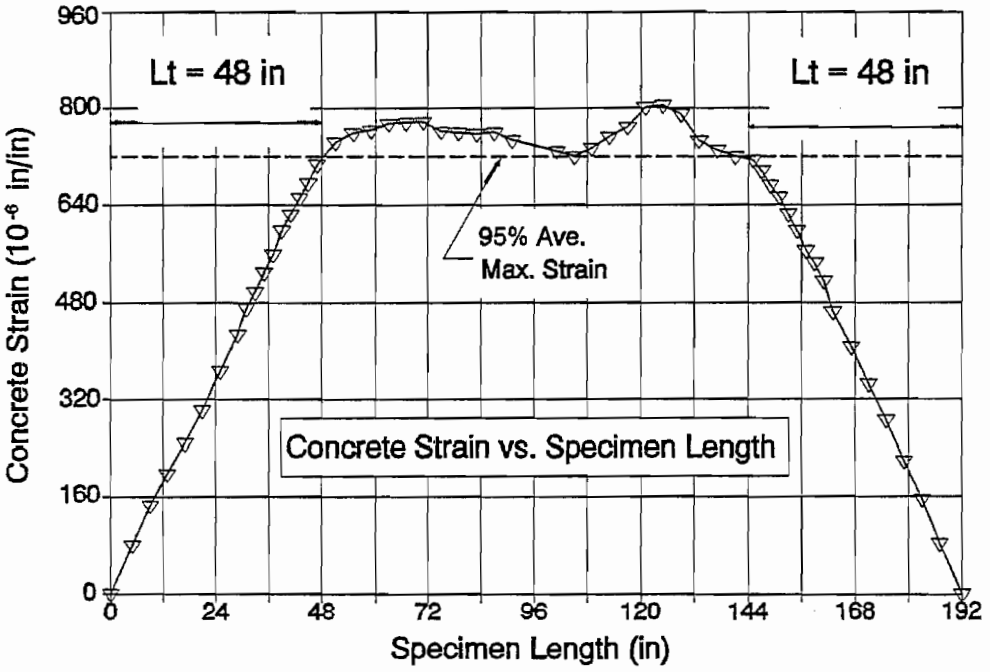

Figure A52. FC560 - 3 , Transfer Length

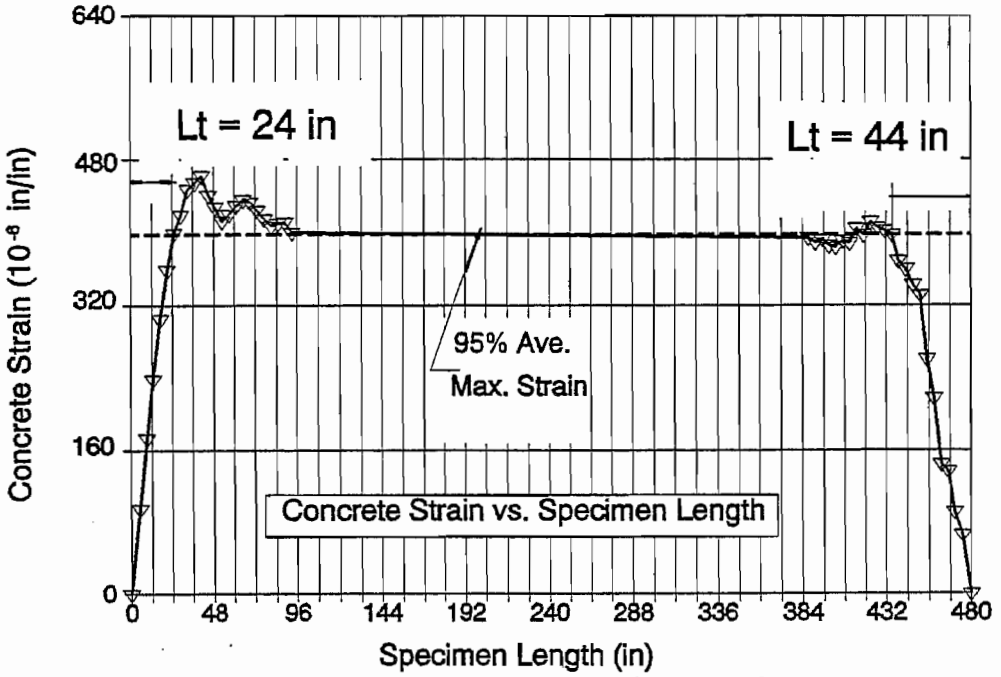

Figure A53. FA460 - 1 , Transfer Length

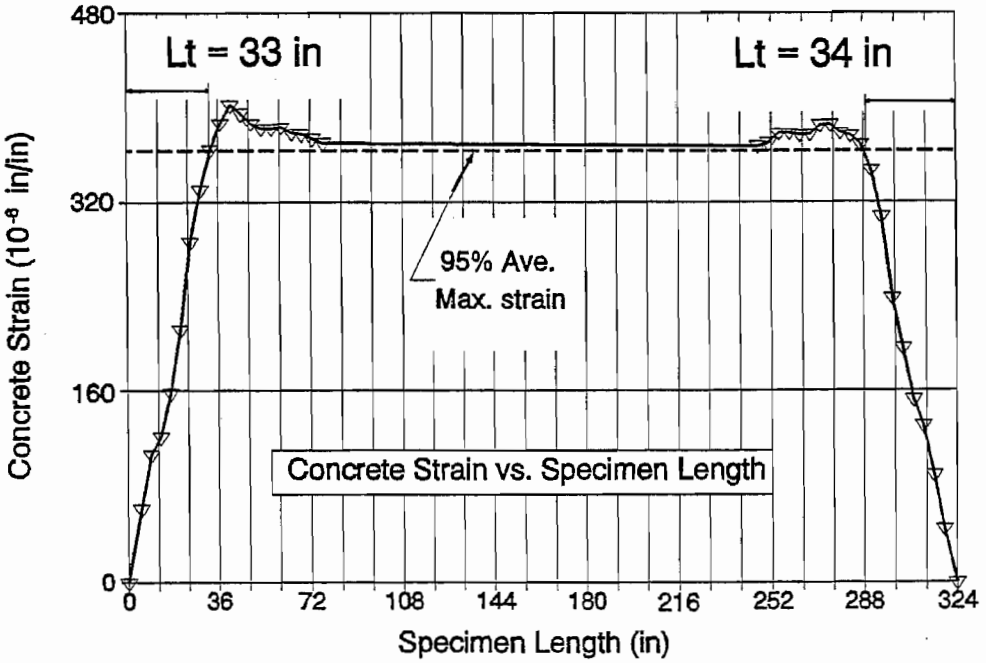

Figure A54. FA460 - 2 , Transfer Length

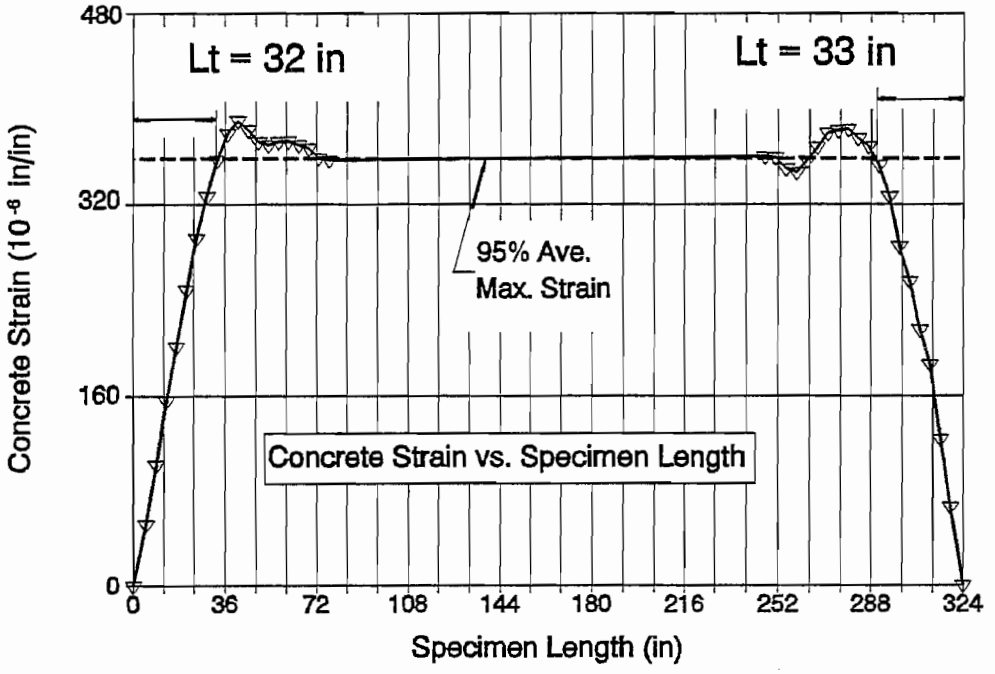

Figure A55. FA460 - 3 , Transfer Length

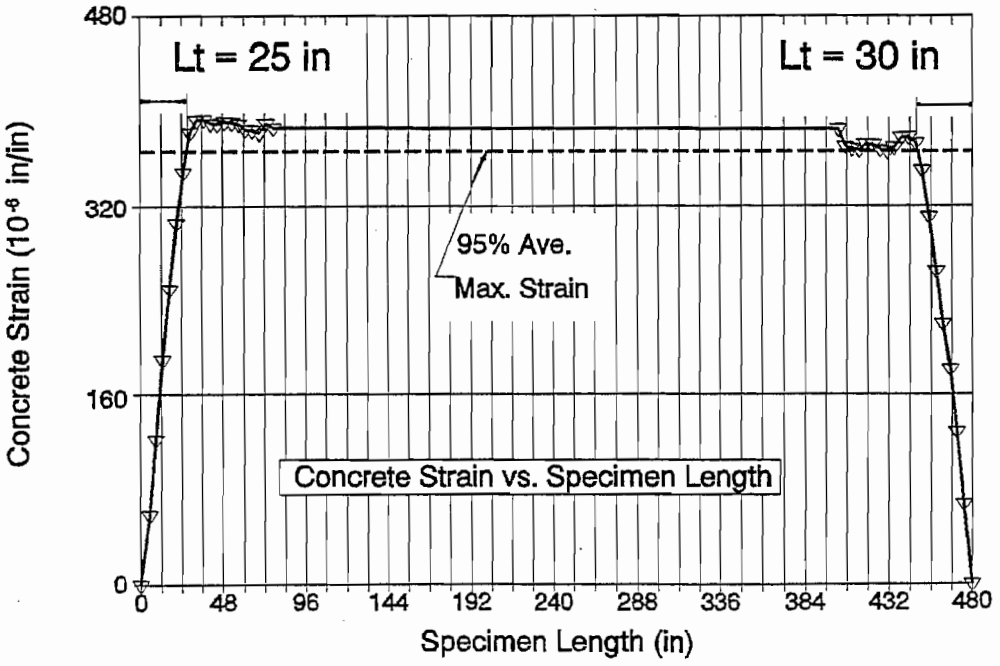

Figure A56. FA460 - 4 , Transfer Length

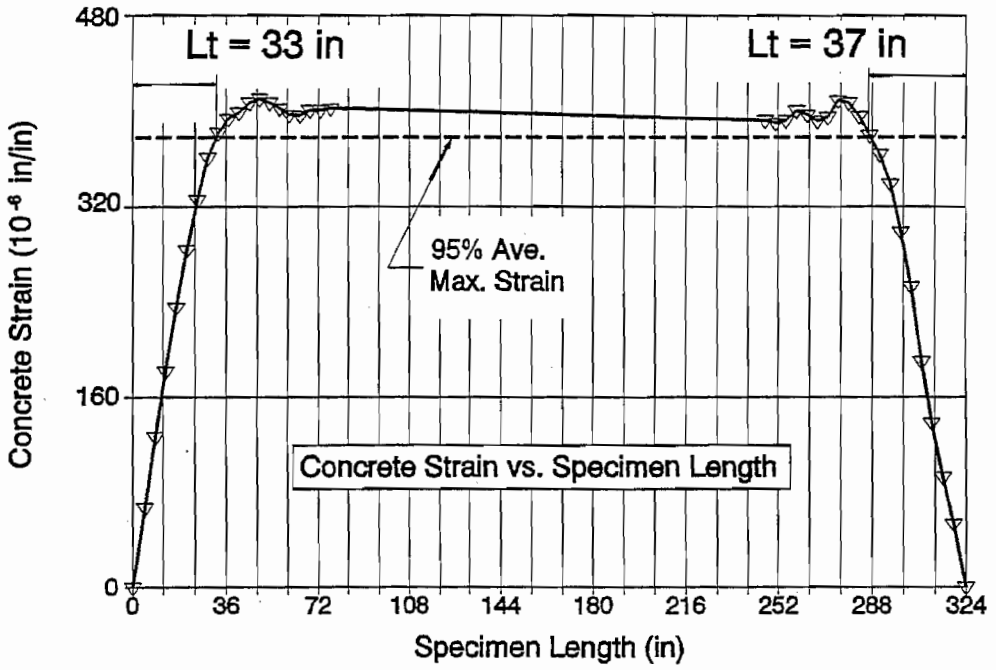

Figure A57. FA460 - 5 , Transfer Length

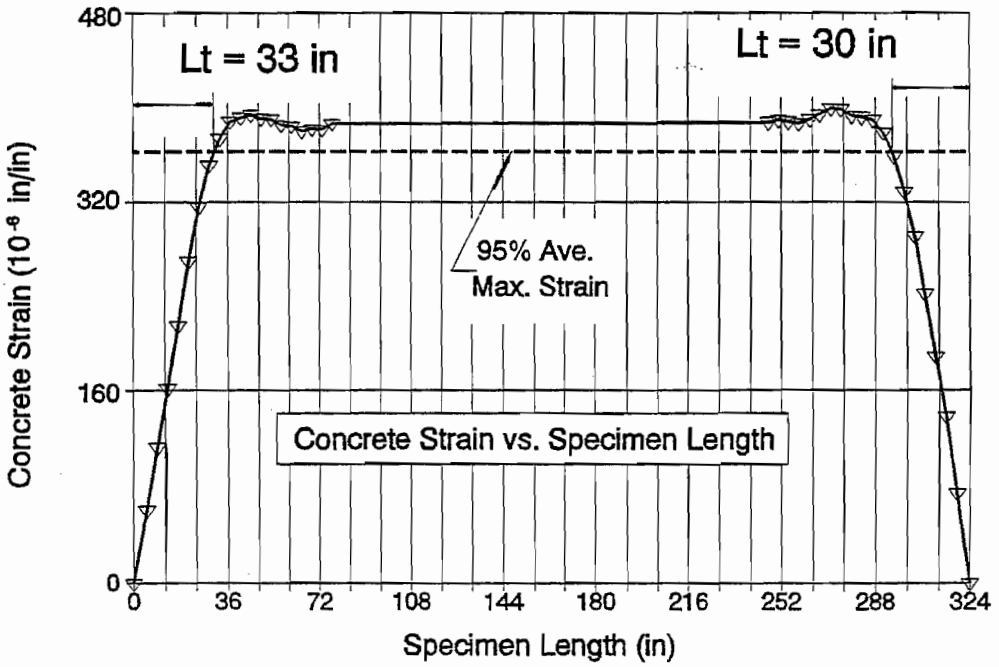

Figure A58. FA460 - 6 , Transfer Length

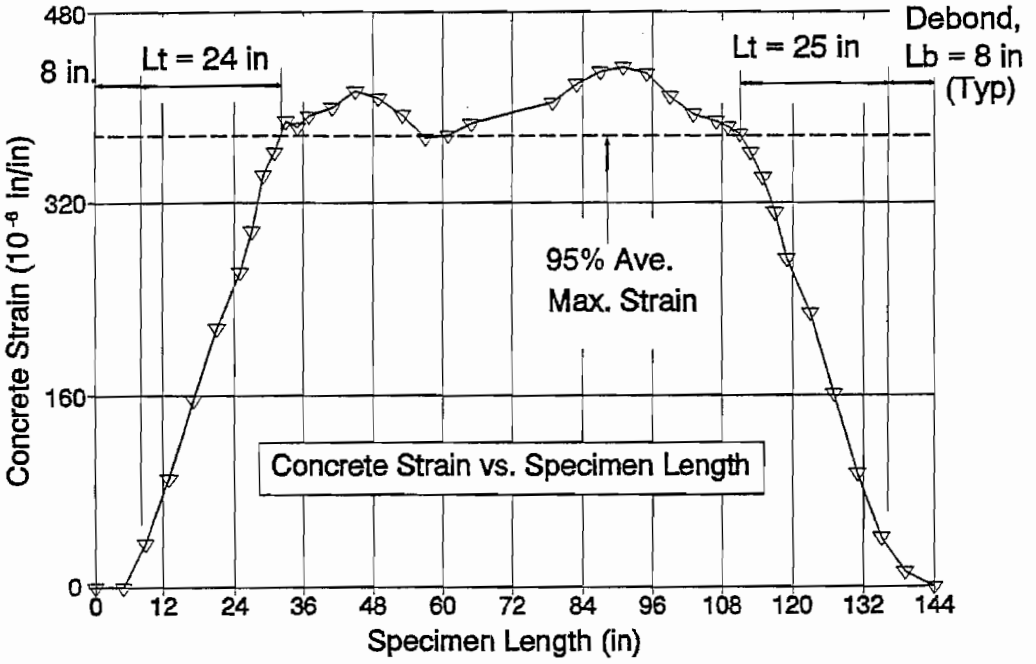

Figure A59. DC150 - 13 , Transfer Length

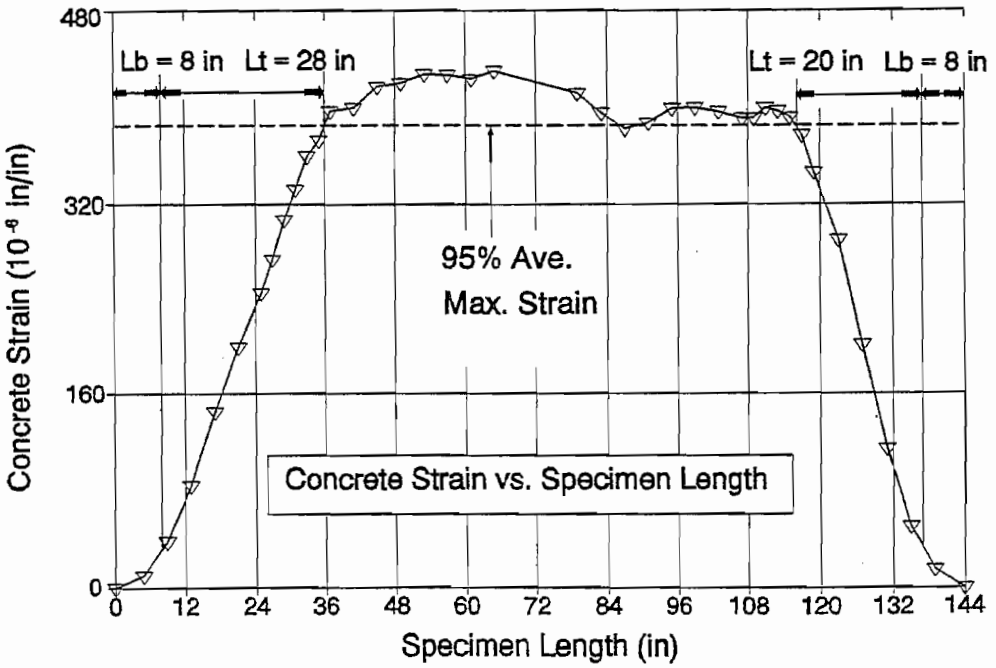

Figure A60. DC150 - 14 , Transfer Length

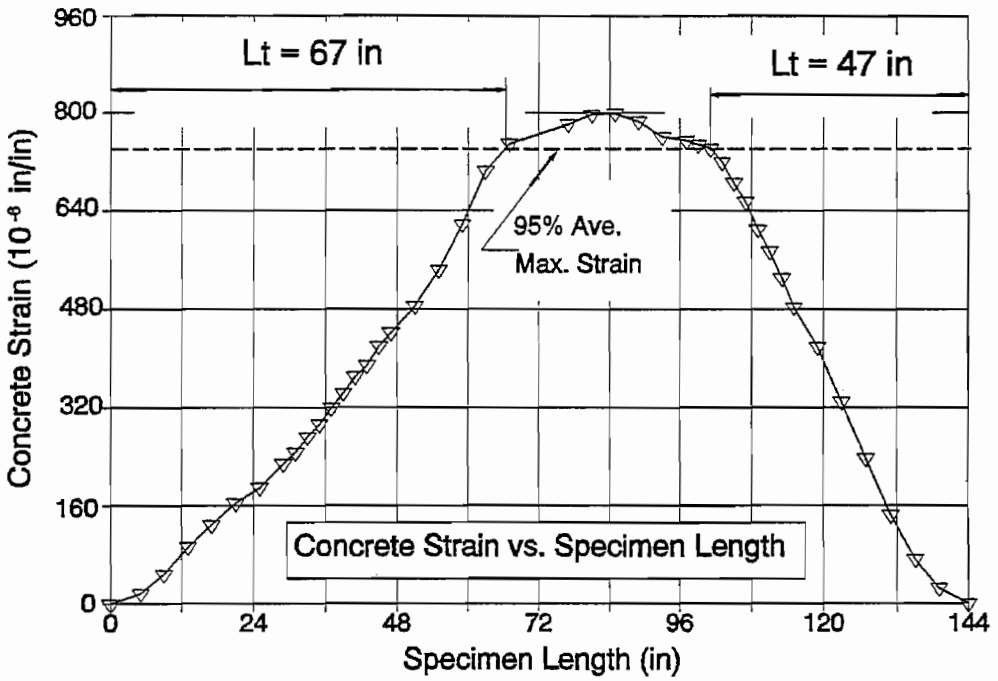

Figure A61. DC160 - 13 , Transfer Length

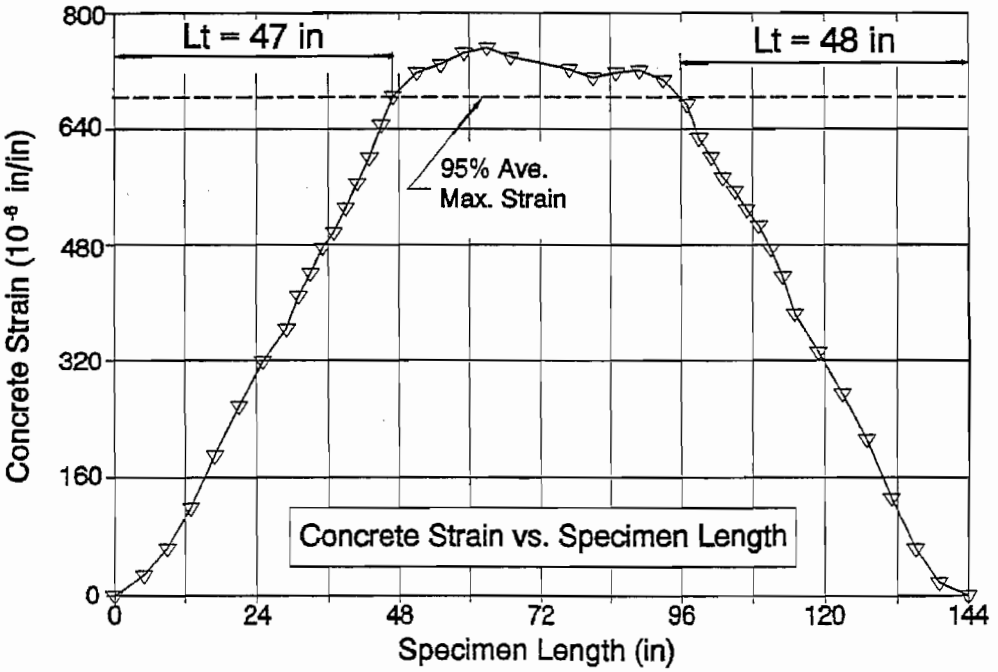

Figure A62. DC160 - 14 , Transfer Length

APPENDIX B
MATERIAL PROPERTIES

Load versus strain curves for the prestressing strand are given in Figure B1. These data were supplied by the manufacturer, Florida Wire and Cable Company. Strand from three different reels was used. Transfer length specimens and the FA550 series development length beams were made with strand from Reel Number 734601. The FR350 and DB850 series used strand from Reel Number 815663. All of the 0.6 inch strand came from Reel Number 742251.

Concrete Strengths are given in Figures B2 through B18. Specimens made with each cast are noted. The casting date is also given in the upper right hand corner of each graph. The shaded areas denote the range of dates the specimens were tested.

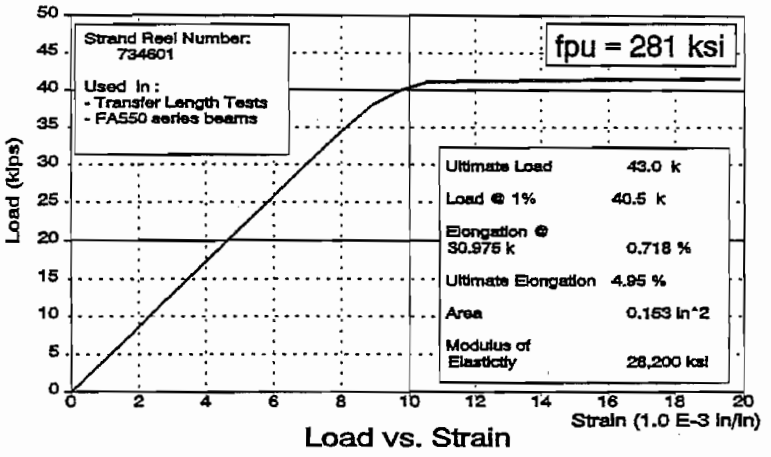

Load vs. Strain

0.5 Inch Diameter Low Relaxation Strand

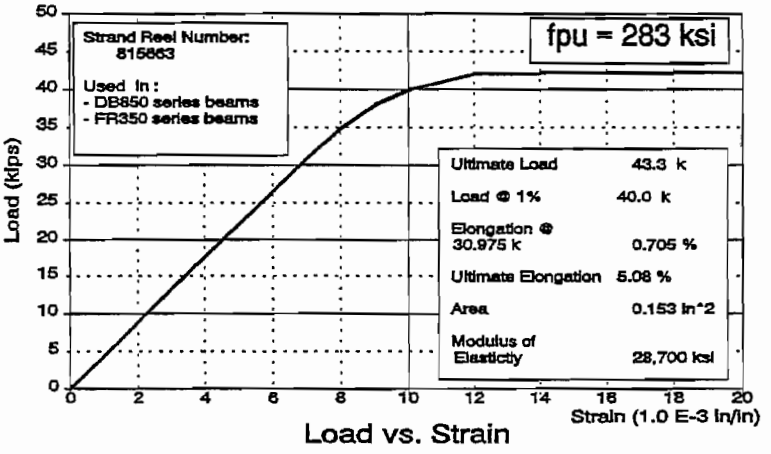

Load vs. Strain

0.5 Inch Diameter Low Relaxation Strand

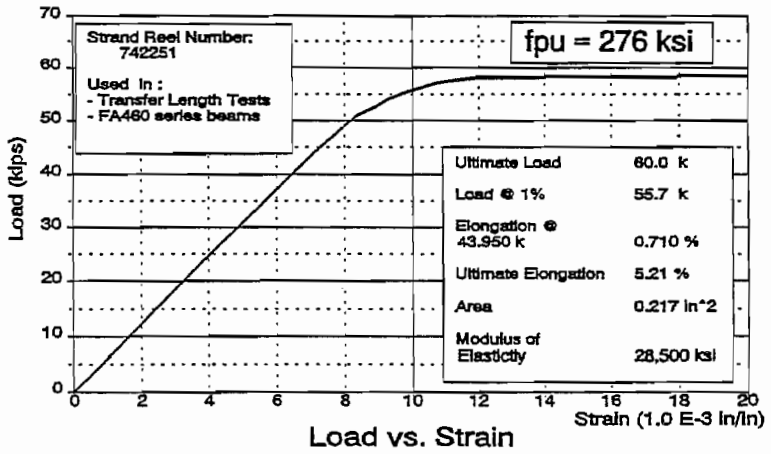

Load vs. Strain

0.6 inch Diameter Low Relaxation Strand

Figure B1. Load vs. Strain for Prestressing Strands

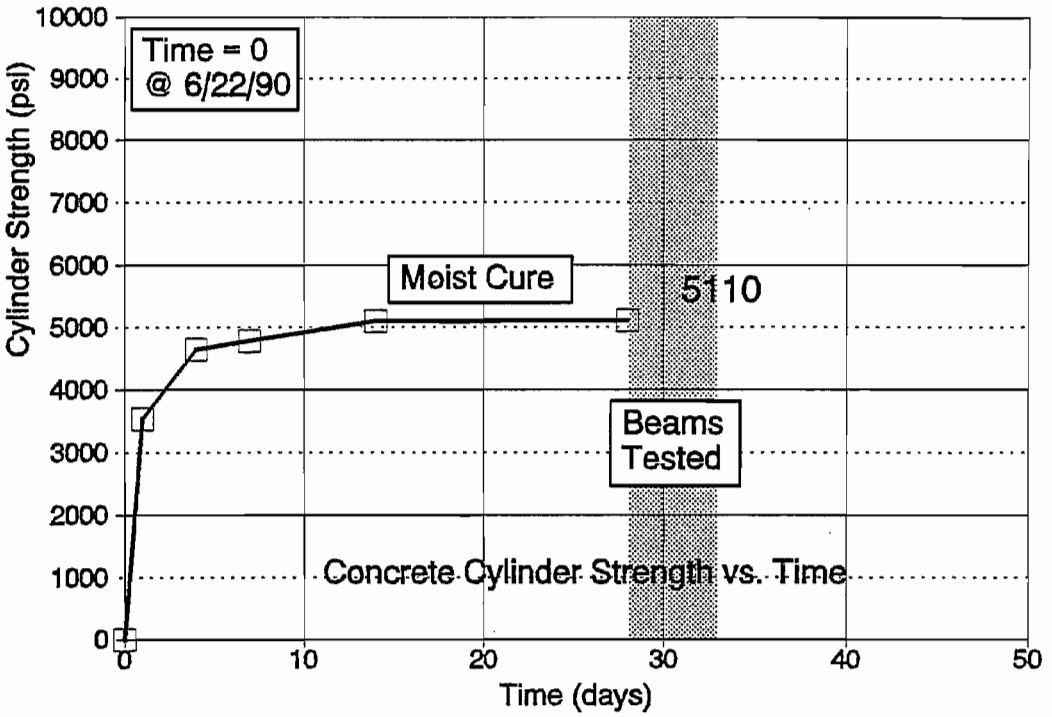

Figure B2. Beams FA550-1 and 2

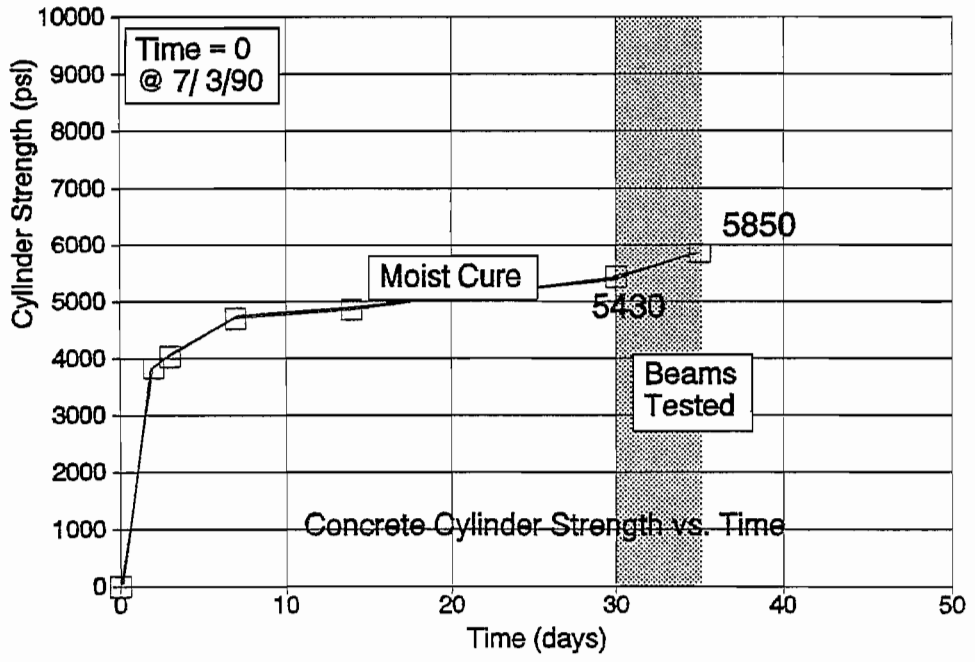

Figure B3. Beams FA550-3 and 4

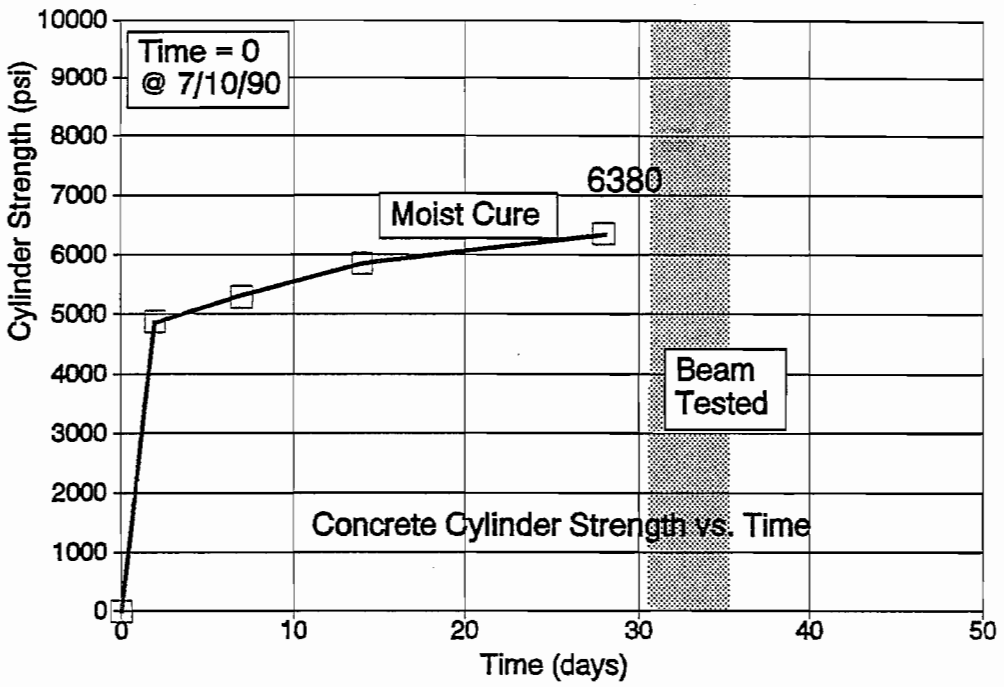

Figure B4. Beam FA460-1

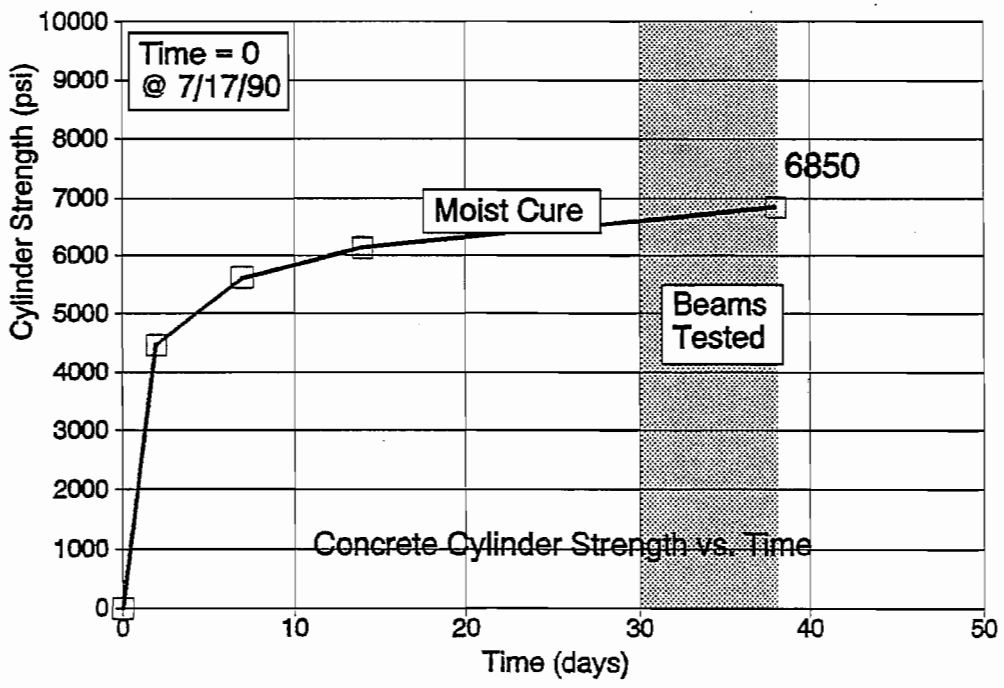

Figure B5. Beams FA460-2 and 3

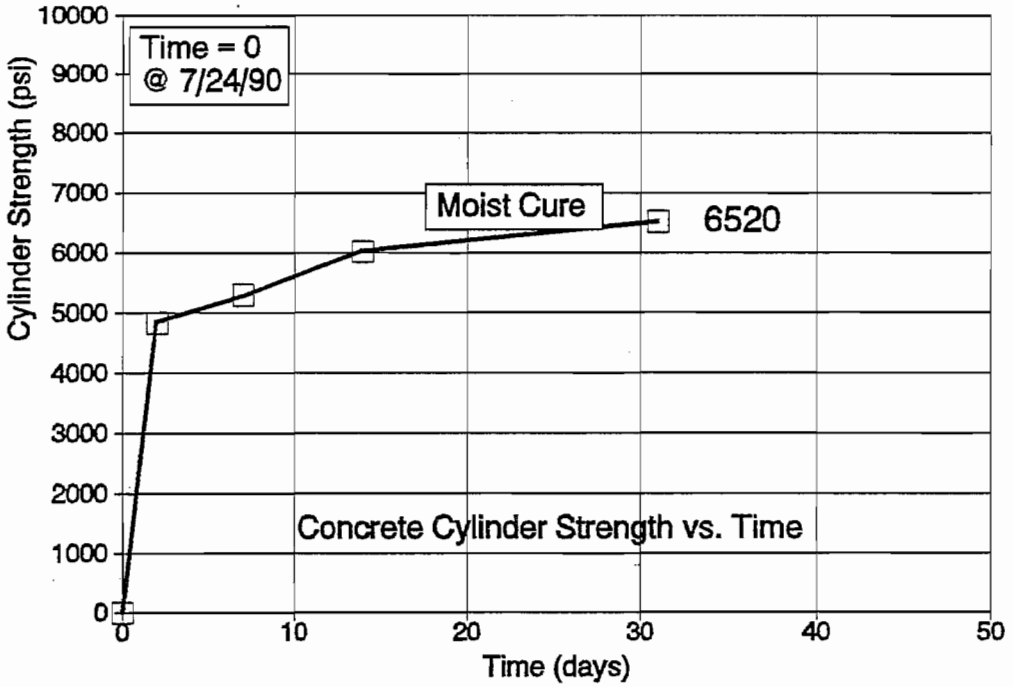

Figure B6. Beams FA460-F4

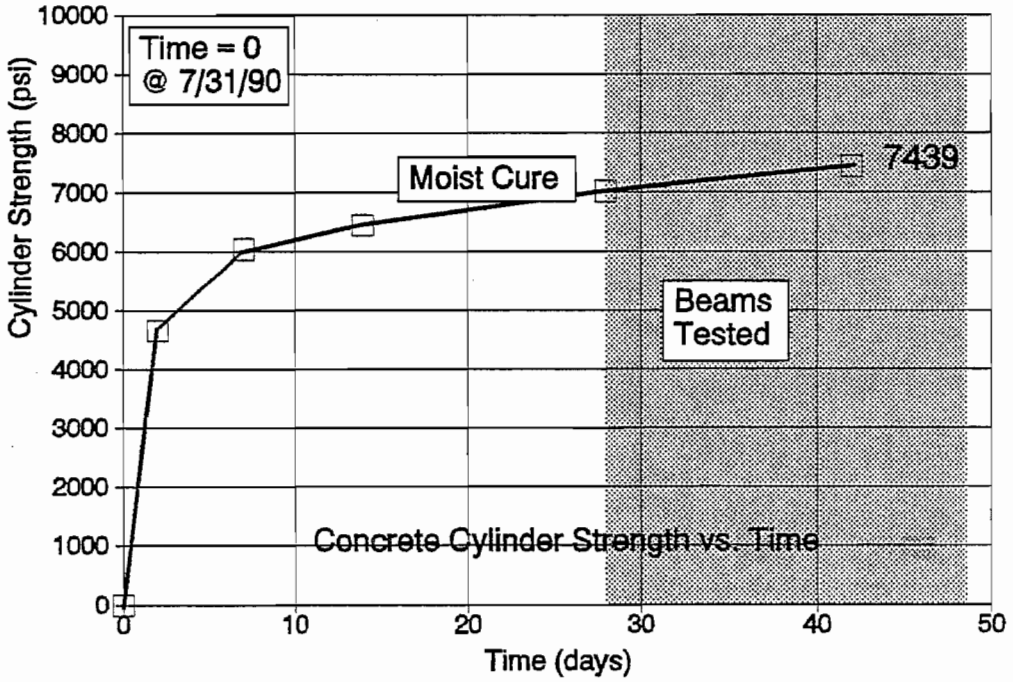

Figure B7. Beams FA460-5 and 6

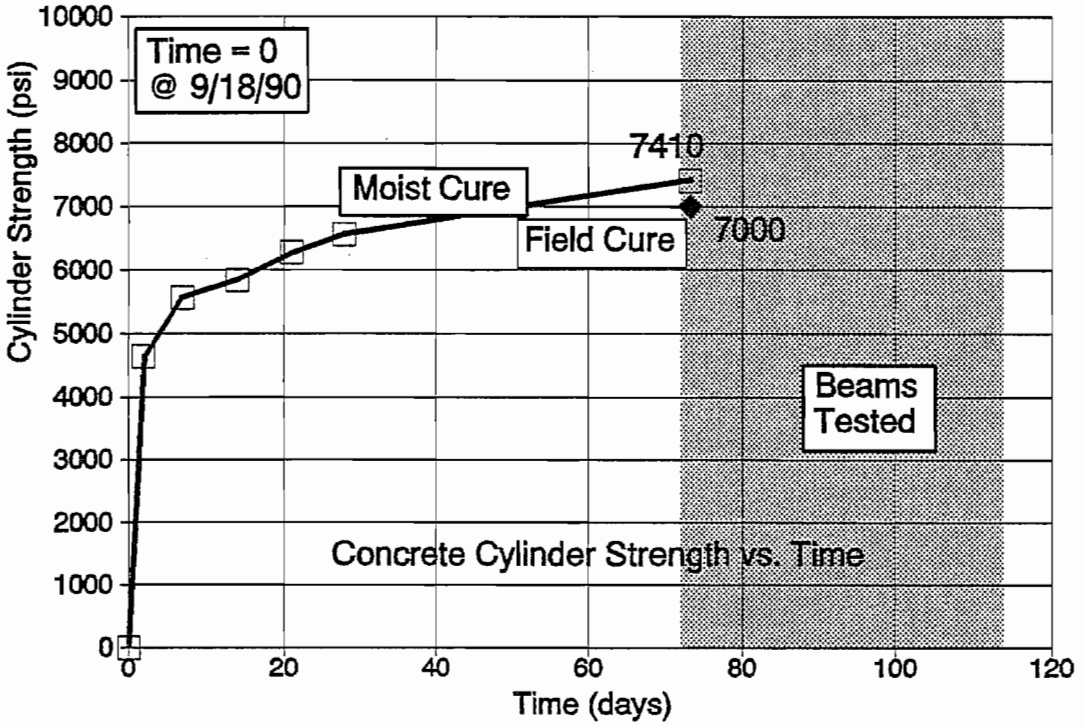

Figure B8. Beams DB850-1 and 2

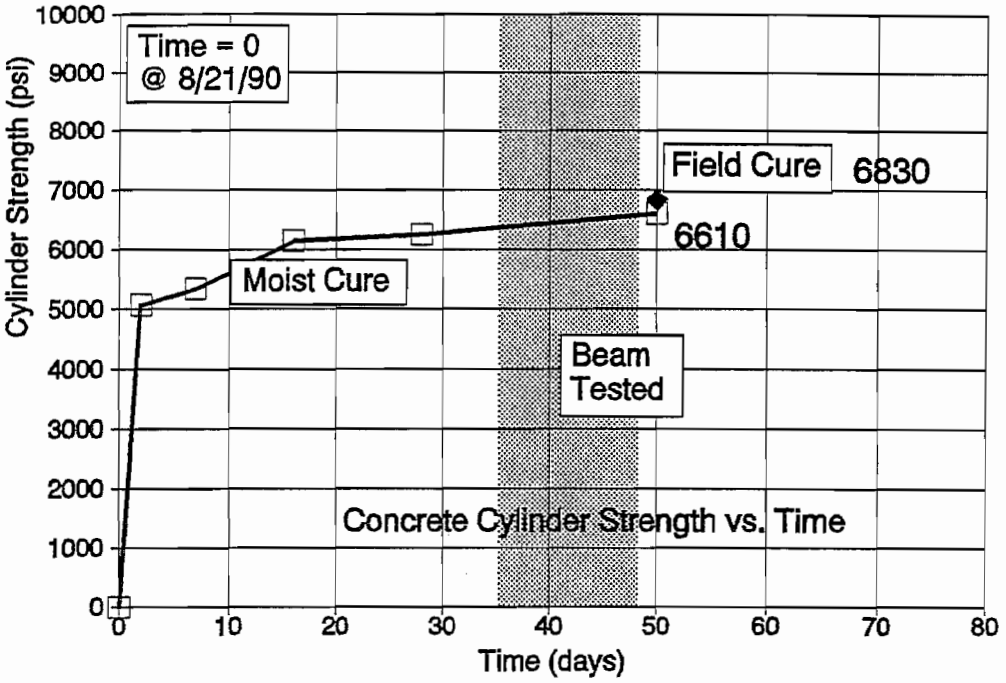

Figure B9. Beam DB850-3

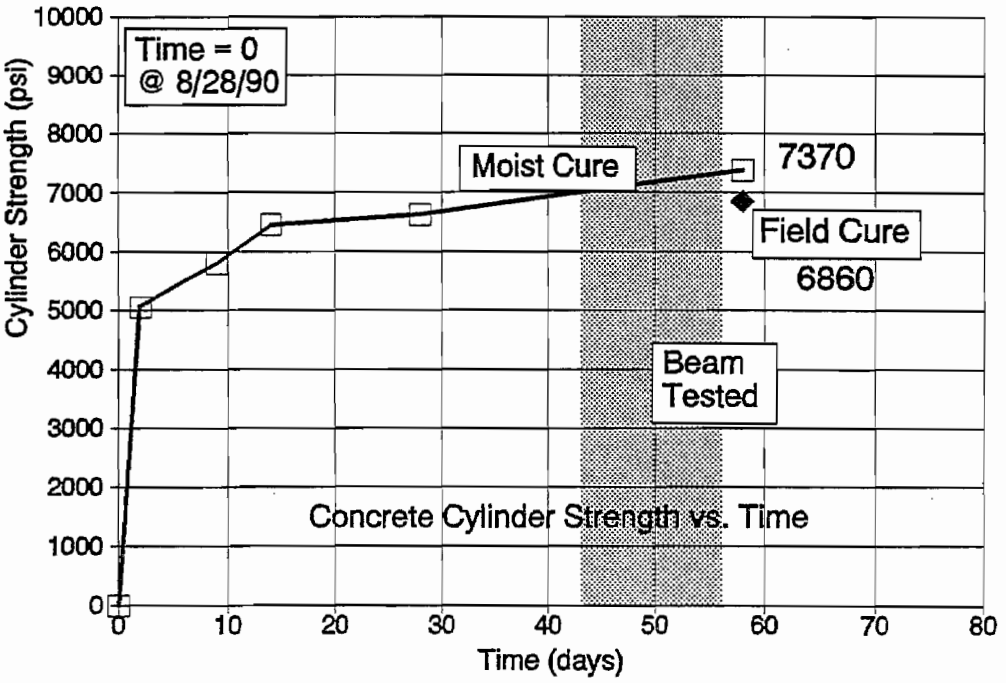

Figure B10. Beam DB850-4

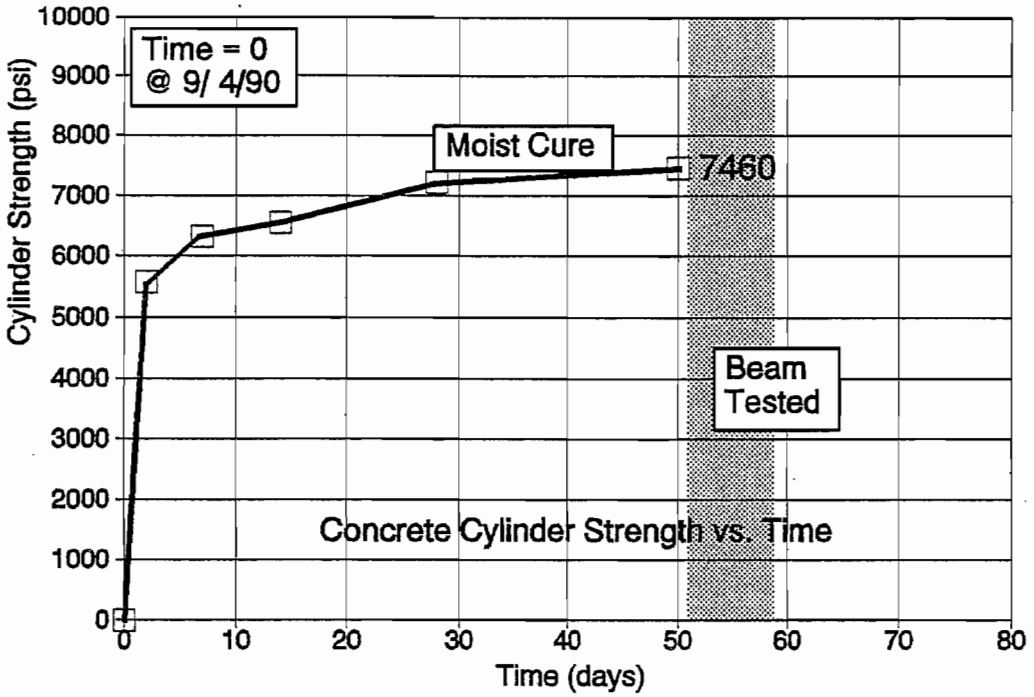

Figure B11. Beam DB850-5

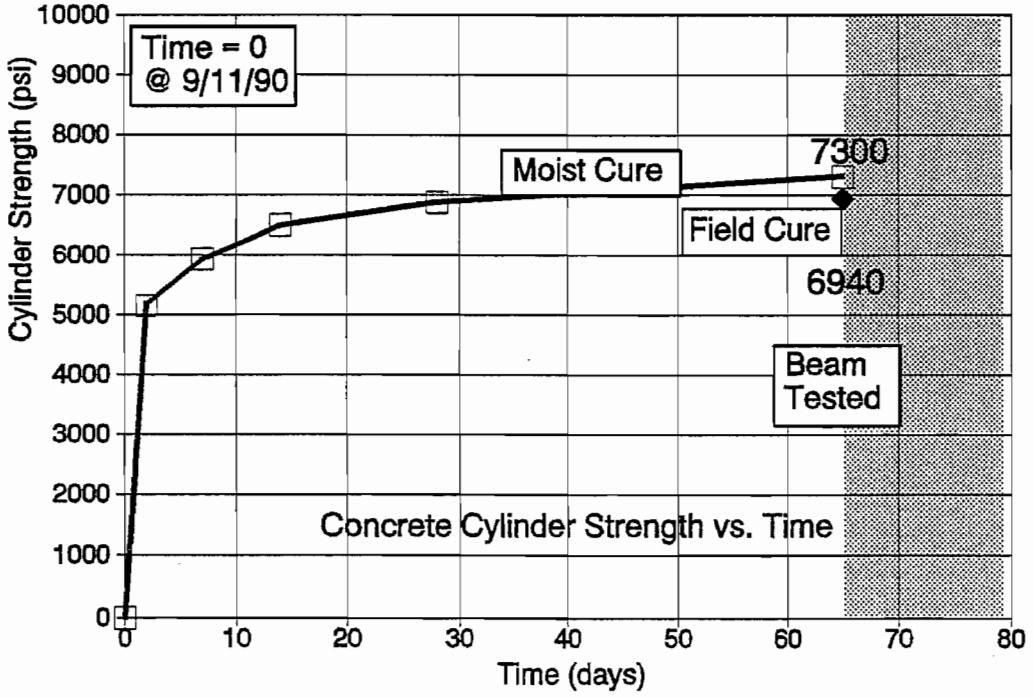

Figure B12. Beam DB850-6

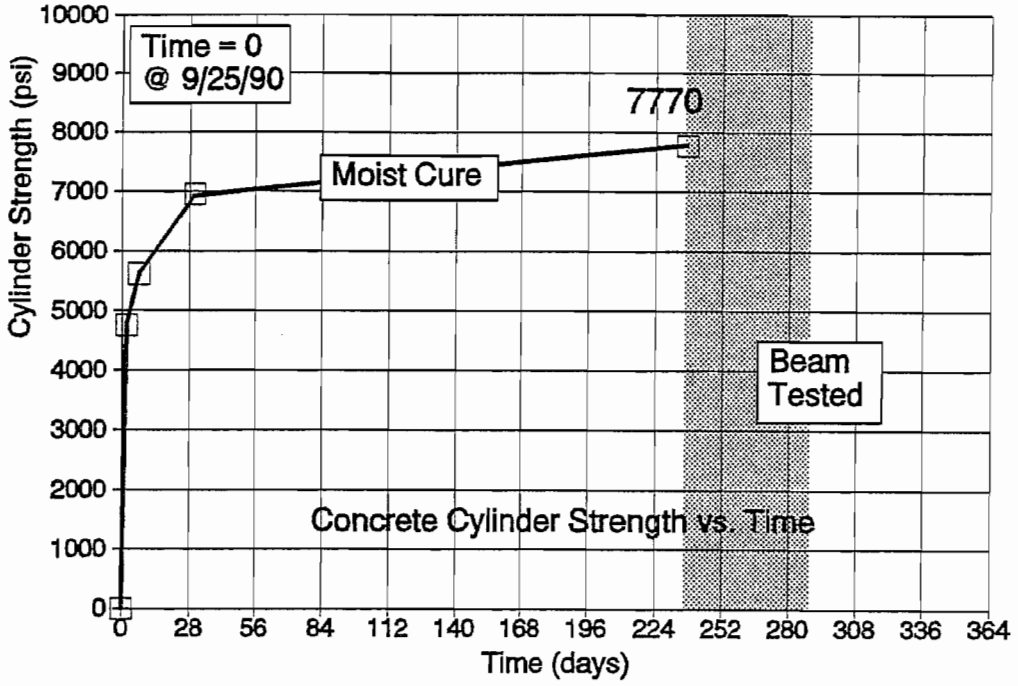

Figure B13. Beam DB850-F1

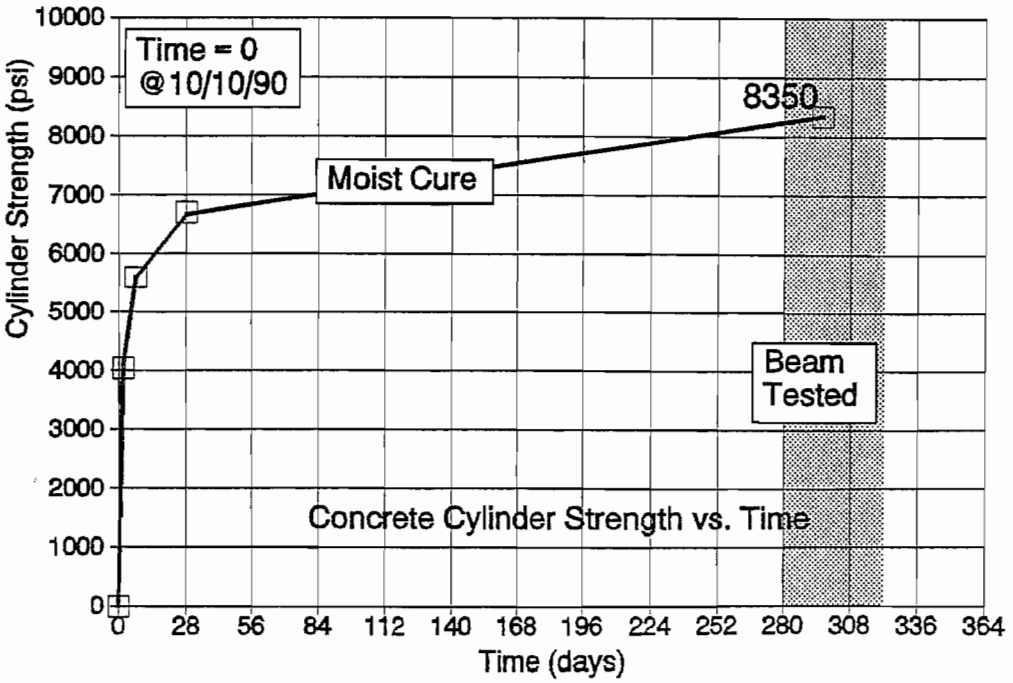

Figure B14. Beam DB850-F2

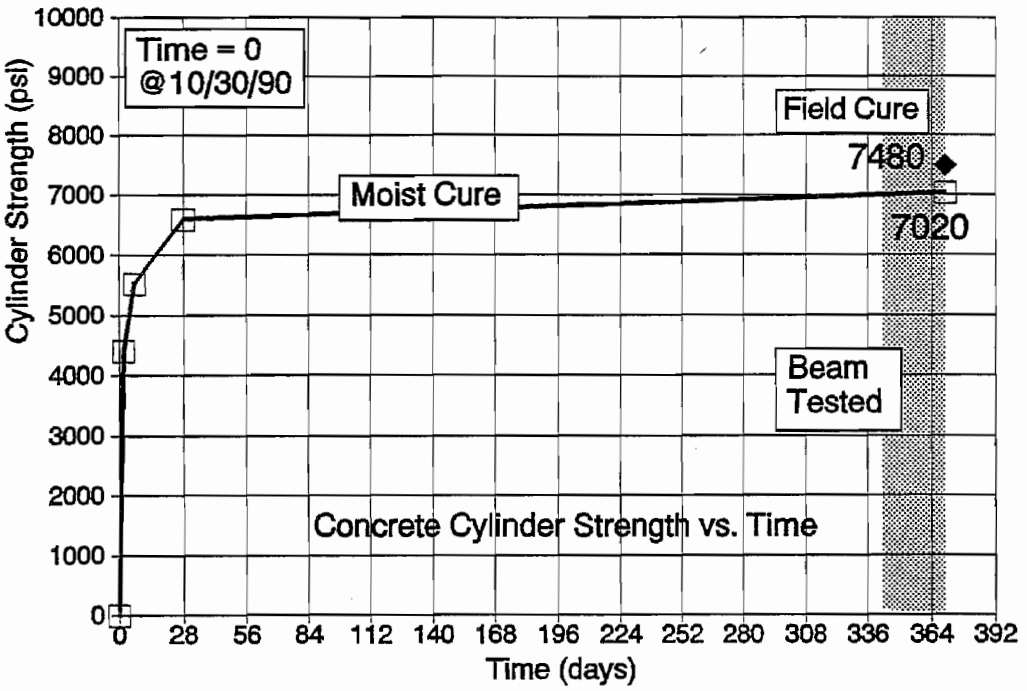

Figure B15. Beam DB850-F3

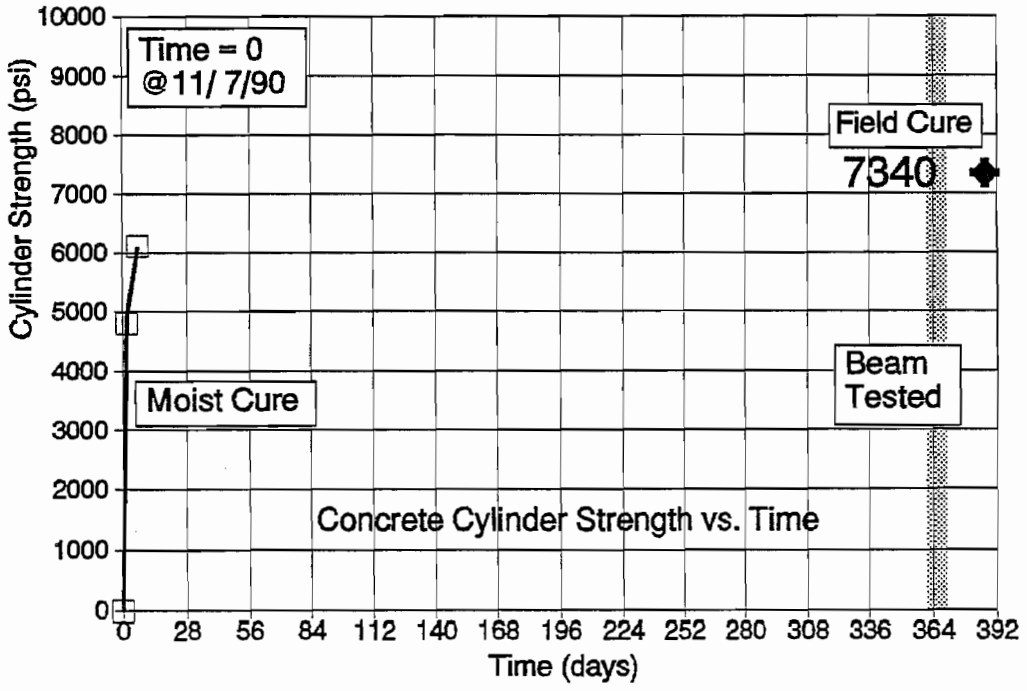

Figure B16. Beam DB850-F4

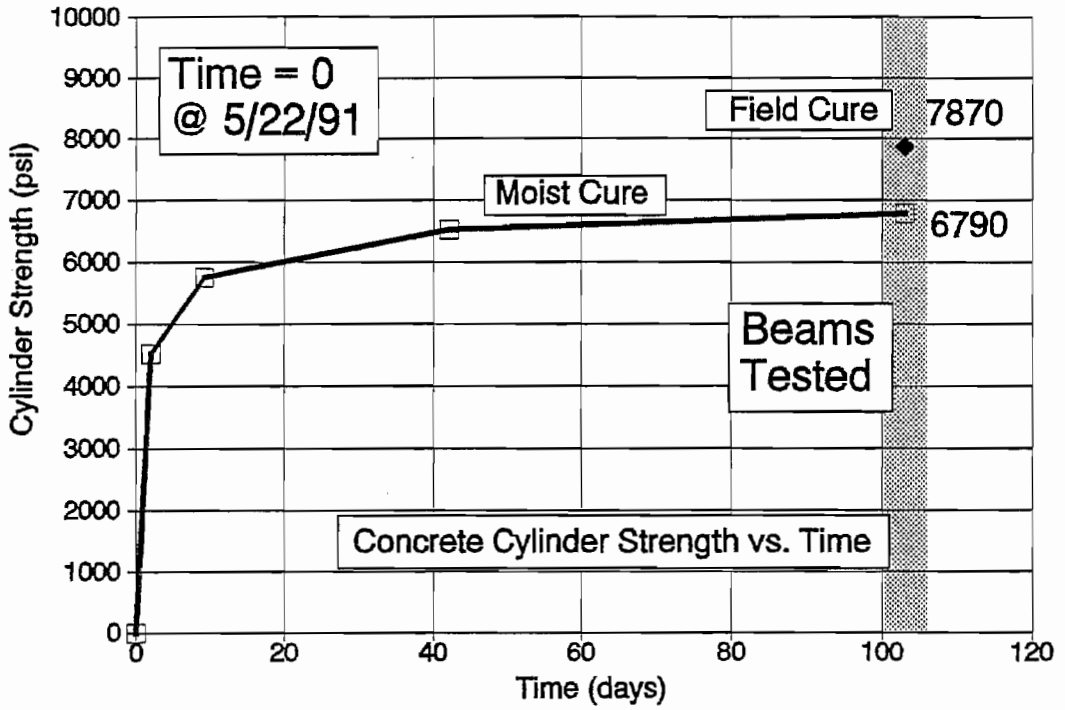

Figure B17. Beams FR350-1 and 2

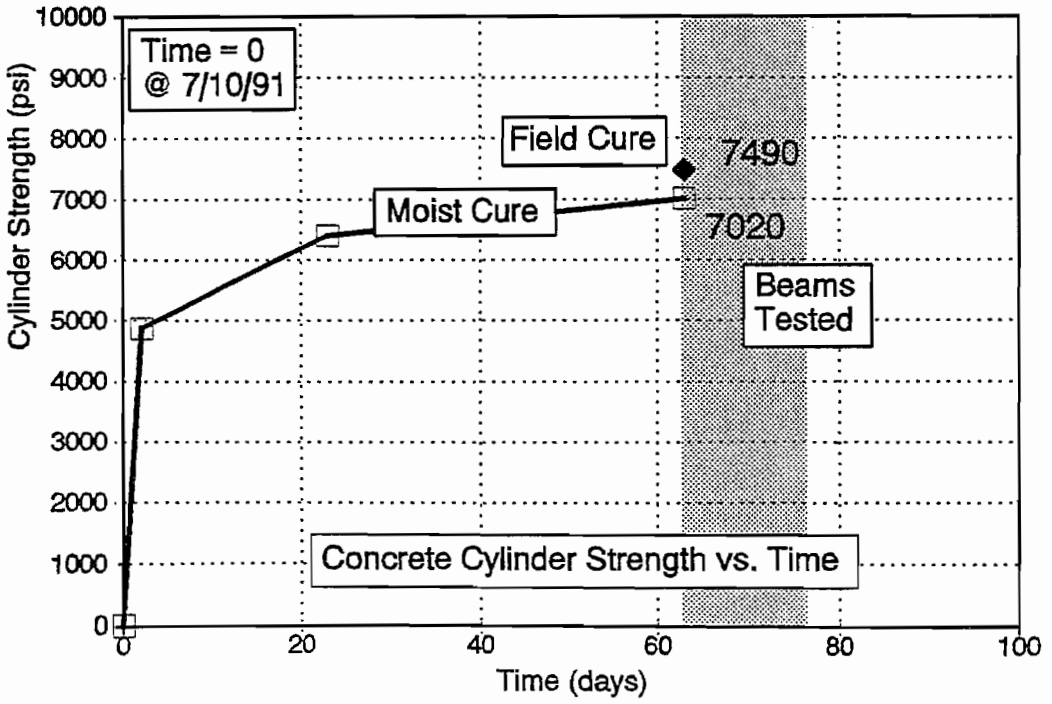

Figure B18. Beams FR360-1 and 2

APPENDIX C
LOAD VERSUS DEFLECTION AND END SLIPS FOR STATIC FLEXURAL TESTS

This Appendix contains the load versus deflection curves for all of the statically loaded development length tests. These tests include AASHTO-type beams, Specimen numbers FA550-1 through 4 and FA460-1 through 3, 5, and 6, and rectangular beams, Specimen numbers FR350-1 and 2 and FR360-1 and 2. End Slips are plotted on the same graphs to illustrate the relationship between cracking and strand slips. Overall beam behavior is demonstrated in these curves. End slips are related to web shear cracking in the case of I-shaped AASHTO-type beams. Significant cracking is noted on the load deflection curves.

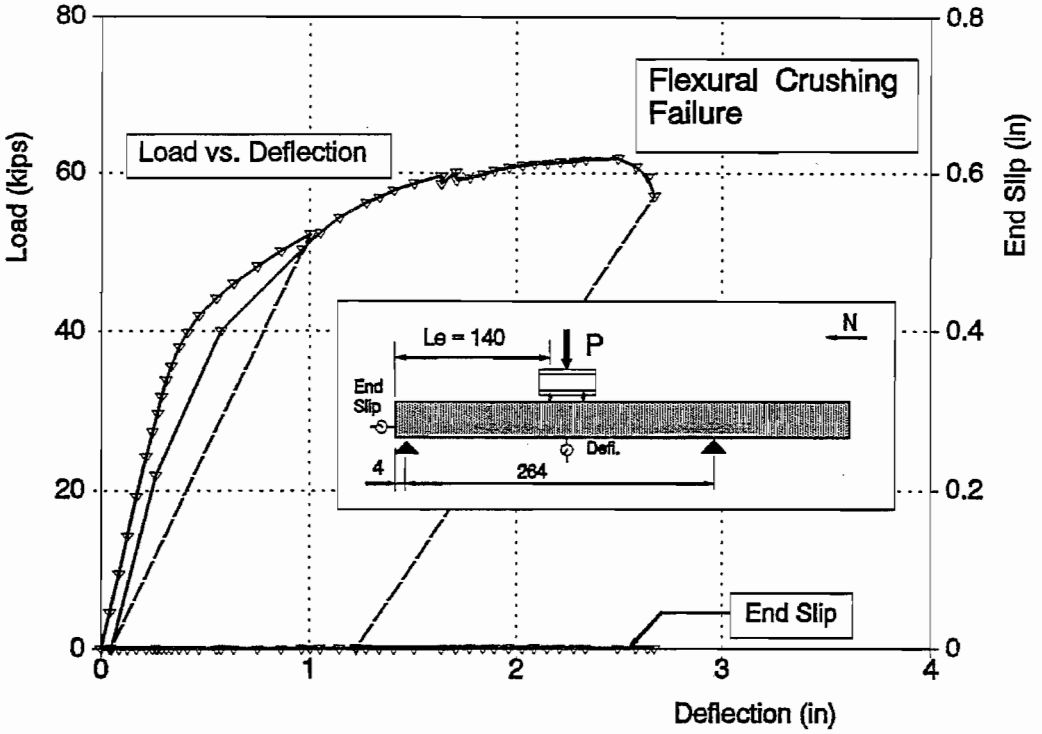

Figure C1. Beam FA550-1 Test A

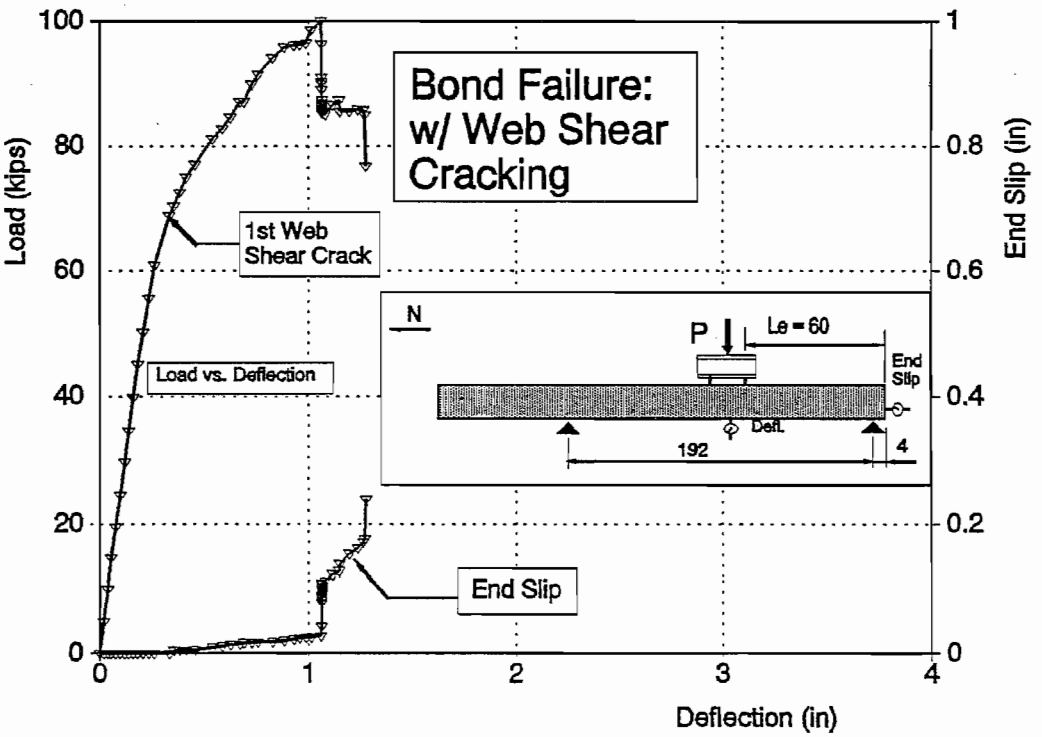

Figure C2. Beam FA550-1 Test B

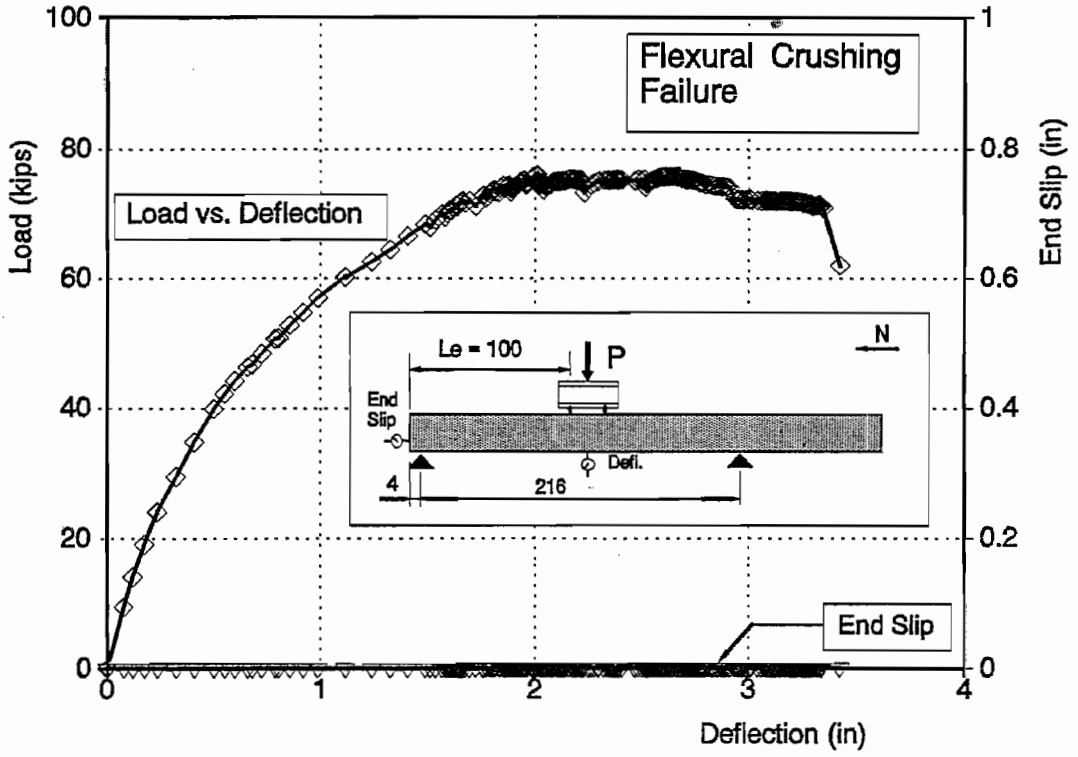

Figure C3. Beam FA550-1 Test C

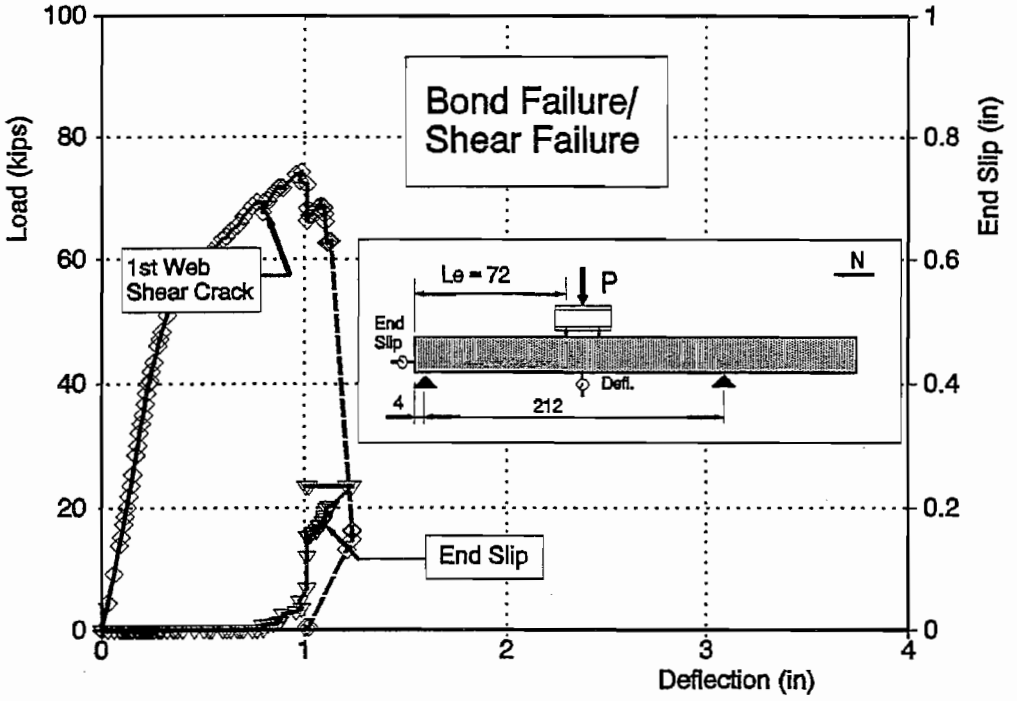

Figure C4. Beam FA550-2 Test A

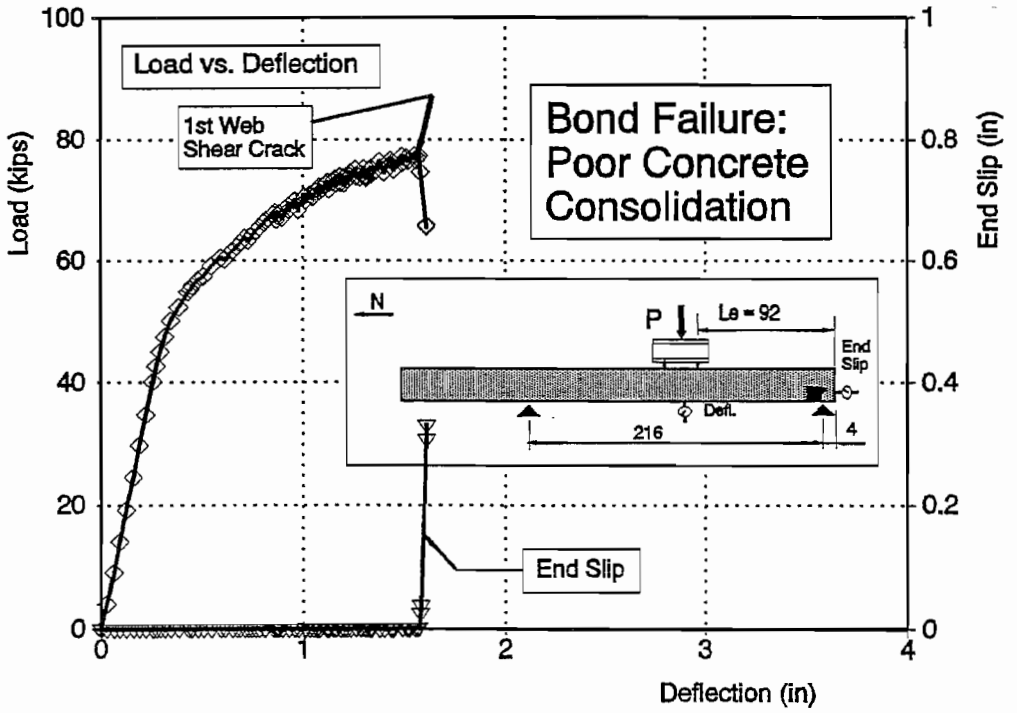

Figure C5. Beam FA550-2 Test B

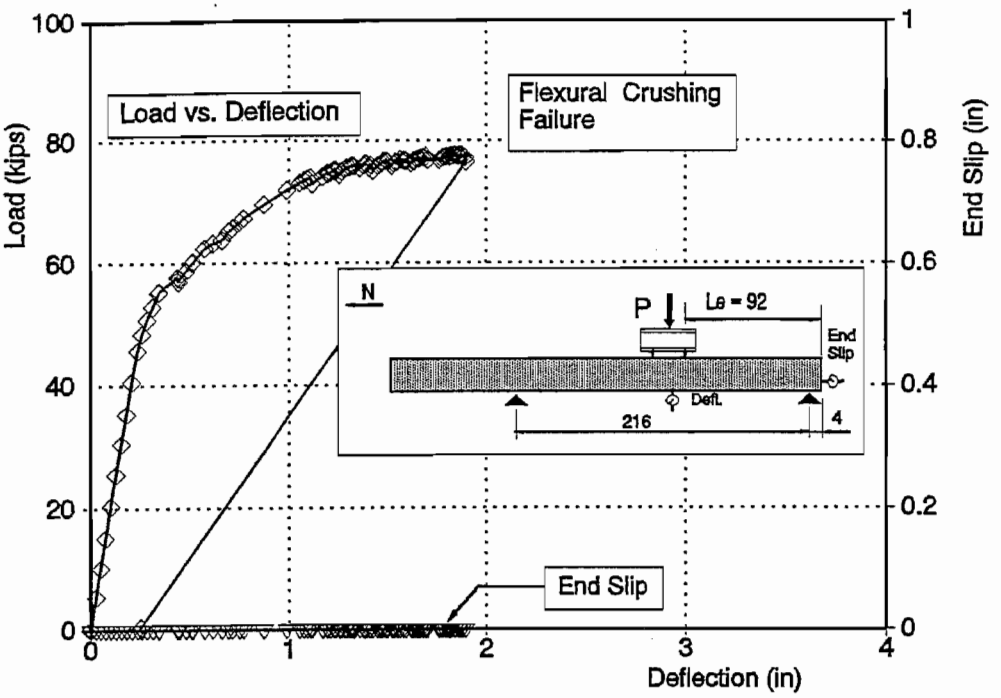

Figure C6. Beam FA550-3 Test A

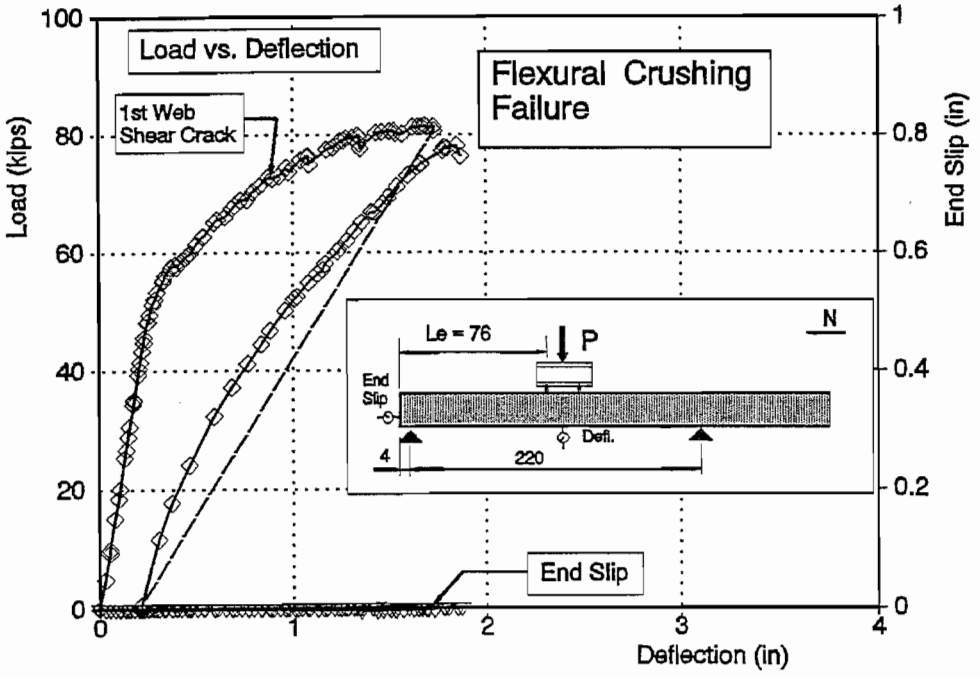

Figure C7. Beam FA550-3 Test B

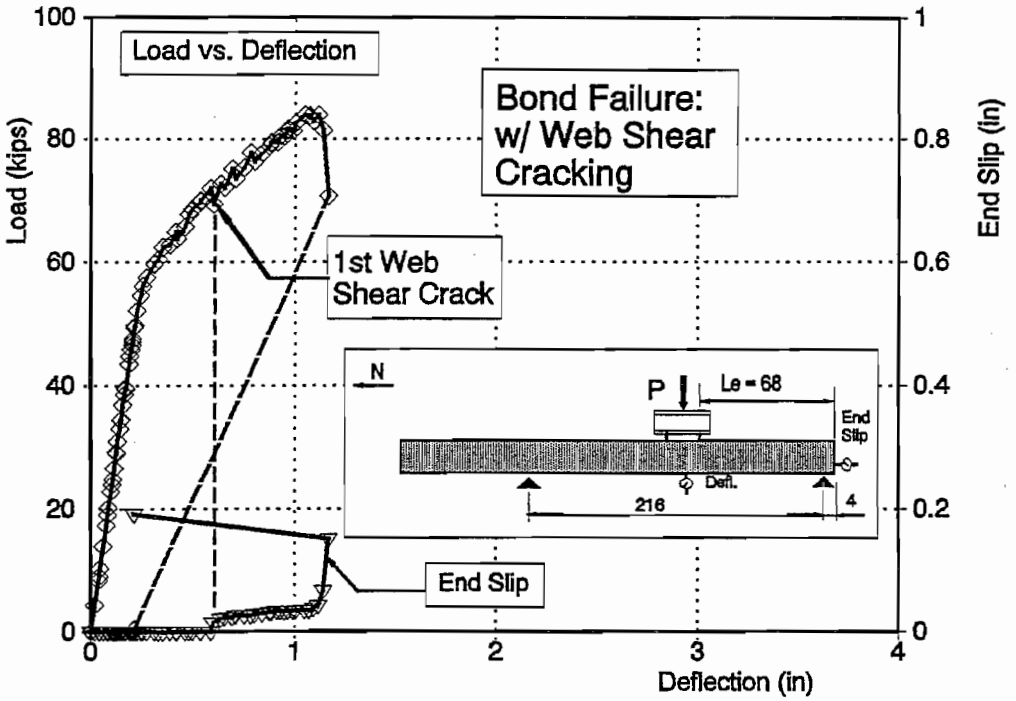

Figure C8. Beam FA550-4 Test A

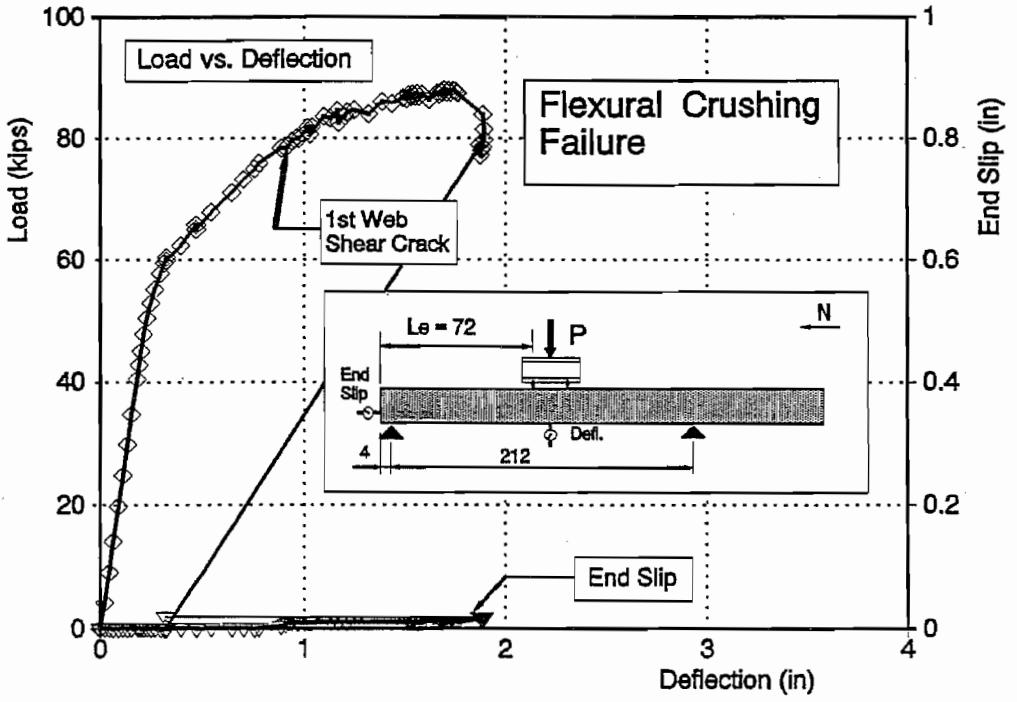

Figure C9. Beam FA550-4 Test B

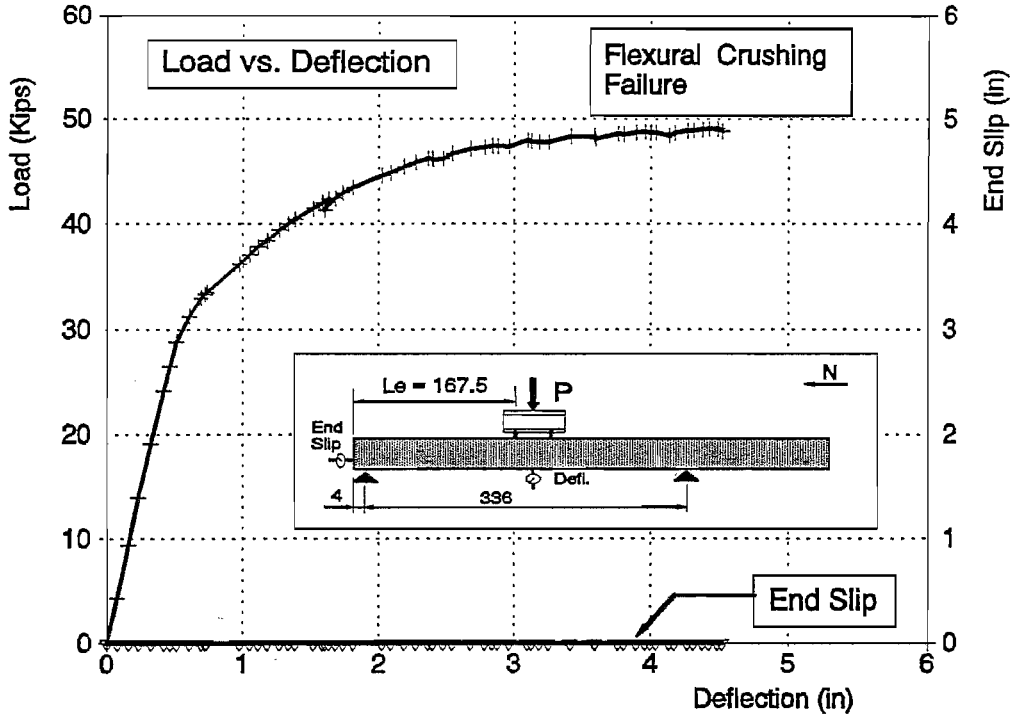

Figure C10. Beam FA460-1 Test A

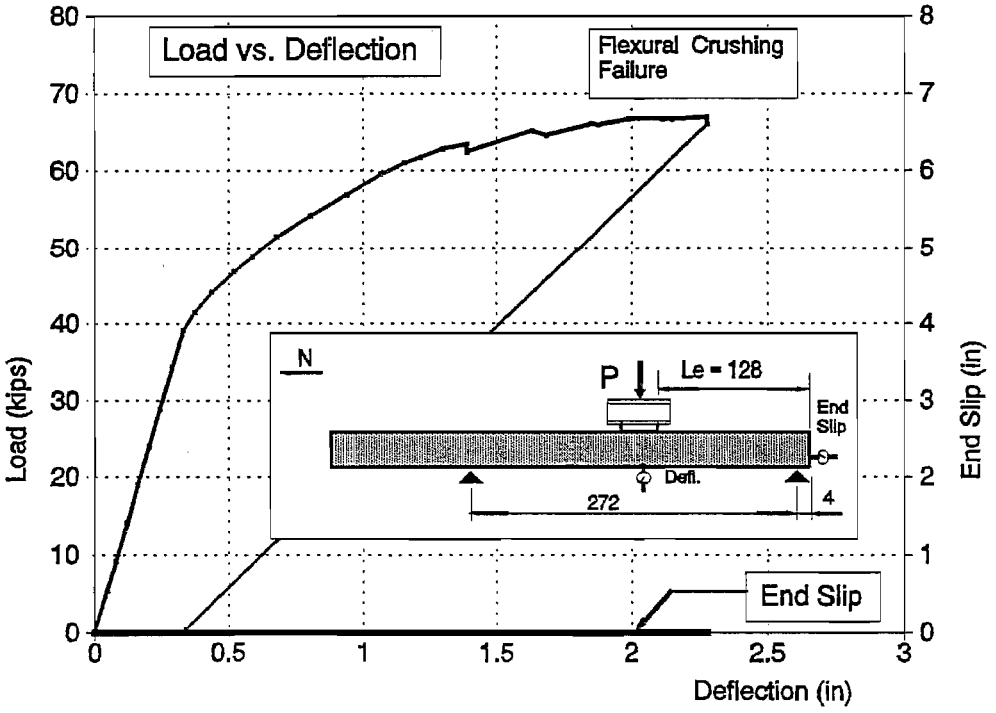

Figure C11. Beam FA460 - 1 Test B

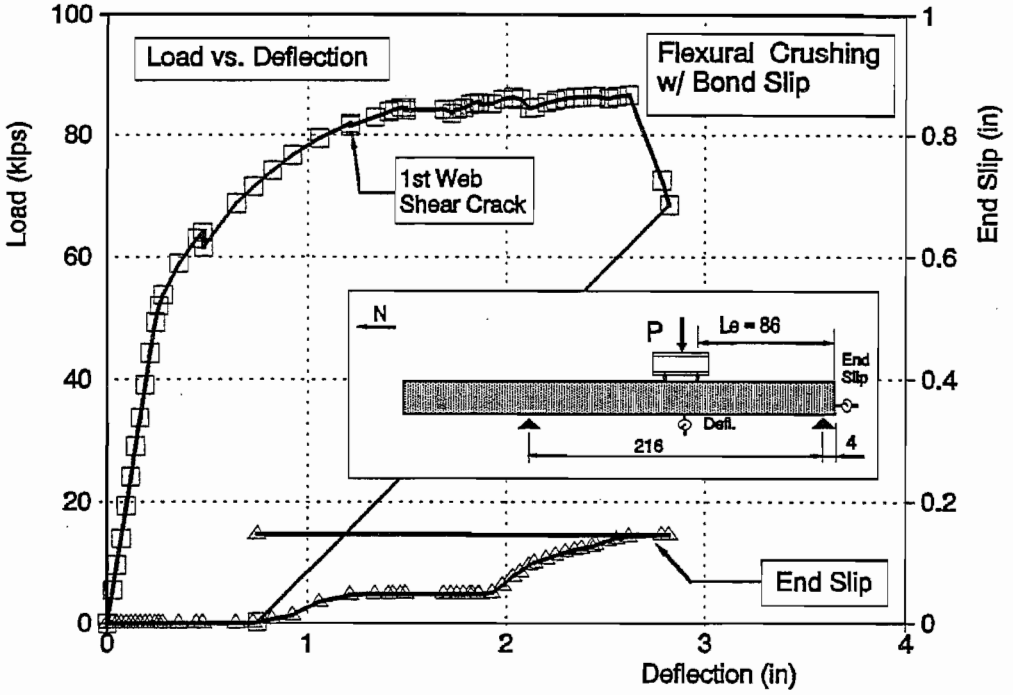

Figure C12. Beam FA460-2 Test A

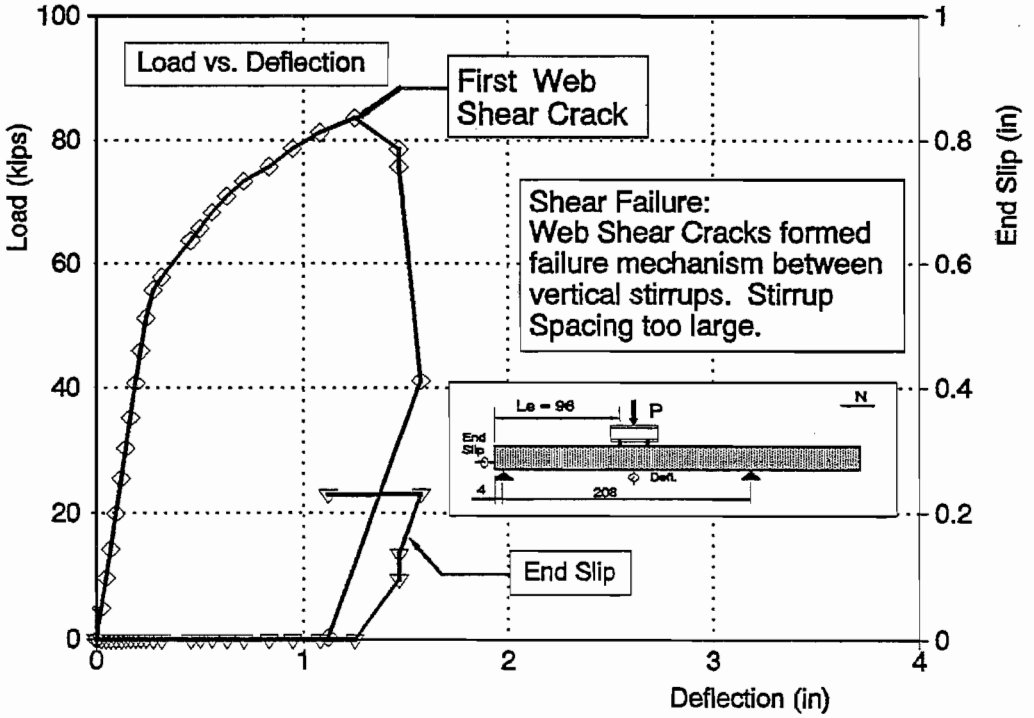

Figure C13. Beam FA460-2 Test B

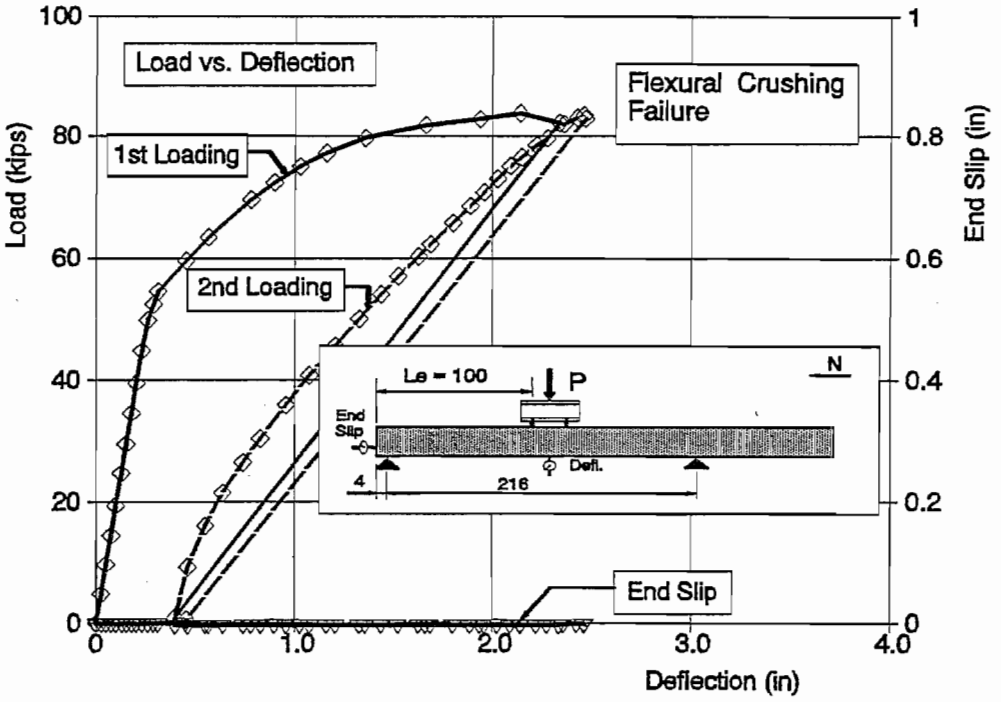

Figure C14. Beam FA460-3 Test A

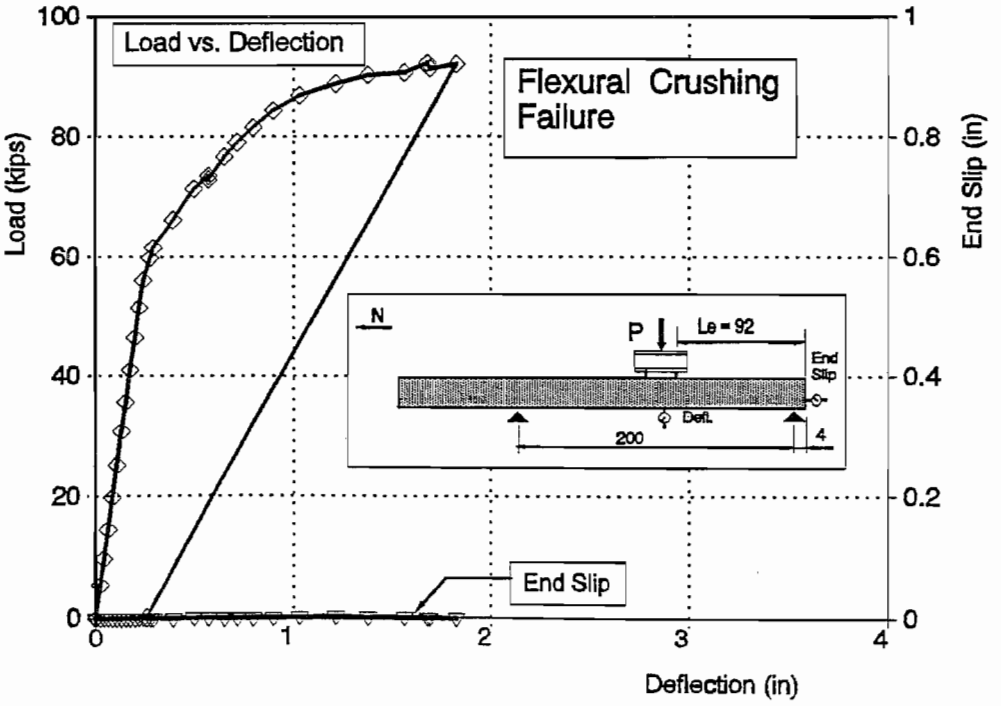

Figure C15. Beam FA460-3 Test B

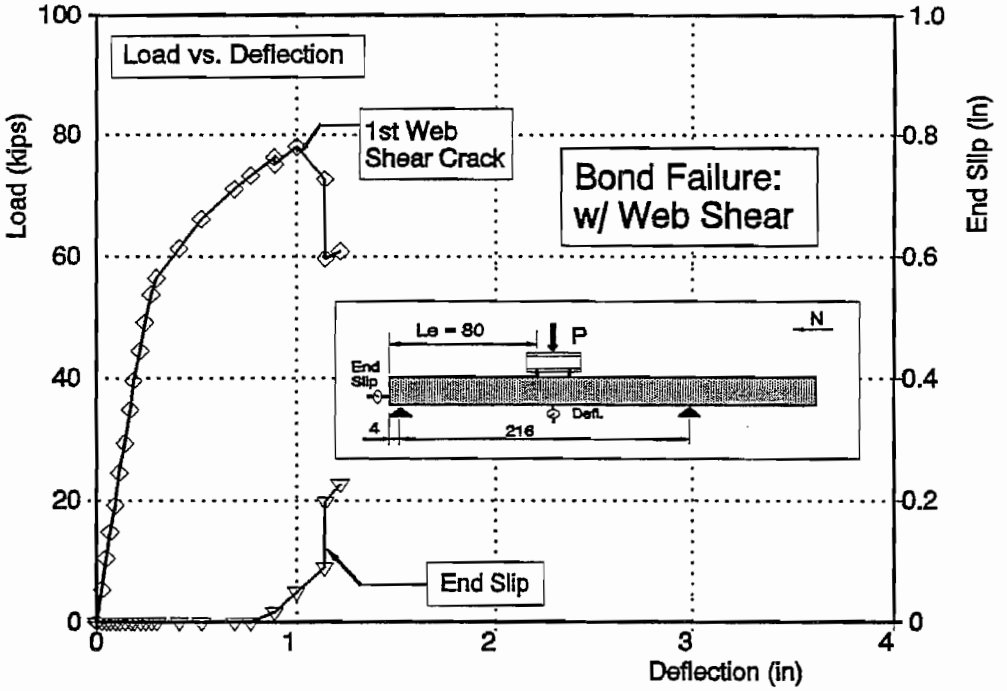

Figure C16. Beam FA460-5 Test A

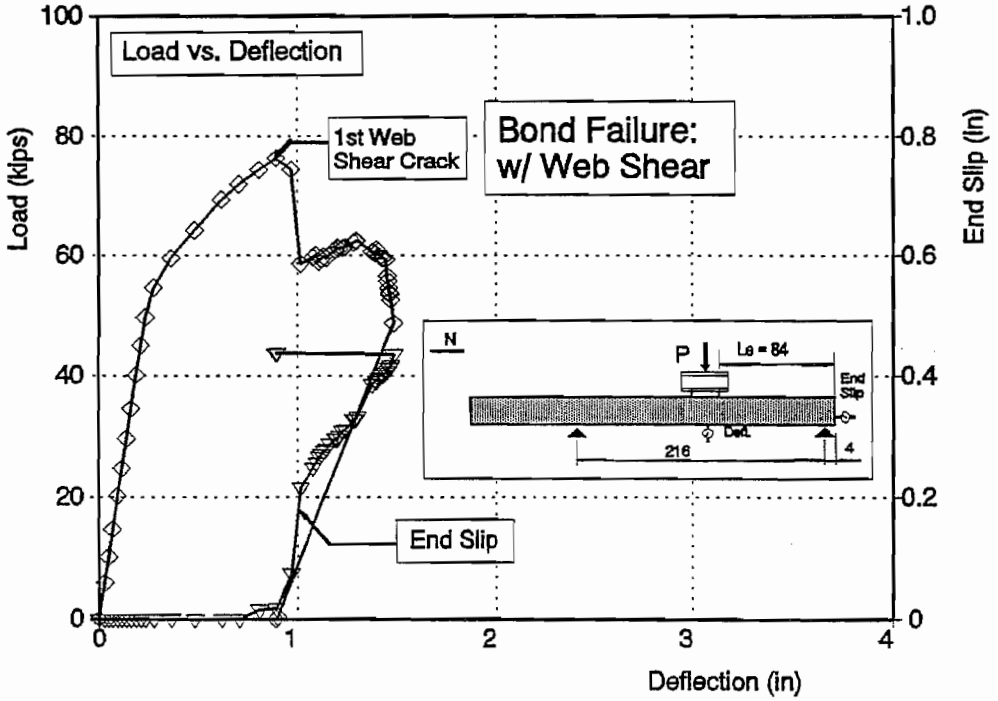

Figure C17. Beam FA460-5 Test B

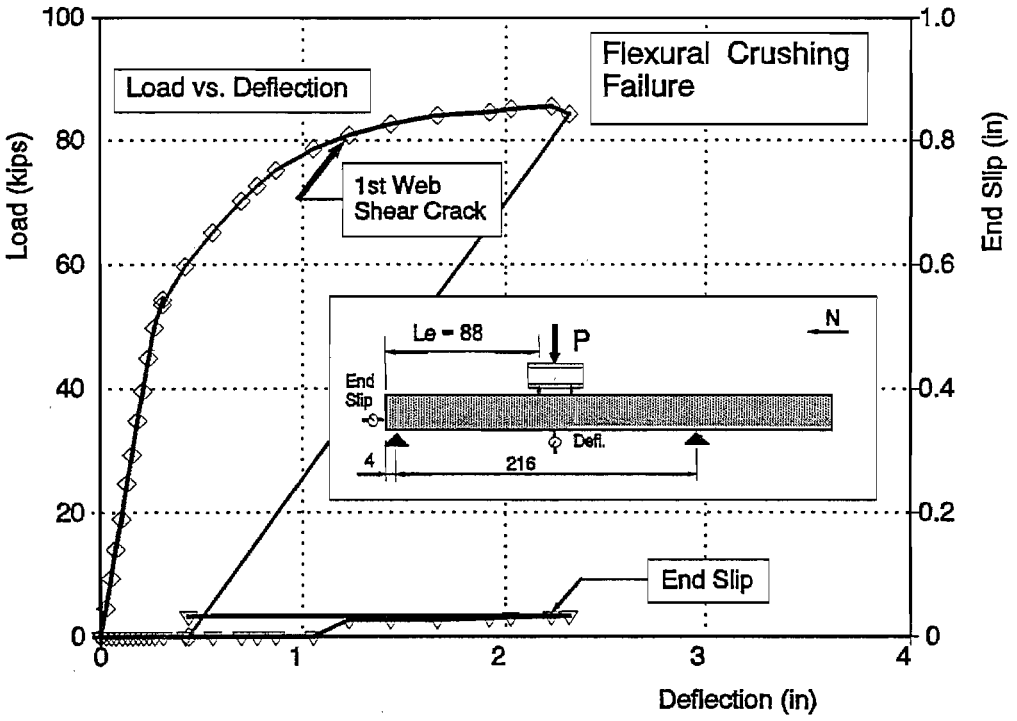

Figure C18. Beam FA460-6 Test A

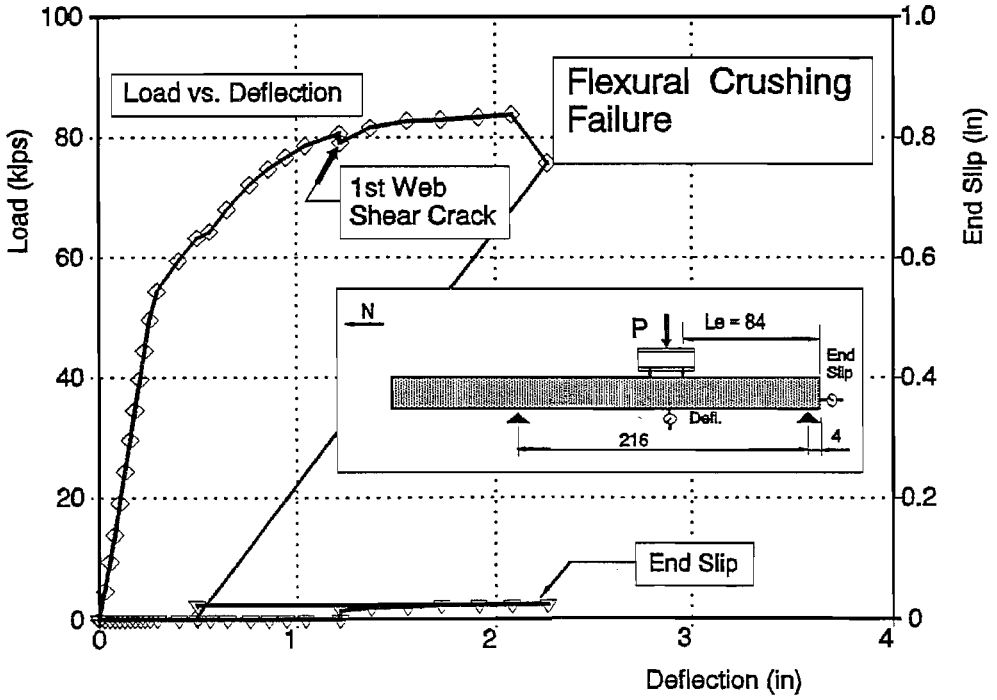

Figure C19. Beam FA460-6 Test B

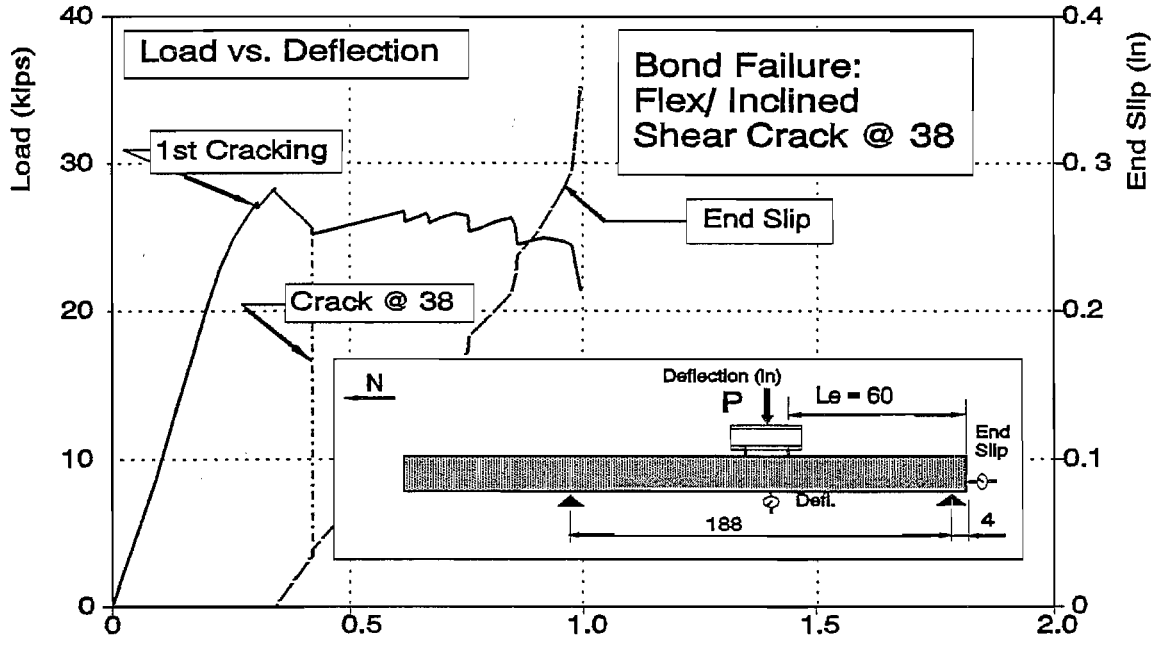

Figure C20. Beam fR350-1 Test A

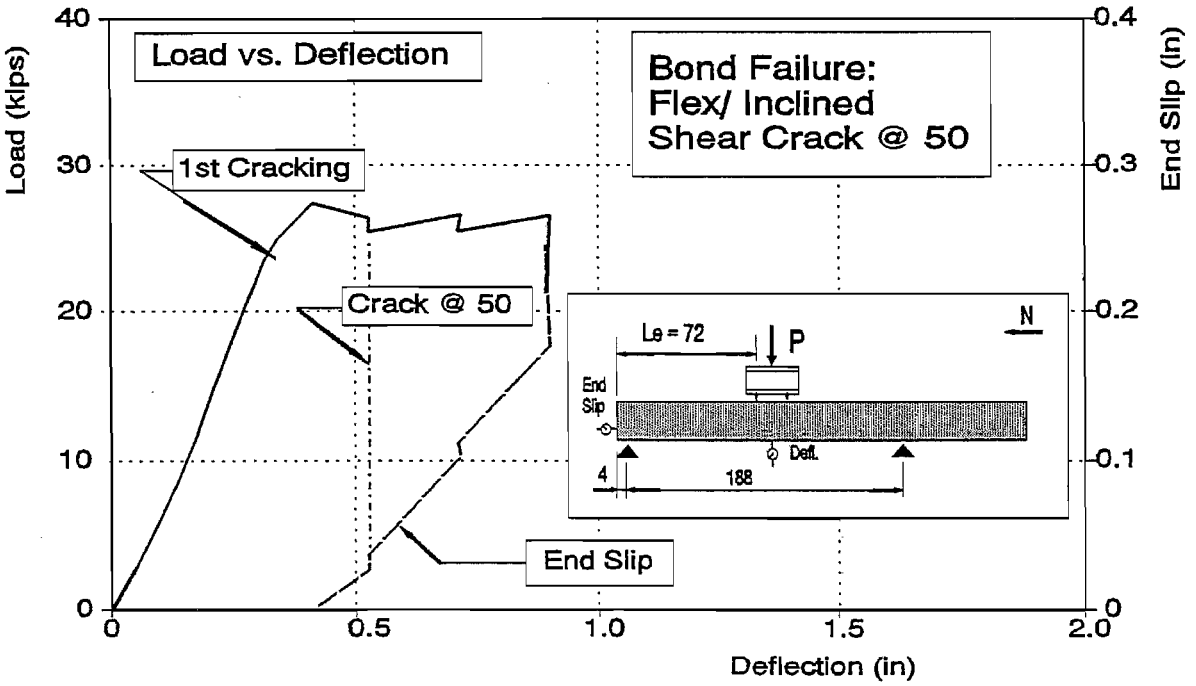

Figure C21. Beam FR350-1 Test B

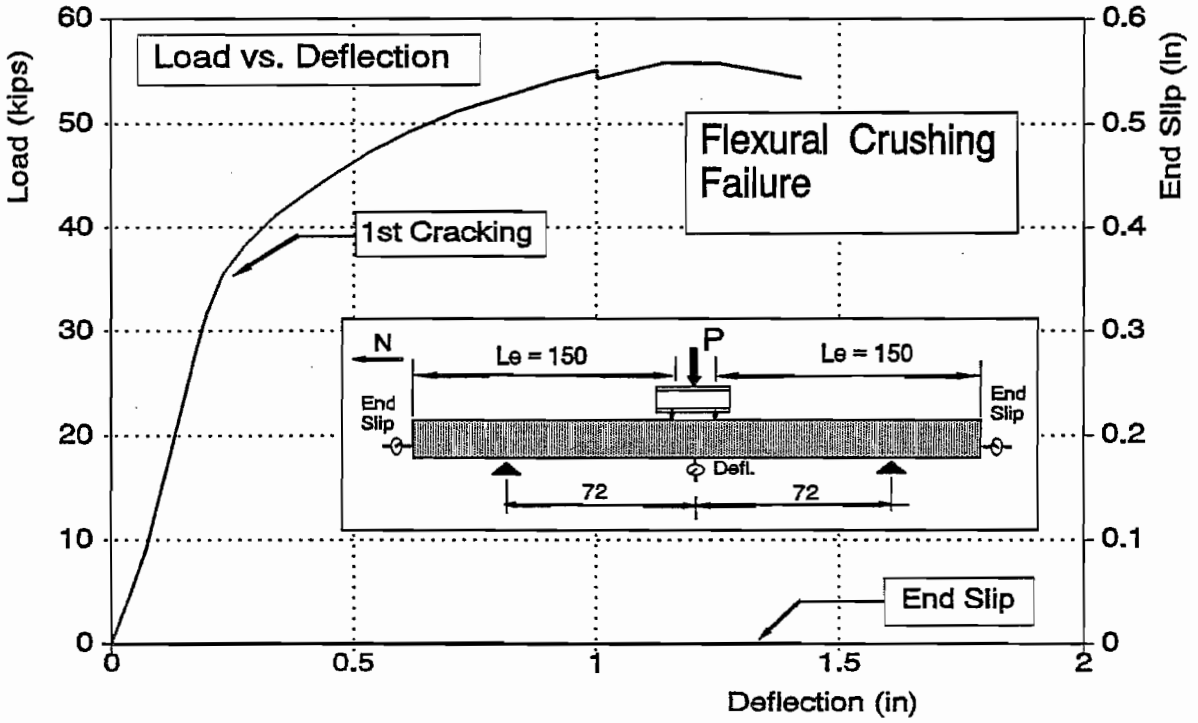

Figure C22. Beam fR350-1 Test C

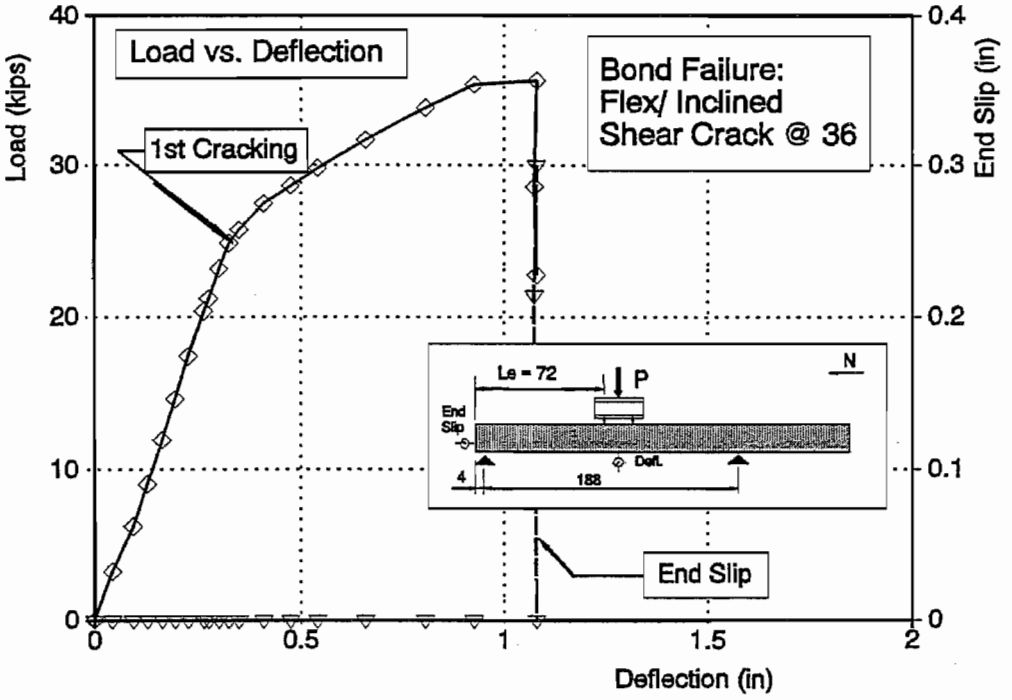

Figure C23. Beam FR350-2 Test A

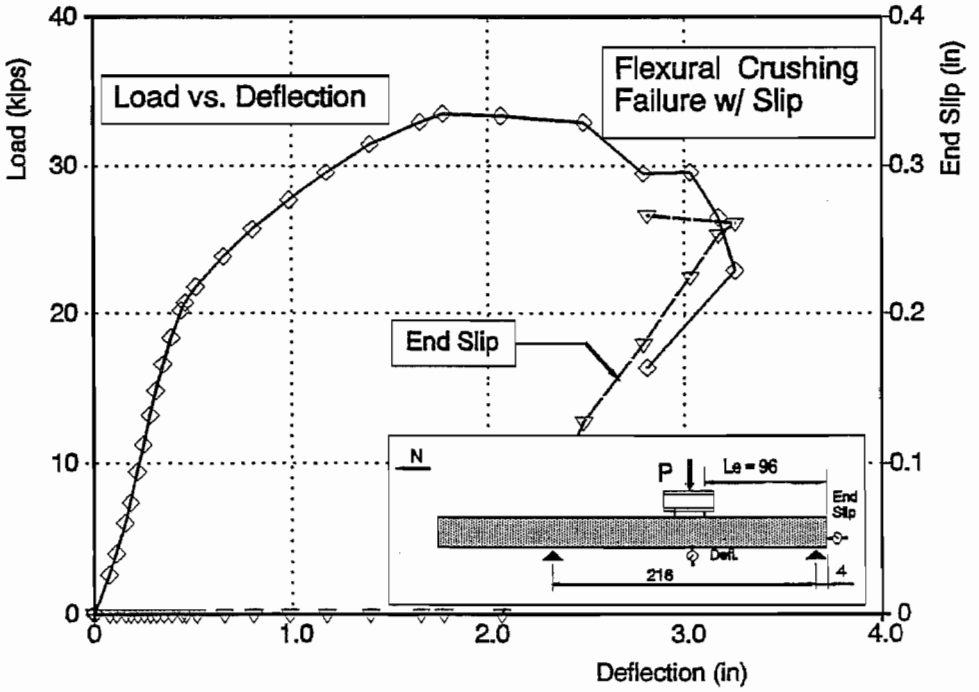

Figure C24. Beam FR350-2 Test B

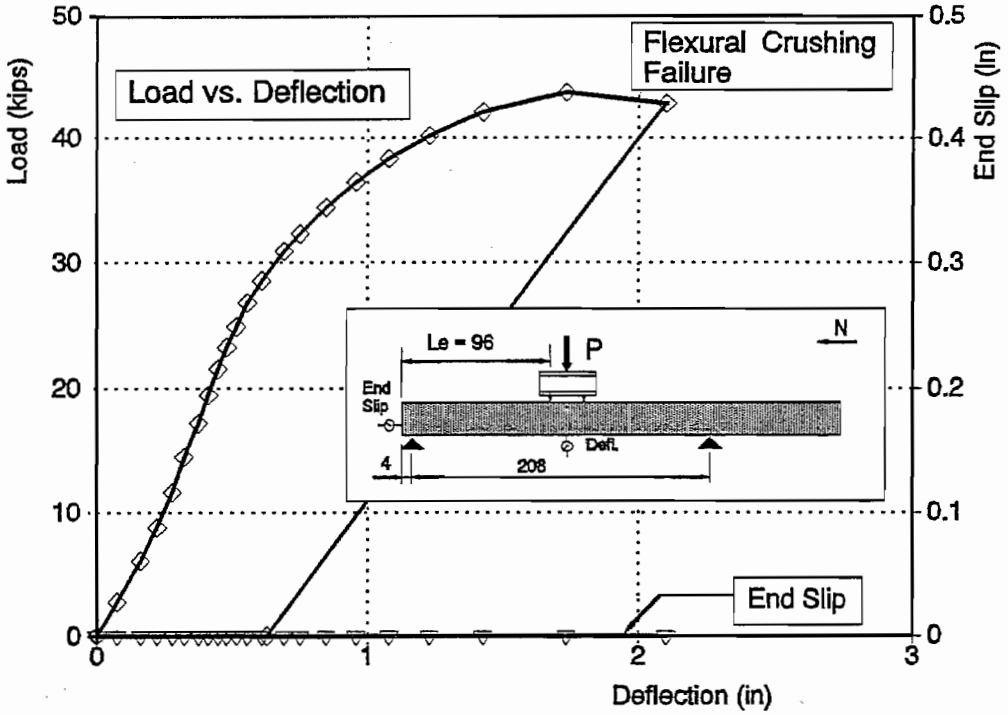

Figure C25. Beam FR360-1 Test A

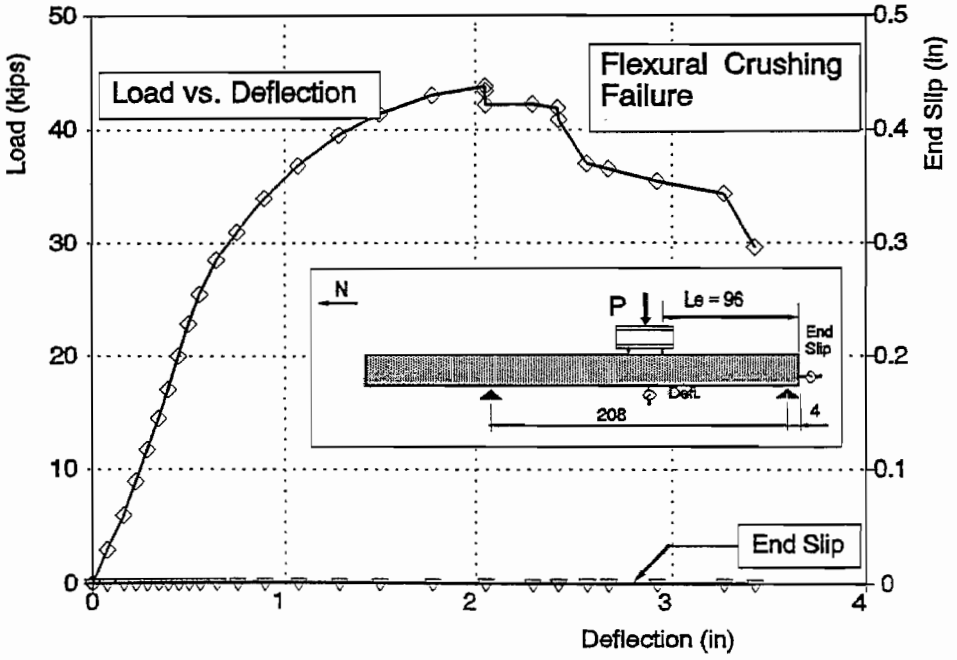

Figure C26. Beam FR360-1 Test B

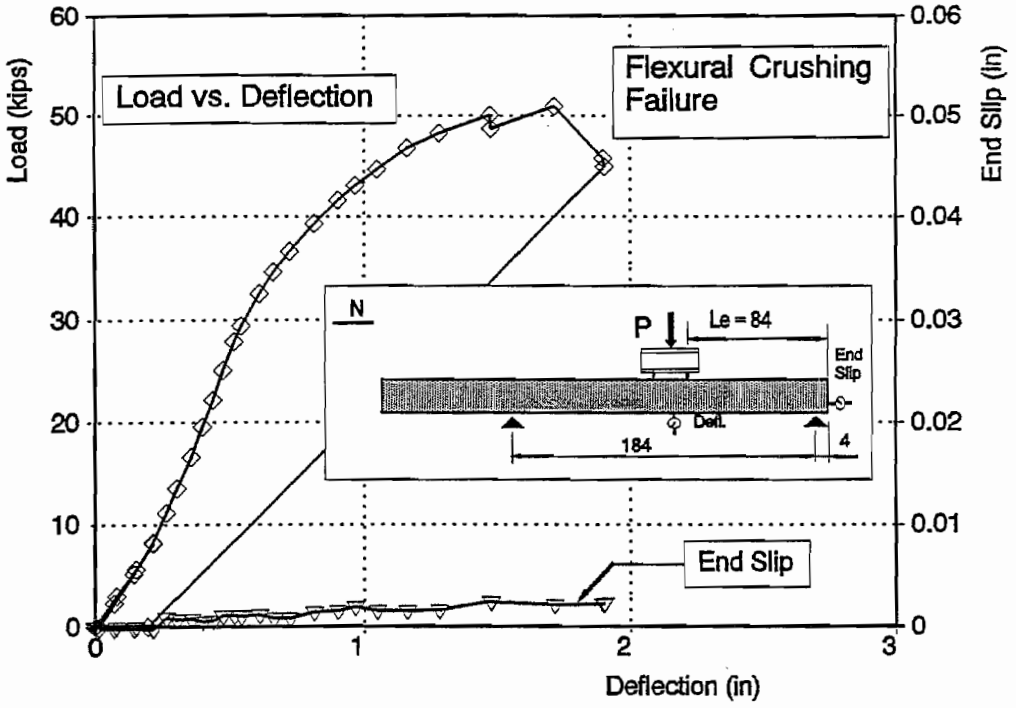

Figure C27. Beam FR360-2 Test A

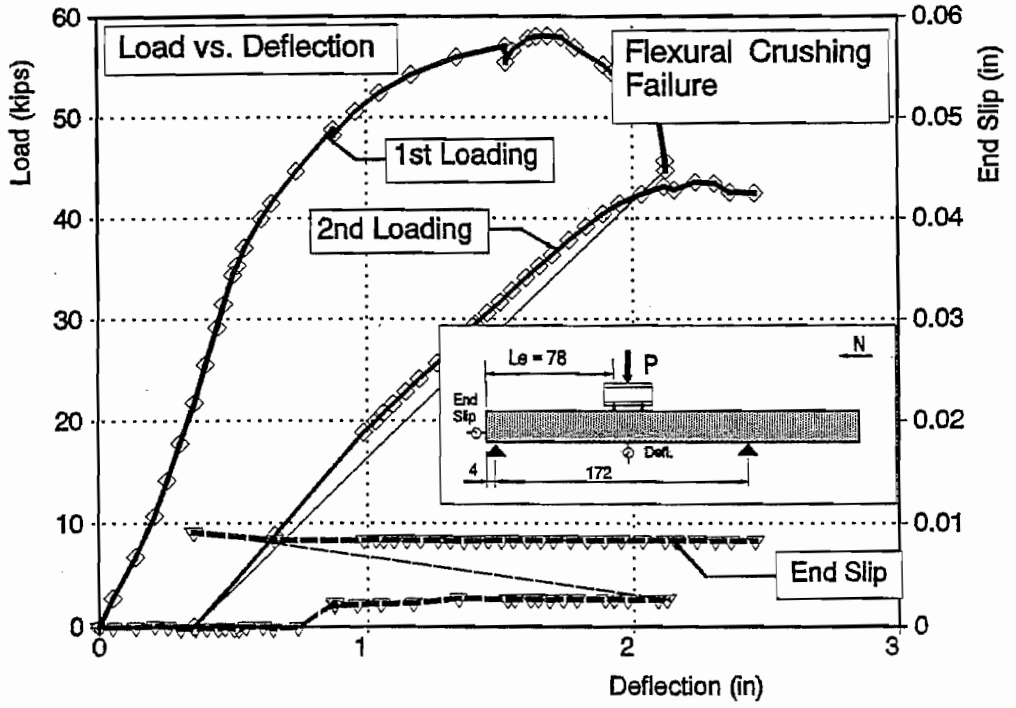

Figure C28. Beam FR360-2 Test B

APPENDIX D
MOMENT CURVATURE FOR FLEXURAL SECTIONS

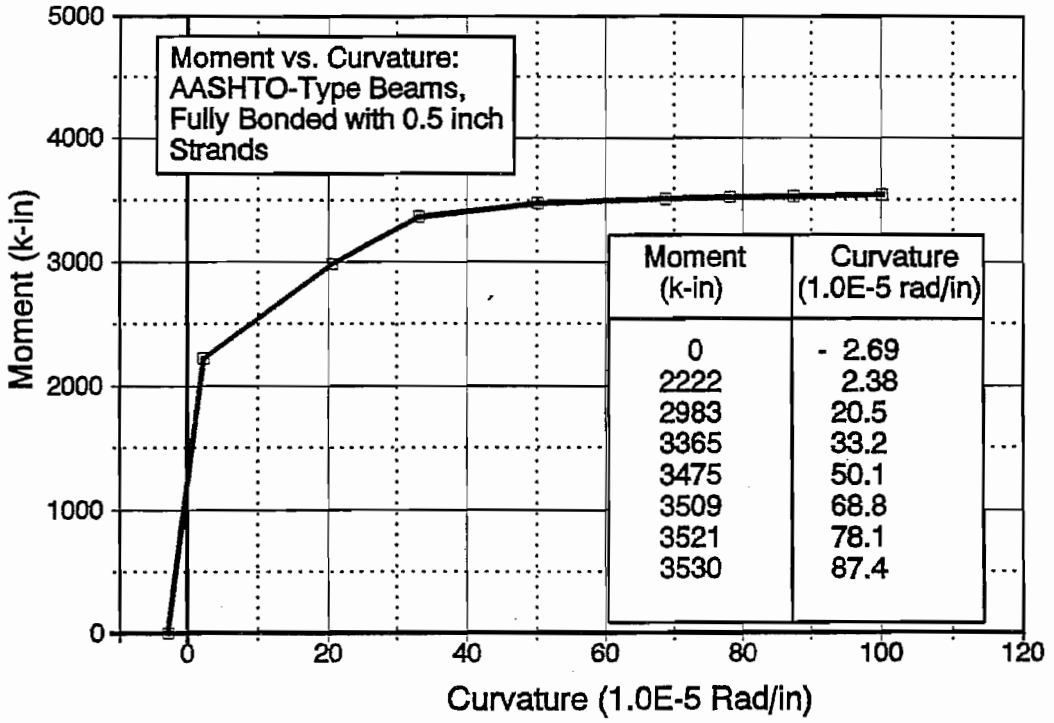

Figure D1. Moment Curvature, Beams FA550

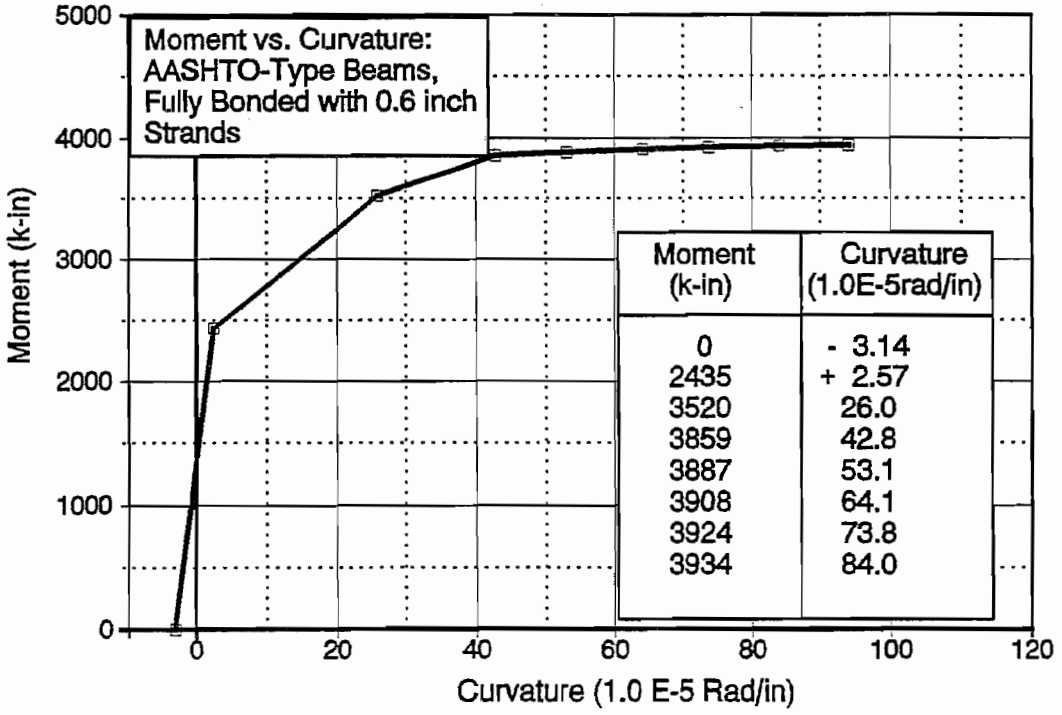

Figure D2 Moment Curvature, Beams FA460

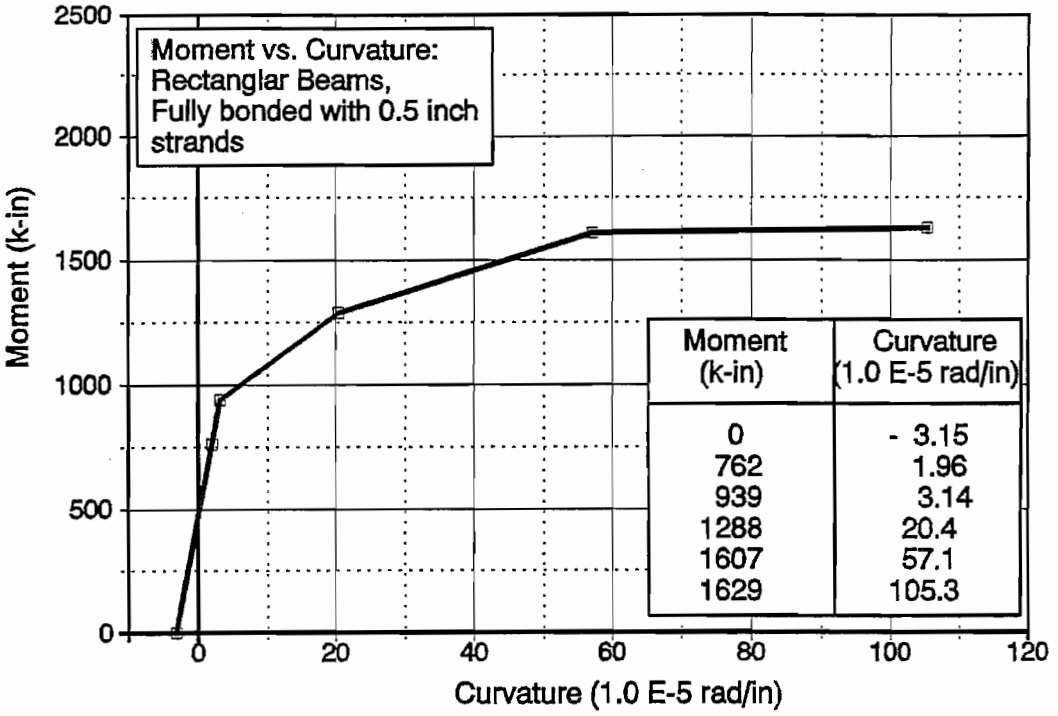

Figure D3. Moment Curvature, Beams FR350

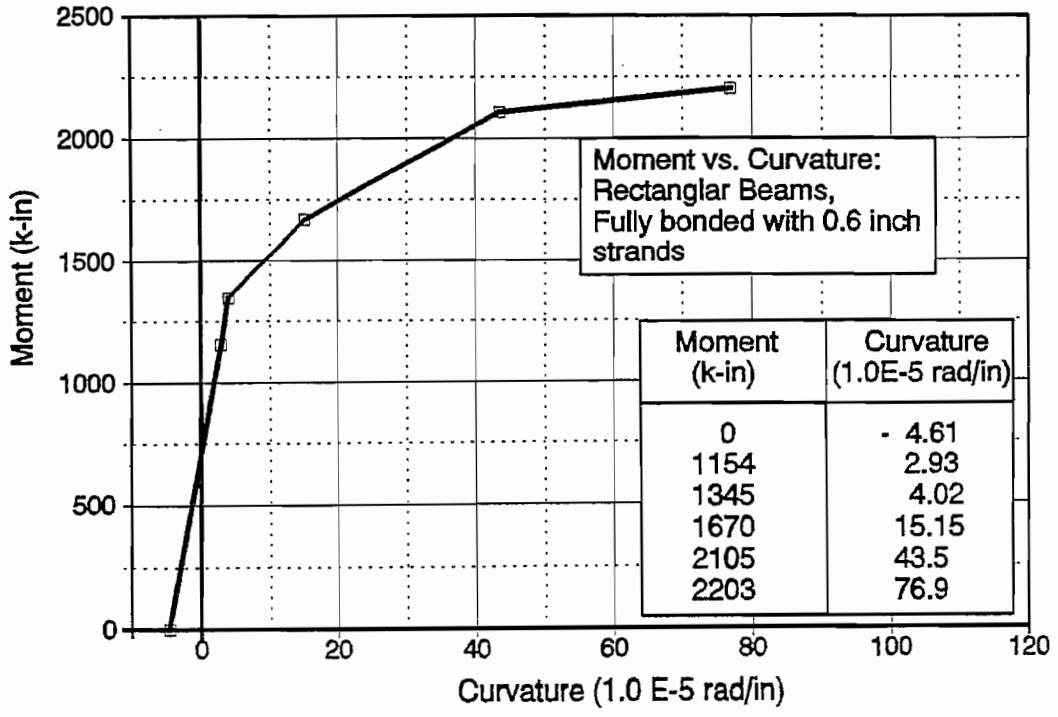

Figure D4. Moment Curvature, Beams FR360

APPENDIX E
GLOSSARY OF TERMS

A_{ps}	–	Area of prestressing steel
d_b	–	Strand diameter
E_{ps}	–	Modulus of elasticity for prestressing strand
f_r	–	Modulus of rupture, or the tensile strength of concrete at the bottom fiber of a flexural member; $f_r = 7.5\sqrt{f'_c}$.
f_{se}	–	Effective prestress after all prestress losses
f_{si}	–	Prestress afer transfer before time dependent losses
L_b	–	Debonded length (length of blanketing)
L_d	–	Development length
L_e	–	Embedment length
L_t	–	Transfer length
M_{cr}	–	Cracking Moment
M_n	–	Nominal Moment, or the calculated moment capacity
M_{sv}	–	Service load moment
M_u	–	Ultimate Moment, usually refers to failure moment
N	–	Number of strands
	–	Number of cycles
N_b	–	Number of blanketed strands
u_{avg}	–	Average bond stress
u_b	–	Bond stress
u_{max}	–	Maximum bond stress
V_c	–	Shear strength of concrete
V_{cw}	–	Web cracking shear of a concrete member
V_u	–	Shear strength at shear failure

REFERENCES

1. Janney, Jack R., "Nature of Bond in Pre-tensioned Prestressed Concrete," *Journal of the American Concrete Institute*, May 1954, pp. 717-736.

2. Thorsen, Niels, "Use of Large Tendons in Pre-tensioned Concrete," *Journal of the American Concrete Institute*, February 1956, pp. 650-659.

3. Peattie, K. R., and Pope, J. A., "Effect of Age of Concrete on Bond Resistance," *Journal of the American Concrete Institute*, February 1956, pp. 661-672.

4. Nordby, Gene M. and Venuti, William J., "Fatigue and Static Tests of Steel Strand Prestressed Beams of Expanded Shale and Conventional Concrete," *Journal of the American Concrete Institute*, August 1957, pp. 141-160.

5. Hanson, Norman W., and Kaar, Paul H., "Flexural Bond Tests of Pretensioned Prestressed Beams," *Journal of the American Concrete Institute*, January 1959, pp. 783-802.

6. Preston, H. Kent, "Characteristics of 15% Stronger Seven-Wire Strand", *Journal of the Prestressed Concrete Institute*, February 1963, pp. 39-35.

7. Janney, J.R., "Report of Strand Transfer Length Studies on 270K Prestressing Strand," *PCI Journal*, February 1963, pp. 41-45.

8. Kaar, Paul H., LaFraugh, Robert W., and Mass, Mark A., "Influence of Concrete Strength on Strand Transfer Length," *Journal of the Prestressed Concrete Institute*, October 1963, pp. 47-67.

9. Lenschow, Rolf J. and Sozen, Mete A., "Practical Analysis of the Anchorage Zone Problems in Prestressed Beams", *Journal of the American Concrete Institute*, November 1965, pp. 1421-1437.

10. Over, R. Stanton, and Au, Tung, "Prestress Transfer Bond of Pretensioned Strands in Concrete," *Journal of the American Concrete Institute*, November 1965, pp. 1451-1460.

11. Kaar, Paul H. and Magura, Donald D., "Effect of Strand Blanketing on Performance of Pretensioned Girders," *Journal of the Prestressed Concrete Institute*, December 1965, pp. 20-34.

12. Hanson, Norman W., "Influence of Surface Roughness of Prestressing Strand in Bond Performance", *Journal of the Prestressed Concrete Institute*, February 1969, pp. 32-45.

13. Coles, Bruce C. and Hamilton, Wayne A., "Repetitive Dynamic Loading on Pretensioned Prestressed Beams", *Journal of the American Concrete Institute*, Sept. 1969, pp. 745-747.

14. Tulin, Leonard G. and Al-Chalabi, Mulaf M., "Bond Strength as a Function of Strand Tension and Cement Paste Content for Lightweight Aggregate Concrete", *Journal of the American Concrete Institute*, October 1969, pp. 840-846.

15. Stocker, M.F., and Sozen, M.A., "Investigation of Prestressed Reinforced Concrete for Highway Bridges, Part V: Bond Characteristics of Prestressing Strand," Engineering Experiment Station 503, The University of Illinois, 1971.

16. Edwards, A. D. and Picard, A., "Bonding Properties of 0.5 inch Diameter Strand", *Journal of the American Concrete Institute*, November 1972, pp. 684-689.

17. Dane, John, III, and Bruce, R.N., Jr., *Elimination of Draped Strands in Prestressed Concrete Girders*, State of Louisiana, Technical Report No. 107, June 1975.

18. Kaar, Paul H. and Hanson, Norman W., "Bond Fatigue Tests of Beams Simulating Pretensioned Concrete Crossties", *Journal of the Prestressed Concrete Institute*, Sept.-Oct. 1975, pp. 65-80.

20. Martin, Leslie D. and Scott, Norman L., "Development of Prestressing Strand in Pretensioned Members," *Journal of the American Concrete Institute*, August 1976, pp. 453-456.

21. Anderson, Arthur R. and Anderson, Richard G., "An Assurance Criterion for Flexural Bond in Pretensioned Hollow Core Units", *Journal of the American Concrete Institute*, August 1976, pp. 457-464.

22. Zia, Paul and Mostafa, Talat, "Development Length of Prestressing Strands," *Journal of the Prestressed Concrete Institute*, Sept.-Oct., 1977.

23. Rabbat, B.G., Kaar, P.H., Russell, H.G., and Bruce, R.N., Jr., *Fatigue Tests of Full-Size Prestressed Girders*, State of Louisiana, Technical Report No. 113, June 1978.

24. Schupack, M. and Mizuma, K., "Bond Properties of High Strength, Low Carbon Bars with Drawn-in Helical Deformation for Use in Pretensioning and as a Special Normal Reinforcement", *Journal of the American Concrete Institute*, Feb. 1979, pp. 249-275.

25. Rabbat, B. G., Kaar, P. H., Russell, H. G., Bruce, R. N., Jr., "Fatigue Tests of Pretensioned Girders With Blanketed and Draped Strands," *Journal of the Prestressed Concrete Institute*, July-August 1979, pp. 88-114.

26. Lin, T.Y., and Burns, Ned H., *Design of Prestressed Concrete Structures*, Third Edition, John Wiley and Sons, New York, New York, 1981.

27. Burnett, Eric F. P., and Anis, Ahmed H., "Bond Characteristics of Initially Untensioned Strands", *Journal of Structural Engineering*, ASCE, May 1981, pp. 953-964.

28. Horn, Daniel G., and Preston, H. Kent, "Use of Debonded Strands in Pretensioned Bridge Members," *Journal of the Prestressed Concrete Institute*, July-August 1981, pp. 42-59.

29. Kennedy, John B. and El-Laithy, A. M., "Cracking at Openings in Prestressed Beams at Transfer", *Journal of Structural Engineering*, ASCE, June 1982, pp. 1250-1265.

30. Ellyin, Fernand and Matta, Rafik, "Bonding and Corrosion Protection for Prestressing Steels", *Journal of the American Concrete Institute*, Sept.-Oct. 1982, pp. 366-371.

31. Ramirez, J.A., and Breen, J.E., *Proposed Design Procedures for Shear and Torsion in Reinforced and Prestressed Concrete*, Research Report 248-4F, Center for Transportation Research, The University of Texas at Austin, November 1983.

32. Ramirez, J.A., and Breen, J.E., *Experimental Verification of Design Procedures for Shear and Torsion in Reinforced and Prestressed Concrete*, Research Report 248-3, Center for Transportation Research, The University of Texas at Austin, November 1983.

33. Keuser, M., Mehlhorn, G. and Cornelius, V., Bond Between Prestressed Steel and Concrete - Computer Analysis Using ADINA", *Computers and Structures*, Pergamon Press Ltd., Great Britain, Vol 17, No. 5, pp.669-676, 1983.

34. Ingraffea, Anthony R., Gerstle, Walter H., Gergely, Peter and Saouma, Victor, "Fracture Mechanics of Bond of Reinforced Concrete", *Journal of Structural Engineering*, ASCE, April 1984, pp.871-890.

35. Overman, T.R., Breen, J.E., and Frank, K.H., *Fatigue Behavior of Pretensioned Concrete Girders*, Research Report 300-2F, Center for Transportation Research, The University of Texas at Austin, November 1984.

36. Yankelevsky, David Z., "New Finite Element for Bond Slip Analysis", *Journal of Structural Engineering*, ASCE, July 1985, pp. 1533-1543.

37. Ghosh, S. K., and Fintel, M., "Development Length of Prestressing Strands, Including Debonded Strands, and Allowable Stresses in Pretensioned Members," *Journal of the Prestressed Concrete Institute*, September-October 1986, pp. 38-57.

39. Cousins, Thomas E., Johnston, David W., and Zia, Paul, *Bond of Epoxy Coated Prestressing Strand,* Center for Transportation Engineering Studies, Department of Civil Engineering, North Carolina State University, December 1986.

40. Bachman, P.M., Kreger, M.E., and Breen, J.E., *An Exploratory Investigation of Shear Fatigue Behavior of Prestressed Concrete Girders*, Research Report 465-1, Center for Transportation Research, The University of Texas at Austin, June 1987.

41. Keuser, M. and Mehlhorn, G., "Finite Element Models for Bond Problems", *Journal of Structural Engineering*, ASCE, October 1987, pp.2160-2173.

42. Ahmed, M. and Bangash, Y., "A Three Dimensional Bond Analysis Using Finite Element", *Computers and Structures*, Vol 25:2, 1987, pp. 281-296.

43. Hartmann, D.L., Breen, J.E., and Kreger, M.E., *Shear Capacity of High Strength Prestressed Concrete Girders*, Research Report 381-2, The Center for Transportation Research, The University of Texas at Austin, January 1988.

44. Castrodale, R.W., Kreger, M.E., and Burns, N.H., *A Study of Pretensioned High Strength Concrete Girders in Composite Highway Bridges- Laboratory Tests*, Research Report 381-3, Center for Transportation Research, The University of Texas at Austin, January 1988.

45. Castrodale, R.W., Kreger, M.E., and Burns, N.H., *A Study of Pretensioned High Strength Concrete Girders in Composite Highway Bridges- Design Considerations*, Research Report 381-4F, Center for Transportation Research, The University of Texas at Austin, January 1988.

46. Brooks, Mark D., Gerstle, Kurt H. and Logan, Donald R.,"Effect of Initial End Slip on the Strength of Hollow-Core Slabs", *Journal of the Prestressed Concrete Institute*, Jan.-Feb. 1989, pp.90-111.

47. Kreger, M.E., Bachman, P.M., and Breen, J.E., "An Exploratory Study of Shear Fatigue Behavior of Prestressed Concrete Girders", *PCI Journal*, July/August 1989, pp. 104-125.

48. *Standard Specifications for Highway Bridges, 14th Edition*, The American Association of State Highway Transportation Officials (AASHTO), Inc., Washington, D.C. 1989.

49. *Building Code Requirements for Reinforced Concrete (ACI 318-89)*, American Concrete Institute, Detroit, Michigan, 1989.

50. *Commentary on Building Code Requirements for Reinforced Concrete (ACI 318-89)*, American Concrete Institute, Detroit, Michigan, 1989.

51. Deatherage, Harold J., and Burdette, Edwin, G., *Development Length and Lateral Spacing Requirements of Prestressing Strand for Prestressed Concrete Bridge Products*, Transportation Center, The University of Tennessee, Knoxville, February 1991.

52. Loov, R.E., and Weerasekera, R., "Prestress Transfer Length," *Annual Conference of The Canadian Society for Civil Engineering*, Hamilton, Ontario, May 1990.

53. Cousins, Thomas E., Johnston, David W., and Zia, Paul,"Development Length of Epoxy-Coated Prestressing Strand", *ACI Materials Journal*, July-August, 1990, pp.309-318.

54. Cousins, Thomas E., Johnston, David W., and Zia, Paul,"Transfer Length of Epoxy-Coated Prestressing Strand", *ACI Materials Journal*, May-June, 1990, pp.309-318.

55. Shahawy, M., and Batchelor, B. Dev, *Bond and Shear Behavior of Prestressed AASHTO Type II Beams*, Progress Report No. 1, Structural Research Center, Florida Department of Transportation, February 1991.

56. Unay, I.O., Russell, B., Burns, N. and Kreger, M., *Measurement of Transfer Length on Prestressing Strands in Prestressed Concrete Specimens*, Center for Transportation Research, The University of Texas at Austin, March 1991.

57. ZumBrunnen, L.G., Russell, B.W., Burns, N.H. and Kreger, M.E., *Behavior of Statically Loaded Pretensioned Concrete Beams with 0.5 inch Diameter Debonded Strands*, Research Report 1210-4, Center for Transportation Research, The University of Texas at Austin, January 1992.

58. Lutz, B.A., Russell, B.W., Burns, N.B. and Kreger, M.E., *Measurement of Development Length of 0.5 Inch and 0.6 Inch Diameter Prestressing Strands in Fully Bonded Concrete Beams*, Research Report 1210-3, Center for Transportation Research, The University of Texas at Austin, February 1992.

59. Shahawy, Mohsen A., Issa, Moussa, and Batchelor, Barrington deV, "Strand Transfer Lengths in Full Scale AASHTO Prestressed Concrete Girders," *PCI Journal*, May/June 1992.

60. Nanni, A. and Tanigaki, M., "Pretensioned Prestressed Members with Bonded Fiber Reinforced Tendons: Development and Flexural Bond Lengths (Static)," *ACI Structural Journal,* July-August 1992, pp.433-441.